Phenomenology at a future 100 TeV hadron collider

Dissertation

zur Erlangung des mathematisch-naturwissenschaftlichen Doktorgrades
„Doctor rerum naturalium“
der Georg-August-Universität Göttingen

im Promotionsprogramm ProPhys
der Georg-August University School of Science (GAUSS)

vorgelegt von

Piero Ferrarese

aus Chioggia (Venedig - Italien)

Göttingen, 2017

Betreuungsausschuss

Prof. Dr. Steffen Schumann
Prof. Dr. Arnulf Quadt

Mitglieder der Prüfungskommission:

Referent:	Prof. Dr. Steffen Schumann II. Physikalisches Institut, Georg-August-Universität Göttingen
Koreferent:	Prof. Dr. Arnulf Quadt II. Physikalisches Institut, Georg-August-Universität Göttingen

Weitere Mitglieder der Prüfungskommission:

Prof. Dr. Laura Covi
Institut für Theoretische Physik, Georg-August-Universität Göttingen

Prof. Dr. Wolfram Kollatschny
Institut für Astrophysik, Georg-August-Universität Göttingen

Prof. Dr. Stanley Lai
II. Physikalisches Institut, Georg-August-Universität Göttingen

Prof. Dr. Salvatore Manmana
Institut für Theoretische Physik, Georg-August-Universität Göttingen

Tag der mündlichen Prüfung:

Ad maiorem Dei gloriam

E anca ancuo la xé andá, e doman pensaremo

Popular wisdom

L'ho pensato anch'io, Capitano, che non dovevo venire, ma mi hai portato lontano fino a dentro il mio cuore, a quest'odore di terra che ora viene dal mare, da amare...

Claudio Chieffo, Capitano, 1992

Phenomenology at a future 100 TeV circular collider

Piero Ferrarese

Abstract

Run 1 of the Large Hadron Collider (LHC) has been one of the most successful experiments in particle physics. We are now approaching the end of LHC Run 2, and whether we will discover new physics or not, the high energy particle physics community is already inspecting various possibilities for the future generation of colliders. One of the most intriguing scenarios deals with the exploration of energies so far not reached, with energy scales up to several TeVs, as for example a $\sqrt{s} = 100$ TeV hadron-hadron collider. This thesis inspects the phenomenological potential of such a machine from two different viewpoints. First, the perturbative Quantum Chromodynamics (QCD) perspective. Monte Carlo event generators play an essential role for data analysis and interpretation at the LHC, and they are vital for exploring the potential of future machines. We aim at improving our current perturbative QCD descriptions with precise predictions through resummation methods. These represent all-orders analytical results which properly account for divergences appearing in the calculations, as those related to the emission of soft gluons. We discuss the automation of soft-gluon resummation within the SHERPA Monte Carlo event generator framework. We present comparisons between resummed and parton-showered predictions, thereby inspecting which are the necessary steps to be taken in passing from Monte Carlo simulations at the LHC to a Future Circular Collider. In the second part of the thesis we discuss the phenomenology related to Vector Boson Scattering at $\sqrt{s} = 100$ TeV in a Composite Higgs model scenario, based on the coset $SU(4)/Sp(4)$. We predict limits for the appearance of resonant and non-resonant excesses in the production channel $pp \to ZZjj$. This process provides one of the most interesting possibilities for finding deviations from the Standard Model at a Future Circular Collider.

Phänomenologie an einem zukünftigen 100 TeV Hadronbeschleuniger

Piero Ferrarese

Zusammenfassung

Run 1 des Large Hadron Colliders (LHC) war eines der erfolgreichsten Experimente in der Teilchenphysik. Wir nähern uns nun dem Ende von LHC Run 2, und ob wir neue Physik entdecken oder nicht, die Hochenergiephysik-Gemeinschaft prüft bereits verschiedene Optionen für die zukünftige Generation von Collider. Eines der faszinierendsten Szenarien beschäftigt sich mit der Erforschung von Energien, die bisher nicht erreicht wurden, mit Energieskalen bis zu einigen Teraelektronenvolt, wie zum Beispiel einem $\sqrt{s} = 100$ TeV Hadron-Hadron-Beschleuniger. Diese Arbeit untersucht das phänomenologische Potenzial einer solchen Maschine aus zwei verschiedenen Gesichtspunkten, einerseits der perturbativen Quantenchromodynamik (QCD) andererseits dem Entdeckungspotenzial für ein spezifisches Szenario neuer Physik. Monte-Carlo Ereignisgeneratoren spielen eine wesentliche Rolle für die Datenanalyse und -interpretation am LHC, und sie sind entscheidend für die Erforschung des Potenzials zukünftiger Maschinen. Gegenstand dieser Arbeit ist die Verbesserung unserer aktuellen perturbativen QCD-Vorhersagen mittels präziser Methoden der Resummation von kinematischen Logarithmen. Diese Resummationsmethoden repräsentieren analytische Ergebnisse für den Einfluss der Abstrahlung weicher Gluonen. Wir diskutieren insbesondere die Automatisierung von Soft-Gluon Resummation im SHERPA Monte Carlo Ereignisgenerator. Wir präsentieren Vergleiche zwischen Resummations- und Parton-Shower-Vorhersagen und machen darauf basierende Extrapolationen vom LHC zu einem zukünftigen 100 TeV Hadron-Hadron-Beschleuniger. Im zweiten Teil der Arbeit diskutieren wir die Phänomenologie des Vektor-Boson-Streuungsprozesses bei $\sqrt{s} = 100$ TeV in einem Composite Higgs-Modell Szenario, basierend auf dem Coset $SU(4)/Sp(4)$. Wir schätzen das Nachweispotenzial für Resonanz- und Nicht-Resonanz Exzesse im Produktionskanal $pp \to ZZjj$. Dieser Prozess bietet eine der interessantesten Möglichkeiten, Abweichungen vom Standardmodell der Teilchenphysik an einem zukünftigen Ringbeschleuniger zu finden.

Contents

CHAPTER 1

Introduction

The last years have been quite successful for the high-energy particle physics community. The Large Hadron Collider (LHC) permitted the exploration of energies that were previously out of reach. Up to 2012, the Standard Model of particle physics (SM) [1–3] was still missing the experimental discovery of one of its building blocks, the Higgs particle. With the discovery of the Higgs boson by the CMS (Compact Muon Solenoid) and ATLAS (A ThoroidaL ApparatuS) collaborations, the Standard Model becomes a theory almost completely tested [4, 5]. The hunt for the Higgs boson lasted almost 60 years, and might be considered one of the greatest achievement for high-energy physics. Still the mechanism that spontaneously breaks Electroweak Symmetry is to be unveiled. Despite several theories for a natural, dynamical explanation of the generation of the Higgs potential being proposed, the exact nature of this mechanism is still unknown. What we need is an explanation without enormous fine-tuning and preferably with a dynamical origin without the ad-hoc terms that occur with the Higgs boson in the Standard Model.

The physics program at the LHC includes not only the search for the main decay channels of the Higgs boson, but also measurements of masses, couplings and parameters, as predicted from the Standard Model of particle physics. While always looking for excesses and deviations of cross sections from the SM predictions, the LHC has repeated almost all of the measurements taken at the Tevatron, the $p\bar{p}$ collider at the Fermi National Laboratory. This has been performed from the perspective of the energy frontier - opposed to what is usually defined as the precision frontier, as in the case of a lepton-lepton collider like the Large Electron-Positron Collider LEP - probing a larger region in the phase space and collecting more data. This has been possible partly thanks to the big developments and efforts of the community for the construction of Monte Carlo software, which allows the calculation of precise predictions to be compared with experimental data. Through Quantum Field Theory principles and prescriptions we are able to compute the cross sections of colliding particles, which are compared to measured

data; though, in the current status, we are able to treat a small number of particles at a time.

Our first principle knowledge, Quantum Field Theory, is only able to treat a small number of particles at a time. A scattering of $2 \to 4$ particles is, in most cases, already quite challenging to compute. Collisions take place in a busy environment, which contains 10^{11} protons per bunch scattering each other in the collision tunnel every 25 ns. The most intriguing part of this picture is the fact that we do not know exactly how the inner part of the proton behaves. The quarks, of which a proton is composed, are, in turn, one of the building blocks of the Standard Model. Any meaningful observable cross section calculation in Quantum Field Theory is performed through the fields representing quarks, not protons.

Monte Carlo algorithms, or the art of generating pseudo-random events for a given - usually quite complicated - probability distribution, allow us to narrow down the integration time of cross sections, and are used to generate sets of momenta for the particles in the events, probabilistically chosen. In this way, performing an analysis, as for the real events collected at the colliders, it is possible to compare measurements and theory predictions. The integration of the matrix element for the process, along with the subsequent showering according to Quantum Chromodynamics (QCD), and the inclusion of low-energy effects, such as hadronisation and further hadron decays, as well as the simulation of multi-parton interactions and other non-perturbative effects, build a complete multi-purpose Monte Carlo software for particle physics.

Perturbation theory organises calculations as a power series expansion in the coupling constant, α_s in the case of QCD, as this keeps a small enough value. For a Monte Carlo event generator it is possible to compute all leading ($\mathcal{O}(\alpha_S(Q^2))$) and next-to-leading $\mathcal{O}(\alpha_S^2(Q^2))$ order cross sections. Currently, some next-to-next-to leading order (NNLO) results, both at integrated and differential level are already fully automated [6–9], and, despite some major issue in the automation process, this is going to be very likely the near future standard precision available for a Monte Carlo simulation software.

Fixed-order calculations, which could provide a great level of precision, even with the increasing number of orders in the perturbative expansion are not complete, therefore it is necessary to include all-order predictions. Due to our lack of knowledge of the behaviour of QCD at low energy scales, we are only able to approximate these effects. Still, parton-shower algorithms, simulating the emissions of QCD partons from a parent one, describe with a good degree of precision the low-energy region of the differential distributions. Then, starting from a fully differential set of events, generated according the matrix element for the given process, it is possible to evolve the particles in the event through the parton-shower, from the production scale down to a cut-off scale, usually around 1 GeV.

Run 1 at the LHC provided, between 2009 and 2013, an integrated luminosity of nearly 30 fb^{-1}, with protons colliding up to a centre of mass energy $\sqrt{s} = 8$ TeV. Run 2 should collect, between 2015 and 2018, events corresponding to an integrated luminosity $L \sim 100\,\text{fb}^{-1}$, with collisions taking place at centre of mass energy of $\sqrt{s} =$ 13 TeV. We want to present here a couple of measurements from the LHC that can help

understanding what we present in this thesis, i.e. jet cross sections and vector-boson-scattering measurements. In fig. 1.1, we present a result from the ATLAS collaboration, the measurement of the inclusive jet multiplicity at $\sqrt{s} = 7$ TeV: QCD is fascinating, but is highly non-perturbative at low energies, around the order of hundreds GeV. The colliding beams scatter giving rise to a di-jet structure, from which further particles are emitted. The increasing energy available for the collision allows for the production of several jet objects. This is a nice example where jet phenomenology studies are allowed

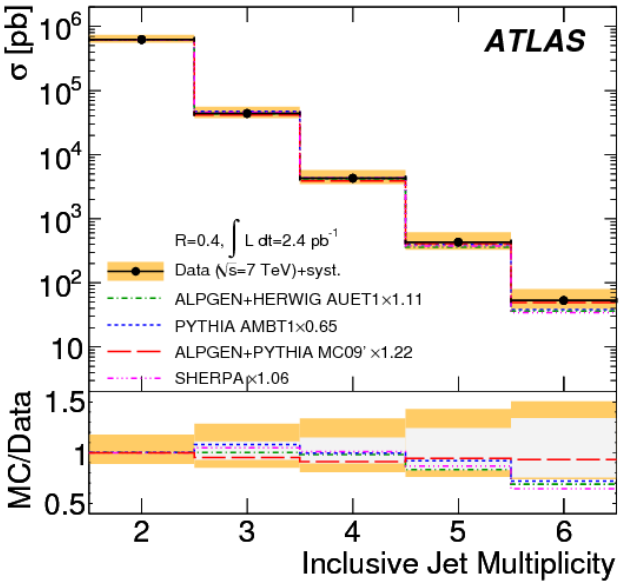

Figure 1.1.: Measurement of the inclusive jet multiplicity in pp collisions at $\sqrt{s} = 7$ TeV from the ATLAS collaboration [10].

by accurate predictions provided by Monte Carlo algorithms [11, 12].

In fig. 1.2 we present the measurement of the differential invariant mass distribution from the CMS collaboration, in ZZ vector-boson-scattering (VBS) events. This is one of the most challenging measurements at LHC, due to its tiny cross section, and a large background. Nonetheless, it could be the door for revealing the true nature of the Higgs boson: it is indeed a handle that could provide a precise measurement of the Higgs tri-linear coupling, and eventual deviation from its Standard Model value could trigger for many interesting Beyond Standard Model scenarios [13–17]. All of this could shed light on the understanding of the real nature of the Higgs particle.

The Standard Model of particle physics is a great success, also because up to now no obvious deviations from the SM predictions were found, and it has become challenging to create new models, which could describe phenomena not yet explained by the SM. Therefore, it is necessary to explore new frontiers, try to reach precision not yet probed,

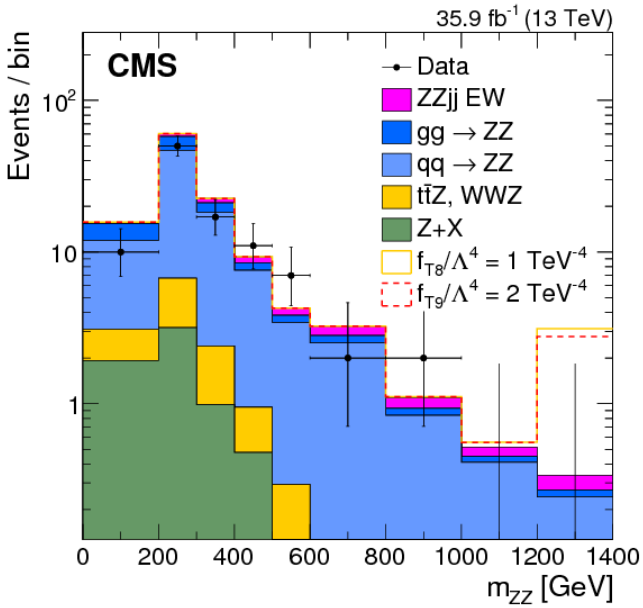

Figure 1.2.: The m_{ZZ} distribution in the $ZZjj$ selection together with the SM prediction and two hypotheses for the anomalous quartic coupling strengths. Points represent the data, filled histograms the expected signal and background contributions. Data collected from the CMS collaboration, at $\sqrt{s} = 13$ TeV and $L = 35.9\,\text{fb}^{-1}$ [18].

or energy scales currently not accessible. It is of paramount importance to understand whether the Higgs particle is indeed the very same predicted by the Standard Model, making it the first fundamental scalar particle, or if some other mechanism is present, that at the TeV energy scale reproduces the particle we detect. On the other hand, there are several open questions, for example, the dynamical generation of the masses, in particular that of the top quark, and it would be of great interest to study the unitarization of WW scattering at high energy.

Already looking at the future, CERN inspects different opportunities for building a future collider able to probe the most interesting processes out there. Several options have been proposed to date, including a linear accelerator [19] and a brand new lepton collider [20]. The possibilities span two different scenarios, as already mentioned: the energy frontier, and the precision one. The latter relies on lepton colliders, which allow for precision measurements, thanks to the fact they do not have composite objects as colliding particles. This avoids lot of issues related to the busy environment typical of the scattering of strongly interacting particles. On the other hand, due to intrinsic design, they allow only for smaller centre of mass energy collisions compared to a hadron-hadron machine. With energy frontier it is meant the idea of pushing forward the centre-of-mass

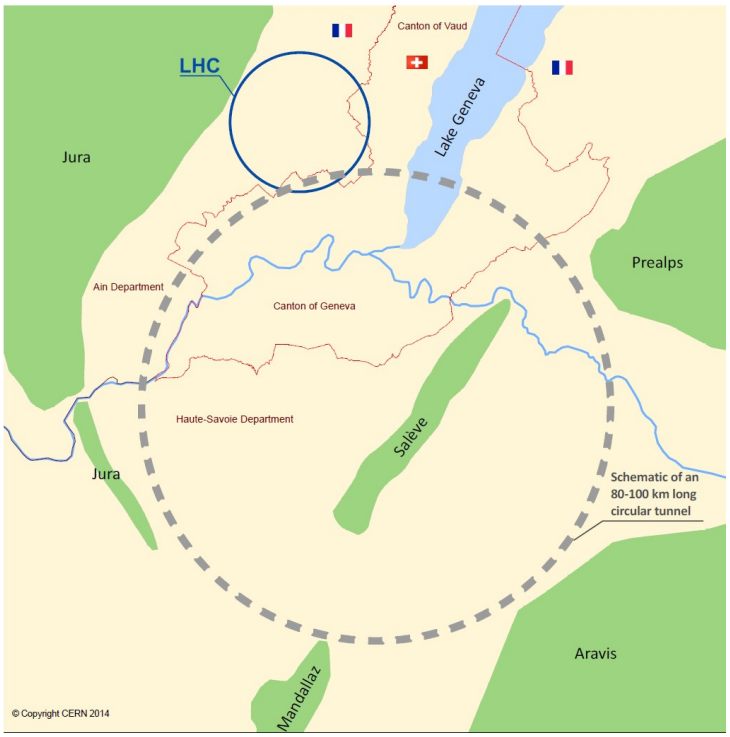

Figure 1.3.: Sketch showing the purpose for the geographical site of a $\sqrt{s} = 100$ TeV hadron collider. In blue the actual LHC ring is shown, in dashed grey the idea for the future hadron collider. The perimeter will be around 100 km, across France and Switzerland.

energy, exploring the so called multi-TeV regime. For some years a group of study has been established to investigate the possibility to build a $\sqrt{s} = 100$ TeV hadron-hadron machine, usually called FCC-hh, Future Circular Collider - hadron-hadron [21, 22].

In fig. 1.3 we can see the sketch of the project for the installation of such a machine. It is definitely an ambitious project, which will break every record set by the LHC. The long-term plan of CERN includes the usage of the LHC tunnel and facilities for at least other 20 years, where the collaborations are scheduling a High Luminosity run, which will reach around $4000\,\text{fb}^{-1}$ of integrated luminosity in 10-12 years of operation. This is the same as the initial luminosity target of the FCC-hh. The luminosity reach for the FCC is the same, as baseline target, with a possible increase.

It is easy indeed to understand how important Monte Carlo simulations are in this particular situation: with their precision and range of applicability, they are of big help in designing future possibilities, predicting what could be possible to detect at hadron colliders with a center of mass energy larger than those employed today. They can help to build analysis strategies. In this sense, it is also important to clarify which approximations, which we are using at the energies of the LHC, will be still valid in a

different environment, at higher energies.

This thesis deals with the physics opportunities and challenges of a $\sqrt{s} = 100$ TeV hadron collider machine. Our aim is to study the validity of present Monte Carlo tools in such an extreme environment, and furthermore, probe the possibility to compare Monte Carlo results with analytical exact methods, such as the resummation of logarithmic enhancements happening in QCD theories. On the other hand, we want to inspect the phenomenological possibilities related to the measurement of the vector boson scattering process. We study a particular Beyond Standard Model realisation to get exclusion limits on the production of exotic modes, with a focus on unitarity of amplitudes.

The outline of the thesis is as follow: in chapter 2 we present the tools and methods developed so far inherent to the Monte Carlo simulations for high-energy particle physics. In chapter 3 we present a study of the relation between numerical implementations like parton showers, with more exact methods such as resummation, comparing predictions for jet rates at a future hadron collider at $\sqrt{s} = 100$ TeV. Finally, in chapter 4 we present a novel treatment of VBS amplitudes within a Composite Higgs realisation.

CHAPTER 2

Perturbative Quantum Chromodynamics and Collider Phenomenology

2.1. Collider phenomenology basics and Monte Carlo simulations

2.1.1. The lagrangian and the coupling constant

Quantum Chromodynamics (QCD) is the theory describing the interactions between quarks and gluons, the fundamental particles that make up composite hadrons such as the proton, neutron and pion. QCD is a non-abelian gauge theory based on the group $SU(3)$. The QCD analog of the electric charge in Quantum Electrodynamics is *colour*. It is the result of several theoretical and experimental efforts starting back in the 1950s. In the present chapter we revise the main features of this successful theory, with particular focus on the main techniques employed in the context of high-energy particle physics Monte Carlo event generators.

The charge associated to the $SU(3)$ symmetry group is called *colour*. The Lagrangian is

$$\mathcal{L}_{\text{QCD}} = \sum_q \bar{\psi}_{q,i} \left(i \not{D}_{ij} - m_q \delta_{ij} \right) \psi_{q,j} - \frac{1}{4} F^A_{\mu\nu} F^{A,\mu\nu}, \tag{2.1}$$

where $\psi_{q,i}$ is the Dirac spinor associated to the quark fields, with an index $i = 1, \ldots, 3$ running through the colour charge, and q labelling the *flavour* index of the fermions;

$$\not{D}_{ij} \equiv \gamma^\mu \left(\partial_\mu \delta_{ij} + i g_s t^A_{ij} \mathcal{A}^A_\mu \right) \tag{2.2}$$

is the covariant derivative, in which we can recognise the strong coupling constant $g_s^2 = 4\pi\alpha_s$ and the boson fields associated to the gluons $\mathcal{A}$. While the quarks belong to the *fundamental* representation of $SU(3)$, the gluons - as mediators of the strong interaction

- live in the *adjoint*, therefore the index runs over the corresponding dimension $A = 1 \ldots, N_C^2 - 1 = 8$. The representation of the Dirac matrices, γ_μ, we use here is shown in appendix A, together with the generators of the $SU(3)$ group t_{ij}. The so-called *field-strength* tensor, $F^A_{\mu\nu}$, is proportional to the commutator of the covariant derivative and reads

$$F^A_{\mu\nu} = \partial_\mu \mathcal{A}^A_\nu - \partial_\nu \mathcal{A}^A_\mu + i f_{ABC} \mathcal{A}^B_\mu \mathcal{A}^C_\nu \,, \tag{2.3}$$

where f_{ABC} are the structure constants of the group, $\left[t^A, t^B\right] = i f_{ABC} t^C$.

One of the most peculiar feature of Quantum Chromodynamics is *asymptotic freedom*. This concept was predicted by Gross, Wilczek and Politzer in 1973 [23, 24], and they have been rewarded with the Nobel prize for their research. Using Wilczek's words from his Nobel lecture: "Antiscreening, or asymptotic freedom, implies instead that a charge of intrinsically small magnitude catalyzes a cloud of virtual particles that enhances its power. I like to think of it as a thundercloud that grows thicker and thicker as you move away from the source." [25]. Differently from what happens in the electroweak sector, the force of the strong interactions becomes large at low energies, $Q^2 \lesssim 10^{-1}$ GeV$^2 \sim \Lambda^2_{\text{QCD}}$, and decreases with the increasing energy. Thanks to this particular behaviour, it is possible to employ perturbation theory to get predictions at energy scales greater than some GeV, computing scattering amplitudes and observables in terms of an expansion in the coupling constant α_s.

Confinement at low energies, with which we mean Λ^2_{QCD} scales, is another important property of QCD. This means that we cannot directly observe colour charged particles, either gluons or quarks, only bound states, that are singlet objects. These are called in full generality *hadrons*, and are divided into *mesons* and *baryons*, if they are composed of 2 or 3 quarks, respectively. Confinement is emerging in QCD as linearly rising term in the potential between strong particles. For example, in a $e^+ - e^-$ scattering in which a quark pair is created, as these start moving away from each other, the linear potential favours the creation of another pair, rather than the separation of the charges. This is a typical behaviour of non-abelian theories, as this is a direct consequence of the fact the the mediators in these theories carry a charge, opposed to what happens in QED.

Although it is hard to get predictions, a rich phenomenology of hadron physics is well described by employing QCD first principles, as it happens with what is called "the eightful Way" [26]. Often, in the regime where perturbation theory is not valid, lattice calculations are employed. In general there is a lack of understanding in what really happens inside a hadron.

Ultraviolet divergences are present also in QCD, as typical of many Quantum Field Theories. Perturbation theory requires *renormalisation* in order to properly take care of these, thus retrieving a divergence-free model. This introduces an energy scale, μ^2_R, at which the renormalisation procedure is performed. Therefore, the definition of observables through the coupling constant, which is not independent of the scale Q^2 at which it is evaluated, is rather depending on the ratio Q^2/μ^2_R. *Running* the coupling constant through the Callan-Symanzik equation, one of the renormalisation group equa-

tions (RGEs),

$$\left(\mu_R^2\frac{\partial}{\partial\mu_R^2}+\mu_R^2\frac{\partial\alpha_s}{\partial\mu_R^2}\frac{\partial}{\partial\alpha_s}\right)\Gamma(Q^2/\mu_R^2,\alpha_s)=0,\quad \text{defining}\quad \beta(\alpha_s)\equiv\mu_R^2\frac{\partial\alpha_s}{\partial\mu_R^2}, \tag{2.4}$$

and solving it using treating the coupling constant in perturbative theory, it is possible to write the expansion

$$\beta(\alpha_s)=-\beta_0\alpha_s\left(1+\beta_1\alpha_s+\beta_2\alpha_s^2+\mathcal{O}(\alpha_s^3)\right)\ , \tag{2.5}$$

which at lowest order gives

$$\alpha_s(Q^2)=\frac{\alpha_s(\mu_R^2)}{1+\beta_0\alpha_s(\mu_R^2)\log Q^2/\mu_R^2},\quad \text{with}\quad \beta_0=(11C_A-4n_fT_R)/(12\pi). \tag{2.6}$$

The constants C_A and T_R arising in the beta function expansion 2.6 can be computed from the structure functions of $SU(3)$: $f_{ACD}f_{BCD}=C_A\delta_{AB}$ and $t^A_{ij}t^B_{ij}=T_R\delta_{AB}$. $C_A=N_C=3$ is the colour factor associated with a gluon emission off a gluon - N_C is the number of colours in the theory, based on the group $SU(N_C)$; $C_F\delta_{ik}=t^A_{ij}t^A_{jk}$, $C_F=(N_C^2-1)/(2N_C)=4/3$ related to gluon emission off a quark. n_f is the number of active quark flavours, to be chosen depending on the energy-scale at which a process takes place. It is possible to rewrite the coupling constant in terms of a more physical quantity, the Λ_{QCD}

$$\alpha_s=\frac{1}{\beta_0\log Q^2/\Lambda^2_{\text{QCD}}}\ , \tag{2.7}$$

which at lowest order appear as a Landau pole. The Λ_{QCD}, being a dimensionful parameter, roughly separates the regime in which QCD can be treated through perturbation theory, to the region of the phase space in which confinement is responsible for the emergence of the hadrons. QCD has stood a long list of measurements over the years, proving itself as a good candidate as theory of the strong interactions. In fig. 2.1 we report as an example the measurement of the strong coupling, that perhaps summarises best this hypothesis.

2.1.2. The cross section

The rate at which a process happens

$$R(s)=\sigma(s)\mathcal{L} \tag{2.8}$$

is proportional to the *cross section*, $\sigma(s)$, and the *luminosity* $\mathcal{L}$. Here $s=(p_1+p_2)^2$ is the Mandelstam variable s. The Large Hadron Collider is in its Run 2 phase, where proton-proton collisions occur at a centre-of-mass energy at $\sqrt{s}=13$ TeV. The luminosity is proportional to the number of particles passing each other per unit time through unit transverse area at the interaction point, and is a parameter related to the design of the collider. The full expression reads

$$L=\frac{f}{\pi}\frac{N_pN_{\bar{p}}}{n_b}\frac{\gamma}{\sqrt{\beta_x\beta_yE_xE_y}}\ , \tag{2.9}$$

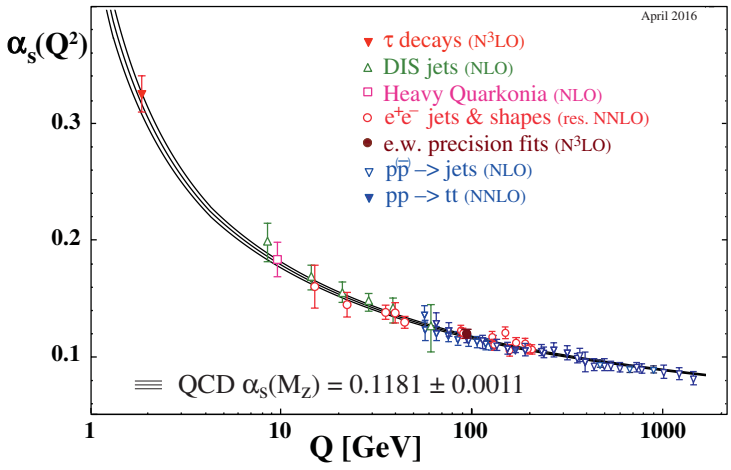

Figure 2.1.: Summary of strong coupling, α_s, measurements as function of the energy scale Q^2. Within the brackets it is indicated the order in the α_s perturbative expansion employed in the calculation. Figure is taken from [27].

where f is the revolution frequency, n is the number of bunches, and N_i is the number of particles (in our case proton and anti-proton); γ is the relativistic factor, and β_i, E_i are respectively the betatron oscillation and the transverse emittance of the beams. The theory understanding is instead fully comprised in the cross section. Experiments like CMS and ATLAS at the LHC measure physical observables and inclusive cross section rates. Cross sections are computed making use of theory models, as perturbative QCD (pQCD), and more in general the full Standard Model theory, or any of its extensions.

In pQCD calculations, we can derive expressions for our building blocks in the theory, *i.e.* quarks and gluons, but not for the physically observed colourless hadrons. In order to directly compare theory predictions with experimental data as collected at colliders, we need to take into account also non-perturbative effects, as we do not have a complete knowledge of how quarks and gluons interact within a hadron. The corner stone of this reasoning is that the hard subprocess occurs at high energies and the interaction can be separated from low-energy - $Q^2 < \Lambda^2_{QCD}$ - phenomena. Therefore, the total cross section for a general process of two scattering hadrons can be written in a *factorised* form. A formal proof of the factorisation property at high energies can be given in the context of operator product expansion (OPE) or within the mass-singularity method [28–30]. The full cross section for the collision between A and B, with final state particles f, is written

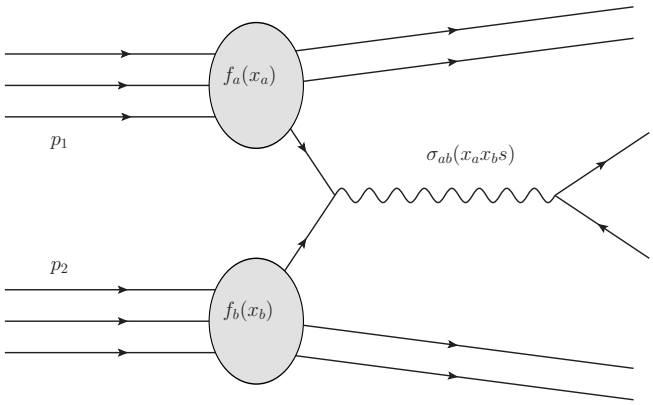

Figure 2.2.: A pictorial representation of a hadron-hadron scattering. $s = (p_1 + p_2)^2$ is the center of mass energy at which the two hadron scatter: in this case 2 partons are chosen according to their PDFs, and thus the partonic cross section $\sigma_a(x_a x_b s)$ is computed.

therefore as

$$\sigma(s)_{\mathrm{AB}\to\mathrm{f}} = \sum_{a,b} \int_0^1 \mathrm{d}x_a \int_0^1 \mathrm{d}x_b f_a(x_a, \mu_F^2) f_b(x_b, \mu_F^2) \sigma_{ab\to f}(Q^2 \equiv x_a x_b s). \tag{2.10}$$

Following Feynman's reasoning [31], a high-energy interaction between two hadrons has to be regarded as an interaction between their components, which are the *partons*. These components carry a fraction of the total momentum of the colliding hadrons. This model is very useful in describing high-energy interactions: in eq. 2.10 we define the probability density functions (PDF) f_a and f_b that exactly describe the probability to find a quark inside a hadron with longitudinal momentum fraction x_i and energy Q^2. μ_F^2 is the *factorisation* scale, describing in some way the separation between perturbative and non-perturbative regimes in the PDF. A pictorial representation for a general process is depicted in fig. 2.2. The PDF is completely independent of the underlying hard subprocess, meaning universal, depending on the hadron involved in the scattering only, and thus it could be experimentally measured in other processes, at lower energies. The differential partonic cross section is expressed through the Fermi Golden Rule,

$$\mathrm{d}\sigma_{ab\to f}(Q^2) = \frac{(2\pi)^4 \delta^4 (p_a + p_b - p_\mathrm{f})}{4\left[(p_a \cdot p_b)^2 - m_a^2 m_b^2\right]^{1/2}} |\mathcal{M}_{ab\to f}|^2 \prod_{j=1}^{n_f} \frac{\mathrm{d}^3 p_j}{(2\pi)^3 2E_j} S\,, \tag{2.11}$$

as usual in Quantum Field Theory. $\mathcal{M}$ is the amplitude of the process, which is derived directly from the Feynman rules. The product over the 3-momenta of the final-state particles accounts for the *phase-space*, encoding all the kinematics of the process. The denominator accounts for the *flux* of incoming particles in the scattering. $S = \prod_i^{n_\mathrm{identical}} 1/i!$ accounts for a symmetry factor in case of identical particles in the final state. For a given

process, AB $\to$ f, the partonic cross section sums over all possible initial states. For example, the $pp \to t\bar{t}\,X$ is given by the sum of all possible partonic scattering. At a hadron collider like the LHC, the detectors are cylindrical and cover the beam line up to certain values for the longitudinal angle θ. Measuring the position and the magnitude of the energy deposits in the detectors,the reconstruction of the energy and momentum p_f the particles is possible. The beam line is identified with the z-axis, and given that the protons center of mass does not coincide with that of the partons colliding, usually variables (or combinations of them) invariant under Lorentz boost along it are employed. One simple example is the transverse momentum p_T

$$p_T = \sqrt{p_x^2 + p_y^2}. \tag{2.12}$$

Rapidity and pseudo-rapidity are defined as

$$y = \frac{1}{2}\log\frac{E + p_z}{E - p_z} \qquad \eta = \frac{1}{2}\log\frac{1+\cos\theta}{1-\cos\theta} = \log\cot\theta/2; \tag{2.13}$$

differences of these two variables are invariant under Lorentz boost along the z-axis, in both laboratory and rest frames, and they are in direct correspondence with the scattering polar angle θ. Of course the azimuthal angle ϕ is itself defined as invariant under longitudinal boost. From these basic variables one can construct observables better characterising the events. It is possible to measure the differential cross sections with respect to these observables, for example $\mathrm{d}\sigma/\mathrm{d}p_T$, $\mathrm{d}\sigma/\mathrm{d}\eta$.

Having defined the coordinates of the system, we can already start to discuss how actual calculations take place. Due to the high dimensionality of any meaningful scattering process ($3n-4$, given n partons in the final state; the -4 factor comes from the momentum-conservation relation), the evaluation of eq. 2.11 is not a trivial procedure. Due to our incapability of getting precise results at non-perturbative energies, PDFs are extracted from experimental data, *e.g.* Deep Inelastic Scattering collisions, data from the Tevatron ($p\bar{p}$ collisions), as well as LHC runs. In addition, the factorised form of the final cross section, eq. 2.10, requires an adequate way to convolute the PDFs and the partonic cross sections. Monte Carlo methods provide an excellent way to solve these puzzling issues. A natural way of generating actual events, *i.e.* momenta according to the respective differential cross section probability, comes directly with the Monte Carlo algorithm itself.

Outcomes from a Relativistic Quantum Field Theory have to be interpreted as well in a probabilistic way. A general observable is constructed as a function of the final momenta,

$$\mathcal{O} = \int \mathrm{d}\Phi(p_1,\ldots,p_n)\frac{|\mathcal{M}|^2}{8I(s)}\Theta(O,p_1,\ldots,p_n), \tag{2.14}$$

where $\mathrm{d}\Phi(p_1,\ldots,p_n)$ denotes the differential phase space and $I(s)$ the flux factor, which is defined in eq. 2.10. The integration is performed using Monte Carlo methods: the integral in 2.14 is evaluated generating a large number of phase-space points. Every generated point comes with a *weight*; these points and weights are stored, and thus a

general expectation value, that is exactly the differential cross section, can be generated in the following way

$$\langle \mathcal{O} \rangle = \frac{1}{N} \sum_i w^i \left(\Phi(p_{i,1}, \ldots, p_{i,n}) \right) \mathcal{O} \left(\Phi(p_{i,1}, \ldots, p_{i,n}) \right), \tag{2.15}$$

where N is the total number of points generated. Eq. 2.15 is a very general statement: currently there are several different software implementations for generating pseudo-events for high-energy scattering at colliders. Many Monte Carlo event generators have been developed in the last 20 years, we cite here three of them, which are defined to be multi-purpose, as they cover several aspects of the process simulation at colliders, HERWIG [32], PYTHIA [33] and SHERPA [34]. The current work has been mainly developed within the SHERPA framework, and the present work focuses on this particular generator.

2.1.3. Fixed-order calculations

The prescription for computing meaningful physical observables has mostly become standardised. We focus for the first two chapters on the Standard Model theory, comprising the QCD Lagrangian and the electroweak one, $\mathcal{L}_{\text{EW}}$, based on the $SU(2) \times U(1)$ symmetry group:

$$\mathcal{L}_{\text{EW}} = -\frac{1}{4} \left(W_{i,\mu\nu} W^{i,\mu\nu} + B_{\mu\nu} B^{\mu\nu} \right) + \bar{\Psi}_{q,i} \not{D}_\mu \Psi_{q,j} + \tag{2.16}$$

$$+ |D_\mu \phi|^2 + \mu^2 \phi^\dagger \phi - \lambda (\phi^\dagger \phi)^2 - y_q \bar{\Psi}_{q,L} \phi \Psi_{q,R}. \tag{2.17}$$

The covariant derivative is defined as $D_\mu = \partial_\mu \delta_{ij} + i g_{\text{EW}} T^a W^{a,\mu}_{ij} + Y \delta_{ij} g'_{\text{EW}} B^\mu$, i and j run with the $SU(2)$ fundamental representation, meaning that the fields $\Psi_{q,j}$ are $SU(2)$ doublets. We stress here the fact that Ψ in this case contains also the leptons flavour families, in addition to the three composed of quarks. W_μ and B_μ are respectively the boson fields associated to the $SU(2)$ adjoint and the U(1) symmetries, and $W_{i,\mu\nu}$ and $B_{\mu\nu}$ their field-strengths. The scalar field , ϕ, acquires a Vacuum Expectation Value VEV v that triggers the spontaneous symmetry breaking at the core of the Higgs mechanism. It is defined in unitary gauge as $\phi^{\text{T}} = \begin{pmatrix} 0 & (h+v)/\sqrt{2} \end{pmatrix}$, where h is the local fluctuation field later associated with the Higgs particle. The y_q are the Yukawa couplings with which we can write mass terms for the fermions, through the gauge invariant $\bar{\Psi}_L \Psi_R$ bilinear, where L and R represent the left and right chiral part of the doublet. In appendix A we give explicitly the representation of the γ_5 matrix. T_i are the $SU(2)$ generators, whose properties are exposed in app. A. Finally we have the full Lagrangian $\mathcal{L}_{\text{SM}} = \mathcal{L}_{\text{QCD}} + \mathcal{L}_{\text{EW}}$, with which we can generate predictions.

In perturbation theory, the amplitude, and thus the cross section, is expanded in powers of the coupling g, providing $g < 4\pi$. From the QCD Lagrangian in eq. 2.1 and the electroweak one in eq. 2.16, the Feynman rules are derived and employed to compute the amplitudes for any process within the Standard Model. This is a fully general procedure that could be extended to any operator appearing in a Lagrangian, for example for arbitrary *beyond* Standard Model theories. The order of a general diagram

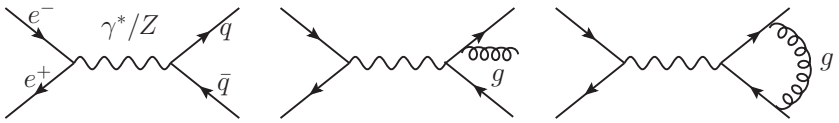

Figure 2.3.: Main Feynman diagrams contributing to the process $e^+e^- \to q\bar{q}$. The left amplitude is LO order accurate, that is $\mathcal{O}(\alpha^2)$; the center and right diagrams contribute to the NLO amplitude, $\mathcal{O}(\alpha^2\alpha_s)$

is equivalent to the number of vertices appearing in the amplitude. For a general process $p_a p_b \to p_1 \dots p_n$ the $n-order$ amplitude reads

$$\mathcal{M}(p_a, p_b; p_1, \dots, p_n) = \underbrace{g\mathcal{A}_1}_{\text{LO}} + \underbrace{g^2\mathcal{A}_2}_{\text{NLO}} + \dots + \mathcal{O}(g^n). \tag{2.18}$$

A basic calculation in pQCD is $e^+e^- \to q\bar{q}$; we want to recall it here, as it is preparatory to the rest of the present work. In fig. 2.3 the diagram topologies contributing to the LO and NLO amplitudes for this process are depicted. The LO cross section arising from the left diagrams reads, at order $\mathcal{O}(\alpha^2)$ in the electromagnetic coupling,

$$\sigma_{\text{LO}} = \frac{4\pi\alpha^2}{3s} Q_f^2 \,, \tag{2.19}$$

where Q_f is the charge of the quark, labeled by the flavour index f. The central and right diagrams constitute the perturbative correction at first order in the strong coupling. Both contributions need to be carefully discussed. The one-loop virtual correction contains ultraviolet divergences, which need to be handled carefully. This contribution contains also infrared divergences, which are embedded in the vertex correction. There are also infrared divergences in the real emission diagram, the central one in fig. 2.3. Looking carefully at the matrix element for the real-emission diagram only,

$$\sigma_{q\bar{q}g} = \sigma_{\text{LO}} 3 \sum_q Q_q^2 \int_0^1 \mathrm{d}x_1 \int_0^1 \mathrm{d}x_2 C_F \frac{\alpha_s}{2\pi} \frac{x_1^2 + x_2^2}{(1-x_1)(1-x_2)} \,, \text{with } x_i = 2E_{q_i}/\sqrt{s}. \tag{2.20}$$

The terms in the denominator diverge clearly; rewriting $1 - x_1 = 2p_q p_g = 2E_q E_g(1 - \cos\theta_{qg})$ it is simple to check that there is a *soft* pole, arising from $E_g \to 0$, and a *collinear* one, $\theta_{qg} \to 0$. We have to regulate these divergences, typically introducing an arbitrary cutoff ϵ in the momentum fraction x_i, and picking afterwards the limit $\epsilon \to 0$. Computing the total cross section, summing up the virtual and real contributions, $\sigma = \sigma_{\text{R}} + \sigma_{\text{V}}$, these divergences cancel out and the resulting cross section is the following one

$$\sigma_{\text{NLO}} = \sigma_{\text{LO}} 3 \sum_q Q_q^2 \frac{3\alpha_s}{4\pi}. \tag{2.21}$$

The cancellation of infrared divergences is a general result, proved by theorems from Kinoshita, Lee and Nauenberg [35,36], that generalise results valid in Quantum Electrodynamics [37].

Soft and collinear divergences appear almost everywhere in pQCD calculations, and from an experimental and physical point of view they necessitate cautious discussion. Experimentally, no detector can resolve a gluon emission at very small angle, or arbitrarily soft energy. This sums up to the fact that we do not observe directly coloured particles in nature, but just their colourless bound states. Therefore, in the PDFs there is a dependence on the factorisation scale μ_F^2: soft emissions below this scale are not considered part of the hard subprocess, but rather in the hadron PDF; collinear ones, belonging to both long and short range interactions, are properly treated through a running procedure. In any case, the dependence of the PDF on μ_F^2 is unphysical. In analogy to the dependence on the renormalisation scale, μ_R^2, there is a running equation for the parton distribution, describing its dependence on the μ_F^2 scale, which was first derived by Altarelli and Parisi [38], later taking the name of DGLAP equations, thanks to contributions from Dokshitzer, Gribov and Lipatov [39, 40]. The parton distribution functions obey the following integro-differential evolution equation:

$$\frac{\partial f(x,Q^2)}{\partial \log Q^2} = \frac{\alpha_s}{2\pi}\int_x^1 \frac{\mathrm{d}\xi}{\xi} f(\xi,Q^2) P\left(x/\xi\right). \tag{2.22}$$

In the equation x is the usual fraction of longitudinal momentum, Q^2 is the scale at which the process takes place. This equation allows one to run the parton distribution function from the scale of the scattering, Q^2, down to the scale where non-perturbative effects happen. The DGLAP equations include the introduction of the *splitting* kernels $P(x)$, which have to be interpreted in a probabilistic way. These splitting functions denote the probability of finding a parton a inside another parton b with momentum fraction x of the parent parton momentum. Due to the characterisation in terms of subsequent emission of a parton from another, it is straightforward to compute as expansion in the coupling α_s, as every emission carries a power of the strong coupling constant. Given the possible combinations of emitted partons and emitter, we have at leading order in α_s the following kernels

$$\begin{aligned}
P_{q\to qg}(x) &= C_F\left[\frac{1+x^2}{(1-x)_+} + \frac{3}{2}\delta(1-x)\right],\\
P_{q\to gq}(x) &= P_{q\to qg}(1-x) = C_F\left[\frac{1+(1-x)^2}{x}\right],\\
P_{g\to gg}(x) &= 2C_A\left[\frac{x}{(1-x)_+} + \frac{1-x}{x} + x(1-x)\right] + \delta(1-x)\frac{11C_A - 4n_f T_R}{6},\\
P_{g\to q\bar{q}}(x) &= T_R\left[x^2 + (1-x)^2\right].
\end{aligned} \tag{2.23}$$

The prescription $(1-x)_+$ indicates the regularisation of the divergent part of the Altarelli-Parisi splitting kernels; higher orders in the strong coupling α_s could be found in refs. [41–43].

2.1.4. The emergence of jets

In high energy physics, a typical pattern observed within a collider detector is that of a jet, a narrow cone of hadrons. After the scattering the partons radiate further and ultimately cluster, forming hadron structures, which in turn decay, evolving in this way down to non-perturbative scales. At hadron colliders the most probable processes to measure - after elastic and diffractive scattering - are di-jet events, originating from simple QCD scattering of *valence* quarks in the protons. But jets can also come from further radiation of a gluon, or from hadronic decays of electroweak particles. Non-perturbative corrections happen at scales $Q^2 \sim \Lambda^2_{\text{QCD}} \ll E$, building intrajet activity. This means they are not emissions that could be classified as a new jet, but rather they modify its internal structure. This phenomenon motivates the idea for the concept of local parton-hadron duality, *i.e.* the fact that we can describe our theory in terms of partons, even though we experimentally observe colourless hadronic jets.

Jets were extensively used to prove QCD as the non-abelian gauge theory of quarks and gluons describing the strong interactions. One initial extremely important result, for example, involves 2- and 3-jet events in electron-positron colliders at the PETRA collider. This also provided an easy connection to a measurement of α_s, as a 3-jet event is interpreted as a gluon emission from a quark, directly proportional to the strong coupling. This is a typical example of *jet rates*, in particular $R_3 = \sigma_{2+1}/\sigma_2$; we will discuss these extensively in sec. 3.2. Afterwards, increasing the centre of mass energy, it was possible to measure 4 jet events, thus having a direct handle to the gluon self-coupling, establishing the non-abelian structure of the strong interactions, providing a nice confirmation of QCD as the right underlying theory for the strong interactions. Later, they were used to characterise the global geometry of the events, with the increasing usage of event-shape variables, that improve the α_s measurements and provide a good handle on pQCD properties, as we will see in sec. 3.1. These measurements and results are now standard concepts well established and known, but would have never happened without the development of jet physics and Monte Carlo generators. With colliders such as the TEVATRON and the LHC, jet machinery and tools became more and more essential for precise measurements in QCD as well as for the analyses of EW processes.

Jets are ubiquitous, so they are the soft and collinear singularities, and they affect, to some extent, almost any experimental search. From a theoretical point of view, it is then important to define appropriate observables, not prone to divergences coming from this particular QCD feature. Theory studies on jet production and definition have a long history; a first attempt to reproduce jet cross sections in perturbation theory is due to Sterman and Weinberg [44] in 1977. However, the definition of a jet is not unique, and the treatment of soft and collinear divergences is not always trivial. Following [45], we define a jet algorithm as a sequence of operations to cluster together final-state particles in a meaningful way. The parameters that define the distance among the particles and the recombination scheme for clustering form together the jet algorithm. We recall some important features jet algorithms must satisfy, already declared back in the 1990s [46]:

- simple to implement in an experimental analysis;

- simple to implement in the theoretical calculation;
- defined at any order in perturbation theory;
- yield a finite cross section at any order in perturbation theory;
- yield a cross section that is relatively insensitive to hadronisation.

The first algorithms were iterative ones, which exploit a top-down strategy, trying to find a suitable cone for energy deposits of the jets. Some of these definitions are infrared and collinear unsafe, meaning that they are too sensitive to the emission of a further soft and/or collinear parton. This leads to serious problems in reconstructing the events, as a soft/collinear emission could completely change the jet reconstruction in the events, leading to very different topologies for the same event. Hence, IR-safe sequential recombination algorithms are preferred to iterative cone algorithms. These relatively new tools follow a bottom-up approach, and they are believed to reflect in a deeper way the underlying pQCD structure of the jet. The first appearing is the JADE algorithm [47, 48]. This is infrared and collinear safe, but has a non-proper handling of soft contributions, leading to complicated logarithmic structures in higher-order calculations. We describe in the following the two algorithms most employed at the LHC: the Cambridge-Aachen and the k_t algorithms (which together form the generalised k_t algorithms).

Cambridge-Aachen algorithm

This algorithm [49,50] is extensively employed especially in jet-tagging techniques, with which electroweak heavy objects decaying to hadrons could be recognised, as we will see in chapter 3.2. The method is implemented by fixing a dimensionless variable R, and then running through the following items:

1. for any pair of particles i,j find the minimum of the distance d_{ij}

$$d_{ij} = \frac{\Delta R_{ij}^2}{R} = \frac{(y_i - y_j)^2 + (\phi_i - \phi_j)^2}{R}; \tag{2.24}$$

2. if $d_{ij} < d_{iB} = 1$, cluster the particles together (*i.e.* a new particle is defined with momentum given by the sum of the respective 4-momenta $p = p_i + p_j$); otherwise this is a final jet, and remove it from the list of particles;
3. go back to 1 until no particles are left.

k_t algorithms

This method includes two different algorithms [51], k_t and anti-k_t, parametrised by a parameter $p = 1, -1$, respectively (actually the Cambridge-Aachen algorithm falls as well in this classification, with $p = 0$). These algorithms first employed at electron-positron

colliders, and later generalised for hadron-hadron environments [52]. This generalisation has been imposed by the necessity of using longitudinally invariant variables: the total energy has been substituted with the transverse momentum variable. The hadron collider version reads:

1. for any pair of particles i,j find the minimum of the distances:

$$d_{ij} = \min\left(p_{T,i}^{2p}, p_{T,j}^{2p}\right)\frac{\Delta R_{ij}}{R^2}, \tag{2.25}$$

$$d_{iB} = p_{T,i}^{2p}, \tag{2.26}$$

2. if $d_{ij} < d_{iB}$, cluster the particles together; otherwise this is a final jet, and remove it from the list of particles;

3. go back to 1 until no particles are left.

In fig. 2.4 we can see the difference in the reconstruction with the three algorithms here described. The plots show the transverse momentum and rapidity of partons in a event, and the coloured ares describe jets reconstructed with the used algorithm.

2.1.5. CS formalism

Due to the need of treating separately divergent pieces in NLO calculations, *subtraction* algorithms have been developed to carefully treat such terms in numerical implementations as in Monte Carlo software. Various methodologies exists, *e.g.* Catani-Seymour [53], FKS [54] and antenna [55, 56] subtraction schemes. We focus here on the Catani-Seymour formalism, as it is largely employed within SHERPA.

Higher order calculations in perturbation theory are often performed for jet observables: the complicated pattern of cancellations of infrared and collinear divergences requires quantities that are insensitive to further low-momentum or small-angle emissions. Fully inclusive calculations are the simplest quantities to be computed in QCD perturbation theory, and do not require any special treatment, thanks to the fact that the cancellation of infrared divergences happens at the integrand level. In exclusive cross-sections, the complicated phase space for multi-parton configurations leads to difficulties not trivial to handle, also due to the different number of final-state particles in the real and virtual terms.

Subtraction methods treat independently real and virtual divergences, isolating them in a process-independent way, such that after the cancellation is achieved, it is possible to perform the remaining part of the calculation with any method - a Monte Carlo algorithm for example. The divergent term from both virtual and real corrections is subtracted, returning a finite, σ_{NLO}:

$$\sigma_{\mathrm{NLO}} = \int_{m+1}\left[\mathrm{d}\sigma_{\mathrm{R}} - \mathrm{d}\sigma_{\mathrm{A}}\right] + \int_{m+1}\mathrm{d}\sigma_{\mathrm{A}} + \int_{m}\mathrm{d}\sigma_{\mathrm{V}}, \tag{2.27}$$

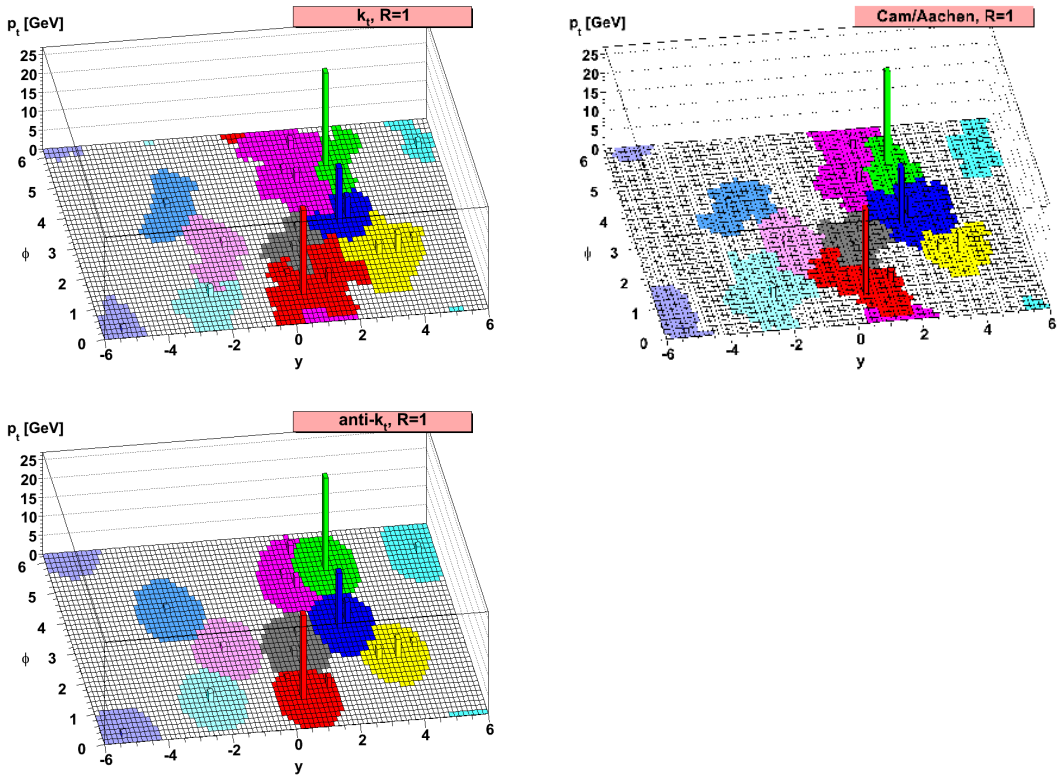

Figure 2.4.: Difference in the jet reconstruction of partons with the anti-k_T, k_T and Cambridge-Aachen algorithms. Figures taken from [52].

where σ_{A} is the diverging subtraction term. Here m is the number of particles in the final state for the LO process, and $m+1$ contains the real emission. We want to stress that the real emission piece belongs to a phase-space with different dimensionality from that of the virtual correction. Thus, for the purposes of the Monte Carlo integration, the term $\int_{m+1} \mathrm{d}\sigma_{\mathrm{A}}$ needs to be integrated over its additional 1-particle phase space, such that it cancels out the divergent part of the virtual correction, giving

$$\sigma_{\mathrm{NLO}} = \int_{m+1} [\mathrm{d}\sigma_{\mathrm{R}} - \mathrm{d}\sigma_{\mathrm{A}}] + \int_{m} \left[\mathrm{d}\sigma_{\mathrm{V}} + \int_{1} \mathrm{d}\sigma_{\mathrm{A}}\right]. \tag{2.28}$$

The Born cross section we are looking at is of the type

$$\mathrm{d}\sigma^{\mathrm{B}} = \sum_{m} \mathrm{d}\phi_n(p_1, \ldots, p_n; Q) |\mathcal{M}_n(p_1, \ldots, p_n)|^2 F_J^{(n)}(p_1, \ldots, p_n)\,, \tag{2.29}$$

where $F_J^{(n)}$ encodes exactly the jet definition in the phase space, and as previously

discussed, infrared/collinear safety ask for the following constraints:

$$F_J^{(n+1)}(p_1,\dots,p_j=\lambda q,\dots,p_{n+1}) \to F_J^{(n)}(p_1,\dots,p_{n+1})\,, \qquad \text{if} \quad \lambda\to 0, \tag{2.30}$$

$$F_J^{(n+1)}(p_1,\dots,p_i,p_j,\dots,p_{n+1}) \to F_J^{(n)}(p_1,\dots,p,\dots,p_{n+1})\,, \tag{2.31}$$
$$\text{if} \quad p_i\to zp\,,\; p_j\to(1-z)p\,.$$

The presence of a universal subtraction term relies on the fact that exactly in the soft/collinear limit, the cross section for the production of an additional parton factorises, being independent of the actual hard process we are evaluating. Factorisation properties of the matrix elements can be inferred from the QED bremsstrahlung, and then generalised to QCD.

In the Catani-Seymour formalism, the subtraction term is generalisable to any process, and is written in term of dipoles:

$$\mathrm{d}\sigma_{\mathrm{A}} = \sum_{\text{dipoles}} \mathrm{d}\sigma^{\mathrm{B}} \otimes \mathrm{d}V_{\text{dipole}}, \tag{2.32}$$

where $\mathrm{d}\sigma^{\mathrm{B}}$ denotes the Born-level differential cross-section, that is the one coming from the LO order accurate matrix-element calculation. The sum over the dipoles is needed since there are various kinematic configurations that mimic the additional emission in $\mathrm{d}\sigma^{\mathrm{R}}$. In this way $\mathrm{d}\sigma^{\mathrm{A}}$ is a local counter-pole for the real emission matrix element. Dipole configurations are shown in fig. 2.5

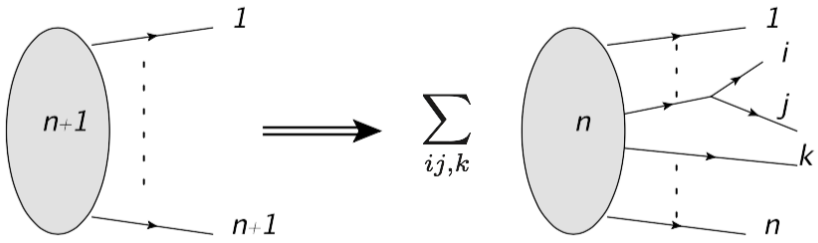

Figure 2.5.: Dipole factorisation: a general $n+1$-parton matrix element is translated into a sum over n-parton diagrams with an emission from a dipole.

The factorisation property could be written as

$$|\mathcal{M}_{n+1}|^2 \to |\mathcal{M}_n|^2 \otimes \sum_{ij,k} V_{ij,k}. \tag{2.33}$$

$\boldsymbol{V}_{ij,k}$ is the dipole, depending on the partons i, j and k. Let us discuss briefly the appearance and factorisation of collinear and soft singularities. The Catani-Seymour formalism defines one parton as the *emitter*, from which an *emitted* particle is radiated;

the *spectator* is needed in order to properly treat the recoil after the emission. In the soft limit we parametrise the 4-momentum p_j^μ of a final-state gluon as

$$p_j^\mu = \lambda q^\mu \, , \; \lambda \to 0 \, , \tag{2.34}$$

where λ is a scale parameter and q^μ and arbitrary 4-vector. The matrix element for a real emission reads

$$|\mathcal{M}|^2_{n+1} \propto \frac{\alpha_s}{\lambda^2} {}_n\langle n+1|\boldsymbol{J}^\mu(q)^\dagger \boldsymbol{J}_\mu(q)|n+1\rangle_n, \tag{2.35}$$

where the $|n\rangle$ is a vector in colour and helicity space; the $\boldsymbol{J}^\mu(q)$ is the *eikonal* current:

$$\boldsymbol{J}^\mu(q) \sim \sum_i \boldsymbol{T}_i \frac{p_i^\mu}{p_i \cdot q} + \boldsymbol{T}_a \frac{p_a^\mu}{p_a \cdot q} \, , \tag{2.36}$$

where the $\boldsymbol{T}$ are the colour generators associated to the charges in the dipole. Eq. 2.36 is not an exact factorisation, since the eikonal current in eq. 2.36 leads to *colour correlations*, and outside the strict limit $\lambda = 0$ the phase space does not factorise exactly. The collinear singularities can be disentangled using the identity

$$\frac{p_k p_i}{(p_k q)(p_i q)} = \frac{p_k p_i}{p_k \cdot q (p_i + p_k) \cdot q} + \frac{p_k p_i}{p_i \cdot q (p_i + p_k) \cdot q}, \tag{2.37}$$

we finally find a more suitable form for our purpose:

$$|\mathcal{M}_{n+1}|^2 = \frac{1}{p_i q} {}_n\langle n+1| \frac{\boldsymbol{T}_k \boldsymbol{T}_i p_k p_i}{(p_i + p_k) q} |n+1\rangle_n + \dots \, , \tag{2.38}$$

where the dots indicate for similar contributions involving other combinations of partons. We highlight that, for the sake of simplicity, we expose here only the final-state final-state case, in which both the spectator and the emitter belong to the final-state particles. Obvious generalisation to initial-state partons involves the PDF distribution.

In order to present the collinear behaviour, we now rewrite the momenta of the involved particles with the help of *Sudakov* variables

$$p_i^\mu = z p^\mu + k_T^\mu - \frac{k_T^2}{z} \frac{n^\mu}{2p \cdot n} \, , \quad p_j^\mu = (1-z) p^\mu - k_T^\mu - \frac{k_T^2}{1-z} \frac{n^\mu}{2p \cdot n} \, , \tag{2.39}$$

where k_T is the transverse momentum of the emitted particle with respect to the dipole, n^μ is an auxiliary light-like vector, specifying the direction in which $k_T \to 0$. Through this adjustment we can approximate the matrix element, neglecting terms $\mathcal{O}(1/k_T^2)$, as

$$|\mathcal{M}_{n+1}|^2 \propto \frac{1}{p_i p_j} {}_n\langle n+1|\hat{P}_{(ij),i}(z, k_T)|n+1\rangle_n. \tag{2.40}$$

From eqs. 2.38, 2.40 we write directly the final, factorised form of the squared matrix element for the production of an additional parton, valid both in the collinear and soft

enhanced regions; this is achieved through the dipole definition:

$$ {}_{n+1}\langle n+1|n+1\rangle_{n+1} = \sum_{k\neq i,j} \mathcal{D}_{ij,k}(p_1,\dots,p_{n+1}) + \text{non-singular terms}\,, \tag{2.41} $$

$$ \mathcal{D}_{ij,k}(p_1,\dots,p_{n+1}) = -\frac{1}{2p_i\cdot p_j}\times \tag{2.42} $$

$$ {}_n\langle 1,\dots,\tilde{ij},\dots,\tilde{k},\dots,n+1|\frac{\boldsymbol{T}_k\cdot\boldsymbol{T}_{ij}}{\boldsymbol{T}_{ij}^2}\boldsymbol{V}_{ij,k}|1,\dots,\tilde{ij},\dots,\tilde{k},\dots,n+1\rangle_n. $$

For a proper treatment of recoil effects, partons i and j in the full $n+1$ matrix element have been replaced by the $\tilde{ij}$ and $\tilde{k}$, respectively the emitter and the spectator, fulfilling the following relations:

$$ \tilde{p}_k^\mu = \frac{1}{1-y_{ij,k}}p_k^\mu\,, \quad \tilde{p}_{ij}^\mu = p_i^\mu + p_j^\mu - \frac{y_{ij,k}}{1-y_{ij,k}}p_k^\mu, \tag{2.43} $$

with

$$ y_{ij,k} = \frac{p_ip_j}{p_ip_j + p_jp_k + p_ip_k}. \tag{2.44} $$

The splitting matrices $\boldsymbol{V}_{ij,k}$, closely related to the Altarelli-Parisi splitting kernels, are defined in the helicity space and depend on the kinematic variables

$$ \tilde{z}_i = 1-\tilde{z}_j = \frac{p_ip_k}{p_jp_k+p_ip_k} = \frac{p_i\tilde{p}_k}{\tilde{p}_{ij}p_k}; \tag{2.45} $$

the $\boldsymbol{T}_i$ are the colour charges, depending on the colour algebra $SU(3)$. It is easy to prove that the correct soft and collinear limits are reached when

$$ y_{ij,k}\to 0\,,\ \tilde{z}_i\to 1\,,\ \tilde{z}_j\to 0 \qquad \text{soft}, \tag{2.46} $$

$$ y_{ij,k}\to \frac{-k_T^2}{2z(1-z)pp_k}\,,\tilde{z}_i = 1-\tilde{z}_j\to z \qquad \text{collinear}. \tag{2.47} $$

Having parametrised in a fully general way the collinear and infrared singularities of a further emission of coloured parton off an ensemble of quarks and gluons, it is possible to define the diverging counter term appearing in eq. 2.32 in terms of the sum over the dipoles $\sum_{k\neq i,j}\mathcal{D}_{ij,k}$

$$ \mathrm{d}\sigma^{\mathrm{A}} = \sum_{n+1}\mathrm{d}\phi_{n+1}\sum_{\text{pairs};i,j}\sum_{k\neq i,j}\mathcal{D}_{ij,k}F_J^{(n)}. \tag{2.48} $$

2.1.6. All order calculations

So far, we have discussed fixed-order calculations, whose technology has been intensively developed over the last 20 years. Nevertheless, the truncation of the perturbative series leads to unpleasant consequences: as we have seen there are regions in the phase-space that are enhanced due to collinear and soft emissions. First of all a miscancellation of

soft and collinear singularities in the higher orders in the series can happen for certain observables, leading to unphysical enhancements. This depends on the fact that there could be regions of the phase space in which the higher-order corrections are of the same magnitude of the calculation at fixed order.

To better characterise this behaviour, we rewrite the emission pattern for an additional parton in the soft and collinear limit in terms of the Catani-Seymour splitting variables, k_T and z:

$$\mathrm{d}\sigma_1 \sim \mathrm{d}\sigma_0 \int_{k_0^2}^{k^2} \frac{\mathrm{d}\kappa_t^2}{\kappa_t^2} \frac{\alpha_s(\kappa_t^2)}{\pi} \int_{z_{\min}}^{z_{\max}} \frac{\mathrm{d}z}{z} P_{ij}(z). \tag{2.49}$$

Using the definition of the splitting kernels and the α_s expression in eq. 2.6, we can straightforwardly integrate and a *double logarithmic* pattern is evident,

$$\mathrm{d}\sigma_1 \sim \mathrm{d}\sigma_0 \log \frac{k_T^2}{k_0^2} \log \frac{1 - z_{\max}}{1 - z_{\min}}. \tag{2.50}$$

This pattern gives enhancements for every kind of observable sensitive to soft or collinear emissions.

In general, large logarithms are ubiquitous in high-energy particle physics, and they are not only originating from soft and collinear emissions: whenever two different scales exist in a process, it is much likely that some variable is plagued by a logarithmic enhancement. Over the years two methods have established for properly treating these kind of issues, *parton showers* and *resummation*. These two methods address respectively numerically and analytically the problem of getting all-order results, providing meaningful distributions for the desired process.

2.1.7. Parton showers

The aim of a parton shower is to evolve incoming and outgoing strongly interacting partons from a high virtuality, $Q^2 \gg \Lambda^2_{\mathrm{QCD}}$ down to a scale $Q^2 \sim \Lambda^2_{\mathrm{QCD}}$ where perturbative results are no more valid. This evolution is performed according to the DGLAP equations 2.22. A typical parton shower associates a probability for its possible branching to every parton in the initial/final state, or for no branching at all, and then the state is evolved generating random successions from this probability distribution. This operation is performed for every subsequent *daughter* parton, and so on, down to the non-perturbative cutoff scale. Although being a numerical implementation, parton showers correctly describe the leading logarithm behaviour, thanks to the correct treatment of collinear emissions coming from the DGLAP evolution. Parton showers make use of the *ordering* of the evolution variable, which allows the treatment of soft emissions. This effect is clearly seen when describing the evolution through the coherent branching formalism, we briefly describe here.

Coherent branching

Coherent branching essentially is a property of QCD emissions that is easily employed in a numerical implementation of a parton shower, as it simply states that subsequent

emissions have to happen inside a cone with opening angle determined by the dipole emitting the daughter parton [57–60]. The argument is present also in electromagnetic theory, known as *Chudakov* effect.

If a parton is radiated from a QCD dipole with inverse wavelength larger than the transverse momentum between the original parton and its colour partner, the radiated quanta can not resolve the individual colour charge of the radiating parton. In this case, radiation can be emitted only with a precise colour charge. Following ref. [41], we recast the general matrix element for an additional emission in terms of the *antenna* pattern

$$\mathrm{d}\sigma_{n+1} = \mathrm{d}\sigma_n \frac{\mathrm{d}\omega}{\omega}\frac{\mathrm{d}\Omega}{2\pi}\frac{\alpha_s}{2\pi}\sum_{i,j} C_{ij} W_{ij}\,, \tag{2.51}$$

$$W_{ij} = \frac{\omega^2 p_i \cdot p_j}{p_i \cdot q\, p_j \cdot q} = \frac{1-\cos\theta_{ij}}{(1-\cos\theta_{iq})(1-\cos\theta_{jq})}\,. \tag{2.52}$$

C_{ij} is a colour factor dependent on the emission pattern, $\mathrm{d}\Omega$ the solid angle for the emission and ω the energy of the emitted gluon. p_i and p_j are the momenta of the partons in the process, and θ_{ij} the angle between the two, and q is the momentum of the emitted gluon. For simplicity we are considering all the partons as massless. The antenna pattern in eq. 2.52 can be separated, thus highlighting the two collinear singularities:

$$W_{ij} = W_{ij,i} + W_{ij,j}\,, \tag{2.53}$$

$$W_{ij,i} = \frac{1}{2}\left(W_{ij} + \frac{1}{1-\cos\theta_{iq}} - \frac{1}{1-\cos\theta_{jq}}\right). \tag{2.54}$$

It is easy to see that after azimuthal integration

$$\begin{aligned}\int_0^{2\pi}\frac{\mathrm{d}\phi_{iq}}{2\pi} W_{ij,i} &= \frac{1}{1-\cos\theta_{iq}} \quad \text{if} \quad \theta_{iq} < \theta_{ij} \\ &= 0 \quad \text{otherwise.}\end{aligned} \tag{2.55}$$

Analogous consideration applies for the other antenna singularity $W_{ij,j}$. In QCD a careful treatment of the colour charge leads to different radiation patterns, depending on the actual emitting dipoles, differentiating the effect from the one happening in QED. For the case of two quarks $q\bar{q}$ forming a colour singlet, we have $C_{ij} = \boldsymbol{T}_i^2 = \boldsymbol{T}_j^2$, with $\boldsymbol{T}^2 = C_F = 4/3$. For a colour singlet with two quarks and a gluon, $i\,, j\,, k$ with $\boldsymbol{T}_l = \boldsymbol{T_i} + \boldsymbol{T_j} = -\boldsymbol{T}_k$, the expression for the emission of a gluon n is more complicated:

$$\begin{aligned}W = \boldsymbol{T}_i^2(W_{ij,i} + \tilde{W}_{jk,i} - \tilde{W}_{ik,j}) + \boldsymbol{T}_j^2(W_{ij,i} + \tilde{W}_{ik,j} - \tilde{W}_{jk,i}) + \\ + \boldsymbol{T}_k^2(\tilde{W}_{jk,i} + \tilde{W}_{ik,j} + \frac{1}{2}W_{ik,k} + \frac{1}{2}W_{jk,k})\,,\end{aligned} \tag{2.56}$$

$$\text{with}\;\; \tilde{W}_{jk,i} = \frac{1}{2}(W_{ik,i} - W_{ij,i}). \tag{2.57}$$

In the limit of i and j collinear, we can approximate $W_{ik,k} \sim W_{jk,k} \sim W_{ik,k}$ and $\tilde{W}_{jk,i} \sim \tilde{W}_{ik,j} \sim \frac{1}{2}\tilde{W}_{lk,ij}$, defining

$$\tilde{W}_{lk,ij} = W_{lk,l}\Theta(\theta_{ln} - \theta_{ij}). \tag{2.58}$$

Thus, the antenna pattern is

$$\boldsymbol{T}_i^2 W_{ij,i} + \boldsymbol{T}_j^2 W_{ij,j} + \boldsymbol{T}_k^2 W_{lk,k} + \boldsymbol{T}_l^2 \tilde{W}_{lk,ij}. \tag{2.59}$$

From eq. 2.59 we interpret that each parton i,j and k emits according to its colour charge squared. Incoherent contributions are suppressed inside the half-angle θ_{ij}, while at larger angles they emit proportional to $\boldsymbol{T}_l^2$. It can be proved [39] through the analysis of the Feynman diagrams contributing to the emission that the dominant contributions come from the so-called *ladder* diagram, as depicted in fig. 2.6, with strongly ordered branchings.

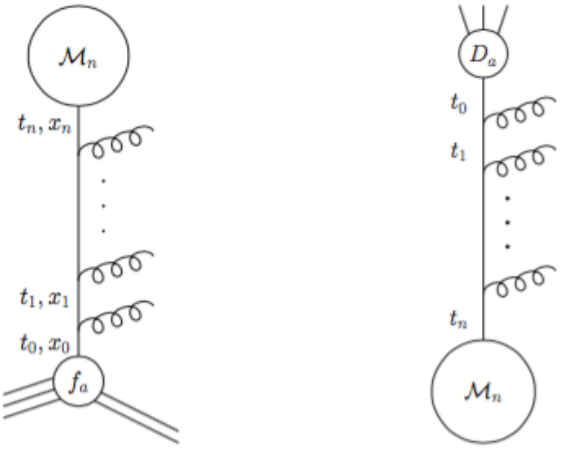

Figure 2.6.: Example of ladder diagrams containing only gluon emissions. The representation on the left shows the evolution of an initial state: from the PDF f_a to the hard subprocess matrix element. On the right-hand side we have instead a final-state evolution: from the hard subprocess down to the fragmentation function where hadronisation occurs. The hard process happens at a scale $t_n \sim Q^2$, the PDF f_a and the fragmentation function D_a are both at a scale t_0, but the ordering is reversed in the two cases. Strong ordering means $t_0 < t_1 < \cdots < t_n$.

The Catani-Seymour dipole inspired shower

The Altarelli-Parisi splitting kernels in eqs. 2.23 defined with the $_+$ prescription are not directly suitable for a Monte Carlo implementation. Some adjustment is therefore needed to properly treat the singular part of the kernels and maintain the accuracy of the shower algorithm.

The unregularised splitting kernels, *i.e.* the kernels without the plus prescription, are regularised, in the parton shower, with the use of a cutoff. The singularities are

still there, as we already know these cancel in the final sum of the real and virtual contributions. The Sudakov form factor [61] is introduced: it resums the singularities below the cutoff scale

$$\Delta_i(t) \equiv \exp\left[\sum_j \int_{t_0}^{t} \frac{\mathrm{d}t'}{t'} \int_{z_{\min}}^{z_{\max}} \mathrm{d}z \frac{\alpha_s}{2\pi} P_{ji}(z)\right], \tag{2.60}$$

modifying the DGLAP equations - in the following the case of an initial state parton shower with the evolution of a PDF $f(x,t)$ - in

$$t\frac{\partial}{\partial t} f(x,t) = \int \frac{\mathrm{d}z}{z} \frac{\alpha_s}{2\pi} P(z) f(x/z,t) + \frac{f(x,t)}{\Delta(t)} t \frac{\partial}{\partial t} \Delta(t). \tag{2.61}$$

A further integration gives

$$f(x,t) = \Delta(t) f(x,t_0) + \int_{t_0}^{t} \frac{\mathrm{d}t'}{t'} \frac{\Delta(t)}{\Delta(t')} \int \frac{\mathrm{d}z}{z} \frac{\alpha_s}{2\pi} P(z) f(x/z,t'). \tag{2.62}$$

We employ here an evolution variable t, since this result is general to various algorithms. The emissions are therefore classified as *resolved* and *unresolved*: if a branching occurs, it is described by the Altarelli-Parisi kernel, where an emission below the cutoff scale results in an emission that cannot be detected, and is properly taken into account through the resummed Sudakov factor, that accounts for the virtual contribution, and is interpreted as the probability of evolving from a scale t down to a scale t_0 without any branching.

Eq. 2.62 is now suitable for a Monte Carlo implementation. The Catani-Seymour algorithm [62] employs as evolution variable the transverse momentum of the emitted parton with respect to the parent dipole k_T^2, defined as in eq. 2.39. The angular ordering constraint is translated up to subleading contributions to

$$k_{T,n}^2 > k_{T,n-1}^2 > \cdots > k_0^2\,, \tag{2.63}$$

where k_0^2 is the cutoff scale of the parton shower algorithm. Using the Catani-Seymour formalism, we can account for the same splitting structure in eq. 2.62 through the sum over the dipoles $\boldsymbol{V}_{ij,k}$. Taking, as an example, the splitting FF, with both emitter and recoiling parton in the final state, the Sudakov form factor reads

$$\begin{aligned}&\Delta_{\mathrm{FF}}(k_{T,\max}^2, k_0^2) = \\ &= \exp\left[-\sum_{ij}\sum_{k\neq ij} \frac{1}{\mathcal{N}_{ij}} \int_{k_0^2}^{k_{T,\max^2}} \frac{\mathrm{d}k_T^2}{k_T^2} \int_{z_-}^{z_+} \mathrm{d}\tilde{z}_i \frac{\alpha_s(k_T^2)}{2\pi} J(y_{ij,k}) \langle \boldsymbol{V}_{ij,k}(\tilde{z}_i, y_{ij,k})\rangle\right].\end{aligned} \tag{2.64}$$

The boundaries of the integration over the splitting kernel are

$$z_{\mp}(k_{T,\max^2}) = \frac{1}{2}\left(1 \mp \sqrt{1 - \frac{k_0^2}{k_{T,\max^2}}}\right), \tag{2.65}$$

and the Jacobian, $J(y_{ij,k}) = 1 - y_{ij,k}$, comes from the fact that we account for the singular structure of the matrix element through the Catani-Seymour variable $y_{ij,k}$. It is possible to prove that $\mathrm{d}k_T/k_T$ corresponds to $\mathrm{d}y_{ij,k}/y_{ij,k}$, at leading logarithm accuracy. It is common practice to evaluate the strong coupling α_s at the actual scale of emission, k_T^2, since this results in the proper treatment of the leading logarithms [63].

With this at hand, it is possible to depict the algorithm in these few steps

1. define the dipoles and choose a dipole configuration;
2. starting from the initial scale Q^2, generate a random number $\mathcal{R}$ and solve for k_T^2 the equation
$$\frac{\Delta(Q^2)}{\Delta(k_T^2)} = \mathcal{R}; \tag{2.66}$$
3. exit the parton-shower if $k_T^2 < k_0^2$
4. generate the momentum fraction z according to the appropriate splitting kernel $P(z)$[1]
5. update the kinematic variables for the new configuration of partons. A new parton has been emitted in this way from the dipole;
6. restart from point 1.

Point 5 and the usage of Catani-Seymour splitting variables allow for a proper treatment of recoil effects in the parton shower, as designed in SHERPA. As last remark we want to stress that in the parton shower approximation only diagrams at orders $1/N_C$ are considered. This means performing a large-N_C approximation, at the price of losing colour correlations between the partons. We perform a deeper analysis of this in chap. 3.

2.1.8. Resummation

In order to perform analyses as one would do with real data, Monte Carlo methods have been preferred over analytical calculations and then over the years the parton-shower technology has become the standard approach for the simulations of high-energy collisions. However, we have to say that an analytical approach is possible, and returns more accurate results. On the other hand, the resummation procedure is less generalisable to any kind of variable, meaning that it is highly process dependent. Nonetheless, it is preferable when looking for high precision computations. Resummation results are invaluable when one wants to extract QCD parameters, such as the strong coupling, the quark masses or parton distribution functions. Usage of resummation analytical results begun already at the HERA collider, the electron-proton collider for Deep Inelastic Scattering studies. There were performed measurements of event shape distributions [65], and were studied the existence of power corrections $1/Q$ to the perturbative series [66]

[1] in SHERPA this is accomplished through an overestimate; this simplifies the procedure because the *inverse* sampling method can be employed, as the primitive function is known.

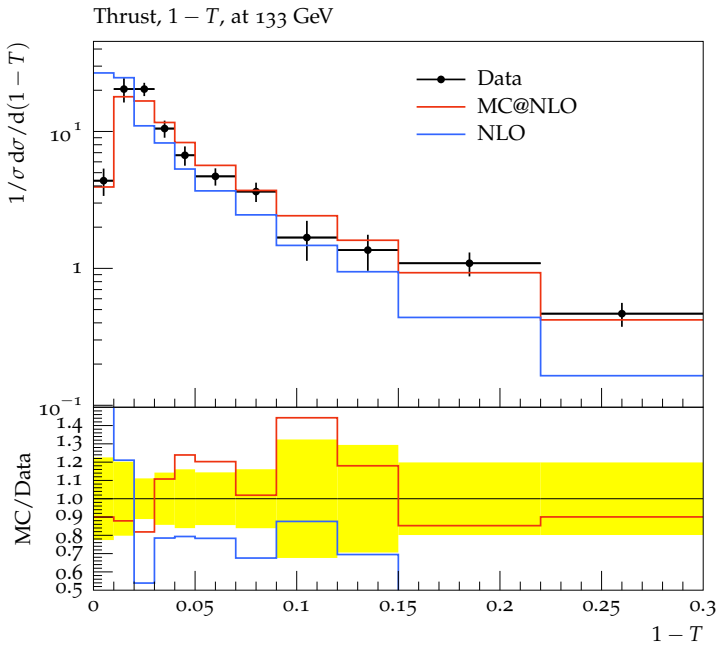

Figure 2.7.: $1-T$ thrust distribution with and without parton shower. The hard process topology is $e^+e^- \to jjj$, where j stays for any of the light quarks. The process is generated with $p_{T,j} = 0.1$ GeV in order to avoid singularities, with the purpose to enhance as much as possible the matrix element. Jets are reconstructed with the anti-k_T algorithm with $R = 0.1$. It is possible, therefore, to see how the non-showered samples, in blue, are enhanced at low values of thrust, and how the parton shower, in red, describes correctly the peak, resumming the double logs. Data points, in black, are taken from OPAL collaboration [64] at $\sqrt{s} = 133$ GeV

and non-global single logarithms [67]. Also at LEP, measurements of the jet rates and of the strong coupling have been performed through the comparison with resummed results [68]. On top of that, resummed results give a good handle to non-perturbative phenomena and therefore are employed in testing the phenomenological models.

Usually it is possible to rewrite eq. 2.18 in terms of an enhanced kinematical variable V

$$\sigma = \alpha_s c_0 \log V + \alpha_s^2 (c_1 \log^2 V + c_2 \log V) + \ldots + \mathcal{O}(\alpha_s^n \log^n V). \tag{2.67}$$

It is indeed clear that if $\log V \gg 1$ the series is not anymore convergent and one finds terms

$$\alpha_s \log V \sim 1. \tag{2.68}$$

These enhanced terms need to be resummed at all orders, thus reorganising the pertur-

bative expansion

$$\sigma = \sum_n \left(\alpha_s^n \log^{2n} V\right) a_{\mathrm{LL}} + \sum_n \left(\alpha_s^n \log^{2n-1} V\right) a_{\mathrm{NLL}} + \dots \,, \tag{2.69}$$

where the dots indicate subleading corrections and the labels LL and NLL stay for leading logarithm and next-to-leading logarithm, respectively. This improved series is valid as $\alpha_s L \lesssim 1$, in the enhanced region of the phase space.

In this work we focus only on the so-called *Sudakov* logarithms, which are those stemming from soft and collinear emissions, such as in eq. 2.49. We stress this, as depending on the type of logarithm to be resummed, the procedures differ slightly: for example there are resummation methods for threshold logarithms [69], for small-x effects in the PDFs [70,71]. Mainly two recipes for resumming Sudakov large logarithms exist, the first based on standard pQCD [72] and the second exploiting effective theory methods, Soft Collinear Effective Theory [73, 74]. All the methods rely on the factorisation properties of the phase space in the region of the enhanced behaviour; as consequence the series *exponentiate*. We now discuss the very first result of pQCD resummation, that is the NLL distribution of the thrust variable [75].

Thrust and soft-gluon resummation

Thrust, T, is a global event shape variable which characterises the geometrical distribution of the energy in the event: it is a very good handle on two jets events, in fact it reaches its maximum value in the case of dijet events, $T \to 1$. It departs from this value when the configuration of the events contains more than two jets. The definition

$$T = \max_{\boldsymbol{n}} \frac{\sum_i |\boldsymbol{p}_i \cdot \boldsymbol{n}|}{\sum_i |\boldsymbol{p}_i|} \,, \tag{2.70}$$

where $\boldsymbol{p}_i$ are the three momenta of the particles in the final state and $\boldsymbol{n}$ is an arbitrary unit vector, is suitable for electron-positron colliders. The hadron-hadron collider version is modified with longitudinal invariant observables, as usual:

$$T = \max_{\boldsymbol{n_T}} \frac{\sum_i |\boldsymbol{p}_{T,i} \cdot \boldsymbol{n}_T|}{\sum_i |\boldsymbol{p}_{T,i}|}. \tag{2.71}$$

Since this variable is maximised for the di-jet event configuration, thrust is highly sensitive to soft and collinear emissions in the region $T \to 1$ of the phase space. The perturbative expansion of the differential distribution contains terms of the form

$$A_n(T) \propto \frac{\log^{2n-1}(1-T)}{1-T} \quad \text{when} \quad T \to 1, \tag{2.72}$$

for every power n of the strong coupling constant. In addition we have to state that other difficulties are present in the perturbative prediction, which are furthermore alleviated by the resummation program, and those are a significant dependence on the renormalisation

scale μ and on hadronisation corrections. Following ref. [72], we introduce the event shape fraction for the thrust distribution

$$f(T) = \int_{1-T}^{1} \mathrm{d}T \frac{1}{\sigma} \frac{\mathrm{d}\sigma}{\mathrm{d}T}, \tag{2.73}$$

that is basically an integrated distribution, retrieving the fraction of events with value of thrust up to T. Exponentiation of this observable means that at high thrust we expect a behaviour

$$f(\tau) = C(\alpha_s) \exp\left[G(\alpha_s, \log 1/\tau)\right] + D(\alpha_s, \tau) \quad \text{with} \quad \tau = 1 - T; \tag{2.74}$$

writing $L = \log 1/\tau$ we define the functions above as

$$C(\alpha_s) = 1 + \sum_{n=1}^{\infty} C_n \bar{\alpha}^n \,, \tag{2.75}$$

$$\begin{aligned} G(\alpha_s, L) &= \sum_{n=1}^{\infty} \sum_{m=1}^{n+1} G_{nm} \bar{\alpha}^n \\ &\equiv L g_1(\alpha_s L) + g_2(\alpha_s L) + \alpha_s g_3(\alpha_s L). \end{aligned} \tag{2.76}$$

The remainder function $D(\alpha_s, \tau)$ vanishes as $\tau \to 0$, as it contains no logarithmic-enhanced terms. This expansion is valid for $\alpha_s L \lesssim 1$, that is a larger phase-space region than $\alpha_s L^2 \ll 1$.

The resummation involves the following steps: first, one has to prove the factorisation of the QCD matrix elements in the soft and collinear region is not spoiled by the particular observable one desires to resum; second, the series has to be reorganised in an exponential form. The coherent branching formalism, relying mainly on the colour coherence property described above is, is very useful for carrying out this program. It is known some variables do not exponentiate, then the factorisation and exponentiation proof has to be performed for every variables one wants to resum. This results in a big dependence of the procedure on the process and variable for which it has to be performed, rendering in this way cumbersome the automatisation of such methods.

Expanding thrust in the enhanced region of phase space we find

$$T = 1 - \frac{k^2}{s} - \frac{\bar{k}^2}{s} - \frac{2k^2\bar{k}^2}{s^2} + \dots \,, \tag{2.77}$$

with s the usual Mandelstam variable; after dividing the event into two hemispheres by the plane orthogonal to the thrust axis, k and $\bar{k}$ are the total momenta of the two different hemispheres. Proving that an emission in one hemisphere remains confined to that hemisphere until the end of the QCD evolution leads to the proper factorisation property. The higher terms are proportional to τ^2 and then they contribute to the remainder function, $D(\alpha_s, L)$. To logarithmic accuracy one finds

$$\Phi_n(\tau) = \Phi_n(k^2 + \bar{k}^2 < s) \,; \tag{2.78}$$

employing the jet mass distribution $J(k^2, s)$ at a scale s, and evolving the state through the coherent branching formalism, the event fraction can be rewritten as

$$f(\tau) = \int_0^{\tau s} \mathrm{d}k^2 \int_0^{\tau s - k^2} \mathrm{d}\bar{k}^2 J(k^2, s) J(\bar{k}^2, s). \tag{2.79}$$

Solving eq. 2.79with the help of the Laplace transform $\tilde{J}(s) = \int_0^\infty \mathrm{d}k^2 e^{-\nu k^2} J(k^2, s)$, it is possible to find the LL and NLL functions g_1 and g_2:

$$g_1(\alpha_s L) = -\frac{C_F}{\pi \beta_0^2 \alpha_s L} \left[(1 - 2\beta_0 \alpha_s L) \log(1 - 2\beta_0 \alpha_s L) - 2(1 - \beta_0 \alpha_s L) \log(1 - \beta_0 \alpha_s L) \right] , \tag{2.80}$$

$$\begin{aligned} g_2(\alpha_s L) = &-\frac{C_F \kappa}{2\pi^2 \beta_0^2} \left[2 \log(1 - 2\beta_0 \alpha_s L) - \log(1 - 2\beta_0 \alpha_s L) \right] + \\ &- \frac{3 C_F}{2\pi \beta_0} \log(1 - \beta_0 \alpha_s L) - \frac{2\gamma_E C_F}{\pi \beta_0} \left[\log(1 - \beta_0 \alpha_s L) - \log(1 - 2\beta_0 \alpha_s L) \right] + \\ &- \frac{C_F \beta_1}{\pi \beta_0^2} \left[\log(1 - 2\beta_0 \alpha_s L) - 2 \log(1 - 2\beta_0 \alpha_s L) + \right. \\ &\left. + \frac{1}{2} \log^2(1 - 2\beta_0 \alpha_s L) - \log^2(1 - \beta_0 \alpha_s L \right] + \\ &- \log \Gamma \left(1 - g_1(\alpha_s L) - \alpha_s L g_1'(\alpha_s L) \right) . \end{aligned}$$

In the above expression are present the Gamma function $\Gamma(z)$, the Euler number $\gamma_E \sim 0.5772$ and $\kappa = (201 - 9\pi^2 - 10 n_f)/18$. We can see that the LL resummation program gives back the correct high-thrust (low τ) behaviour

$$f(\tau) \sim \exp(-2\bar{\alpha}_s C_F L^2) , \tag{2.81}$$

in the limit $\alpha_s L \ll 1$. This is a typical Sudakov suppression, an effect we already encountered in the parton shower approach. At low values of thrust it can be noted that the LL resummed result is no longer reliable: this is in full agreement with the fact that the resummation is valid when $\alpha_s L \ll 1$. The thrust distribution has kinematical limits, depending on the number of jets, but the values cannot be less than 0.5 for multi-jet observables. Adding the NLL function shifts this spurious effect. In fig. 2.8, we plot the integrated thrust distribution at NLO and at NLL. The NLO distribution is divergent, as expected: the thrust variable is completely insensitive to virtual corrections, therefore terms coming from that contribution have no effect on the differential distribution. The NLL curve nicely shows the Sudakov-like structure, and the spurious terms introduced in the right side of the distribution.

2.1.9. Matching fixed and all order

Parton showers and resummation lead to an improvement of the perturbative prediction, adding all-orders effects, thus reducing the uncertainties and better predicting the shapes of the distributions - we have to note, in fact, that fixed-order calculations are important

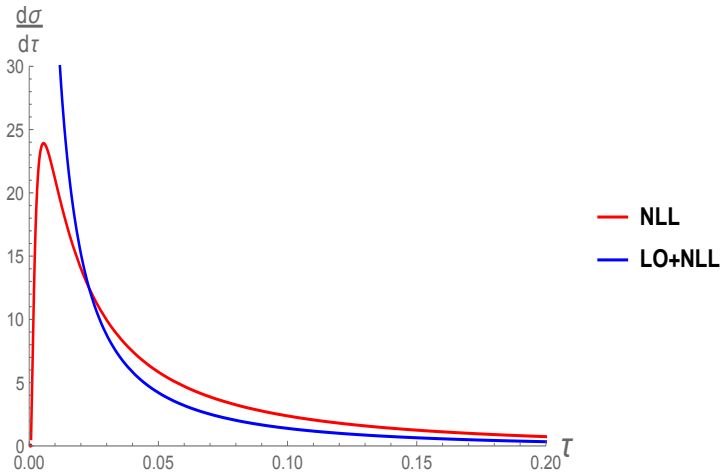

Figure 2.8.: Integrated thrust distributions for the NLO case (red) and the resummed one NLL accurate (blue). The Sudakov peak is evident in the resummed distribution, and also the fact that the resummed distribution gives results outside the kinematical limits for thrust.

for the normalisation, where all-order methods are necessary for the correct shape of the distribution. In any case both methods, and in particular parton showers, rely on several assumptions and are valid mostly in the soft and collinear limit of additional emissions. That means we better trust these results in some regions of the phase space, which are exactly those characterised by low energy emissions. Regarding the leftover phase space, it is better to employ fixed-order calculations, which better describe the hard part of the collision.

Two methods have been developed over the years: *matching* and *merging*. Matching exactly indicates the procedure of unifying the emissions from the parton shower and the matrix element in different region of the phase space. While this is relatively simple for a LO calculation, it becomes non-trivial for a NLO one, as the real emission of the matrix element calculation could be double-counted, given that an additional hard parton is already generated in the NLO cross section. Two matching techniques exist nowadays, MC@NLO [76] and POWHEG [77,78]. On the other hand a merging prescription allows us to add real-emission matrix elements to a fixed-order calculation, properly treating double-counting issues and naturally choosing the starting conditions for the showering. This approach improves the accuracy of the leading logarithmic approximation that one can reach through a standard parton shower, which is *de-facto* an approximated real-emission calculation. The inclusion of exclusive real-emission samples, although not being a full higher-order calculation, improves the description of variables involving additional hard jets. The basic idea relies on the fact that the real emission matrix element is rather simple to compute when compared to the virtual part that contains loop diagrams, which makes the calculation more complicated. Several algorithms exist:

CKKW [79–81] and MLM [82] for merging samples with tree-level calculations; generalisation to NLO fixed-order matrix elements are available [83, 84]. In fig. 2.9 we present the transverse momentum of the Z boson, in Drell-Yan events at the LHC. Date are taken from ATLAS collaboration, [64]. The samples generated comprise the LO order one, labeled as 0-jet case, the sample with an additional parton emitted, 1-jet, and with 2 additional partons, 2-jets. We can see how the merging prescription is relevant for the prediction of variables which are sensitive to the modelling of additional emissions, such as the transverse momentum of the Z gauge boson.

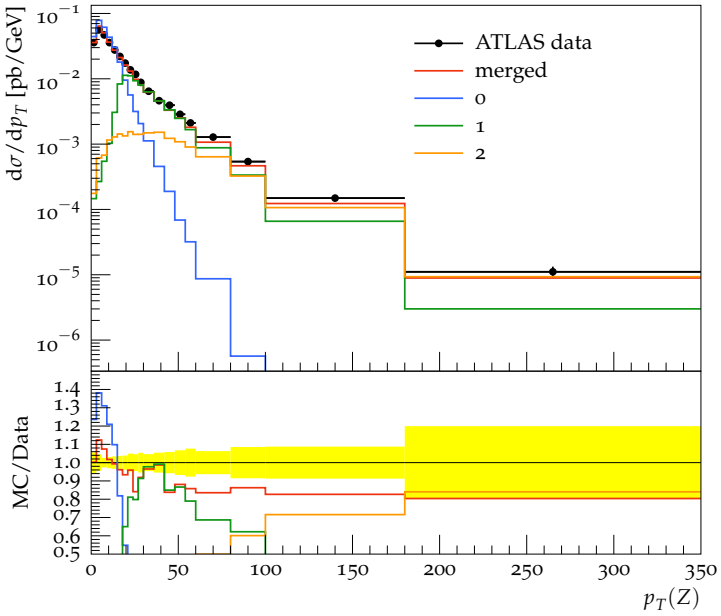

Figure 2.9.: Merging of real-emission fixed-order calculation and showering samples, generated with SHERPA. Comparison to data measured at LHC by ATLAS [85] shows agreement for the merged sample. The process under consideration is Drell-Yan Z production decaying to leptons.

Matching in the MC@NLO version [76] could be summarised using the NLO formalism of Born-weighted NLO cross section

$$d\tilde{\sigma}_B(\phi_n) = d\sigma_B(\phi_n) + d\sigma_V(\phi_n) + d\sigma_I(\phi_n) - \int d\phi_1 \sigma_D(\phi_{n+1}\theta(t - \mu_Q^2)) \,, \qquad 2.82$$

where B, V, I and D stand for Born, virtual, real integrated and subtraction terms, respectively. t is the evolution variable, and μ_Q^2 is the scale at which matching is performed. Introducing the hard remainder function, that accounts for the region of the phase space where the NLO calculation is trusted - opposed to a soft one, where parton

shower emissions are employed -

$$\mathrm{d}\sigma_{\mathrm{H,n}}(\phi_{\mathrm{n+1}}) = \mathrm{d}\sigma_{\mathrm{R,n}}(\phi_{\mathrm{n+1}}) - \mathrm{d}\sigma_{\mathrm{D}}(\phi_{\mathrm{n+1}})\theta(\mu_{\mathrm{Q}}^2 - \mathrm{t}), \tag{2.83}$$

the Sudakov form factor now reads

$$\Delta_n(t_0, t) = \exp\left[-\int_{t_0}^{t} \mathrm{d}\phi_1 \frac{\sigma_D(\phi_n, \phi_1)}{\mathrm{d}\sigma_{\mathrm{B}}(\phi_{\mathrm{n}})}\right], \tag{2.84}$$

and events are generated according to

$$\mathrm{d}\sigma = \int \mathrm{d}\phi_{\mathrm{n}} \mathrm{d}\tilde{\sigma}_{\mathrm{B}}(\phi_{\mathrm{n}}) \left[\Delta_{\mathrm{n}}(\mathrm{t}_0, \mu_{\mathrm{Q}}^2) + \int_{\mathrm{t}_0}^{\mu_{\mathrm{Q}}^2} \mathrm{d}\phi_1 \frac{\sigma_{\mathrm{D}}(\phi_{\mathrm{n}}, \phi_1)}{\mathrm{d}\sigma_{\mathrm{B}}(\phi_{\mathrm{n}})} \Delta_{\mathrm{n}}(\mathrm{t}, \mu_{\mathrm{Q}}^2)\right] + \int \mathrm{d}\phi_{\mathrm{n+1}} \mathrm{d}\sigma_{\mathrm{H}}(\phi_{\mathrm{n+1}}). \tag{2.85}$$

Regarding merging, we briefly describe the simplest case, MEPS@LO. We summarise the generation of events through the following expression for the mean value of an observable

$$\sigma = \int \mathrm{d}\phi_n \sigma_{B,n}(\phi_n) \left[\Delta_n(t_0, \mu_Q^2) + \int_{t_0}^{\mu_Q^2} \mathrm{d}\phi_n \frac{\alpha_s}{2\pi} \sum_j P_j(z) \Delta_n(t_{n+1}, \mu_Q^2)\right] + \tag{2.86}$$
$$+ \int \mathrm{d}\phi_{n+1} \left[\sigma_{B,n+1}(\phi_{n+1}) - \sigma_{B,n}(\phi_n) \frac{\alpha_s}{2\pi} \sum_j P_j(z)\right] \Delta(t, \mu_Q^2) \theta(Q_{n+1} - Q_{\mathrm{cut}}),$$

where $P_j(z)$ is the Altarelli-Parisi splitting kernel, σ_B denotes the Born cross section, $n+1$ is the number of final state partons and ϕ_n in general is the phase space for the process. From this formulation we can highlight the procedure for a multi-jet merging: the *merging* scale Q_{cut} defines the two regions where parton shower emissions and real-emission matrix elements interchange. Matrix element emissions are vetoed for $Q < Q_{\mathrm{cut}}$, conversely for what concerns parton shower radiation. Multi-jet merging has been challenging due to the introduction of a *backward clustering* algorithm: from a fully showered sample we need to reconstruct the history of branchings in order to identify the corresponding core process. *Truncated* shower is the paradigm employed within SHERPA to implement numerically eq. 2.86. Vetoing shower emissions leads to additional weights, which must be considered during the showering; the Sudakov Veto Algorithm is therefore employed [86, 87]. This happens multiplying every line with an additional acceptance or rejection probability and in this way it is possible to avoid double-counting effects. The dependence on the merging scale is therefore canceled by the combination of vetoed matrix-element events and shower emissions.

We state here that for resummation calculations matching prescriptions are also needed, as we have seen that results as in eq. 2.80 are not fully reliable outside the proper region $\alpha_s L \lesssim 1$: we discuss in detail novel matching methods for resummed calculations in chapter 3.

2.1.10. Non-perturbative effects

After discussing perturbative results, in order to achieve a result comparable to any meaningful measurement performed at hadron-hadron colliders, non-perturbative effects have to be taken into account. These reactions happen at a scale $Q^2 \sim \Lambda^2_{\mathrm{QCD}}$, and are therefore classified as long-range interactions, meaning that they should not affect the short-range, high-energy part of the calculations. However, they account for important aftermaths that would render a perturbative calculation not as precise in the direct comparison with data. This approach is known as *parton-hadron duality* [88], basically stating

$$\int \mathrm{d}s\omega(s)\rho_{\mathrm{theory}}(s) = \int \mathrm{d}s\omega(s)\rho_{\mathrm{exp}}(s), \tag{2.87}$$

where ρ is the spectral density and $\omega(s)$ is a weight function - to be identified with the distribution of an observable. This would be a trivial statement if we would have known the full perturbative series at all orders. Since this is not the case, and we actually do not know how to describe QCD below Λ_{QCD}, how gluon and quarks condensate and behave at those energy, to assume eq. 2.87 is definitely not self-evident. Proofs of this rely on the Operator Product Expansion of Wilson lines [89, 90]. Hence, the task is to phenomenologically model the irreducible smearing of order Λ_{NP} due to hadron formation.

When speaking of adding non-perturbative effects to the generated samples we indicate a handful of tools, implementing different processes. First of all, a *string* [91, 92] or *cluster* [93] model connects the showered particles into colour singlets. In the former model this is performed simulating a linear potential between the quarks, in the latter by creating colour-singlet clusters, directly from $q\bar{q}$ pairs or from non-perturbative splittings of gluons. Common to both models is the fact of joining colour connected partons, that is always the case with a shower, which implements only *planar* diagrams, in the large-N_C approximation. In the last few years several novel *colour reconnection* models have been implemented, which take into account subleading effects coming from non-planar diagrams [94–96]. Finally, hadrons are decayed. Another source of non-perturbative physics lays in the remnants of the scattering beams: models of *primordial* k_T exist, trying to describe the average transverse momentum of the parton selected for the hard scattering within the proton. This effect could come from different sources: Fermi motion within the hadron, some unresolved initial state radiation or low-x effects in the PDFs. Usually a Gaussian primordial k_T is chosen. Last, *multiple parton interactions* [97] are simulated: in a realistic scenario the particles not taking part in the hard scattering do interact in some way, what usually is defined as *underlying event*; one must take into account for the elastic and inelastic parts of the scattering, classifying and treating the *diffractive* and *non-diffractive* terms therein. More extensive discussion of these effects could be found in ref. [98]. Due to the phenomenological nature of these models, tuning to actual data from the experiments is performed, in order to choose the proper parameters that better describe the interactions.

Despite the focus of the current work on pQCD methods, the usage of non-perturbative results is necessary for comparing to data, especially for observables directly sensitive

to hadron properties, as could be the energy distribution within a jet. We present in fig. 2.10 the comparison of a simulated di-jet sample with and without the non-perturbative corrections, for the ρ and ψ observables. These are defined as

$$\rho(r) = \frac{1}{N_{\text{jet}}} \sum_{\text{jets}} \frac{p_T(r - \delta r/2, r + \delta r/2)}{p_T(0, R)} \,, \tag{2.88}$$

$$\psi(r) = \frac{1}{N_{\text{jets}}} \sum_{\text{jets}} \frac{p_T(0, r)}{p_T^{\text{jet}}(0, R)} \,, \tag{2.89}$$

where r is the radius within a reconstructed jet with R parameter. The differential jet shape ρ describes the average fraction of jet momentum within an annulus of $r - \delta r/2$ and $r + \delta r/2$, where the integrated ψ represents the average jet momentum inside a cone of radius r concentric to the jet axis. Good agreement with data, taken from [99], is present only after the inclusion of these.

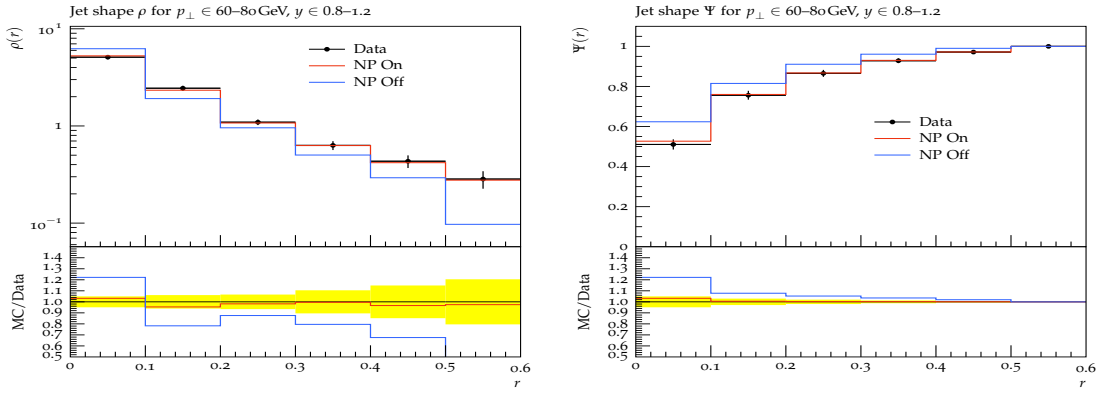

(a) (b)

Figure 2.10.: ρ and ψ jet-shape variables are here compared to measured data at the LHC, showing the agreement of the Monte Carlo simulations with data only after the inclusion of hadronisation and multiple-parton interactions. Measurement of jet shapes in inclusive jet production in pp collisions at $\sqrt{s} = 7$ TeV based on $L = 3\,\text{pb}^{-1}$ of data. Jets are reconstructed in $|\eta| < 5$ using the anti-k_T algorithm with $30 < p_T < 600$ GeV and $|y| < 2.8$ [99].

2.1.11. Presentation of the tools

We want to stress here, that for the purpose of Monte Carlo generation, where pseudo-events are generated and compared with the data measured at colliders, parton showers are usually preferred. A chain of different software tools, comprising

- fixed order calculation and decay of hard particles,

- QCD showering and other all-order effects,
- hadronisation,
- hadron decays,
- other non-perturbative effects,

has become a standard procedure for generating Monte Carlo events. Resummation techniques, on the other hand, provide a deeper understanding of the underlying pQCD structure of the all-order results. We discuss in chapter 3 how the two methods relate to each other.

A vast variety of tools for the hard process integration have been implemented over the years. Due to the high number of amplitudes which must be evaluated, helicity amplitudes methods (see [100] for a nice overview) are preferred to the academic summing of spinors and polarisation vectors through completeness relations. In this framework, the amplitudes are treated as complex numbers, then summed and finally squared. Within SHERPA, two fully automatic matrix element generators are offered, AMEGIC and COMIX [101, 102]. These implementations are results of independent methods and efforts, therefore have slightly different features. AMEGIC implements the Catani-Seymour subtraction method, generating the local counter-term for the given process. COMIX implements the Berends-Giele recursion relations [103], and is particularly suited when computing final states with high multiplicity.

Due to the intrinsic diversity in the calculation of virtual processes, loop diagrams underwent a different development history. Several Monte Carlo implementations have been released, and SHERPA interfaces to some of them in order to provide NLO QCD cross sections: BLACKHAT [104], OPENLOOPS [105] and in the latest versions also RECOLA [106, 107], in order to implement EW corrections to the hard process.

These tools are relevant for the computation of the matrix elements; as these are at hands, SHERPA takes care of integrating the phase space differential in eq. 2.14, through a multi-channel algorithm dividing the complicated phase space into channels identifying the peaks coming from the dominant Feynman diagrams, treating them independently [101]. VEGAS optimisation is available [108], as well as other basic Monte Carlo integrators, like RAMBO [109], SARGE [110] or HAAG [111].

Two parton showers are available in the latest version of SHERPA, one based on the Catani-Seymour dipole, CSSHOWER and the other implementing a slightly different form of the dipoles in the soft and collinear limit, DIRE [112]. Results for both showers have been cross checked against the other major Monte Carlo programs.

Concerning soft QCD, SHERPA implements a cluster hadronisation model, described in [113] and implemented in the module AHADIC; the HADRONS++ module further decay the primordial hadrons and other unstable particles, such τ leptons. Multiple parton interactions are accounted for through the AMISIC module, implementing the model in [114].

2.2. Collider phenomenology at a 100 TeV hadron collider

After presenting the main tools and concepts used for studies and analyses of high energy particle physics experiments, we want to better outline the target machine we are going to use as benchmark for the present work. It is better to characterise such a project through a comparison to the actual running machine, LHC.

A big role in differentiating a $\sqrt{s} = 100$ TeV machine with respect to a $\sqrt{s} = 13$ TeV one is played by the PDFs. Still unexplored kinematical regions, as the very low x regime, $x < 10^{-5}$ or the high-Q^2, $\sqrt{Q^2} \gtrsim 10^4$ GeV [115], could be probed with an FCC machine. An understanding of how *parton luminosities* scale with the increasing centre of mass energy is needed. Given that, forecasting the knowledge of the PDFs contents from now to the next generation of colliders is not trivial, since more data have been collected at Run I and also now at Run II of LHC, and for sure we will have improvements from a High Luminosity Run in the coming years. Nevertheless, we can speculate a little with the current knowledge in our possession. Additional information and progress about global PDFs will come from other possible experiments, *e.g.* electron-nucleon, electron-ion colliders.

Parton luminosities, as the name suggests, are a concept inherited from the definition of luminosity in eq. 2.9. Since the overall energy carried by a parton in the hadron is less than the center of mass energy, it is useful to define the differential parton luminosity:

$$\tau \frac{\mathrm{d}L_{ij}}{\mathrm{d}\tau} = \frac{1}{1+\delta_{ij}} \int_0^1 \mathrm{d}x_1 \mathrm{d}x_2 \times \tag{2.90}$$

$$\times \left[(x_1 f_i(x_1, \mu^2) x_2 f_j(x_2, \mu^2)) + (1 \leftrightarrow 2) \right] \delta(\tau - x_1 x_2). \tag{2.91}$$

The Kronecker's delta in front of the definition applies to the case in which we are considering the same parton. We can recast the usual eq. 2.10 as

$$\sigma(s) = \sum_{ij} \int_{\tau_0}^1 \frac{\mathrm{d}\tau}{\tau} \left[\frac{1}{s} \frac{\mathrm{d}L_{ij}}{\mathrm{d}\tau} \right] \hat{s}\hat{\sigma}_{ij}. \tag{2.92}$$

From eq. 2.92 we notice that the scaling is driven by the parton luminosities: the partonic cross section in fact is dependent on the coupling, which in turn depends slightly on the energy scale. τ_0 acts as a cutoff scale, indicating the lowest center of mass energy at which the hard subprocess can be initiated. In figs. 2.11 parton luminosities for the LHC and the FCC are represented. Lines indicating equal energy scale Q and same luminosity are depicted. We show distributions for the case of quark-quark, quark-antiquark, quark-gluon, gluon-gluon. For a meaningful comparison of the actual setups employed at the LHC PDFs containing top quarks have been separated from those considering just the light quarks - up to the b quark. We can note in fact the mass threshold $m_{\mathrm{top}} = 173$ GeV at which the top quarks start comparing within the proton. One can easily see how big is the role of QCD radiation in an FCC environment, as gluon-gluon initiated processes are enhanced with respect to the quark-antiquark ones luminosity at 13 TeV. In fig. 2.12 a ratio of the LHC and FCC luminosities are shown; this quantity helps us to inspect,

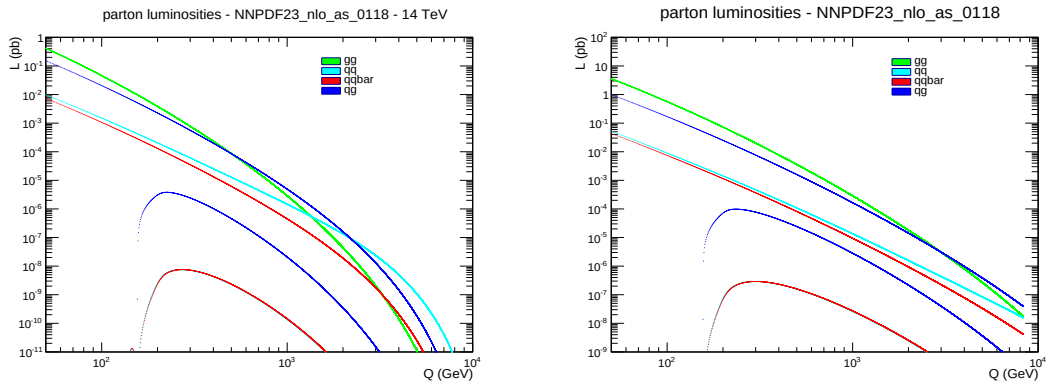

(a) (b)

Figure 2.11.: Parton luminosities for the quark-quark, quark-antiquark, quark-gluon and gluon-gluon cases. In (a) $\sqrt{s} = 13$ TeV, in (b) $\sqrt{s} = 100$ TeV. PDF set NNPDF 2.3 NLO with $\alpha_s = 0.118$ has been employed. Top quark contributions are excluded and plotted separately, but with the same colour code, and have sensitively lower values. Lines of equal Q and luminosity are depicted.

in detail, the occurrence of the production of object of mass M_X at the two colliders. For example, we can estimate that an object with $M_X \sim 5$ TeV produced through the gluon-gluon combination will have roughly an increased probability of being produced $R \sim 10^5$, demonstrating how relevant are QCD processes and tools for computing these predictions in such an environment. In chapter 3 we further discuss the need for precise calculation in pQCD; in chapter 4 we estimate the scaling of production cross sections for background processes for our Beyond the Standard Model search exactly through the help of parton luminosities.

To support the validity of this argument, we present in fig. 2.13 the theoretical cross sections for some relevant processes at a future 100 TeV collider. These have been obtained with SHERPA, with $\sqrt{s} = 100$ TeV with the NNPDF 3.0 NLO PDF set; jets are reconstructed with the anti-k_t algorithm with a parameter $R = 0.4$, requiring a minimum transverse momentum for the jets $p_{T,\text{min}} = 50$ GeV. Photons have additional cuts $R = 0.4$ and $p_{T,\text{min}} = 50$ GeV. Standard Model parameters are imposed through the G_μ scheme, $G_\mu = 1.6639 \times 10^{-5}$ GeV^{-2}, $m_Z = 91.188$ GeV, $m_H = 125$ GeV and $\alpha_s = 0.118$. Cross sections are leading-order accurate; GF and VBF stay for the Higgs production modes, gluon fusion and vector boson fusion, respectively. These results have to be compared to the corresponding measurements at the LHC: for example $t\bar{t}$ production, we can estimate roughly a factor 20×10 from the ratio of the PDFs as in fig. 2.12 from the relevant production modes, gg and $q\bar{q}$. This would account for an increase of the cross section of order 10^2, as it turns out comparing figs. 2.14 and 2.13, from which we can assess $\sigma_{13\ \text{TeV}} \sim 200\,\text{pb}$ and $\sigma_{100\ \text{TeV}} \sim 10^4\,\text{pb}$.

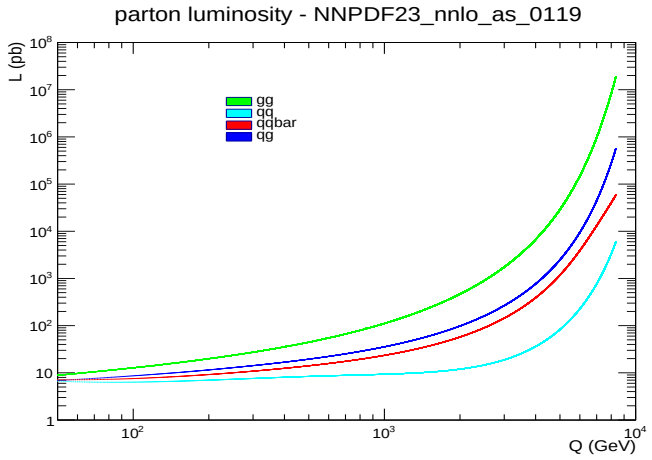

Figure 2.12.: Parton luminosities ratio for the quark-quark, quark-antiquark, quark-gluon and gluon-gluon cases, between $\sqrt{s} = 13$ TeV and $\sqrt{s} = 100$ TeV. Top quarks are excluded when considering quark PDFs. The PDF set employed is NNPDF 2.3 NNLO with $\alpha_s = 0.119$.

2.3. Conclusion

In this chapter we presented a general introduction to Quantum Chromodynamics aspects of the physics at colliders, with a particular focus to hadron-hadron machines. We described the whole process of computing predictions suited for physics studies at such colliders. In particular we aimed at presenting how all-order calculations, in the α_s coupling constant, could be achieved, both through numerical methods - like the parton showers - and more analytical methodologies - as resummation. We reviewed the state-of-the-art material on the subject from the point of view of the comparison between these two approaches.

This material has been introductory to our presentation of physics opportunities at a hadronic future collider. In particular, after looking at the scaling of PDF luminosities and at the overall cross sections for the main processes, we would like to briefly discuss what is the aim of such a collider, and its potential. In general, the machine can be regarded as an unprecedented opportunity to directly probe new physics up to scale of multi-TeVs, with mass reaches spanning from few TeV, to 40-50 TeV [117]. The main branches of study in this direction comprehends potential dark matter candidates, and new symmetries of the space time, as supersymmetry. Whatever will be the solution to the Standard Model puzzle, a big part of the theory community is convinced that new physics should be around this scale.

Thanks to its high luminosity, the FCC could be regarded also as a precision machine. It is estimated that the Higgs self-coupling could be measured at order of some percentage points, whereas the top Yukawa coupling could be probed with more accuracy than

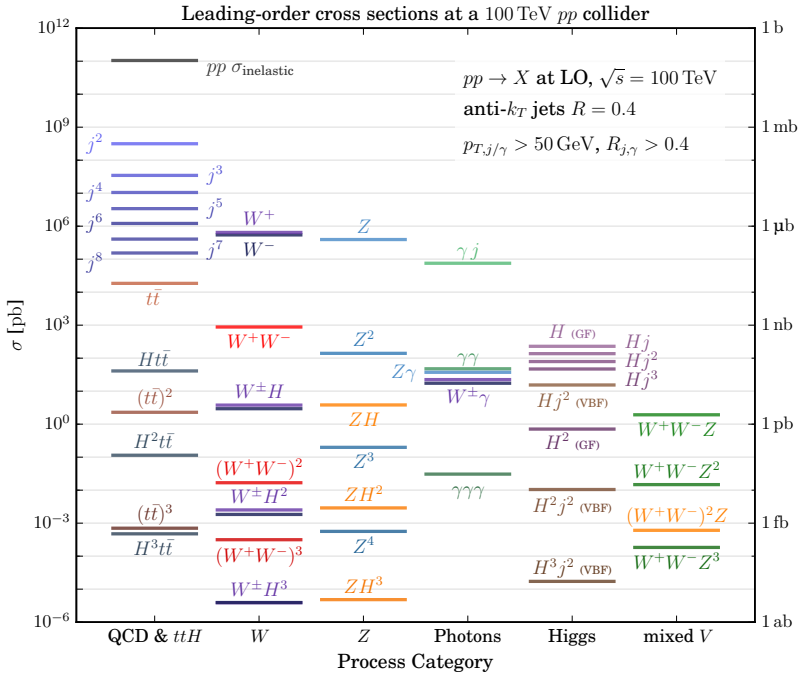

Figure 2.13.: We present inclusive cross sections for different categories of processes, simulated with SHERPA at a 100 TeV hadron-hadron collider. QCD, single- and multiple-gauge-bosons, photons, Higgs are presented. Setup is fully described in ref. [116].

LHC nowadays [118]. Another important test of the Standard Model would be the measurement of triple and quadruple Higgs couplings, for which test scenario and theory analyses are not yet fully clear. Of course, from the precision point of view, the FCC has to be regarded as a complementary machine to a real precision collider, as a lepton-lepton machine would be. In any case, new directions in how theoretical uncertainties, systematical ones and background estimations are balancing are opened by the potential reach of such a machine.

Challenges are posed either when considering highly boosted objects, which will require also a careful design of the detectors resolution and depths, or from a crowded environment that arise from such energetic collisions. Overall, from a purely theoretical point of view, higher order corrections will for sure be an important topic, in order to lower the amount of theoretical uncertainties. The interplay of these with all-order effects, either computed by means of numerical algorithms, or with analytical methods such resummation, will be a challenge, especially in the integration of multi-purpose tools, as Monte Carlo event generators in the LHC era.

Although being a great opportunity for the study of still unexplored regions of the phase space, providing inestimable amount of data useful for the understanding of the

dynamic of the Higgs mechanism, the presence of new physics, as well as the direct and indirect measurements of the Higgs self-couplings, a 100 TeV collider is challenging also from the point of view of the detector design.

The phase space coverage of the produced particles will allow us to measure events in regions of pseudo-rapidity not covered by the multi-purpose detectors as ATLAS and CMS [116]: one of the first challenges is the large η acceptance for the detectors. In addition, a huge quantity of *pileup* events are expected: these are effects accounting for the non-negligible probability for a single bunch to produce several separate interactions. Pile-up is classified as either in-time or out-of-time: the former regards additional interactions in the detectors overlapping with the hard-scattering process; the latter refers to events belonging to the successive bunch crossings (for example, at the LHC, the bunch-crossing interval is of 25 ns, therefore, the electronics and detectors has to take this specification into account). Pile-up has an impact on jet kinematics and substructure, leading to non-negligible contributions. Some jet reconstruction techniques [119–123] are already designed explicitly to subtract these contributions, but $n_{\text{pileup}} \sim 1000$, as expected at the FCC-hh, is nevertheless challenging for the further development of these techniques. Furthermore, pileup contributions account for much more radiation, which is not relevant for the analyses but anyway present and detected by the trackers and calorimeters. This intense environment requires a careful study and design of the future

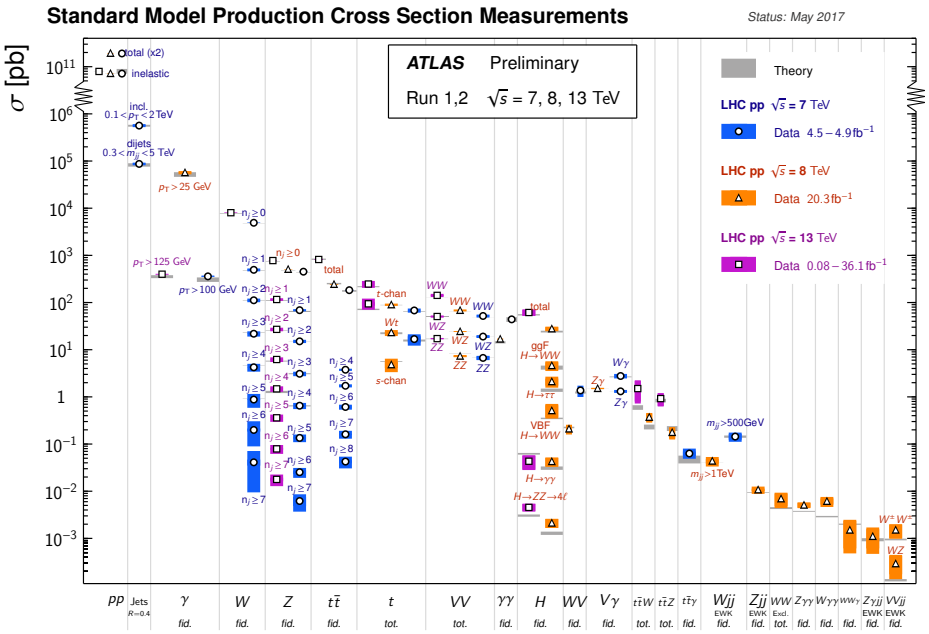

Figure 2.14.: The measurements at the LHC of inclusive cross sections for different categories of processes; data taken from the ATLAS experiment.

detector systems.

The conceptual design report of the detectors and of the overall FCC-hh experiment is due for the end of 2018. Due to the larger η acceptance and a bigger interest in forward physics compare to the LHC, one of the purposes for a possible detector is to have an ATLAS/CMS-like central region detector, with higher resolution trackers and calorimeters, and a forward region detector similar to that of the LHCb experiment running in these days, as designed in [124]. The combination of the two layouts should enhance the overall acceptance, giving access to regions currently not covered by the two main multi-purpose detectors, ATLAS and CMS. The conceptual design comprises a central magnet of 4 T, meaning double the magnetic field compared to ATLAS. Barrel electromagnetic calorimeters with energy resolution of $\sigma_E/E \sim 10\,\%/\sqrt{E}$ and hadronic calorimeters with $\sigma_E/E \sim 50\,\%/\sqrt{E}$; trackers are designed to have energy resolution of $\sigma_E/E \sim 10\,\%$. The rapidity coverage, calorimeters comprised, aim to a goal of $|\eta| \sim 6.0$; the forward detectors will be located farer from the central region and they will be properly shielded, to reduce radiation load and contamination. Target for the muon resolution is around 5 %, with a rapidity coverage $|\eta| < 4.0$. The focus is overall on "low-p_T" physics, coming for example from W/Z/Higgs or top decays, but shifted more to forward angles with respect to the beams.

The latest updates in ref. [125] on the overall layout of the FCC-hh setup comprise two high-luminosity experiments and two other experiments combined with injection, meaning the possibility to vary the incoming particles of one of the beam, allowing for example heavy-ions or leptons collisions with protons.

With this information at hand, we discuss in the coming chapters possible directions on how Monte Carlo event generators at the present state can help us understanding the challenges posed by such a collider, and to design possible analysis strategies for processes not yet probed at the LHC.

CHAPTER 3

Resummation

This chapter presents the study of precise calculations for a future hadron collider. At a $\sqrt{s} = 100$ TeV, negligible effects at LHC energies begin to have an impact on the simulations. We employ resummation in the forthcoming discussion, not only as a valid alternative to the parton-shower, but rather as a tool to gain a greater insight into the accuracy of calculations. We would like to demonstrate how such method could be automated within a Monte Carlo multi-purpose software, and how it could be used to trace the logarithmic structure and accuracy of the parton-shower algorithms. Resummation methods, despite being fully analytical, are highly process dependent, whereas the parton shower can easily adapt to different processes, and for this reason is today the usual tool employed for producing all-order results. Automation of resummation methods therefore could be one important target for the particle physics community, having an alternative to parton showers, which could even gain more insights in the physics at colliders.

First resummed calculations were specially employed in predictions for global variables at lepton colliders. Event shape variables, like thrust in section 2.1.8 have been successfully employed at LEP and in DIS experiments in order to measure the strong coupling. These observables measure the flow of energy-momentum in the event, for example, continuously encoding the transition from a two-jet to a three-jet event, as in the case of thrust. This information would not be available through jet finder algorithms, which would always give a discrete jet structure, also in the case of absence of prong-like shapes in the event. Globalness, *i.e.* being sensitive to radiation at any point of the phase space, leads to a remarkable simplification in the factorisation property of the phase space with respect to QCD radiation. The enhancements coming from soft and collinear emissions, typically at values of the event-shape variable related to the di-jet structure, have pushed the research towards the understanding of QCD dynamics itself and in the development of all-order techniques as soft-gluon resummation itself.

This property allows to have a good handle to the QCD parameters, like the quark and gluon colour factors and the β function of the strong coupling. Tests of QCD colour structure [126] and Monte Carlo generators validations [127, 128] have been carried out thanks to the presence of resummed results for event-shape variables. In fact, the presence of power corrections of order $(\Lambda/Q)^2$, which stem from hadronisation corrections, have been computed in this framework and permit a better understanding of soft QCD corrections.

Despite the busy QCD environment typical at hadron colliders, such as the LHC, an unprecedented number of experimental measurements have been carried out by both the ATLAS and CMS collaborations, including the Higgs boson discovery [129, 130]. For many of these experimental analyses, several non-global event shapes are used. These are defined "non-global", in the sense that they characterise the events in a confined region of the phase space, usually within a jet.These variables are a generalisation of global event-shape variables. They are employed to characterise energy-momentum flow within a jet, in order to both better understand QCD radiation and to construct tagging algorithms for the decays of heavy resonances such as weak bosons, top quarks and Higgs bosons. Among others, we present jet subjettiness:

$$\tau_N = \frac{\sum_k p_{T,k} \min \Delta R_{1,k}, \Delta R_{2,k}, \ldots, \Delta R_{N,k}}{\sum_k p_{T,k} R_0}, \tag{3.1}$$

where $p_{T,k}$ is the transverse-momentum of the k-th constituent in a reconstructed jet, and $\Delta R_{i,k} = \sqrt{\Delta\eta_{i,k}^2 + \Delta\phi_{i,k}}$ is the distance in the rapidity-azimuth plane between a candidate subjet, i, and the given constituent k; R_0 is the jet radius of the original reconstructed jet. Subjettiness is widely employed at the LHC, in order to reconstruct heavy objects decaying to hadrons, giving rise to two- and three-prong structures within a fat jet. A characterisation in terms of logarithmic accuracy of these new variables is mandatory, but the loss of globality in the definition of the variable renders resummed calculations cumbersome, leading to a non-trivial factorisation of the phase space. In spite of that, resummed results have recently been achieved, within Soft and Collinear Effective Theory [67, 131], and in section 3.2 we will show a valuable approach to study subjet rates. The extension of resummation methods to non-global observable is a key point for starting employing on a wider range of variables analytical resummed results. It is a topic that lies outside the scope of this thesis, but it is important to stress out its importance in the running experiments.

We start discussing soft-gluon resummation as developed within the CAESAR framework [132], showing how resummed results could be achieved generalising this approach within SHERPA [133] for events at hadron-hadron colliders. Next, we directly compare resummed results obtained through the generating functional method to events generated at a 100 TeV collider.

3.1. Soft-gluon resummation: the semi-numerical CAESAR approach

At the level of the integrated cross section, soft and/or collinear QCD radiation leads to divergences proportional to $\alpha_S \log^2(\tau)$ and $\alpha_S \log(\tau)$. In general, at hadron colliders, the divergences are classified in terms of the strong coupling, α_S, and the particular enhanced logarithm, $L \equiv \log 1/v$, where the logarithm is enhanced in the phase-space region sensible to soft and collinear emission, $v \to 0$, where $v \equiv \tau$ in the thrust case. Our distribution depends on combinations of powers of the strong coupling and logarithm like $\alpha_S^n \log^{2n} v$, leading logarithms (LL), $\alpha_S^n \log^{2n-1} v$ next-to-leading logarithms (NLL) and so on. Following ref. [72], it is possible to resum to all-orders in α_S these divergences using the coherent-branching algorithm in QCD, getting a reliable prediction for the process. This approach, fully analytical, is process dependent, and in most cases involves lots of calculations, which are hard to generalise and automate. Over the past few years the community has begun to focus more on the parton-shower formalism to get an all-orders prediction that relies on some approximations but it is more convenient and easy to automate than the resummation one.

In the early 2000's, a framework has been developed to account for a semi-automatic generalised resummation of a large class of event-shape variables at lepton and hadron colliders, including, among others, thrust, jet broadening, F-parameter and the exclusive k_t-algorithm jet-rates [132]. The Caesar approach defines a resummation program for a general observable, $V = V(q_1, q_2, \ldots, q_n)$, which has to be infrared and collinear safe. After a certain number of particles, n, the variable tends smoothly to zero for momentum configurations that approach the n-jet limit. The cross section is defined through the introduction of a function, $\mathcal{H}(q_1, q_2, \ldots)$, selecting the hard jets:

$$\sigma_{\mathcal{H}} = \sum_{N=n-n_i}^{\infty} \int \mathrm{d}\Phi_N \frac{\mathrm{d}\sigma_N}{\mathrm{d}\Phi_N} \mathcal{H}(q_1, \ldots, q_N). \tag{3.2}$$

The integrated cross section is conveniently rewritten through the introduction of the event fraction we already employed in chapter 2:

$$\Sigma_{\mathcal{H}} = \sum_{\delta} \int \mathrm{d}\sigma_B \frac{\mathrm{d}\sigma_\delta}{\mathrm{d}\sigma_B} f_{\sigma_B,\delta}(v) \mathcal{H}(p_{n_i+1}, \ldots, p_n), \tag{3.3}$$

where σ_B is the Born cross section and $\mathrm{d}\sigma_\delta/\mathrm{d}\sigma_B$ represent the probability to produce a Born event with $n - n_i$ outgoing hard momenta, $p_{n_i+1}, \ldots, p_n$, in a given scattering channel δ, and v is the actual value taken by the general variable V in the given event. $f(v)$ is the integrated event fraction, which represents the probability of having a value for the observable smaller than v. The variable value should vanish for a Born hard event consisting of n hard legs, which allows a simple parametrisation for an additional emission k, soft and collinear to the Born leg ℓ

$$V(k, \{p\}) = d_\ell \left(\frac{k_t}{Q}\right)^{a_\ell} e^{-b_\ell \eta_\ell} g_\ell(\phi_\ell). \tag{3.4}$$

$\{p\}$ denotes the ensemble of Born legs momenta. k_t^ℓ, η_ℓ are computed with respect to the original parent Born dipole (the one before the emission). a, b, d and g are set to parametrise the observable under consideration. For the case of thrust τ for example, we have $a_\ell = b_\ell = d_\ell = g_\ell(\phi_\ell) = 0$ for every ℓ in the event.

For the resummation program to work, two conditions have to be valid: *recursive infrared and collinear safety* (rIRC) and *continuous globalness*. These are not at all new concepts in typical resummation calculations, instead they harden the standard globalness and infrared collinear safety prescriptions.

- Asking for a global observable means that the variable departs from the null value, which, by definition, is reached in the case where only the Born legs are present in the event, for any additional emission. This translates into the following requirements to the Caesar parametrisation

$$\left.\frac{\partial V(k,\{p\})}{\partial \log k_t^\ell}\right|_{\text{fixed } \eta_\ell,\phi_\ell} = a\,, \qquad \left.\frac{\partial V(k,\{p\})}{\partial \log k_t^\ell}\right|_{\text{fixed } z_\ell,\phi_\ell} = a + b_\ell\,, \tag{3.5}$$

  having defined z_ℓ to be the longitudinal momentum fraction of the emission, always with respect to the original parent dipole. The two formulations exhibit the same constraint, but in the soft (and eventually collinear) and collinear (eventually soft) limits respectively.

- rIRC imposes that, any further soft/collinear emission has the same scaling property for the observable; in addition it could be shown that there exists some $\epsilon \ll 1$ such that emissions below ϵv do not contribute significantly to the observable value. These conditions can be formulated in two limits:

  1. the limit
  $$\lim_{\bar{v}\to 0} \frac{1}{\bar{v}} V(\{p\}, k_1(\bar{v}_1\xi_1), \ldots, k_m(\bar{v}_m\xi_m)) \tag{3.6}$$
  is well-defined and non-zero; in eq. 3.6 $\bar{v}_i = v/\xi_i$;
  2. the following limits are identical and well-defined
  $$\lim_{\xi_{m+1}\to 0} \lim_{\bar{v}\to 0} \frac{1}{\bar{v}} V(\{p\}, k_1(\bar{v}_1\xi_1), \ldots, k_m(\bar{v}_m\xi_m), k_{m+1}(\bar{v}_{m+1}\xi_{m+1})) \tag{3.7}$$
  $$= \lim_{\bar{v}\to 0} V(\{p\}, k_1(\bar{v}\xi_1), \ldots, k_m(\bar{v}\xi_m))\,. \tag{3.8}$$

3.1.1. The radiator and the multiple emissions terms

We now discuss the parametrisation in eq. 3.4 in the concrete case of the thrust variable. Defining one momentum for each hemisphere S_i in the plane orthogonal to the thrust axis $\boldsymbol{n}_T$,

$$q_1 = \sum_{i\in S_1} p_i = z_1 p + k_{t1} + \bar{z}_1 \bar{p}\,, \tag{3.9}$$

$$q_2 = \sum_{i\in S_2} p_i = z_2 p + k_{t2} + \bar{z}_2 \bar{p}\,, \tag{3.10}$$

where p and $\bar{p}$ are light-like momenta. We can rewrite thrust $\tau = 1 - T$ as

$$\tau = 1 - \frac{1}{Q}(|\boldsymbol{q}_1 \cdot \boldsymbol{n}_T| + |\boldsymbol{q}_2 \cdot \boldsymbol{n}_T|) = 1 - \sqrt{1 + 2\left(\frac{q_1^2}{Q^2} + \frac{q_2^2}{Q^2}\right)}. \tag{3.11}$$

This simplifies in the case of soft and/or collinear emissions $(q_1^2 + q_2^2)/Q^2 \ll 1$ as

$$\tau = \frac{q_1^2}{Q^2} + \frac{q_2^2}{Q^2} + \mathcal{O}(q_i^2 q_j^2/Q^4) = \sum_{i=1}^{n} V(k_i)\,, \tag{3.12}$$

where we omit the $\{p\}$ ensemble of Born legs.

We recast the cumulative distribution defined in eq. 3.3 as a Sudakov exponential, comprising the virtual corrections to the Born process, times an infinite tower of n additional emissions, according to the matrix element M, in the following equation

$$\Sigma(v) = \exp\left[-\int [\mathrm{d}k] M^2(k)\right] \times \sum_{n=0}^{\infty} \frac{1}{n!} \int \prod_i [\mathrm{d}k_i] M^2(k_i) \Theta(v - V(\{k_i\}))\,. \tag{3.13}$$

Introducing a small parameter, ϵ, which has the same purpose as the shower cutoff, it is possible to further divide the phase space of the emissions, encoding those with $V < \epsilon v$ in the exponentiated virtual correction term, and counting the other as resolved emissions. Thanks to rIRC, in particular eq. 3.7, unresolved emissions do not contribute significantly at NLL. Thus, the cumulative distribution becomes

$$\Sigma(v) = \exp\left[-\int [\mathrm{d}k] M^2(k)(1 - \Theta(\epsilon v - V(k)))\right] \times \tag{3.14}$$
$$\times \sum_{n=0}^{\infty} \frac{1}{n!} \int_{\epsilon v}^{v} \prod_{i=1}^{n} [\mathrm{d}k_i] M^2(k_i) \Theta(v - V(\{k_i\})) \Theta(V(\{k_i\}) - \epsilon v).$$

We can recombine the virtual corrections, which account for the appropriate running of the coupling in a similar fashion to what is performed in the parton showers, evaluating the coupling at the scale of the emission, $\alpha_s(k_t^2)$. This recombination is done by expanding the exponential around the single emission matrix element coming from the first emission. That is the one accounting for the most important effect on the value of the observable

$$\exp\left[-\int_{\epsilon v_1} [\mathrm{d}k] |M^2(k)|\right] = e^{-R(\epsilon v_1)} = e^{-R(v) - R' \log v/\epsilon v_1 + \mathcal{O}(R'')}\,, \tag{3.15}$$

where $R' \equiv \partial R/\partial L$. $R(v)$ is often called the gluon radiator, and can be computed directly from the single-emission matrix element, with the adequate boundaries coming from the event-shape variable constraints

$$R(v) = \sum_{\ell=1}^{2} C_F \left[\int_{Q^2 v^{2/(a+b_\ell)}}^{Q^2} \frac{\mathrm{d}k_t^2}{k_t^2} \frac{\alpha_s(k_t^2)}{\pi} \left(\log \frac{Q_{12}}{k_t} + B_\ell\right) + \right. \tag{3.16}$$
$$\left. + \int_{Q^2 v^{2/a}}^{Q^2 v^{2/(a+b_\ell)}} \frac{\mathrm{d}k_t^2}{k_t^2} \frac{\mathrm{d}\phi}{2\pi} \frac{\alpha_s(k_t^2)}{\pi} \left(\log \frac{Q_{12}}{2E_\ell} + \frac{1}{b_\ell} \log\left(\left(\frac{k_t}{Q}\right)^a \frac{d_\ell g_\ell(\phi)}{v}\right)\right)\right],$$

where Q_{12} is the energy scale of the emitting dipole and B_ℓ includes the contribution from the large-η integration over the splitting function

$$B_\ell = \int_0^1 \frac{\mathrm{d}z}{z}\left(\frac{zp(z)}{2} - 1\right). \tag{3.17}$$

In fig. 3.1.1 we show the splitting of the phase space for the emission as in the integral of eq. 3.16, in which it is possible to note that, for the purpose of NLL resummation, the allowed phase space is that constrained by the transverse-momentum lower cutoff, in terms of ϵ, the upper k_t boundary, coming by the kinematics, and the constraints due to the variable parametrisation.

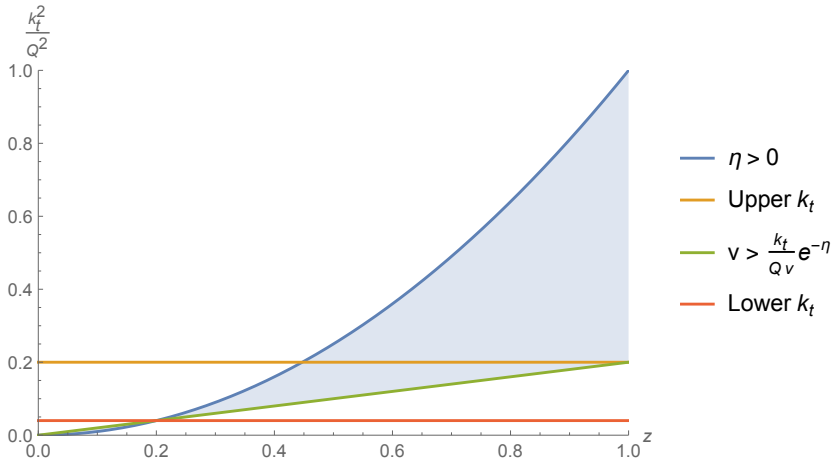

Figure 3.1.: Constraints on the single-emission contributions in the Lund plane, defined by the longitudinal fraction momentum, z, and the ratio of the transverse momentum of the emission, k_t^2, and the hard scale of the process, Q^2. Different areas are highlighted, coming from boundaries of the integrals (lower and upper k_t) and from requirements on the variable, as in eq. 3.16.

From the splitting of the virtual contributions as in eq. 3.15 we can define a function, $\mathcal{F}(v)$, which encodes a dependence on single-emission independent contributions, *i.e.*

$$\Sigma(v) = \exp\left[-\int [\mathrm{d}k] M^2(k)\Theta(V(k) - v)\right] \times \mathcal{F}(v)\,, \text{with} \tag{3.18}$$

$$\mathcal{F}(v) = \exp\left[-\int_{\epsilon v}^{v} [\mathrm{d}k] M^2(k)\right] \sum_{n=0}^{\infty} \frac{1}{n!} \int_{\epsilon v}^{v} \prod_{i=1}^{n} [\mathrm{d}k_i] M^2(k_i). \tag{3.19}$$

The reasoning above is valid for a simple $e^+e^- \to jj$ process and to arbitrary logarithmic accuracy and is fully general and easily generalisable. In going from a lepton-lepton collider to a hadron-hadron one, two complications arise: there is a non-trivial colour structure, already for relatively simple processes like $pp \to jj$, and we have to account

for DGLAP-like effects coming from the evolution of the hadronic initial state. Defining $L \equiv \ln 1/v$ and $\lambda \equiv \alpha_S \beta_0 L$, the general integrated distribution at hadron-hadron colliders, accurate to NLL is

$$\ln f(v) = -\sum_{\ell=1}^{n} C_\ell \Bigg[r_\ell(L) + r'_\ell(L) \left(\log \bar{d}_\ell - b_\ell \ln \frac{2E_\ell}{Q} \right) + B_\ell T\left(\frac{L}{a+b_\ell}\right) + \sum_{\ell=1}^{n_i} \ln \frac{q^\ell(x_\ell, e^{-\frac{2L}{a+b_\ell}}\mu_F^2)}{q^\ell(x_\ell,\mu_F^2)} + \ln S(T(L/a)) + \ln \mathcal{F}(C_1,\ldots,C_n;\lambda) \Bigg], \tag{3.20}$$

where $C_\ell = C_F, C_A$ are the colour factors for the respective leg. We have defined

$$r_\ell(L) = \int_{Q^2 e^{-2L/(a+b_\ell)}}^{Q^2} \frac{\mathrm{d}k_t^2}{k_t^2} \frac{\alpha_s(k_t^2)}{\pi} \log \frac{Q}{k_t} + \int_{Q^2 e^{-2L/a}}^{Q^2 e^{-2L.(a+b_\ell)}} \frac{\mathrm{d}k_t^2}{k_t^2} \frac{\alpha_s(k_t^2)}{\pi} \left(\frac{L}{b_\ell} + \log \left(\frac{k_t}{Q} \right)^{a/b_\ell} \right), \tag{3.21}$$

$$r'_\ell(L) \equiv \frac{\partial r_\ell(L)}{\partial L} = \frac{1}{b_\ell} \left[T\left(L/a\right) - T\left(L/(a+b_\ell)\right) \right], \quad \text{with} \tag{3.22}$$

$$T(L) = \int_{Q^2 e^{-2L}}^{Q^2} \frac{\mathrm{d}k_t^2}{k_t^2} \frac{\alpha_s(k_t^2)}{\pi}. \tag{3.23}$$

Contributions in eqs. 3.22 all come from the radiator, $R(v)$, which was discussed in eq. 3.16. Substituting in the one-loop accurate expression for the running coupling, it is possible to evaluate the integrals in eq. 3.22 and recovering the result in eq. 2.80. S encodes the colour flow of the underlying Born event. It is relevant only for hadron colliders, as the colour flow for simple processes in lepton machines is trivial. We discuss them separately in the following. The evolution of the PDFs is taken into account through the ratio of the two parton distribution functions

$$\frac{q(x, \mu_F^2 v^{2/(a+b_\ell)})}{q(x,\mu_F^2)}; \tag{3.24}$$

in fact, collinear emissions are properly taken into account up to the factorisation scale, as usual, but placing a limit, v, on the value of the observable actually implies vetoing emissions $(k_t/Q)^{a+b_\ell} \lesssim v$. Hard collinear emissions, by construction, do not affect the values of observables, and the parton density function scales with a factor of the order, $Qv^{1/(a+b_\ell)}$. The old parton density function at scale μ_F^2 is then replaced by the parton density evaluated at lower scale $\mu_F^2 v^{2/(a+b_\ell)}$.

3.1.2. The soft function

When considering more than 2 QCD charged partons in a resummed calculation, the only difference is in the radiator function. This function becomes a sum over dipoles, which are constructed by pairing the various colour-charged particles in the event, such

that we rewrite the function R(v) as

$$R(v) = \sum_{\text{dipoles}} C_{\text{dipole}} \left(\sum_{\ell \in \text{dipole}} \left[r_\ell(L) + r'_\ell(L) \left(\log d_\ell - b_\ell \log \frac{2E_\ell}{Q} \right) + \right. \right. \tag{3.25}$$
$$\left. \left. + B_\ell T(L/(a+b_\ell)) \right] + 2T(L/a) \log \frac{Q_{\text{dipole}}}{Q} \right).$$

By rearranging the sum over dipoles and over the associated legs, it is possible to write the radiator function as a single sum over Born legs and a function encoding all the dependence over dipoles, the latter being what we have defined to be the S "soft" function:

$$R(v) = \sum_\ell C_\ell \left[r_\ell(L) + r'_\ell(L) \left(\log d_\ell - b_\ell \log \frac{2E_\ell}{Q} \right) + B_\ell T(L/(a+b_\ell)) + \right. \tag{3.26}$$
$$\left. - \log S\left(T(L/(a))\right) \right],$$

where, in the case $n = 3$, the S function takes the form

$$\log S(t) = -t \left[C_A \log \frac{Q_{qg} Q_{q'g}}{Q_{qq'}} \right]. \tag{3.27}$$

From $n = 4$ legs, the situation is more complicated, because loop-corrections that are included through the proper treatment of the running coupling must be taken into account when computing the colour flow. A loop diagram appearing in a $q\bar{q} \to q\bar{q}$ exchange would already introduce a non-trivial colour flow; this is indeed one of the simplest processes we could think for the colour algebra. Needless to say, for diagrams involving gluons, in order to resum to all orders, the number of colour-flow combinations increases almost exponentially. Looking at eq. 3.26, it is evident that contributions ending up in the soft function are exactly soft - *i.e.* unresolved - large-angle contributions.

As we have seen in the parton shower formalism, the treatment of colour flow in the hard QCD event is not simple. There, the large N_C approximation is employed, where N_C denotes the number of colour charges, *i.e.* $SU(N_C)$. This approximation was introduced by 't Hooft [134] to simplify the treatment of meson-meson exchanges. Basically, one considers the limit $N_C \to \infty$, while keeping $\alpha_s N_C$ fixed. This introduces considerable simplification, and mainly we have some topologies of diagrams contributing most; diagrams are classified in powers of $1/N_C$. Graphically, a large-N_C theory depicts the quarks as a single colour-flow line, and gluons as a double line, with opposite flow, as it would be if the gluon is regarded as a $q\bar{q}$ pair. It is then simple to count the $1/N_C$ powers of a diagram: in fig. 3.2 bottom, for example, we can see the introduction of two gluon lines overlapping, a typical non-planar diagram. Following the colour flow, it is evident to see that this diagram is $1/N_C$ suppressed with respect to a planar diagram as in fig. 3.2 right.

The function S appearing in eq. 3.20 [135, 136] can be expressed as a matrix element in the colour space of the hard scattering: defining $|m_0\rangle$ a vector in the colour space,

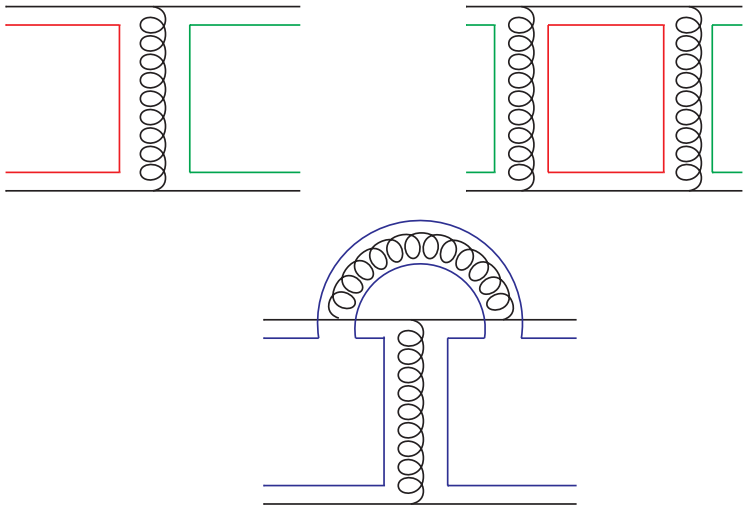

Figure 3.2.: Example diagrams for visualising the colour flow in the large N_C approximation. Large-N_C flow is projected over the Feynman diagrams for the process $qq \to qq$ with additional gluon exchange, at order α_s^2,α_s^4.

such that the Born amplitude is $|M_{\text{Born}}|^2 = \langle m_0|m_0\rangle$, one can write

$$S(\xi) = \frac{\langle m_0|e^{-\Gamma^\dagger \xi/2} e^{-\Gamma \xi/2}|m_0\rangle}{\langle m_0|m_0\rangle}\,, \tag{3.28}$$

where Γ is the soft anomalous dimension, resumming to all orders the soft, large-angle contribution and ξ is the single-logarithmic evolution variable. The dependence on the strong coupling is completely contained in the evolution variable. For global event-shape variables, the soft anomalous dimension can be written as

$$\Gamma = -2\sum_{i<j} \boldsymbol{T}_i \cdot \boldsymbol{T}_j \log\frac{Q_{ij}}{Q} + i\,\pi \sum_{i,j=II,FF} \boldsymbol{T}_i \cdot \boldsymbol{T}_j\,, \tag{3.29}$$

where $Q_{ij}^2 = 2p_i \cdot p_j$, is the invariant mass of the dipole, as before. II and FF denotes the fact that dipoles are initial-initial or final-final. Being Γ and $\Gamma^\dagger$ non-commutative, the evaluation of eq. 3.28 is not trivial. This results in an additional phase for the soft function, that accounts for the exchange of Coulomb-Glauber partons.

In the $2 \to 2$ case the dipoles are classified in terms of the Mandelstam variables, $\sqrt{s} = Q_{12} = Q_{34}$, $\sqrt{-t} = Q_{13} = Q_{24}$ and $\sqrt{-u} = Q_{14} = Q_{23}$. Therefore, the soft anomalous dimension becomes

$$\Gamma = -\left(\boldsymbol{T}_1 \cdot \boldsymbol{T}_3 + \boldsymbol{T}_2 \cdot \boldsymbol{T}_4\right) T - \left(\boldsymbol{T}_1 \cdot \boldsymbol{T}_4 + \boldsymbol{T}_2 \cdot \boldsymbol{T}_3\right) U\,, \tag{3.30}$$

where we defined

$$T = \log \frac{-t}{s} + i\pi \quad \text{and} \quad U = \log \frac{-u}{s} + i\pi \,. \tag{3.31}$$

In eq. 3.30 we employed the conservation of the overall colour charge in the event, which can be expressed as

$$\left(\sum_{i=1}^{4} \boldsymbol{T}_i \right) |m_0\rangle = 0 \,. \tag{3.32}$$

Hence, an automation of the soft function calculation should define and compute the colour basis and metric, calculate of the operators $\boldsymbol{T}_i \cdot \boldsymbol{T}_j$ and finally decompose the amplitude in this colour basis. Despite the difficulties, technologies to deal with the colour bases and mixing matrices exist, [137–139], through the construction of appropriate and optimised bases for the general $SU(N_C)$ algebra. This topic is intrinsically connected to the construction of multi-leg QCD partial-amplitudes [140]. The approach pursued by ref. [133] in particular exploits existing tools which provide colour-ordered amplitudes, such as computed in COMIX, in order to calculate the soft function. In this approach, the Γ matrix is expressed in the same basis of the colour amplitudes within in COMIX.

A colour basis is defined through the rules for the interaction vertices of the process, and in general simplification rules for three-gluon vertices and exchange of a gluon in $qq' \to qq'$ scattering diagrams exist, depicted in figs. 3.3 and 3.1.2.

(a) (b)

Figure 3.3.: Factors associated to the qqg and the ggg vertices in QCD.

Nevertheless, the colour bases employed are non-orthogonal, meaning

$$\langle c_\alpha | c_\beta \rangle \equiv c_{\alpha\beta} \neq \delta_{\alpha\beta} \quad c^{\alpha\beta} = (c_{\alpha\beta})^{-1} \,, \tag{3.33}$$

where we define a general element of the basis $|c_\alpha\rangle$, for which by definition $c_{\alpha\gamma} c^{\gamma\beta} = \delta_\alpha^\beta$. The soft function in such a basis is rewritten as

$$S(\xi) = \frac{\mathrm{Tr}\left(H e^{-\Gamma^\dagger \xi/2} c e^{-\Gamma \xi/2} \right)}{\mathrm{Tr}\,(cH)} = \frac{c_{\alpha\beta} H^{\gamma\delta} \mathcal{G}^\dagger_{\gamma\rho} c^{\rho\beta} c^{\alpha\delta} \mathcal{G}_{\delta\sigma}}{c_{\alpha\beta} H^{\alpha\beta}} \,. \tag{3.34}$$

The matrix, $\mathcal{G}$, is the exponential of the Γ anomalous dimension contracted with the proper metric

$$\mathcal{G}_{\alpha\beta}(\xi) = c_{\alpha\gamma} \exp\left(-\frac{\xi}{2} c^{\gamma\delta} \Gamma_{\delta\beta} \right) \,. \tag{3.35}$$

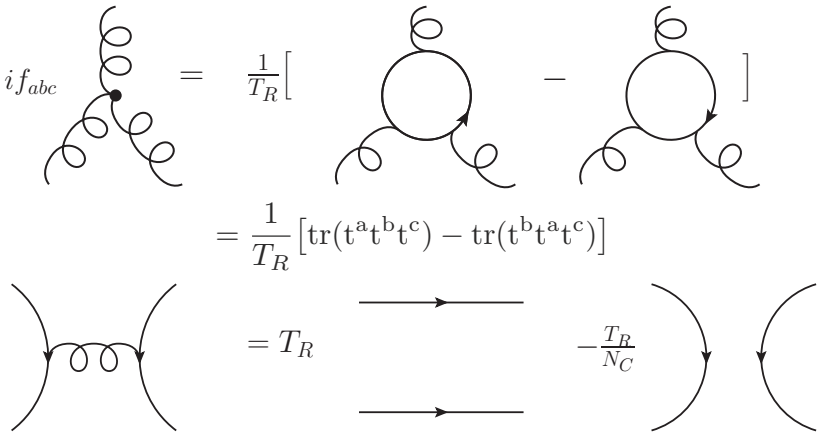

Figure 3.4.: Simplification of the *qqg* and the *ggg* vertices in the colour flow formalism in QCD.

As a concrete example, we present the quark-quark scattering case. In fig. 3.5 the two contributing diagrams to the process are presented, showing in the large-N_C limit the colour connection between the external lines. The basis elements could be read from the figure directly,

$$c_1 = \frac{1}{N_C}\delta_{i_1}^{j_2}\delta_{i_3}^{j_4} \quad , \quad c_2 = \frac{1}{N_C}\delta_{i_1}^{j_4}\delta_{i_3}^{j_2}\,. \tag{3.36}$$

The metric and its inverse, which are defined in eq. 3.33, are therefore

$$c_{\alpha\beta} = \begin{pmatrix} 1 & \frac{1}{N_C} \\ \frac{1}{N_C} & 1 \end{pmatrix} \quad , \quad c^{\alpha\beta} = \begin{pmatrix} 1 & -\frac{1}{N_C} \\ -\frac{1}{N_C} & 1 \end{pmatrix}, \tag{3.37}$$

thus, the soft anomalous dimension is

$$\Gamma_{\alpha\beta} = \frac{N_C^2 - 1}{N_C^2}\begin{pmatrix} T & \frac{1}{N_C}(T-U) \\ \frac{1}{N_C}(T-U) & 0 \end{pmatrix}. \tag{3.38}$$

In this simple example it is easy to see that off-diagonal elements are suppressed by a N_C factor: this feature is present in any process, and therefore the large-N_C approximation can be implemented by simply extracting the diagonal matrix from the soft-anomalous dimension. This is a nice approximation, which helps us to relate and compare the resummed results to the standard parton shower approach.

In an ordinary calculation, given the size of this matrix and the dimensionality of the bases as in tab. 3.1, one of the intrinsic complications is the evaluation of the exponential of this matrix. Within SHERPA the software libraries chosen allow the computation of up to 8 legs in the final state in a reasonable amount of time. This is far beyond the previous state of the art for NLL resummed calculation at hadron colliders.

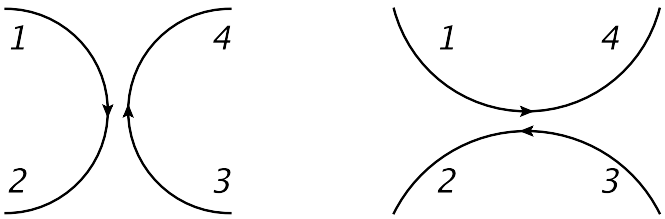

Figure 3.5.: The two colour flow diagrams contributing to the qq' scattering. They are related to the s and t or u Feynman diagrams, respectively.

Subprocess	gggg	5g	6g	7g
Dim. basis	5	16	79	421

Table 3.1.: Dimension of the non-orthogonal bases for subprocesses with gluons. The colour flow is rapidly increasing with the further addition of a gluon leg. Results extracted from [133].

Combining the colour-ordered partial amplitudes available through COMIX, and the soft anomalous dimension computed in the proper basis, it is possible to obtain a prediction for the soft function in a Monte Carlo-fashion. We have to note that some pathologies related to $N_C = 3$ due to the non-orthogonality, and therefore over-completeness of the basis, have to be taken into account [133].

In fig. 3.6 we show a comparison of the resummed result for the thrust distribution $1/\sigma \mathrm{d}\sigma/\mathrm{d}\tau$, for the subprocess $gg \to gg$, at $\sqrt{s} = 14\,, 100\,,$ TeV: the difference in the two distributions comes from the evaluation of the colour flow, that is exactly the computation of the Γ matrix. The red line describes the full colour evaluation, whereas the blue one labels the large-N_C approximation. It is worth noting that the difference in the colour evaluation does not change between the two different centre of mass energies, meaning that the kinematics does not affect the colour flow. The large-N_C approximation is there obtained simply keeping the diagonal Γ matrix, suppressing all off-diagonal entries. The only effect of the increased energy is to shift the maximum value for thrust to higher values: this is understood when noting that more energy allows for a larger phase space. Nevertheless, matching is here not considered, and in any case the maximum allowed value for thrust would not change between the LHC and an FCC. From this reasoning, we could derive that in principle, the leading colour behaviour could already be well described by the parton shower also at higher energies, given that the colour flow contribution seems not to dramatically change the results. We stress here that, by construction, the gluonic channels are widely influenced by the colour algebra. The overall effect on $pp \to jj + X$ is reduced when considering all the scattering channels:

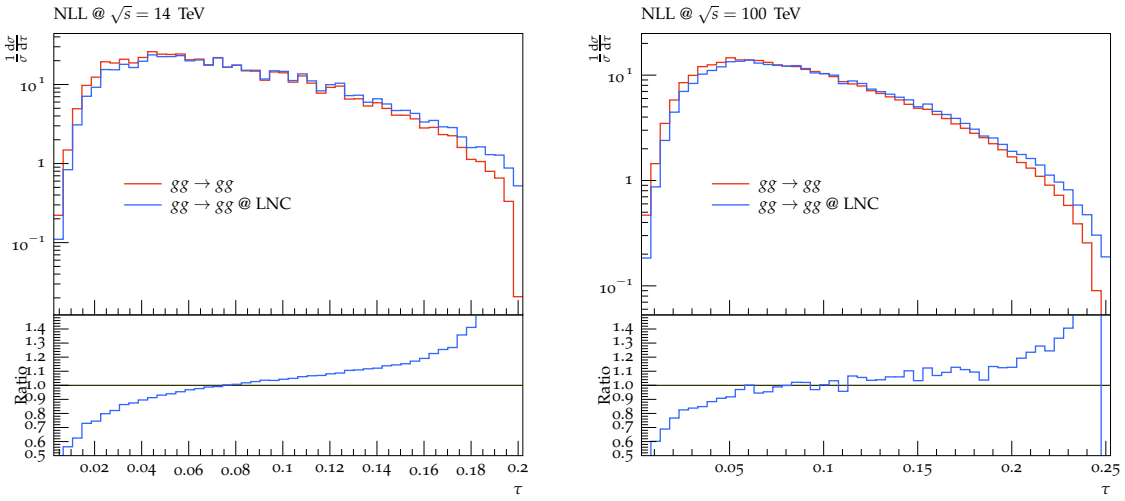

(a) (b)

Figure 3.6.: Resummed distributions for subprocess $2 \to 2$ with 4 gluons, at 8 GeV. Comparison between the large-N_c and full color-flow at $\sqrt{s} = 14$ TeV in (a) and $\sqrt{s} = 100$ TeV in (b).

this is indeed due to the fact that the matrix element is contributing less to the overall process, and the effect is averaged out by the other kinematic channels, with less colour flow contributions, as those represented in fig.3.5.

3.1.3. Matching fixed-order to all-order

In complete analogy to what happens when matching matrix element to the parton shower, a matching prescription is needed for the resummation. The resummation approach is valid in the logarithmic enhanced region of the phase space of the observable under consideration, $\alpha_s L \lesssim 1$. Outside this regime the resummed prescription adds spurious terms that spoil the perturbative calculation.

Some techniques have been developed already in [72]; the difficulty arises from the ambiguity in the matching prescription which comes from the non-logarithmic terms, what we have defined for a general exponentiated expression the "remainder" in eq. 2.74, and in general by the truncation of the perturbative expansion at a given order. The only rigorous statement of the factorisation theorem is

$$\log f(v) = \log C(\alpha_s) + \log \exp[G(\alpha_s, \log 1/v)] + \text{vanishing terms} \qquad v \to 0\,, \qquad 3.39$$

where we label with *vanishing terms* contributions canceling order by order in perturbation theory. Thus, in general it is possible to construct a resummed prescription with different functions, which fulfil eq. 3.39

$$f(v) = \tilde{C}(v, \alpha_s) \exp\left[\tilde{G}(\alpha_s, \log 1/v)\right] + \tilde{D}(v, \alpha_s)\,, \qquad 3.40$$

leading to the uncertainty in defining a unique recipe.

The "log-R" prescription [72] and the multiplicative "mod-R" ones [141] are the most widely employed in order to compare experimental measurements and analytical resummation, as in [142]. They are defined at lowest order, respectively by

$$f(v) = \frac{\tilde{f}(v)}{\tilde{f}_{\max}(v)}\,, \qquad \tilde{f}_{\text{log-R}}(v) = \frac{1}{\sigma_0+\sigma_1}\left[\tilde{\Sigma}_r \exp\left(\frac{\Sigma_1(v)-\tilde{\Sigma}_{r,1}(v)}{\sigma_0}\right)\right] \tag{3.41}$$

$$\tilde{f}_{\text{mod-R}}(v) = \frac{1}{\sigma_0+\sigma_1}\left[\tilde{\Sigma}_r(1-v/v_{\max})\left(1+\frac{\Sigma_1(v)-(1-v/v_{\max})\tilde{\Sigma}_{r,1}}{\sigma_0}\right)\right]. \tag{3.42}$$

We have defined $\Sigma(v)$ as the partial integrated cross section as in eq. 3.3. The algorithms are based on the subtraction of the divergent terms in the fixed-order result, which are correctly described by the resummed result. The r superscript labels the resummed distribution, and the $r,1$ denotes the expanded resummed result at first order, that cancels the divergence in the fixed-order calculation. The 0 and 1 indices label the order in the perturbative expansion and $\tilde{\Sigma}$ indicates the usage of the modified logarithmic prescription

$$\tilde{L} = \frac{1}{p}\log\left(\left(\frac{1}{x_V v}\right)^p - \left(\frac{1}{x_V v_{\max}}\right)^p + 1\right), \qquad x_V = X\cdot X_V\,, \tag{3.43}$$

where $v_{\max}$ is the maximum kinematically allowed value for the event shape under consideration. This modification of the logarithmic structure is indeed necessary for the matching to get the proper maximum kinematical value, defining $\tilde{L}(v_{\max}) = 0$. x_v and p modifies the logarithm respectively at low and high values of the observable v, and they introduce terms that are subleading at NLL accuracy [142].

For a more convenient Monte Carlo implementation, quantities should be differentials, in this way suitable for an event by event generation and analysis. Therefore, the following matching to fixed-order perturbative result is adapted [133]

$$\frac{\mathrm{d}\sigma^{\text{matched}}}{\mathrm{d}v} = \frac{\mathrm{d}\sigma^{\text{r}}}{\mathrm{d}v} + \left(\frac{\mathrm{d}\sigma^{\text{FO}}}{\mathrm{d}v} - \frac{\mathrm{d}\sigma^{r,1}}{\mathrm{d}v}\right), \tag{3.44}$$

where σ^{r},σ^{FO} and $\sigma^{r,1}$ are the full resummed, perturbative fixed-order and first order expansion of the fully resummed cross-section, respectively. The last two terms are separately divergent, but the combination is finite. In fig. 3.7 we present the matching prescription of eq. 3.44 for a single event in the phase space for three-jet production at a lepton-lepton and DIS colliders respectively. The modified logarithmic prescription in eq. 3.43 is in these results already implemented, such that the maximum value for the resummed distribution matches exactly the maximum kinematical value allowed, $v = 1/3$, for thrust with three jets in the final state.

In the SHERPA implementation, this proceeds as follow. The resummed and expanded differential distributions in eq. 3.44 are directly computable within the CAESAR framework, exploiting the soft function described in section 3.1.2. The expanded resummed

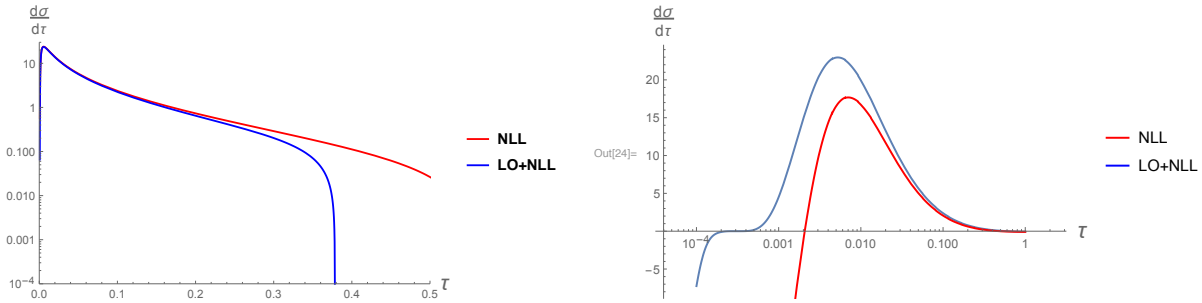

Figure 3.7.: Complete NLL and matched to LO resummed distribution for thrust τ at e^+e^- (left) and for DIS process (right). Arbitrary units. The distribution is not integrated over the whole phase space, but evaluated just for one point. To note, especially in the left case, the right behaviour of the matched distribution, that falls to 0 reaching the physical maximum allowed value of thrust for a final state of 3 partons - that is 1/3.

functions are defined as following

$$G_{12} = -\sum_{\ell=1}^{n} \frac{C_\ell}{a+b_\ell} \,, \tag{3.45}$$

$$G_{11} = -\left[\sum_{\ell=1}^{n} C_\ell \left(\frac{B_\ell}{a+b_\ell} + \frac{1}{a(a+b_\ell)}\left(\log \bar{d}_\ell - b_\ell \log\frac{2E_\ell}{Q}\right) + \frac{1}{a}\log\frac{Q_{12}}{Q}\right)\right. \tag{3.46}$$
$$\left. + \frac{1}{a}\frac{\mathrm{Re}[\Gamma_{\alpha\beta}]H^{\alpha\beta}}{c_{\alpha\beta}H^{\alpha\beta}} + \sum_{\ell=1}^{n_{\text{initial}}} \frac{\int_{x_\ell}^1 P^0_{\ell k}(x_\ell/z)q^{(k)}(z,\mu_F^2)}{2(a+b_\ell)q^{(\ell)}(x_\ell,\mu_F^2)}\right] .$$

It is sufficient to note that the divergent structure and the colour flow in the Γ soft anomalous dimension in eq. 3.29 is comparable to the soft and collinear limit of the Catani-Seymour matrix elements. This is accomplished in SHERPA exploiting the Catani-Seymour subtraction method, as implemented in AMEGIC, after taking into account two major differences:

- replace the kernel $V_{ij,k}$ by the factor $2\log Q_{(ij)k}/Q_{12}$ and rescaling by the a value of the observable parametrisation;
- restrict the splitting function $P_{ij,k}$ on the region of the phase space belonging to the enhanced double-logarithmic term.

In fig. 3.8 are presented the matched and resummed-only results for the process $pp \to jj$ at $\sqrt{s} = 8$ TeV, with asymmetric cuts on the leading jets, $p_{T,1} = 100$ GeV and $p_{T,2} = 80$ GeV. As expected, the resummed distributions considerably differ towards the high values of the τ observable, whereas for $\tau \to 0$ they approach the same value.

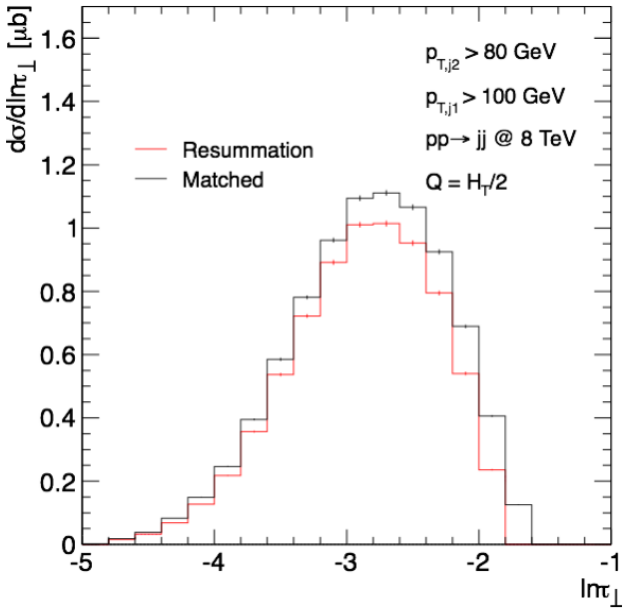

Figure 3.8.: Matched and resummed-only distributions for the process $pp \to jj$ at a hadron collider with $\sqrt{s} = 8$ TeV

3.1.4. A Monte Carlo evaluation of the multiple emissions contribution

Eq. 3.19 is composed of a suppression term coming from the virtual contribution, and an infinite sum over resolved, correlated, emissions:

$$\mathcal{F}(v) = \lim_{\epsilon\to 0} \frac{\epsilon^{R'(v)}}{R'(v)} \sum_{m=0}^{\infty} \frac{1}{m!} \left(\prod_{i=1}^{m+1} \sum_{\ell_i=1}^{n} C_{\ell_i} r'_{\ell_i} \int_\epsilon^1 \frac{\mathrm{d}\zeta_i}{\zeta_i} \int_0^{2\pi} \frac{\mathrm{d}\phi_i}{2\pi} \right) \delta(\log \zeta_1) \times \qquad 3.47$$
$$\times \exp\left(-R'(v) \log \lim_{\bar{v}\to 0} \frac{V(\{p\}, k_1, \ldots, k_{m+1})}{\bar{v}} \right) ,$$

where $\zeta_i = v_i/\bar{v}$. The explicit limit $\epsilon \to 0$ and $\bar{v} \to 0$ and the rIRC conditions ensure that the $\mathcal{F}$ function contains only single logarithms, thanks to the ordering $\log 1/\bar{v} \gg \log 1/\epsilon \gg 1$. The results presented so far for τ at lepton and hadron colliders exploit the fully integrable form of the $\mathcal{F}$ function. Thanks to the simple factorisation of this observable, it is possible to write

$$\tau(\{p\}, \kappa_1(\bar{v}\zeta_1), \ldots, \kappa_m(\bar{v}\zeta_m)) = \sum_i^m \tau(\{p\}, \kappa_i(\bar{v}\zeta_i)) = \bar{v} \sum_i \zeta_i \,, \qquad \text{with } \zeta_i = v_i/\bar{v} \,, \quad 3.48$$

from which we derive a factorised expression for eq. 3.19

$$\mathcal{F} = \lim_{\epsilon\to 0} \frac{\epsilon^{R'}}{R'} \sum_{m=0}^{\infty} \frac{1}{m!} \left(\prod_{i=1}^{m+1} \int_\epsilon^1 \frac{\mathrm{d}\zeta_i}{\zeta_i} \right) \delta(\log \zeta_1) e^{-R' \log \sum_{j=2}^{m+1} \zeta_j} \,. \qquad 3.49$$

The main simplification in eq. 3.49 comes from the last term in eq. 3.47. Because thrust is additive, we can factorise the complex exponential, thus allowing a direct integration. Following ref. [72], we introduce a Mellin transformation, which allows to compute the integral

$$e^{-R' \log \sum_{j=2}^{m+1} \zeta_j} = R' \int \frac{\mathrm{d}Z}{Z} e^{-\log Z} \int \frac{\mathrm{d}\nu}{2\pi i \nu} e^{\nu Z} \prod_{j=2}^{m+1} e^{-\nu \zeta_j} \,, \tag{3.50}$$

through which we obtain the final expression

$$\mathcal{F}(R') = \int \frac{\mathrm{d}\nu}{2\pi i \nu} e^{\nu - R' \log \nu - R' \gamma_E} = \frac{e^{-\gamma_E R'}}{\Gamma(1 + R')} \,, \tag{3.51}$$

where γ_E is the Euler-Mascheroni constant, and Γ is the Euler function.

In general, the evaluation of $\mathcal{F}(v)$ is not as simple as in the case of thrust: in general the event-shape observable parametrisation is not additive, and there could be different coefficients for every leg. This has already been addressed by authors in ref. [132], through a Monte Carlo algorithm. In the following we want to stress the similarity of the Monte Carlo evaluation of the $\mathcal{F}(v)$ with the parton-shower formalism, in order to establish some connections.

The integrals in eq. 3.47 can be evaluated with the *importance sampling* method, carefully described in app. B, with sampling function $g(v) = 1/v$. There are two numerical issues arising, which are the presence of the limit $\lim_{\epsilon \to 0}$ and the sum over an infinite number of emissions. These two elements are however related, since the cutoff ϵ divides exactly the domain in the phase space belonging to the unresolved emissions, providing the exponential Sudakov-like suppression, and the resolved correlated emissions, accounted for exactly through the infinite sum over the index m. We take the fully analytical result for thrust in eq. 3.51 as a benchmark and present two versions of the Monte Carlo evaluated $\mathcal{F}$ function in fig. 3.9, respectively with $\epsilon = 0.01$ and 0.001. As expected, reducing the value of the cutoff increases the number of additional emissions which must be considered: in agreement with the fact that more radiation becomes resolved. In fig. 3.10 is evident how the choice of the cutoff and of the number of additional emissions affect the Monte Carlo evaluation, especially at low values of the cutoff and of the number of legs.

As, for a general observable, for which the $\mathcal{F}(v)$ function is not additive, a full resummed result is not available, in order to generate pseudo-events in a Monte Carlo fashion we have to consider the treatment of the convergence of the series and, therefore, the stopping point of the algorithm. This will depend on the number of subsequent emissions, and on the cutoff scale. This is complete similarity to what happen in the parton shower, but within a fixed theoretical scheme. Hence, we could interpret the values thrown by the Monte Carlo algorithms as the momenta of the particles emitted, as we do in the parton shower approach. For the purpose of the convergence, we sketch the following prescription:

- fix the value of the cutoff, ϵ, and the number of additional legs m;

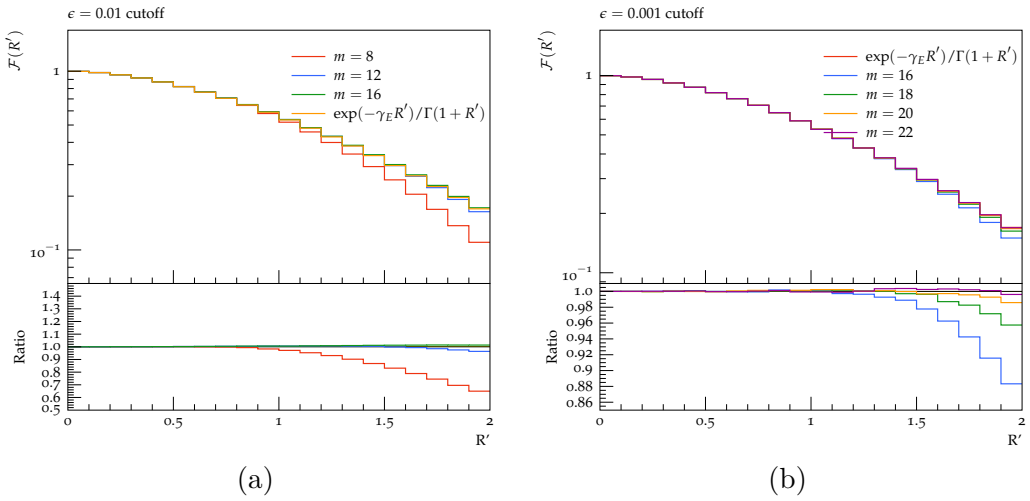

Figure 3.9.: Independent evaluation of the $\mathcal{F}$, with importance sampling, $g(x) = 1/\xi_i$. Different numbers of additional emissions are presented, for a cutoff $\epsilon = 0.01$ in (a) and $\epsilon = 0.001$ in (b). The benchmark is the analytical result for thrust. A different cutoff implies an higher number of additional emissions for the function to converge.

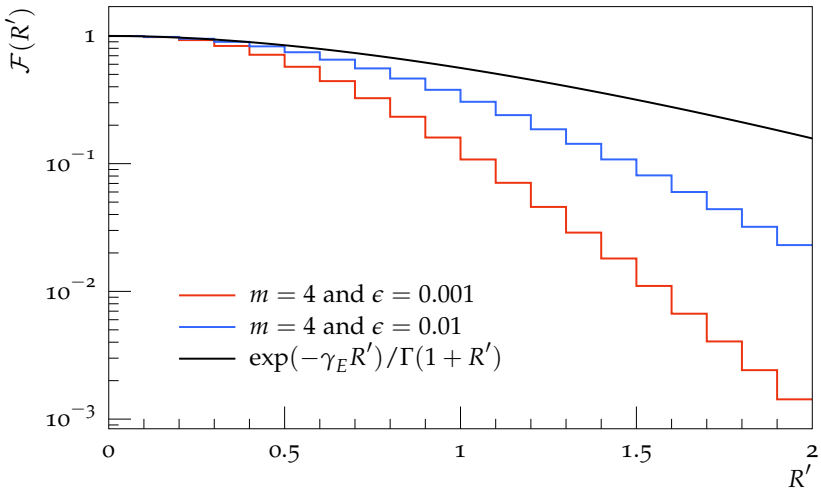

Figure 3.10.: Comparison of the convergence of the Monte Carlo numerical evaluation with different cutoffs $\epsilon = 0.01$ and $\epsilon = 0.001$ and fixed number of additional emissions, $m = 4$.

- divide the R' domain into bins;
- integrate the $\mathcal{F}(R')$ for each bin;
- check the convergence bin-per-bin
- increase the number of legs and restart the algorithm until the convergence coefficient is $c < 0.05$ for each bin.

We use the following estimator for the convergence:

$$c = 1 - \frac{\ell_{n+1}}{\ell_n} \,, \tag{3.52}$$

where we indicate with ℓ the $\mathcal{F}(v)$ evaluated with n additional emissions. This estimator has to be interpreted as the impact of adding a new emission to the previous one. As we know that the emission is in any case ordered in transverse momentum, when we reach a sufficient small cutoff, we can easily say that the convergence is reached. This happens again thanks to the CAESAR initial hypothesis of recursive infrared safety and to the globalness of the observable under consideration. In fig. 3.11 we present results for the last 4 bins in the distribution with $\epsilon = 0.001$ of fig. 3.9. The series converges with $m = 22$.

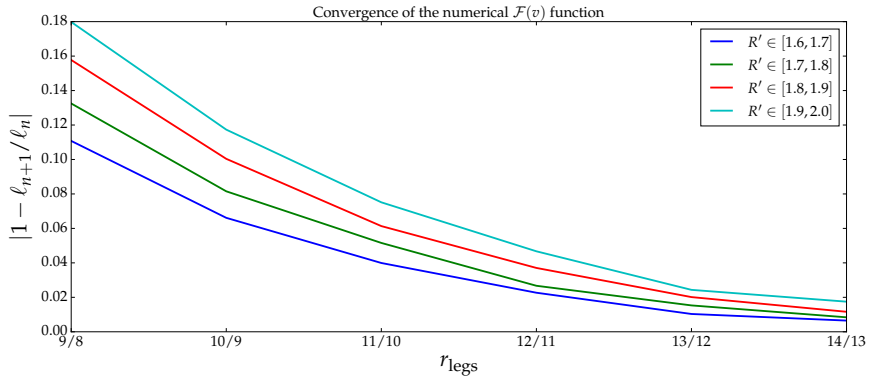

Figure 3.11.: Convergence of the series of integrals in eq. 3.47. We stop adding emissions when the ratio between the values of the evaluation of $1 - \mathcal{F}(v)_{n+1}/\mathcal{F}(v)_n$ at the last bin on the right of the plot is smaller than 0.05.

The Catani-Seymour inspired shower generates momenta, therefore particle candidates, according to the Sudakov form factor

$$\begin{aligned} &\Delta(k^2_{\perp,\max}, k^2_{\perp,0}) = \\ &= \exp\left(-\sum_{ij}\sum_{k\neq ij}\int_{k^2_{\perp,0}}^{k^2_{\perp,\max}} \frac{\mathrm{d}k^2_\perp}{k^2_\perp}\int_{z_{\min}}^{z_{\max}} \frac{\alpha_S(k^2_\perp)}{2\pi} J(y_{ij,k})\langle V_{ij,k}(z_i y_{ij,k})\rangle\right). \end{aligned} \tag{3.53}$$

Here, $k_\perp$ is the transverse momentum of the emission, computed with respect to the parent dipole, that is, with respect to the dipole before any emission. $V_{ij,k}$ is the splitting function for the given spectator, emitter and emitted particles (ij, k), and could be found in chapter 2; $J(y)$ is a jacobian factor emerging from the change of variable, from the transverse momentum $k_\perp$ to the Catani-Seymour y. It has been already shown in ref. [132] that the difference between this and the Caesar one, k_T, gives contributions at order NNLL. Therefore, we can neglect these effects in this analysis. Concerning the z_i longitudinal fraction of the momentum, we can write

$$\xi_i = \frac{v_i}{v_1} = \frac{k_T}{Qv_1}\exp(-\eta) = \frac{k_T^2}{Q^2\tilde{z}_1} \qquad \Longrightarrow \qquad \frac{\mathrm{d}\xi_i}{\xi_i} = \frac{\mathrm{d}z_i}{z_i}, \tag{3.54}$$

using $\eta = \frac{1}{2}\log\frac{\tilde{z}_1}{\tilde{z}_2}$ and $k_T^2 = z_1 z_2 Q$. Here, $\tilde{z}_i$ is computed with respect to the original (parent) dipole. Choosing the proper z, i.e. the one with respect to the emitter, coincides with the choice of the z_i computed in the Catani-Seymour formalism, up to some recoil correction. This correction contributes anyway beyond next-to-leading log accuracy. In addition, the CAESAR formalism for NLL resummation only takes into account the primary emission off a leg, which avoids furthermore big differences in the recoil contribution, given that the difference in the transverse momentum and longitudinal fraction is of order $\sim z_{i-1}k_\perp$. In Fig. 3.12 the sampling of k_T and z from properly

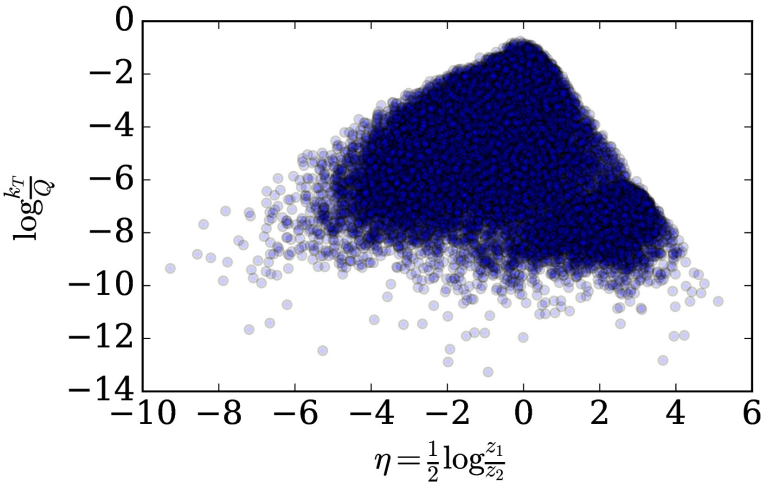

Figure 3.12.: Lund plane pattern of emissions with k_T and z computed as in the Caesar prescription.

adapted SHERPA is shown. This is in agreement with the boundaries of the typical Lund-plane variables plot, as one could argue from fig. 3.1.1, by remapping the variables. This suggests that further studies could be performed in order to directly employ the parton shower as a sampler for the $\mathcal{F}$ integration.

In this paragraph we have shown one example of how the resummation formalism can play a role in foreseeing how QCD phenomena evolve with the increasing centre of mass energy at a hadronic collider. We have presented original results on the colour flow, and an approach to compute the single logarithmic function $\mathcal{F}(v)$ exploiting Monte Carlo algorithms, and that could be easily implemented within SHERPA. In the following we describe another, different, case, in which resummation and analytical QCD results can help improve the understanding of current techniques, and how the evolution of these will look like in an FCC-like environment.

3.2. All-orders average jet multiplicities

Jet production at hadron colliders is one of the most striking signatures of the validity of QCD as the theory of strong interactions. As introduced in chapter 2, the generalised k_t algorithms are widely employed at colliders. With these kind of prescriptions, it is, in fact, possible to have a good handling on the underlying theoretical properties of the event. Through the coherent branching formalism and the related *generating functionals*, it is possible to compute jet rates and jet average multiplicities in a similar fashion to resummation. These are global quantities, as the phase space is sliced in term of the resolution parameter of the particular jet algorithm, and therefore do not suffer of the presence of any non-global logarithms. The boundary condition coming from the jet algorithm is equivalent to the IR cutoff condition appearing in the branching algorithm or in the parton shower, as in eq. 2.65.

Our aim is to revise the generating function formalism, following ref. [143], and to employ the analytical results there achieved to predict the inner structure of jets produced at a future hadron collider at $\sqrt{s} = 100$ TeV. In collisions at the LHC, in particular during Run II, several techniques for reconstructing hadronically decaying boosted objects have been developed and widely employed [144–154]. They are all joined by the fact that they exploit jet substructures: the main idea behind this being that a jet originating from QCD radiation is intrinsically different from one stemming from the decay of heavy resonances. The more these objects are boosted, the narrower decay products become, such that, by reconstructing the object as jet with a slightly larger cone size than usual, $R \approx 1.0$, it is possible to capture all the radiation from the parent particle within a single jet. By boosted objects we mean particles with scales $p_T^2 \gg m_V^2$, where m_V is the mass of the particle under consideration. Variables are then constructed in order to highlight the intrinsic differences between the objects. For example, one of the variables employed is subjettiness. The theoretical question arising is: are we able to predict jet substructures? In particular, in our work, we try to address whether the all-order methods employed at the LHC will also be valuable in an extreme environment such as a 100 TeV hadron collider.

3.2.1. Generating functional formalism

The generating functional formalism allows for a precise treatment of the soft and collinear singularities arising in QCD radiation. This is accomplished through successive derivations of the generating functionals, that are differently defined for gluons and quarks and for different processes. The algorithms for which the following discussion applies are described in sec. 2.1.4. In particular, the good theoretical properties of the generalized k_t algorithms are optimal, when combined with this analytical approach, in order to gain further understanding of QCD evolution within a jet. The logarithms we discuss here always stem from the existence of soft and collinear radiation, and are mainly of the form $\log 1/R$ and $\log Q/E_R$, where R is the resolution parameter of the algorithm, Q the hard scale of the process and E_R the minimum jet energy.

The evolution scale for coherent parton showering is $\xi \equiv 1-\cos\theta$ with θ the emission angle. The probability to have a single resolvable gluon, emitted from a quark of energy E at a scale ξ is computed in term of the Altarelli-Parisi splitting kernels,

$$\mathcal{P}_q(E,\xi) = \int_{\xi_R}^{\xi} \frac{d\xi'}{\xi'} \int_{E_R/E}^{1} dz \frac{\alpha_s(k_t^2)}{2\pi} P_{gq}(z) \ , \tag{3.55}$$

where the running coupling is evaluated at the transverse momentum scale of the emission, $k_t^2 = z^2E^2\xi'$, as shown also in the last section,

$$\frac{\alpha_s(k_t^2)}{\pi} = \frac{1}{b_0 \ln(z^2E^2\xi'/\Lambda^2)} \tag{3.56}$$

with $b_0 = (11C_A - 2n_f)/12$. Defining $\bar{\alpha}_s = \alpha_s(E^2\xi)/\pi$, i.e. in terms of the coupling at the hard scale, we can rewrite at next-to-double-log accuracy (NDLA)

$$\frac{\alpha_s(k_t^2)}{\pi} = \bar{\alpha}_s - b_0\bar{\alpha}_s^2 \left[2\ln z + \ln\left(\frac{\xi'}{\xi}\right)\right] \tag{3.57}$$

and

$$\begin{aligned}\mathcal{P}_q(E,\xi) = {} & C_F\bar{\alpha}_s \ln\left(\frac{\xi}{\xi}_R\right)\left[\ln\left(\frac{E}{E_R}\right) - \frac{3}{4}\right] + \\ & \frac{1}{2}C_F b_0\bar{\alpha}_s^2 \ln\left(\frac{\xi}{\xi}_R\right)\ln\left(\frac{E}{E_R}\right)\left[2\ln\left(\frac{E}{E_R}\right) + \ln\left(\frac{\xi}{\xi}_R\right)\right] \ .\end{aligned} \tag{3.58}$$

The probability for no-resolvable emissions is expressed in term of the Sudakov form factor

$$\Delta_q(E,\xi) = \exp\left[-\mathcal{P}_q(E,\xi)\right] \ . \tag{3.59}$$

By definition, the generating function for resolved jets from a quark ($i=q$) or gluon ($i=g$) of energy E at scale ξ is [41, 42, 155]

$$\Phi_i(u,E,\xi) = \sum_{n=0}^{\infty} u^n \, R_n^i(E,\xi) \ , \tag{3.60}$$

where R_n^i is the corresponding n-jet rate, which is the probability of finding n resolved jets. The jet rates can be recovered from the generating function by successive differentiation at $u = 0$:

$$R_n^i(E,\xi) = \frac{1}{n!}\frac{\partial^n}{\partial u^n}\Phi_i(u,E,\xi)\bigg|_{u=0} . \tag{3.61}$$

The average multiplicity of resolved jets is obtained by differentiating at $u = 1$. Writing the average jet multiplicity from a quark or gluon of energy E at scale ξ as $\mathcal{N}_i(E,\xi)$, we have

$$\mathcal{N}_i(E,\xi) = \sum_{n=0}^{\infty} n\, R_n^i(E,\xi) = \frac{\partial}{\partial u}\Phi_i(u,E,\xi)\bigg|_{u=1} . \tag{3.62}$$

The generating functions, $\Phi_{q,g}$, must thus satisfy the boundary condition

$$\Phi_i(u,E,\xi_R) = 1 + (u-1)\Theta(E - E_R) . \tag{3.63}$$

The generating function for e^+e^- annihilation at centre of mass energy E_{cm} is that for two quarks of energy $E_{\mathrm{cm}}/2$, each filling one hemisphere:

$$\Phi_{ee} = [\Phi_q(u, E_{\mathrm{cm}}/2, 1)]^2 . \tag{3.64}$$

We expect that initial state radiation does not significantly affect the parton content in the reconstruction of a boosted object, and therefore we employ the results obtained in ref. [143], though in principle one should take the showering effects from the initial PDFs into account. In any case, we expect that the contribution of the initial radiation to the jet substructure to be negligible. Defining suitable variables

$$\kappa \equiv \log E/E_R \qquad , \qquad \lambda \equiv \log \xi/\xi_R , \tag{3.65}$$

we write the average jet multiplicity from the jet rates, obtaining at order $\mathcal{O}(\alpha_s^3)$

$$\begin{aligned}\mathcal{N}_{LL} = 2 &+ \bar{\alpha}_s\left(2\kappa\lambda - \frac{3}{2}\lambda\right)C_F \\ &+ \bar{\alpha}_s^2\left(\frac{1}{2}C_A\kappa\lambda + 2b_0(2\kappa+\lambda) - \frac{5}{3}C_A\lambda + \frac{1}{6}n_f\lambda\right)C_F\kappa\lambda \\ &+ \bar{\alpha}_s^3\left(\frac{1}{18}C_A^2\kappa\lambda + \frac{1}{2}b_0C_A(2\kappa+\lambda) + \frac{1}{18}n_fC_F\lambda - \frac{31}{72}C_A^2\lambda\right)C_F\kappa^2\lambda^2 .\end{aligned} \tag{3.66}$$

Here, the terms in b_0 originate from including the running coupling expression. We see that these terms enhance the average jet multiplicity with respect to a fixed-coupling calculation.

To achieve a NDLA result as in ref. [156], we write in terms of the generating functions,

$$\mathcal{N}(E,\xi) = \frac{\partial\Phi_{ee}}{\partial u}\bigg|_{u=1} = 2\,\frac{\partial\Phi_q}{\partial u}\bigg|_{u=1} = 2\mathcal{N}_q \tag{3.67}$$

where $\mathcal{N}_{q,g}$ is the average quark and gluon jet multiplicities and satisfies the equations

$$\mathcal{N}_q(E,\xi) = 1 + \int_{\xi_R}^{\xi} \frac{d\xi'}{\xi'} \int_{E_R/E}^{1} dz \frac{\alpha_s(k_t^2)}{2\pi} P_{gq}(z) \mathcal{N}_g(zE,\xi') \tag{3.68}$$

$$\begin{aligned}\mathcal{N}_g(E,\xi) = 1 + \int_{\xi_R}^{\xi} \frac{d\xi'}{\xi'} \int_{E_R/E}^{1} dz \frac{\alpha_s(k_t^2)}{2\pi} \{ & P_{gg}(z) \mathcal{N}_g(zE,\xi') \\ & + P_{qg}(z) \left[2\mathcal{N}_q(E,\xi') - \mathcal{N}_g(E,\xi') \right] \} \, .\end{aligned} \tag{3.69}$$

It can be shown [143] that the expressions for the average jet multiplicities in terms of the logarithmic variables in eq. 3.65 are equivalent to the following partial derivatives equation (PDE)

$$\frac{\partial^2 \mathcal{N}_q}{\partial\kappa\partial\lambda} = C_F \bar{\alpha}_s \left(\mathcal{N}_g - \frac{3}{4} \frac{\partial \mathcal{N}_g}{\partial \kappa} \right) \, , \tag{3.70}$$

with boundary conditions $\mathcal{N}_q(\kappa,0) = \mathcal{N}_q(0,\lambda) = 1$.

Similarly, we find from eq. 3.69

$$\frac{\partial^2 \mathcal{N}_g}{\partial\kappa\partial\lambda} = \bar{\alpha}_s \left[C_A \mathcal{N}_g - \left(\frac{11}{12} C_A + \frac{n_f}{6} \right) \frac{\partial \mathcal{N}_g}{\partial \kappa} \right] + \frac{n_f}{3} \bar{\alpha}_s \frac{\partial \mathcal{N}_q}{\partial \kappa} \, , \tag{3.71}$$

where to the required accuracy, we may set, in the last term

$$\frac{\partial \mathcal{N}_q}{\partial \kappa} = \frac{C_F}{C_A} \frac{\partial \mathcal{N}_g}{\partial \kappa} \, , \tag{3.72}$$

so that finally

$$\frac{\partial^2 \mathcal{N}_g}{\partial\kappa\partial\lambda} = \bar{\alpha}_s \left[C_A \mathcal{N}_g - \left(\frac{11}{12} C_A + \frac{n_f}{6} - \frac{n_f C_F}{3 C_A} \right) \frac{\partial \mathcal{N}_g}{\partial \kappa} \right] \, , \tag{3.73}$$

with boundary conditions $\mathcal{N}_g(\kappa,0) = \mathcal{N}_g(0,\lambda) = 1$.

Note that the n_f dependence in eq. 3.73 is very weak and vanishes in the large-N_C limit:

$$\frac{n_f}{6} - \frac{n_f C_F}{3 C_A} = \frac{n_f}{6 N_C^2} = \frac{n_f}{54} \, . \tag{3.74}$$

This is because at large N_C a $q\bar{q}$ pair from gluon splitting radiates like a gluon, due to the similar overall charge.

Dropping the non-singular parts of the splitting functions, we have

$$\mathcal{N} = 2\mathcal{N}_q = 2 + 2 \frac{C_F}{C_A} \left(\mathcal{N}_g - 1 \right) \, , \tag{3.75}$$

where

$$\frac{\partial^2 \mathcal{N}_g}{\partial\kappa\partial\lambda} = C_A \bar{\alpha}_s \mathcal{N}_g \, . \tag{3.76}$$

In the leading double log approximation DLA , α_s is constant. Then the solution to eq. 3.76 is a modified Bessel function:

$$\mathcal{N}_g(\kappa,\lambda) = \sum_{n=0}^{\infty} \frac{(C_A \bar{\alpha}_s \kappa\lambda)^n}{(n!)^2} = I_0 \left(2\sqrt{C_A \bar{\alpha}_s \kappa\lambda} \right) \, . \tag{3.77}$$

The asymptotic behaviour for large argument of the modified Bessel function, $y \propto \bar{\alpha}_s \kappa \lambda$,

$$I_0(y) \sim \frac{e^y}{\sqrt{2\pi y}} \,, \tag{3.78}$$

implies that, for high energy and small cone size,

$$\mathcal{N}_{ee} \sim 2\left(1 - \frac{C_F}{C_A}\right) + \frac{C_F}{\sqrt{\pi} C_A} \left[C_A \bar{\alpha}_s \ln\left(\frac{E_{\text{cm}}}{2E_R}\right) \ln\left(\frac{1}{\xi_R}\right)\right]^{-\frac{1}{4}} \times \exp\left[2\sqrt{C_A \bar{\alpha}_s \ln\left(\frac{E_{\text{cm}}}{2E_R}\right) \ln\left(\frac{1}{\xi_R}\right)}\right] . \tag{3.79}$$

Taking into account the running of $\bar{\alpha}_s$ to NLO, we have

$$\frac{\partial^2}{\partial\kappa\partial\lambda} I_0\left(2\sqrt{C_A \bar{\alpha}_s \kappa\lambda}\right) = [1 - b_0(2\kappa + \lambda)\bar{\alpha}_s + \mathcal{O}(\alpha_s^2)] I_0\left(2\sqrt{C_A \bar{\alpha}_s \kappa\lambda}\right) \,. \tag{3.80}$$

Thus, if we drop terms of relative order α_s^2, the solution to eq. 3.76 is

$$N_g = [1 + b_0(2\kappa + \lambda)\bar{\alpha}_s]\, I_0\left(2\sqrt{C_A \bar{\alpha}_s \kappa\lambda}\right) \,, \tag{3.81}$$

which agrees with the b_0-dependent terms in eq. 3.66. However, for large κ and/or λ, $b_0(2\kappa + \lambda)\bar{\alpha}_s \sim 1$ and therefore we need to take into account the running of α_s to all orders.

Treating the running of α_s to all orders but still neglecting the finite parts of the splitting functions, we have in place of eq. 3.76

$$\frac{\partial^2 \mathcal{N}_g}{\partial\kappa\,\partial\lambda} = c_g \frac{\mathcal{N}_g}{(2\kappa + \lambda + \mu)} \,, \tag{3.82}$$

with $c_g = C_A/b_0$. These equations are not easy to solve and a solution could be more easily found through a numerical discretisation method, which we describe in detail in app. C. The building blocks are now ready, and we can use these results for generating predictions and comparing with simulations at a potential 100 TeV future hadron-hadron collider.

3.2.2. Results at a 100 TeV hadron collider

In light of the formalism just described, we discuss in the following how the generating functionals could be used in order to trace results obtained with parton showers, in particular with Sherpa. Furthermore, as we did for the thrust case, we discuss which implications these results can have in the design of a future circular collider. Results presented in this paragraph were first presented in [116].

Large-area QCD jets, "fat-jets", are assumed to contain the hadronic decay products of the produced resonance, as well as the majority of the associated QCD radiation. Their use at colliders is prototypical for jet substructure analyses. Subjet methods are based

on the fact that the subjet structures originating from the decay of heavy boosted objects appear substantially different from a standard QCD jet. Two-body decay kinematics, as in the gauge bosons or the Higgs decays, lead to two-prong subjet structures, while the top quark originates a three-prong one. Mass constraints on the reconstructed subjets help to increase the discriminating power of these techniques.

At the LHC, typical radii for such fat-jets are of the order of $R \approx 1$, but it is clear that larger boosts – larger transverse momenta – will necessitate smaller radii, usually of the order of $R \approx 2M/p_T$, where M is the mass of the heavy particle. Assuming a top quark with a transverse momentum of around 3.5 TeV, originating from a hypothetical 7 TeVresonance, the resulting fat-jet will have a radius of around $R \approx 0.1$ only. This clearly poses a considerable challenge for the granularity of future detectors, and it is nicely depicted in fig. 3.13. In this figure we show the distances between the jet axis and the first subjet in p_T are shown. It is evident how with the increasing boost of the jet, the subjets become narrower, up to be collimated in a region of $\mathrm{d}R \sim 0.01$.

We simulate with SHERPA the W and top productions and hadronic decays at $\sqrt{s} =$ 100 TeV; the simulation comprises showering and hadronisation. We reconstruct the *fat* jet with the anti-k_t algorithm with a parameter $R = 1.0$, and match it to the truth-particle in the Monte Carlo parton level event. Subjets are reconstructed with the anti-k_t algorithm with a parameter $R = 0.1$. In fig. 3.13 we present the $\Delta R(j, j_{0,1})$, the distance between the first subject and the jet-axis; subjets are ordered in transverse momentum. We present events for top quark, W gauge boson and QCD di-jet processes. The reconstruction is organised such that we divide in different slices of transverse momentum the reconstructed jets: results are depicted for the ranges $p_T \in (0.5, 1)$-$(1, 2)$-$(2, 5)$-$(5, 10)$ TeV. Boosted objects with $p_T > 2$ TeV become so collimated that the subjects lay within the $R = 0.05$ region of the fat jet. This indicates that the decaying objects are so near in the phase space that the $\eta-\phi$ resolution of the detector will probably not be enough for observing two different objects. This is just an assumption based on the fact that nowadays detectors have a resolution $\eta - \phi \sim 0.05 \times 0.01$[1], motivating a deeper study and design of detectors and techniques for a 100 TeV collider project.

However, assuming suitable fat-jets have been identified, specialised tagging methods are used, which analyse their substructure. This is achieved through, for example, re-clustering the large-jet constituents into smaller subjets, or in terms of jet-shape like measures. For reviews of the currently available techniques see Refs. [144,157–159]. Vital for all these approaches is a good theoretical understanding of both the backgrounds from pure QCD jets and the radiation pattern of the heavy resonance and its decay products. The complexity of the tagging methods used often allows for a comparison of the response from different Monte-Carlo generators only. However, there is a lot of activity to develop predictive analytical techniques, see for instance Refs. [160–165].

In the following the focus will be on some rather coarse feature of large-area QCD jets at high transverse momentum, namely the mean number of small-R subjets $\langle n_{\text{subjets}} \rangle$ found inside fat-jets. Results will be finally compared to the corresponding observable

[1] for what concern trackers - calorimeters have usually less resolution power

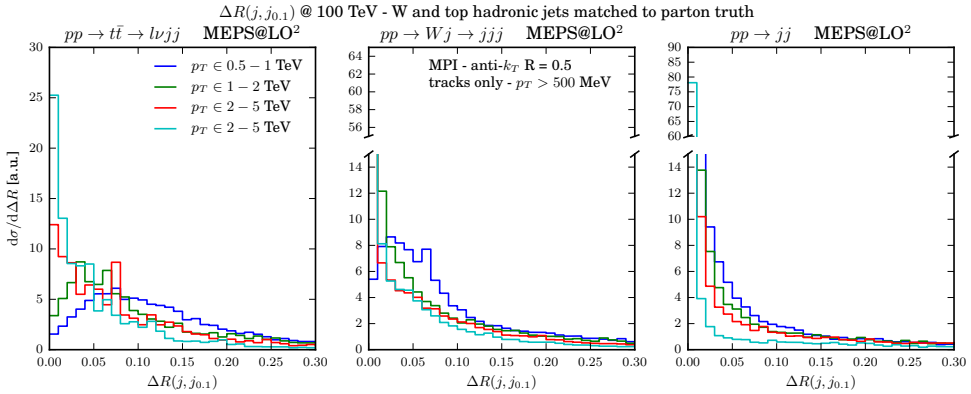

Figure 3.13.: $\Delta R(j_i)$ of different topologies of boosted jets, reconstructed with the Cambridge-Aachen algorithm. This is the distance between the jet axis and the first subjet (ordered in transverse momentum). Categories fall in different slices of the transverse momentum of the reconstructed jet, p_T. We can notice how with the increasing boost, the subjets become narrower. Process simulated for top hadronic decay, W hadronic decay and QCD jets samples with SHERPA, at $\sqrt{s} = 100$ TeV. MEPS@LO^2 stands for the fact we merged samples up to the second real emission for the process under consideration.

for highly-boosted hadronic decays of top quarks and W-bosons. The number of subjets found inside a larger jet is expected to carry information on the QCD colour charge of the jet initiating particle. Broadly speaking, at lowest order one expects the scaling behaviour $\langle n_{\text{subjets}} \rangle \propto C_A$ for colour octets and $\langle n_{\text{subjets}} \rangle \propto C_F$ for colour triplets. Based on such considerations one can attempt to discriminate gluon from quark jets [166, 167], i.e. assign a corresponding likelihood based on the jet-internal QCD activity. For hadronic decays of colour singlets, a reduced and more collimated QCD radiation can be expected, resulting in a smaller number of subjets to be found. Considering the physics case of highly-boosted hadronic decays, rather small radii R_{subjet} need to be considered.

To set the stage, Fig. 3.14 compiles the expectation for the average number of anti-k_T subjets found inside large-area Cambridge–Aachen jets of size $R_{C/A} = 1.0$ [168] as a function of the fat-jet transverse momentum. This potentially allows contact to be made with LHC results in the future. Results are obtained from a SHERPA dijet simulation, invoking parton showers but neglecting any non-perturbative corrections, like parton-to-hadron fragmentation and the underlying event. While the results shown here were obtained from the parton shower based on Catani–Seymour dipoles [62], they have carefully been checked and confirmed using the independent DIRE shower implementation [169] in SHERPA.

In all results, two benchmark values for R_{subjet} are considered, $R_{\text{subjet}} = 0.05$ and 0.1.

Furthermore, two threshold values for the subjet transverse momentum are used, namely $p_T^{\text{subjet}} > 20$, 10 GeV. Clearly, $\langle n_{\text{subjets}} \rangle$ grows with smaller R_{subjet} and p_T^{subjet} cut. For the mixture of quark and gluon jets given by the LO matrix elements in this calculations setup, a mean number of subjets of $\langle n_{\text{subjets}} \rangle \approx 5$ for $p_T^{\text{fat}} = 3.5$ TeV, $p_T^{\text{subjet}} > 10$ GeV and $R_{\text{subjet}} = 0.1$ is found. In the following, the LO matrix elements for quark and gluon production will be considered separately, in order to contrast them individually. However, for all considered parameter choices the slope of the $\langle n_{\text{subjets}} \rangle$ distributions levels off for large values of the fat-jet p_T, corresponding to very collimated jet-energy profiles. In this regime of large p_T, the actual jet inside the fat-jet area becomes to be of a size comparable to the subjet size, and it becomes increasingly harder to push more subjets into the jet.

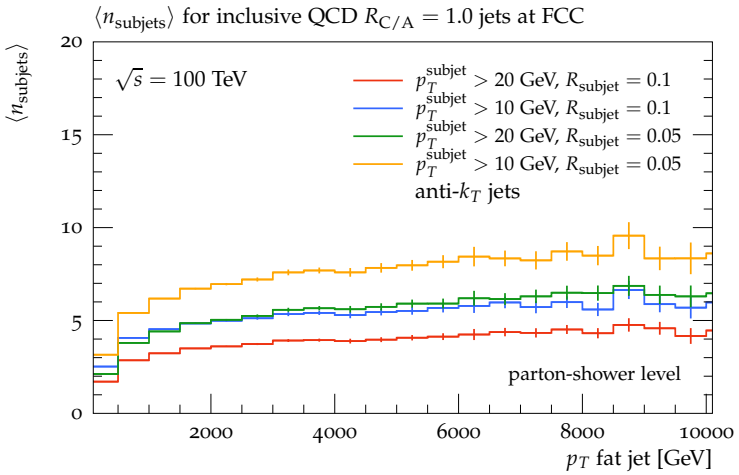

Figure 3.14.: Average number of subjets inside Cambridge–Aachen jets of $R = 1.0$ in inclusive QCD-jet production. Subjets are reconstructed using the anti-k_T jet finder with $R_{\text{subjet}} = 0.05$, 0.1 and $p_T^{\text{subjet}} > 10$, 20 GeV. Results are presented at parton level.

Using very small R_{subjet} and p_T^{subjet} is not only an experimental challenge for reconstruction algorithms but also induces large logarithms that need to be resummed in order to obtain a reliable prediction. We employ in the following generalised longitudinally-invariant k_T algorithms, k_T, anti-k_T and Cambridge-Aachen, we already described in chapter 2. For this class of jet algorithms there are predictions resummed for small R to all-orders of $(\alpha_s \log R^2)$ [170, 171], and for small R and small transverse-momentum threshold $p_{T,\text{min}}$ of $(\alpha_s \log R^2 \log(p_T/p_{T,\text{min}}))$ to double and next-to-double logarithmic approximation [143, 167]. In particular, Ref. [143] derived resummed predictions for jet rates and the mean number of jets to double-logarithmic (DLA) and next-to-double-logarithmic approximation (NDLA), accounting for effects of the running of the strong coupling. It should be noted that at this level of accuracy the results are independent of the parameter p that distinguishes the jet algorithms.

In Fig. 3.15, resummed predictions to DLA and NDLA accuracy including the effect of the running of α_s to one-loop order are presented for $\langle n_{\text{subjets}} \rangle$ for both light-quark and gluon initiated jets of size $R = 1.0$. It can be observed that for all combinations of R_{subjet} and $p_{T,\text{min}}^{\text{subjet}}$ gluons induce a larger mean number of subjets than quarks, as naively expected from the colour charges. The NDLA corrections are most sizeable for $R_{\text{subjet}} = 0.05$, where they reduce the DLA prediction significantly.

In Fig. 3.16 the comparison of the $\langle n_{\text{subjets}} \rangle$ distribution for a SHERPA parton-shower simulation and the corresponding NDLA prediction for quark- and gluon-initiated jets is presented. For the shower simulation, the processes $pp \to q\bar{q}$ and $pp \to gg$ at parton level have been considered, respectively. Given the large jet transverse momenta investigated here, initial-state parton-shower effects are rather suppressed and a comparison to the pure final-state evolution hypothesis of the resummed calculation is applicable[2]. For the case of quark-initiated jets, the resummed predictions agree well with the parton-shower results, and the dependence on the fat-jet transverse momentum is very well reproduced. For $R_{\text{subjet}} = 0.05$ the resummation overshoots the shower prediction by about 10%. When comparing the results for gluon jets, somewhat larger deviations are observed. Once again the parton shower nicely reproduces the shape of the resummed prediction. However, the NDLA results overshoot the Monte-Carlo simulation by about 20% for $R_{\text{subjet}} = 0.1$ and 25% when $R_{\text{subjet}} = 0.05$. It has been observed before that resummed predictions for gluon jets tend to produce larger deviations from shower generators [167] and that the latter predict somewhat lower rates, in particular when considering small jet radii. Since in general gluons radiate more than quarks, they are thus more sensitive to missing higher-order terms. For R_{subjet} values as small as 0.1 or even 0.05 the analytic resummation of terms like $(\alpha_s \log(1/R_{\text{subjet}}^2))^n$ to all orders [170] or jet-clustering logarithms as discussed in [172] might need to be considered. Furthermore,

[2]This hypothesis has explicitly been checked and confirmed by switching off initial-state splittings in the SHERPA parton shower.

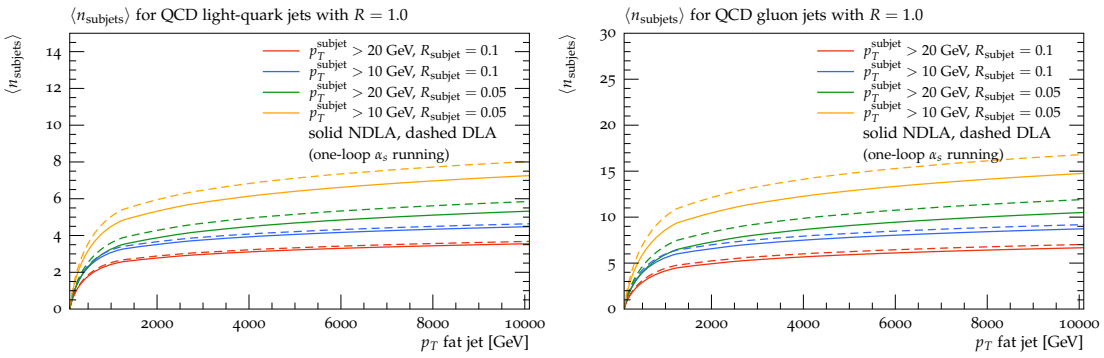

Figure 3.15.: NDLA (solid) and DLA (dashed) predictions for the mean number of subjets inside $R = 1.0$ light-quark (left panel) and gluon (right panel) initiated jets for different choices of p_T^{subjet} and R_{subjet}.

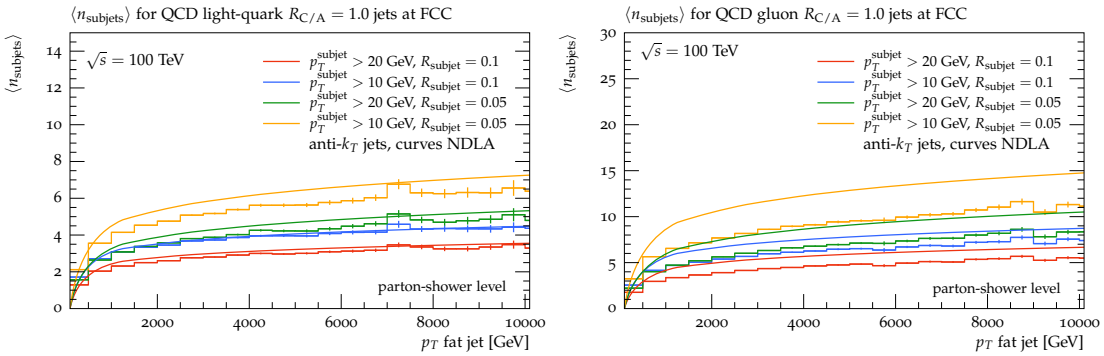

Figure 3.16.: Average number of subjets inside $R = 1.0$ light-quark (left panel) and gluon (right panel) initiated jets. A SHERPA parton-shower simulation (histograms) is compared to a corresponding NDLA resummed predictions (solid curves) for different choices of p_T^{subjet} and R_{subjet}.

explicit calculations of the NNDLA contributions to k_T jet rates turn out to give sizeable corrections and improve the agreement with parton-shower simulations[3].

Overall, one can conclude that parton-shower predictions for the mean-number of subjets in large-area jets give reliable results that are in reasonable agreement with analytical estimates from resummed calculations. However, in particular for the case of gluon jets higher-logarithmic contributions seem to yield sizeable corrections. However, for subjet radii not too small the techniques presented allow for realistic perturbative predictions to be made for very large jet transverse momenta and rather small subjet p_T thresholds. Certainly, for a dedicated comparison against data, non-perturbative corrections from hadronisation and the underlying event need to be included. However, these are largely independent of the flavour of the particle that seeds the jet evolution and thus will not critically change the above picture. Instead, apart from slightly washing out some of the differences between quark and gluon jets, only a modest offset in the mean number subjets is expected.

The observable at hand, $\langle n_{\text{subjets}} \rangle$ as a function of the transverse momentum of a large-area jet, will now be considered as a discriminator for QCD jets and hadronic decays of heavy particles. In Fig. 3.17, a comparison for the mean number of subjets found inside Cambridge–Aachen jets of $R = 1.0$ containing the hadronic decay products of top-quarks, W-bosons and light-quark QCD jets is presented. In the analysis of the top-quark and W-boson decays, the reconstructed fat-jet that is closest to the direction of the actual resonance is being analysed. The quark-jet distribution is obtained from the analysis of $pp \to q\bar{q}$ events. For R_{subjet} and p_T^{subjet} the values 0.1 and 10 GeV are considered, respectively.

Most notably, jets containing the decay jets of boosted $W \to q\bar{q}'$ decays feature a rather small number of subjets. This is related to the colour-singlet nature of the W-boson. Its

[3]Private communication with Bryan Webber based on unpublished results.

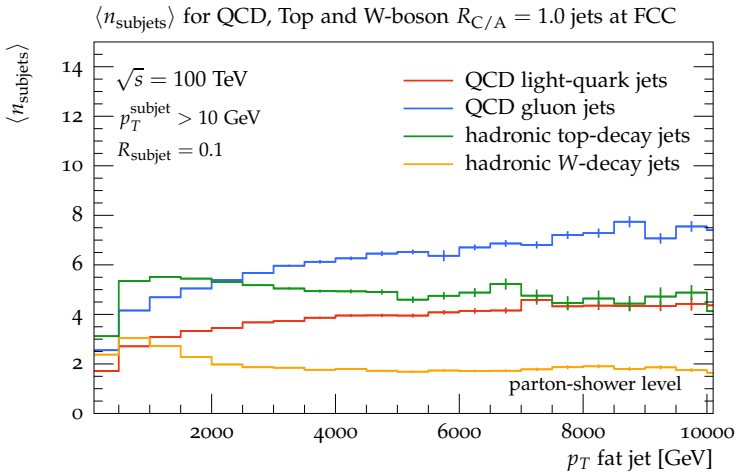

Figure 3.17.: Average number of subjets inside Cambridge–Aachen jets of $R = 1.0$ originating from hadronic top-quark and W-boson decays, and QCD quark-jet production. Subjets are reconstructed using the anti-k_T jet finder with $R_{\text{subjet}} = 0.1$ and $p_T^{\text{subjet}} > 10$ GeV. Results are presented at parton level.

decay jets are very collimated at high transverse momentum, with no colour–connection to the rest of the event, that characterise the quark or gluon jets. This results in a rather constant expectation of just two subjets for $p_T^{\text{fat}} > 2$ TeV. At $p_T^{\text{fat}} \approx 1$ TeV three subjets are resolved on average, corresponding to the emission of one additional jet from the two decay partons. This prominent feature makes it easily possible to distinguish hadronic W-boson decays, or similarly Higgs-boson decays, from QCD jets.

The identification of top-quark decays based on $\langle n_{\text{subjets}} \rangle$ seems much harder. The distribution peaks around $p_T^{\text{fat}} \approx 1$ TeV with a value of $\langle n_{\text{subjets}} \rangle \approx 5.5$. This is significantly higher than what is observed for light-quark jets and even for gluon jets, and it is due to the hadronic decays assumed for the tops, i.e. $t \to bW^+ \to bq\bar{q}'$, which yield three jets – two more than the original quark. With increasing transverse momentum the top-jet distribution approaches the light-quark result, reflecting the fact that beyond $p_T^{\text{fat}} \approx 4$ TeV the decay products are extremely collimated and basically radiate with their combined colour charge C_F as light-quark jets do. To illustrate this fact Fig. 3.18 compiles the $\langle n_{\text{subjets}} \rangle$ distribution for undecayed top quarks and bottom quarks. Three values of p_T^{subjet} are considered, 5, 10 and 20 GeV while R_{subjet} is fixed to 0.1. Mass effects, namely the shielding of collinear singularities, yield a suppression of radiation off top quarks up to p_T values of 4 TeV. The radiation off bottom-quarks is at high transverse momenta as considered here compatible with the light-quark distributions presented in fig. 3.16. It can be concluded that at FCC collisions energies the identification of very boosted hadronic decays becomes extremely challenging. The observable presented here, i.e. $\langle n_{\text{subjets}} \rangle$ of large-area jets, provides sensitivity to the QCD

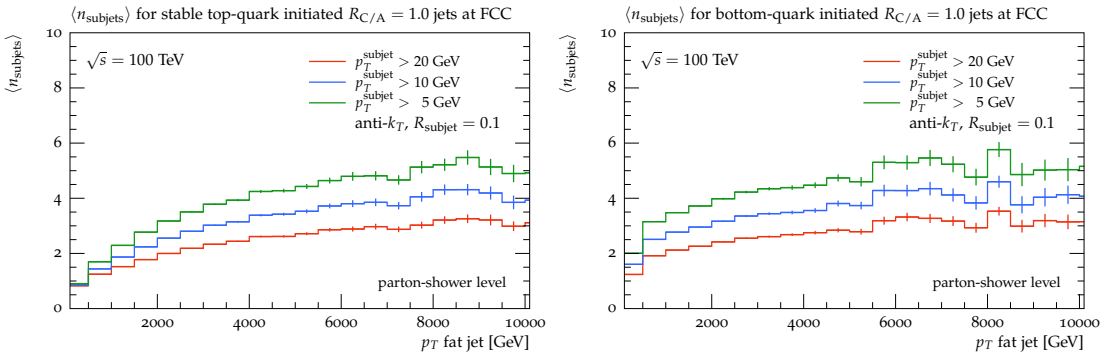

Figure 3.18.: Average number of subjets inside Cambridge–Aachen jets of $R = 1.0$ originating from stable top-quark and bottom-quark production. Subjets are reconstructed using the anti-k_T jet finder with $R_{\text{subjet}} = 0.1$ and $p_T^{\text{subjet}} > 5\,, 10,\, 20\,\text{GeV}$. Results are presented at parton level.

colour charge of the jet-initiating particle, either a QCD parton or a heavy resonance. For QCD quark and gluon jets the results obtained from parton-shower simulations are in reasonable agreement with predictions from all-orders resummation calculations at NDLA accuracy.

3.3. Conclusion

In the present chapter resummation effects in simulations at a future collider have been presented. The first approach discussed is the CAESAR one, which is a general framework that accounts for the resummation of soft and collinear logarithms in global event shapes, at a hadronic collider. After introducing the main concepts, results on the colour flow in pp collisions have been presented, with a comparison between LHC and FCC collisions. These have been obtaining by combining existing tools within the SHERPA multi-purpose event generator. The colour flow, accounted for in the CAESAR framework by the soft function, which comprises an evolution equation, parametrised by an anomalous dimension matrix, can be evaluated by mean of the large-N_C approximation too. Through this simplification, it has been possible to make a connection between the resummation approach and the parton shower one, as the latter is by default large-N_C accurate. Events at FCC and LHC energies have been generated, showing that the overall contribution of the full-N_C colour flow to the process is marginal, and therefore, the large-N_C approximation, as used in the parton shower could be valuable also in the scenario of a future collider.

We present a discussion over the single-logarithmic function present in the CAESAR approach. An independent Monte Carlo evaluation has been presented, and possible integration within a Monte Carlo event generato discussed. Due to its similarity to the Sudakov factor in the parton shower, it could be an interesting tool again helping us in

comparing resummation effects as performed in the parton shower approach.

In the second part of the chapter we continue our diagnosis of resummation in parton showers by mean of another analytical resummation method, the so called generating functionals one. After a short introduction of the prescription, direct comparison between showered and fully NDLA have been presented, showing an overall agreement between the two methods at 100 TeV. Our analysis focuses on the average number of subjets within a "fat" jet. This kind of objects are widely employed in boosted searches, and as starting point for the reconstruction of several hadronically decaying particles, as top quarks, Higgses and gauge bosons.

The present discussion shows from one side that parton showers, although being a numerical Markov chain employed for iteratively solving the evolution equation, is a good tool, with accurate prediction properties. This comparison goes in the direction of carefully describing jet substructure techniques from a theoretical point of view, as in ref. [173]. Further studies could also improve the understanding of new technologies. For example recent results [174,175] discuss NLO accurate parton-shower, and a careful understanding and check of the parton-shower log-accuracy is needed, before going to the next accuracy level.

CHAPTER 4

Beyond Standard Model

This chapter discusses the phenomenology of a particular Beyond Standard Model theory at a proton-proton future circular collider with centre of mass energy $\sqrt{s} = 100$ TeV. The ultimate goal is to study the scattering of gauge bosons, a handle to the intrinsic nature of the Standard Model, and of its BSM completion, whatever it will be. We perform the study within the context of Composite Higgs models, in particular employing the symmetry breaking pattern $SU(4)/Sp(4)$. We make use of unitarity methods to set natural parameters for the model, in order to generate predictions. We first present the necessary context following refs. [176, 177], understanding what is still missing to the Standard Model, and what inconsistency we try to address; in between, we present the unitarity method we employ. In section 4.2 we present the actual $SU(4)/Sp(4)$ Composite Higgs model, and finally we describe the procedure we apply for getting reliable predictions, and an analysis to be performed at a future $\sqrt{s} = 100$ TeV hadron collider.

4.1. Going Beyond

The Standard Model of particle physics, whose Lagrangian is summarised in eqs. 2.16 and 2.1, successfully describes almost all measured high-energy physics data to date. The Higgs boson discovery [178,179] in 2012 by the ATLAS and CMS collaborations [4,5,180] confirm the last missing piece of the puzzle. Despite its success, the Standard Model is not a complete nor final theory. Gravitational interactions are not included, and seemingly there is not yet a satisfactory quantum theory for them. Also, non-vanishing neutrino masses are not predicted within the Standard Model, and, in general, the Hierarchy problem is posed by the simple formulation of the Higgs boson mass and its introduction through the Electroweak Symmetry Breaking. The current paradigm largely employed when trying to describe the Standard Model is that of Effective Field

Theory. Following other historical working example, such as the Fermi theory, we should look at the Standard Model as an effective theory, valid up to some scale $\Lambda^2_{\rm SM}$, before or near to the so-called Planck scale, $m^2_{\rm Planck} = \hbar c/G = (10^{19})^2$ GeV^2. The Fermi theory with four-fermion interactions is valid below the scale of the gauge-boson masses $\Lambda^2 \sim m_Z^2$, and afterwards the Standard Model is the right theory to employ, which describes the same mechanism as the Fermi theory through the introduction of boson mediators. We also expect that, for the Standard Model, a more complete theory exists, enlarging its validity domain and describing the phenomena with a deeper understanding, just as what happens for the Fermi theory. Usually, such a theory is referred to as the UltraViolet (UV) completion.

In an effective field theory, operators in the Lagrangian are classified according to their mass dimension

$$\mathcal{L}_{\rm SM} = \mathcal{L}^{\rm d=4} + \frac{1}{\Lambda_{\rm SM}}\mathcal{L}^{\rm d=5} + \frac{1}{\Lambda^2_{\rm SM}}\mathcal{L}^{\rm d=6} + \dots \ . \tag{4.1}$$

The dimensional analysis of the operator composing the Lagrangian is a powerful tool when we want to match the effective theory with the fundamental one. Some new physics must exist in some form, and it might arise at very high energy scales that we cannot currently access. Since a Quantum Field Theory describing Nature has to be renormalizable (meaning $d \leq 4$ for the Standard Model), in order to not contain divergences, from power counting it directly follows that operators with d > 4 have to be suppressed by a power of the Standard Model cutoff in order to restore the right dimension for the term in the Lagrangian density. From this point of view, we understand why the effects of operators with $d > 4$ are not included in the "canonical" Standard Model Lagrangian of the previous section: they are suppressed by powers of the cut-off energy so that they give very small contributions and can be safely neglected. It is worth noting that the Lagrangian with operators d $= 4$ already accounts for almost every process measured today, and those not yet accounted for could be regarded as in the following.

A key role in the SM description is played by the so-called "accidental" symmetries. These are not imposed in the theory, as for example the Poincaré and gauge symmetries, but they are a consequence of the truncation of the Lagrangian up to 4-dimensional operators. For the lagrangian with operators $d \leq 4$, baryon and lepton number conservation belong to this class. The fact that those symmetries are not imposed as principles means that the fundamental theory could violate them. Accidental symmetries are a big phenomenological success of the theory, so it is remarkable that they could arise at the typical Standard Model energy scale. One such symmetry is baryon number conservation, which forbids the proton decay - in other words proton lifetime is greater than the age of the universe.

At the level of $d = 4$ operators, baryon number is exact and the proton is exactly stable. However there are $d = 6$ operators [181] like, for example,

$$\mathcal{O}_{abcd} = \frac{1}{\Lambda^2}\epsilon^{\alpha\beta\gamma}\epsilon_{ij}\epsilon_{kl}(\bar{q}_{L,\alpha,i,a}q^c_{L,\beta,j,b})(\bar{q}_{L,\gamma,k,c}\ell^c_{L,l,d}) \ , \tag{4.2}$$

where ϵ is the Levi-Civita anti-symmetric tensor, the qs are quarks spinors and ℓ denotes a lepton doublet; α, β, γ are $SU(3)$ indices, i, j are $SU(2)$ ones, and a, b, c, d refers to the generation. This operator violates baryon number, thus leading to proton decay. We can give a crude estimate, based on dimensional analysis,

$$\Gamma(p \to e^+\pi^0) \simeq 1/\tau \sim \frac{1}{8\pi}\frac{1}{\Lambda_{SM}^4} m_p^5 . \tag{4.3}$$

The proton can thus be made arbitrarily long lived, for large enough energies $\Lambda_{\rm SM}$. The Super-Kamiokande experiment in Japan has set an experimental bound on the decay of the proton $\tau = 1/\Gamma(p \to e^+\pi^0) \geqslant 1.4 \times 10^{34}$ years [182]; this incredibly long lifetime is very easy to understand in the Standard Model. Given the present bound we estimate the decay width Γ_p

$$\Gamma_p \lesssim \frac{1}{3.2 \times 10^{32}} \frac{1}{1.5 \times 10^{24}} \,\text{GeV} = 2 \times 10^{-64}\,\text{GeV} \tag{4.4}$$

$$\Rightarrow \Lambda_{SM} \geq m_p \left(\frac{m_p}{8\pi\Gamma_p}\right) \simeq 3.7 \times 10^{15}\,\text{GeV} . \tag{4.5}$$

The second important accidental symmetry is *lepton* flavour conservation. After diagonalising the lepton Yukawa's, we find that the $d = 4$ Lagrangian is invariant under the transformations

$$U(1)_{Le} \times U(1)_{L\mu} \times U(1)_{L\tau} , \tag{4.6}$$

under which the three leptons families rotate independently. This symmetry forbids any flavour-changing transition in the lepton sector. Experimentally, processes like flavour-violating decays of the μ are indeed largely suppressed [27]

$$Br(\mu^- \to e^-\gamma) \leq 3.3 \times 10^{-8} \tag{4.7}$$

$$Br(\mu^- \to e^-e^+e^-) \leq 2.7 \times 10^{-8} , \tag{4.8}$$

in the Standard Model with large Λ_{SM}, as expected . However by the observation of neutrino masses and oscillations, we know that lepton flavour is a good approximate symmetry, but not an exact one. But this is not a failure of the Standard Model, actually could be a great success. At $d = 4$, lepton flavour is exact and neutrinos are massless, but both these features are violated by a five-dimensional operator [183]

$$\frac{1}{\Lambda_{SM}}(\bar{\ell}_L H)(\ell_L H^c) , \tag{4.9}$$

where ℓ is the lepton doublet, H the Higgs doublet field and the superscript c indicates the charge conjugates. After the Higgs acquires a Vacuum Expectation Value, the operator in eq. 4.9 leads to a Majorana neutrino mass

$$m_\nu \sim \frac{v^2}{\Lambda_{SM}} , \tag{4.10}$$

that can lead to neutrino oscillation and masses. The stringent limit on m_{ν_e} comes from the Troitsk experiment [184] $m_{\nu_e} < 2.3\,\text{eV}$, and an overall limit $\sum_\nu m_\nu < 0.23\,\text{eV}$, which could be naturally accounted for if $\Lambda_{SM} \sim 6 \times 10^{14}$ GeV. It is interesting to note that the first evidence of new phenomena beyond Standard Model, such as neutrino masses and oscillations, could come from the first sector with higher dimensionality than d = 4, which is the least suppressed by the scale of new physics.

By the arguments presented up to now, it seems extremely plausible that the Standard Model is the valid theory of Nature up to very high energies, far above the current and foreseen experimental reach, to the order of the so-called Grand Unification Scale, $M_{GUT} \sim 10^{16}\,\text{GeV}$. This is however contradicted by another argument, the so-called *Hierarchy Problem*, which can be formulated as follows. By power-counting, i.e. dimensional analysis, we estimate that an operator with $d > 4$ must be suppressed by the appropriate power of Λ_{SM}, but exactly the same argument leads us to conclude that an operator with $d < 4$ must instead be enhanced by the appropriate power of the scale Λ_{SM}

$$\mathcal{L} = \mathcal{L}^{d\geq 4} + \Lambda_{SM}^{d'} \mathcal{L}^{d'<4} \,. \tag{4.11}$$

The only such operator actually contained in the Standard Model Lagrangian is the Higgs boson mass term

$$m_H^2 H^2 \simeq c\Lambda_{SM}^2 H^2 \,, \tag{4.12}$$

where c is an unknown coefficient. Then, comparing $\Lambda_{\text{SM}} \sim 10^{16}$ GeV with the measured Higgs mass $m_H = 125\,\text{GeV}$

$$\frac{(m_H^2)_{true}}{(m_H^2)_{estimate}} \sim 10^{-16} \,. \tag{4.13}$$

Why the power-counting estimate is so badly violated? This is the essence of the Hierarchy Problem. This is not a mathematical inconsistency of the theory. The fact that the Higgs mass estimated by dimensional analysis as in the previous section is so large does not forbid us to obtain the correct Higgs pole mass, 125 GeV. As made very clear in the Wilson approach to Quantum Field Theory, $m_{phys}^2 = m_{UV}^2 + \delta^2 m$, where $\delta^2 m$ comes from radiative corrections and it is associated with physics below the cut-off Λ_{SM}^2. Classifying the Higgs boson as fundamental scalar particle means that this is not protected by large radiative corrections, so that δm can be very large and compensate for $m_{H,UV}$. The main correction at one-loop order g^2 comes from the particle with largest Yukawa coupling, the top quark. Its radiative contribution to the Higgs mass is not the only one, there are others arising from the gauge bosons, Higgs self-coupling, and almost every other particles, and they are summing with different signs. They are considerably smaller compared to the top-quark contribution, due to their smaller masses.

We compute δm^2 by regularising the integral appearing in the loop correction with a cut-off, obtaining

$$\delta m_H^2 = 3\lambda_t^2 \int_{|k|\leq\Lambda_{SM}} \frac{d^4k}{(2\pi)^4} \frac{1}{k^2} \sim -\frac{3\lambda_t^2}{2\pi^2} \left[\Lambda^2 + ...\right] \simeq 0.1\Lambda_{SM}^2 \,, \tag{4.14}$$

where λ_t is the Yukawa coupling and Λ is the regularising cut-off. The correction is quadratically divergent in the energy scales. To quantify the precision with which the UV and IR term have to cancel, we can define

$$\Delta = \frac{\max\left[c\Lambda_{SM}^2, \delta m_H^2\right]}{m_{H,pole}^2} \geq \left(\frac{125\,\text{GeV}}{m_H}\right)^2 \left(\frac{\Lambda_{SM}}{400\,\text{GeV}}\right)^2, \tag{4.15}$$

where Δ defines the amount of cancellation we need to reproduce the experimentally observed Higgs mass. In the scenario of no new physics below the Planck scale it would be needed to set the Δ parameter down to a precision of a very unnatural number of digits. Briefly, the unknown coefficient, c, appearing in eq. 4.12 has to be $c \sim 10^{-28}$ in order to reproduce $m_H = 125$ GeV. This inconsistency is introduced by the fact that we do not yet know exactly the origin of the Higgs boson.

The Hierarchy Problem regards only scalar particles, as the Higgs boson in the Standard Model. For example, let us consider the electron, a fermion, and compute its main radiative correction. Using a cut-off regularisation as before to renormalise our theory, we find that

$$\delta m_e = \frac{3\alpha_{em}}{4\pi} m_e \log\frac{\Lambda}{m_e} \tag{4.16}$$

In this case the dependence of the correction from the energy scale is logarithmic, than we can say that the contribution of the self-energy diagram gives a small correction to the electron mass. This is very simply understood in terms of symmetry: in the limit of vanishing mass $m_e \to 0$, the theory acquires a global chiral symmetry, the left-handed and right-handed component of the electron spinor are decoupled: the action is invariant under phase transformation:

$$\psi_L' \to e^{i\theta_L}\psi_L \qquad\qquad \psi_R' \to e^{i\theta_r}\psi_R \tag{4.17}$$

Since $m_e \neq 0$, chiral symmetry is not exact, but approximate, the correction to the electron mass is proportional to the fermion mass itself. A small break implies a small correction. All fermion masses are protected by this mechanism, since the Standard Model is a chiral theory. So we may think that a similar mechanism based on symmetries could preserve the Higgs mass to its right value. We know Electroweak Symmetry Breaking is the paradigm to solve the puzzle of the masses in the Standard Model Lagrangian, but we do not know much more, nor we understand exactly its dynamics: it is sufficient to think of the hierarchy in the fermionic masses between the different families, that has not yet an explanation. Up to now there is no satisfactory theory explaining why we have three different generations of quarks and leptons, with mass spectra at different energy scales.

The existence of new physics beyond the Standard Model is also suggested by other experimental evidence, in particular the existence of Dark Matter and of neutrino masses. Other problems arise if we try to explain baryogenesis and the existence of flavours. The power spectrum of the Cosmological Microwave Background allows to estimate the density of the various components of the universe, in particular we have experimental

confirmation that invisible (i.e. Dark Matter and Dark Energy) components are largely dominating over the baryonic component. We have $\Omega_{invisible}h^2 = 0.127$ [185]; Ω_i is defined as the ratio between the density of the i-th component of the universe and critical density $\rho_c = (3H_0^2)/(8\pi G)$ - currently we have $\Omega_{tot} \sim 1$ and $\Omega_{baryonic}h^2 = 0.0222$ (here h^2 is the Hubble parameter) within a very precise range. This shows that the relative abundance of baryonic constituents compared to that of invisible matter is low, confirming the fact that there has to be something else in the universe. Experimental evidence for neutrino masses are given by neutrinos flavour oscillations, measured in the relative abundance of neutrinos coming from the sun. However, currently we have no direct information that such problems are directly related to energies we are going to explore at the Large Hadron Collider, $13 - 14\,\text{TeV}$. So which are the possible scenarios? One is fine-tuning: we choose the parametrizations of the model in such a way that the cancellation happens. But with this situation rises the *naturalness* problem: how is it natural to fine-tune quantities to reach the values we want? If we want to make the cancellation accidental, we do not also want a large fine-tuning, and so this argument implies that new physics must arise at energies explored by the LHC, for example,

$$\Delta \leq 100 \Rightarrow \Lambda_{SM} \sim \text{13-14 TeV}\,. \tag{4.18}$$

The other possibility is that new physics arises and so new particles, new phenomena, or something else that goes beyond what we actually know, could cancel out these divergences. For example, one of the solutions to the Hierarchy problem, studied in the last thirty years, is Supersymmetry, in which boson masses are related to their fermionic superpartners, then there is a chiral symmetry protecting from large radiative corrections. The Composite Higgs [186–188] is another solution, different from Supersymmetry.

The mechanism that protects the Higgs mass in the composite scenario is dimensional transmutation. This is the phenomenon, happening in QCD too, if we would not consider quark masses, for which we derive from a dimensionless quantity, like α_s, a dimensionful one, like Λ^2_{QCD}, that is exactly the typical scale of confinement for the theory. Above that scale, the composite particles are insensitive to corrections. This could be shown making use of the renormalisation group equation, as in ref. [189].

Pictorially, if we treat the Higgs is a composite state of a new-strongly interacting sector, the dimensionality of the Higgs mass operator, written in terms of the constituents of the new strong sector, is not $d = 2$, but it could be even $d > 4$, so we have no problem explaining why the Higgs mass is relatively light. The mass is also protected by symmetry, so the radiative corrections do not imply divergences. For example, if the Higgs is a composite state made of two ψ fermions of the new strong sector, we could write

$$dim\,[H] \sim dim\left[\bar{\psi}\psi\right] \rightarrow dim\left[H^2\right] = 6\,. \tag{4.19}$$

From the altered dimension of the field corresponding to the Higgs boson, it follows that correction are suppressed by powers of Λ_{SM}, and, as it was for the example of the proton decay, the Higgs is protected by corrections from $E \sim M_{GUT}$. The theory is therefore parametrised in term of the only scale of this new strong sector, at which confinement happens, as for QCD.

Rather being a fundamental, point-like particle, the Higgs would now be an object with a proper and finite geometric size l_H. The typical confinement scale would be something like $m_* = 1/l_H$. In this way, quanta with wavelength bigger than l_H would treat the Higgs as a fundamental particle. Conversely, the Higgs would be transparent to objects with higher energy scales than m_*^2, that is, with wavelength bigger than the its typical size. This is completely in analogy to a gluon hitting a $q\bar{q}$ pair, giving rise to colour coherence effect: if the gluon is soft, it will not resolve the quark pair, and display them as colour neutral particle. In this way the Higgs particle is insensitive to corrections of energy order bigger than its confinement scale m_*^2.

In this picture, all the resonances (we globally call ρ) must have the same mass, within an energy range determined by an order of magnitude, for example. Then if the Higgs boson belongs to this picture, it would be surrounded by other strong resonances (of spin 1/2, 1 , 2), all at the same mass. To get a Higgs mass of about 125 GeV the energy scale of the new strong sector would be 100 GeV, and we have strong bounds on the production of such particles, since they would be at an energy range explored so far. For example, a large splitting between the Higgs and spin-1 resonances is strongly suppressed by comparison with Electroweak Precision Test (EWPT), and such a situation would require

$$\left(\frac{m_H^2}{m_\rho^2}\right) \lesssim 1/400\,, \tag{4.20}$$

that is a large fine-tuning. However, in the QCD picture we also know of particles lighter than the other resonances: these are the pions, that we construct as *pseudo-Nambu-Goldstone bosons*. This is the same feature that we require for the Higgs boson in our Composite Higgs model, it has to be a pseudo-Nambu Goldstone boson coming from the spontaneous breaking of the global group $\mathcal{G} \to \mathcal{H}$. If the symmetry were exact, the Higgs would be massless; a symmetry breaking induces the Higgs to acquire a relatively high mass, but are protected by the underlying Goldstone symmetry. We present in the following briefly the case of pions in QCD, as it works as an example both for understanding the idea beneath the Composite Higgs models in general, and has been the inspiration for our work on unitarity and Goldstone Boson Scattering in section 4.3.

4.1.1. A case of study

In QCD we have scalar particles: the pions are the lightest mesons in the mass spectra with $m_\pi \sim 100\,\text{MeV}$. How are their masses protected from being close to other composite states (resonances), with $m_\rho \sim 1\,\text{GeV}$? The chiral symmetry is the answer to this question. If only the two lightest quarks, u and d, are considered, the quark sector of the QCD Lagrangian reads

$$\mathcal{L} = \sum_{j=u,d} \bar{q}_j \left(i\not{D} + m\right) q_j\,. \tag{4.21}$$

This Lagrangian is invariant under various global symmetries. The first one is a phase transformation of the quark fields. This is the accidental baryon symmetry described

above, and it leads to the conservation of *baryon* number, by which we classify the hadrons in mesons and baryons.

$$q'^i \to e^{i\alpha/3} q^i \qquad B[q] = \frac{1}{3} \qquad B[\bar{q}] = -\frac{1}{3} \tag{4.22}$$

Thus, the classification splits in:

- *mesons*: $B[q\bar{q}] = 0$;
- *baryons*: $B[qqq] = 1$.

Introducing a notation that manifestly shows symmetries that couple different flavours, we write:

$$q = \begin{pmatrix} u \\ d \end{pmatrix} . \tag{4.23}$$

The lagrangian becomes:

$$\mathcal{L} = \bar{q} \left(i \not{D} \right) q . \tag{4.24}$$

We have neglected the masses of the quarks, which are small compared to the energy scale we are dealing with. This Lagrangian is invariant under a 2×2 unitary transformation:

$$q' = \exp \left[\sum_0^3 \alpha_i \sigma_i \right] q \tag{4.25}$$

$\sigma_i \, , (i = 1, 2, 3)$ are the Pauli matrices and σ_0 is the unit matrix. So this $U(2)_V$ is the $U(1)$ phase transformation mentioned above, composed with a $SU(2)_V$ transformation. This is an exact symmetry in the case that the u and d masses are degenerate. The subscript V stands for *vectorial*, since the associated current is vectorial:

$$J^i_\mu = \bar{q} \gamma_\mu \sigma^i q . \tag{4.26}$$

Decomposing the quark fields in terms of their chiral components, and neglecting the quark masses, the Lagrangian becomes

$$\mathcal{L} = \bar{q}_L i \not{D} q_L + \bar{q}_R i \not{D} q_R \tag{4.27}$$

We can note that QCD with two massless flavours of quarks possesses chiral symmetry: $SU(2)_L \times SU(2)_R$. This symmetry does not appear in the observed spectrum of QCD. If it existed, every hadron would have a symmetric partner with opposite parity (since the chirality is opposite). Colour condensation (which means the operator $\bar{q}q$ has a non-zero expectation value, $\langle 0 | \left(\bar{u}u + \bar{d}d \right) | 0 \rangle \sim (250\,\mathrm{MeV})^3$, breaks down the chiral symmetry to $SU(2)_V \times U(1)_B$. The composite operator $\bar{q}q$ connects left and chiral components of the quark fields. Three broken generators implies three massless Nambu-Goldstone bosons. In the spectrum there is not anything like these, but we can note that three low-mass hadrons exist: π^0,$\pi^\pm$. The explanation for such a pattern of the spectrum is again spontaneous symmetry breaking: u and d are not massless, though their masses

are very small compared to Λ_{QCD}. In addition, electromagnetic interactions split the mass spectrum of the three pions: $\pi^{\pm}$ have different mass than π^0, because u and d have different charge with respect to electromagnetic interactions. These pions are particles we call them pseudo Nambu-Goldstone (NG) bosons. In fact, they do not come from a broken exact symmetry, but from a broken approximate one.

4.2. The Fundamental Minimal Composite Higgs Model

Composite Higgs (CH) models are among the most promising candidates to address some of the SM weaknesses, dynamically generating the EW scale through a vacuum condensate and at the same time explaining the mass gap between the Higgs boson and the other composite states by the identification of the Higgs with one of the pseudo-Nambu Goldstone boson (NGB) of the underlying global symmetry breaking [176, 186–188, 190]. The Fundamental Minimal Composite Higgs Model (FMCHM) is based on the coset SU(4)/Sp(4), which is the simplest global symmetry breaking pattern which can be realised in terms of an underlying fermionic gauge theory[1]. The simplest underlying theory realising this symmetry breaking is based on the SU(2) gauge theory with two Dirac fermions transforming according to the fundamental representation of the gauge group [192–194]. This scenario has been studied as CH model in Refs. [193, 194].

The Fundamental Minimal Composite Higgs Model describes the composite dynamics of the electroweak sector in the Standard Model; such a unified description has first been presented in [194]. A new strong sector is introduced, and the breaking of the related global symmetry produces the Higgs, as a pseudo Nambu-Goldstone boson. Depending on the representation of the new fermions, (pseudo-)real or complex, the unbroken quantum flavour symmetries are bounded to be of the type $SU(2N_f)$ or $SU(N_f) \times SU(N_f)$. In the case of pseudo-real representation, we expect a symmetry breaking pattern $SU(2N_f) \to Sp(2N_f)$. The fermionic condensate of the new sector therefore transforms in the antisymmetric 2-index representation of $SU(2N_f)$. We focus on the symmetry breaking $SU(4) \to Sp(4)$. The dimensions of the groups are 15 and 10, respectively, according to the Goldstone Theorem we end up with 5 different massless Goldstone bosons, transforming as $(2,2) \oplus (1,1)$ in the $SU(2) \times SU(2)$ subgroup of the $Sp(4)$ group. A fourplet is present, from which we can construct the Higgs and the three Goldstones which we identify with the Standard Model gauge-boson longitudinal polarisations.

The new Lagrangian is

$$\mathcal{L} = -\frac{1}{4} F^a_{\mu\nu} F^{a,\mu\nu} + \bar{U} \left(i\gamma^\mu D_\mu - m \right) U + \bar{D} \left(i\gamma^\mu D_\mu - m \right) D \, . \tag{4.28}$$

U and D are the two new fermionic fields, each with mass m. A global symmetry $SU(4)$ is present for massless fermions , which is broken down to $Sp(4)$ through the introduction

[1] The minimal CH model, SO(5)/SO(4), can be realised with the inclusion of 4-fermion operators [191].

of the mass. Thus, it is possible to rewrite the Lagrangian as

$$\mathcal{L} = -\frac{1}{4}F^a_{\mu\nu}F^{a,\mu\nu} + i\bar{U}\gamma^\mu D_\mu U + i\bar{D}\gamma^\mu D_\mu D + \frac{m}{2}Q^T(-i\sigma^2)CEQ + \frac{m}{2}\left(Q^T(-i\sigma^2)CEQ\right)^\dagger , \tag{4.29}$$

where

$$Q = \begin{pmatrix} U_L \\ D_L \\ \tilde{U}_L \\ \tilde{D}_L \end{pmatrix} \qquad E = \begin{pmatrix} 0 & 0 & 1 & 0 \\ 0 & 0 & 0 & 1 \\ -1 & 0 & 0 & 0 \\ 0 & -1 & 0 & 0 \end{pmatrix} . \tag{4.30}$$

C is the charge conjugation operator and $\tilde{U}_L = -i\sigma^2 C\bar{U}_R^T$. Under infinitesimal transformation of $SU(4)$, the Lagrangian transforms as

$$Q \to \left(1 + i\sum_{n=1}^{15}\alpha_n T^n\right) , \tag{4.31}$$

$$\mathcal{L} \to \mathcal{L} + \frac{im}{2}\sum_{n=1}^{15}\alpha^n Q^T(-i\sigma^2)C\left(ET^n + (T^n)^T E\right)Q + \text{h.c.} . \tag{4.32}$$

Here T^n are the 15 $SU(4)$ generators. Therefore, the Lagrangian is invariant if

$$ET^n + (T^n)^T E = 0 , \tag{4.33}$$

leading us to the definition of the $Sp(4)$ algebra. The condensate state

$$\langle\bar{U}U + \bar{D}D\rangle \neq 0 \tag{4.34}$$

originates the symmetry breaking. Standard Model electroweak fermions are identified as $Q_L = (U_L, D_L)$ for a $SU(2)_L$ doublet with $Y = 0$, $\bar{U}_L$ and $\bar{D}_L$ for two $SU(2)_L$ singlets with $Y = \pm 1/2$.

In these models the fermionic condensate generating the EW scale is misaligned with respect to the vacuum that breaks the EW group, thus the acquisition of a vacuum expectation value (*vev*) by the fermionic condensate creates a hierarchy between the NGB decay constant f and the EW scale v. Two different vacuum values exist, $\langle QQ\rangle = \Sigma_0$,

$$\Sigma_B = \begin{pmatrix} i\sigma_2 & 0 \\ 0 & -i\sigma_2 \end{pmatrix} \qquad \text{and} \qquad \Sigma_H = E = \begin{pmatrix} 0 & 1 \\ -1 & 0 \end{pmatrix} , \tag{4.35}$$

with σ_2 being the second Pauli matrix and E the $Sp(4)$ metric. The first conserves electroweak symmetry, the latter instead breaks it completely, leading to a Technicolor model.

We can construct the Lagrangian for the first vacuum by defining the 10 generators of the unbroken group, as they transform as $\Sigma \to u\Sigma u^T$ with $u \in SU(4)$, so they transform as

$$T^a \cdot \Sigma_B + \Sigma_B \cdot T^{a,T} = 0 . \tag{4.36}$$

We define the 10 S_i generators to be normalised as in app. A. We can there identify the generators of $SU(2)_L$ rotations with S_i with $i = 1, 2, 3$ and S_6 as the generator of the hypercharge $U(1)_Y$ group. The 5 broken generators are reported in app. A, and through them it is possible to write the Lagrangian through the non-linear Σ construction

$$\mathcal{L} = f^2 \operatorname{Tr} D_\mu \Sigma^\dagger D^\mu \Sigma \,, \tag{4.37}$$

having constructed the Goldstone field

$$\Sigma = e^{i\frac{\phi_i}{f} X^i} \cdot \Sigma_B \,, \tag{4.38}$$

and using the covariant derivative obtained from the minimal coupling approach. Expanding the Lagrangian in powers of the Goldstone fields ϕ_i it could be seen that no mass term for the Standard Model gauge bosons appears. As the generator S_6 has been chosen such that $Q = T^3 + Y = S_3 + S_6$, one could note $Q \cdot \Sigma_H + \Sigma_H \cdot Q^T = 0$, where $\Sigma_H = 2\sqrt{2} i X_4 \cdot \Sigma_B$. It is then easy to see that if the ϕ_4 acquires a *vev*, $\langle \phi_4 \rangle = v$, the electroweak symmetry is therefore broken, the ϕ_i , $i = 1, 2, 3$ are eaten by the W and Z bosons, the fluctuations around ϕ_4 are identified with the Higgs field and an additional singlet scalar particle is present, $\phi^5 \equiv \eta$.

To construct the full phenomenological model, the authors in [193] use a superposition of the two different vacua Σ_B and Σ_H, parametrised by an angle θ interpolating through the two different extremes, *i.e.* electroweak symmetry conserved or fully broken. The Σ_0 vacuum therefore reads

$$\Sigma_0 = \cos\theta \Sigma_B + \sin\theta \Sigma_H \,, \tag{4.39}$$

and $\Sigma_0^\dagger \Sigma_0 = 1$. The broken generators are defined in term of the previously defined X_i with $i = 1, \ldots, 5$ and the unbroken S_i:

$$\begin{aligned} &Y_1 = \cos\theta X_1 - \sin\theta \frac{S_1 - S_4}{\sqrt{2}} \,, Y_2 = \cos\theta X_2 + \sin\theta \frac{S_2 - S_5}{\sqrt{2}} \,, Y_3 = \cos\theta X_3 + \sin\theta \frac{S_3 - S_6}{\sqrt{2}} \\ &Y_4 = X_4 \,, Y_5 = \cos\theta X_5 - \sin\theta S_8 \,. \end{aligned} \tag{4.40}$$

Unbroken and broken generators are defined through $V_a \cdot \Sigma_0 + \Sigma_0 \cdot V_a = 0$ and $Y_i \cdot \Sigma_0 - \Sigma_0 \cdot Y_i = 0$..

We use the Callan-Coleman-Wess-Zumino (CCWZ) construction [195,196] to write the effective Lagrangian. We construct the Lagrangian through the gauge Maurer-Cartan one-forms ω_μ

$$\omega_{0,\mu} = \phi_0^\dagger D_\mu \phi_0, \tag{4.41}$$

$$D_\mu = \partial_\mu - i W_\mu^i S_i - i B_\mu S_6 \qquad i = 1, 2, 3 \tag{4.42}$$

$$x_\mu = 2 \operatorname{Tr}\left[Y_a \omega_\mu\right] Y^a \tag{4.43}$$

$$\mathcal{L} = f^2 Tr[x_\mu x^\mu], \tag{4.44}$$

where f is the Goldstone decay constant. Imposing the W boson mass we recover an explicit expression of the Goldstone constant in term of Standard Model quantities and the vacuum alignment angle

$$v = f \sin\theta \ . \tag{4.45}$$

where θ is the misalignment angle. Standard Model couplings between the Higgs and gauge bosons can be read off the Lagrangian in eq. 4.41.

Generally, the alignment angle of the condensate matters for the gauge bosons, as the $SU(2)_L$ is just one of the subgroup of the bigger $SU(4)$, and also for the mechanism that generates the top mass. The potential is written exploiting the formalism by Coleman and Weinberg [197], in which the loop contributions are computed. The minimisation of the loop-induced potential with respect to the misalignment angle fixes its value. In refs. [193, 198, 199] the following contributions were derived:

1. loops of gauge bosons

$$V_{\text{gauge}} = -C_g g^2 f_0^4 \sum_{i=1}^{3} \text{Tr}\left(S^i \cdot \Sigma_0 \cdot (S^i \cdot \Sigma_0)\right) - C_g g'^2 f_0^4 \,\text{Tr}\left(S^6 \cdot \Sigma_0 \cdot (S^6 \cdot \Sigma_0)\right) \ , \tag{4.46}$$

   where C_g is an unknown loop factor, g and g' are the usual Standard Model couplings for the electroweak symmetry;

2. top-loops, where the top mass is generated through a 4-fermion operator

$$\frac{y_t}{\Lambda_t^2} (Qt^c)^\dagger_a \, \psi^T P^\alpha \psi \ . \tag{4.47}$$

   The potential reads

$$V_{\text{top}} = -C_t y_t' f_0^4 \sum_\alpha \left|\text{Tr}\left[P_\alpha \Sigma\right]\right|^2 \ , \tag{4.48}$$

   where α is the $SU(2)_L$ index, and the projectors P^α select the components $\psi^T\psi$ that transform as a doublet under $SU(2)_L$; Λ_t is some new dynamical scale, and C_t an unknown loop factor, as before. We note here that the first term in the expansion of the 4-fermion operator gives rise to the top mass, always parametrised by the vacuum misalignment angle θ and the new dynamical scale f, $m_{\text{top}} = y_t' v/(2\sqrt{2})$.

3. Terms explicitly breaking the $SU(4)$ symmetry are present, giving rise to other contributions to the Higgs potential and mass. A possible way to embed such terms is to add the masses of the techni-fermions through $SU(4)$ violating terms. We could assume the masses to be aligned with the gauged sector, having, for example, $M = \mu\Sigma_B$, where Σ_B is the vacuum configuration in eq. 4.36, and μ is a free parameter. The potential is written as

$$V_m = C_m f^4 \,\text{Tr}\left(\Sigma_B \cdot \Sigma\right) \ . \tag{4.49}$$

   As above, C_m is an unknown loop coefficient, and Σ is the Goldstone field.

The first contribution coming from gauge bosons is quite small compared to the top and the explicitly breaking ones, and it is therefore neglected. The minimisation of the top quark piece of the potential would bring us to a vacuum aligned with a Technicolor scenario, $\theta = \pi/2$; the explicitly breaking term V_m on the other hand contributes to offset the ground state from the $\theta = \pi/2$ value. The combined minimisation implies

$$\cos\theta_{min} = \frac{2C_m}{y'_t C_t}, \quad \text{for } y'_t C_t > 2|C_m|\,, \tag{4.50}$$

where $y'_t = 2\sqrt{2}m_{\text{top}}/v$. This indicates a naturally not so small angle, since this would require $y'_t C_t$ very close to $2C_m$, which is not in principle justified due the different origins of these two terms. On the other hand, large angles are not favoured by data due to deviations of the Higgs couplings from the SM predictions, which upset EW precision observables (EWPO) resulting in an upper bound [200]

$$\sin\theta \lesssim 0.2 \quad \text{EWPO} \tag{4.51}$$

This limit depends mildly on the fermion content and dynamics of the underlying theory but is dominated by Higgs coupling modification. It can also be alleviated by cancellations from other composite states [201].

4.2.1. Vector Resonances

The composite vector resonances in FMCHM have been studied in Ref. [201] making use of the hidden local symmetry (HLS) approach [202]. We write two replicas of the Goldstones living both in the **5** representation of $SU(4)$

$$\xi_0 = \exp\left[\frac{i}{f}\sum_a \pi_{0,a} Y_a\right] \quad , \quad \xi_1 = \exp\left[\frac{i}{f}\sum_a \pi_{1,a} Y_a\right] \quad a = 1,\dots,5 \tag{4.52}$$

and then we gauge the first field with the Standard Model respective vectors, and the second with the new vectors:

$$\omega_{\mu,i}(x) = i\xi_i^\dagger(x) D_\mu \xi_i(x) \tag{4.53}$$

$$D_{0,\mu} = \partial_\mu - igW_\mu^i S_i - ig' B_\mu S_6 \qquad i = 1,2,3 \tag{4.54}$$

$$D_{1,\mu} = \partial_\mu - i\tilde{g}\sum_a^{10} V_\mu^{\hat{a}} V_{\hat{a}} - i\tilde{g}\sum_a^{5} A_{a,\mu} Y_a \qquad i = 1,2,3 \tag{4.55}$$

$$x_{\mu,i} = 2\,\text{Tr}\left[Y_a \omega_{\mu,i}\right] Y^a, \tag{4.56}$$

where $x_{\mu,i}$ are the projections onto the broken generators Y_a, which we used to construct the Chiral Lagrangian, as before.

In the FMCHM a vast spectrum of 15 heavy composite vector resonances is expected, with very peculiar phenomenology. They can be associated with the broken generators Y_a and the unbroken ones V_a,

$$\boldsymbol{\mathcal{F}}_\mu = \boldsymbol{\mathcal{V}}_\mu + \boldsymbol{\mathcal{A}}_\mu = \sum_{a=1}^{10} \mathcal{V}_\mu^a V_a + \sum_{a=1}^{5} \mathcal{A}_\mu^a Y_a, \tag{4.57}$$

forming a **10** and a **5** multiplet of Sp(4). The lowest dimension Lagrangian is given by

$$\begin{aligned}\mathcal{L}_v &= -\frac{1}{2\widetilde{g}^2}\,\langle \boldsymbol{\mathcal{F}}_{\mu\nu}\boldsymbol{\mathcal{F}}^{\mu\nu}\rangle + \frac{1}{2}f_0^2\,\langle x_{0\mu}x_0^{\mu}\rangle \\ &+ \frac{1}{2}f_1^2\,\langle x_{1\mu}x_1^{\mu}\rangle + r f_1^2\,\langle x_{0\mu}Kx_1^{\mu}K^{\dagger}\rangle \\ &+ \frac{1}{2}f_K^2\,\langle D^{\mu}K\; D_{\mu}K^{\dagger}\rangle\,. \end{aligned} \tag{4.58}$$

$\boldsymbol{\mathcal{F}}_{\mu\nu}$ is the field strength tensor of $\boldsymbol{\mathcal{F}}_{\mu}$. The K field is introduced to break the two remaining copies of $Sp(4)$, $Sp(4)_0 \times Sp(4)_1$ to the diagonal final $Sp(4)$:

$$K = \exp\left[ik^a V^a/f_K\right]\,, \tag{4.59}$$

and it transforms like

$$K \to K' = h(g_0,\pi_0)\,K\,h^{\dagger}(g_1,\pi_1)\,, \tag{4.60}$$

thus its covariant derivative takes the form

$$D_{\mu}K = \partial_{\mu}K - iv_{0\mu}K + iKv_{1\mu}\,. \tag{4.61}$$

The 10 pions contained in K are needed to provide the longitudinal degrees of freedom for the 10 vectors $\mathcal{V}_{\mu}^a$, while a combination of the other pions π^i acts as the longitudinal degrees of freedom for the $\mathcal{A}_{\mu}^a$. It should be reminded that out of the 5 remaining scalars, 3 are exact NGBs *eaten* by the massive W and Z bosons, while 2 remain as physical scalars in the spectrum: one Higgs-like state plus a singlet η.

The EW *vev* is

$$v^2 = \left(f_0^2 - r^2 f_1^2\right)\sin^2\theta = f_{\pi}^2\sin^2\theta\,, \tag{4.62}$$

where $f_{\pi} = \sqrt{f_0^2 - r^2 f_1^2}$. We neglect possible direct couplings of $\boldsymbol{\mathcal{F}}_{\mu}$ to fermions, which are generated in our set-up only through the mixing with EW gauge bosons.

The masses of $\boldsymbol{\mathcal{V}}_{\mu}$ and $\boldsymbol{\mathcal{A}}_{\mu}$ (without EW interactions) are given respectively by

$$M_V \equiv \frac{\widetilde{g}f_K}{\sqrt{2}} \quad \text{and} \quad M_{\boldsymbol{\mathcal{A}}} \equiv \frac{\widetilde{g}f_1}{\sqrt{2}}\,. \tag{4.63}$$

These masses have been estimated with lattice calculations for the FMCHM SU(2) gauge theory with 2 Dirac fermions, $M_V = 3.2(5)\ \text{TeV}/\sin\theta$ and $M_{\boldsymbol{\mathcal{A}}} = 3.6(9)\ \text{TeV}/\sin\theta$ [203].

Once the masses are fixed there are 2 extra free parameters which were not computed from first principles: $\widetilde{g}$ and r. These parameters basically determine the branching ratios into fermions or bosons. If $r = 1$ the fermion decays dominate, once $|r-1| \gtrsim 0.1$ the diboson decays dominate.

We now evaluate the trilinear couplings between heavy vectors and the Goldstone bosons, which will be important for our analysis of the Goldstone Boson Scattering. They come from the f_K term in 4.58. Only couplings to $\boldsymbol{\mathcal{V}}_{\mu}$ are generated, which can be expressed as

$$\begin{aligned}\pi_a\pi_b\mathcal{V}_{\mu}^c:\qquad & \frac{2\widetilde{g}f_K^2(1-r^2)}{f^2}\,\mathrm{Tr}(Y^aY^bV^c)(p_a-p_b) \\ & = ig_V(p_a-p_b)\Xi^{abc}, \end{aligned} \tag{4.64}$$

where

$$g_V = -\frac{M_V}{2f} a_V = -\frac{M_V^2(1-r^2)}{\sqrt{2}\tilde{g} f^2}\,, \tag{4.65}$$

and $\Xi^{abc} = 1$ for (c,a,b)= (1,3,2), (2,3,1), (3,1,2), (4,1,4), (5,2,4), (6,3,4), (7,5,3), (8,5,4), (9,5,1), (10,2,5), $\Xi^{abc} = -1$ by interchanging $a \leftrightarrow b$ above and $\Xi^{abc} = 0$ otherwise.

4.2.2. Scalar isosinglet σ

Additional scalars are a common feature in composite extensions of the SM, see *e.g.* [204, 205]. The scalar singlet σ can be incorporated in a simple general way

$$\mathcal{L}_\sigma = \frac{1}{2}\kappa(\sigma) f^2 \langle x_\mu x^\mu \rangle + \frac{1}{2}\partial_\mu \sigma \partial^\mu \sigma - \frac{1}{2} M_\sigma^2 \sigma^2\,, \tag{4.66}$$

with $\kappa(\sigma) = 1 + \kappa'\sigma/f + \kappa''\sigma^2/(2f) + \cdots$. The potential (which must be added to $\mathcal{L}_\sigma$) generates a tadpole term that drives the *vev* to σ. In addition, it also generates a mixing term with the Higgs boson, $h \equiv \phi_4$. These effects are however small when a very heavy scalar is considered. Mixing between h and σ is, for small θ, approximately $\alpha \sim \frac{2m_h^2}{m_\sigma^2}$ [200]. For $M_\sigma \gtrsim 5$ TeV, $\alpha \lesssim 0.00125$ is very small and will be neglected in the following analysis.

The relevant parameters here are M_σ and κ'. The lattice prediction for the SU(2) gauge theory with 2 Dirac fermions has large uncertainty, $M_\sigma = 4.7(2.6)\ \text{TeV}/\sin\theta$ [203]. We will see that unitarity of VBS provides more stringent limits on the parameters of this state. The trilinear couplings between σ and the NGBs read

$$\sigma\pi_a\pi_b : -2i\frac{g_\sigma}{f} p_a \cdot p_b\,, \tag{4.67}$$

with $g_\sigma = \kappa'/2$.

4.3. Unitarity Implications

Striking evidence of new strong dynamics at high scales is the presence of strong Vector Boson Scattering (VBS) [206–211], or more generally strong Goldstone Boson Scattering (GBS), including physical pseudo-NGBs (the Higgs boson itself and others in non-minimal CH realisations) and longitudinal VBS, which are related to the GBS by the Goldstone Boson Equivalence Theorem (GBET) [212]. The strong nature of the NGBs in CH models manifests itself in GBS through the miscancellation of Feynman diagrams and the divergent behaviour of the scattering amplitudes according to the Low Energy Theorems (LET) [213]

$$\mathcal{A}(\pi\pi \to \pi\pi) \sim \frac{s}{f^2} = \frac{s}{v^2}\sin^2\theta\,, \tag{4.68}$$

with π a NGB and s the Mandelstam variable. This is in contrast with the well behaved amplitudes of the SM, which approach $-m_h^2/v^2 \sim 0.26$ at high energies. The growing behaviour of GBS amplitudes must eventually be controlled by strong effects at high

energies, either in the form of broad *continuum* enhancements or in the form of composite resonances, saturating unitarity in a similar way to what happens in hadron physics. In this case, the possibility to probe such high scales at the LHC, or at a higher energy machine such as the FCC 100 TeV collider, remains to be quantified.

To tackle this problem the first question that arises is how to estimate the actual scale of resonance formation or strong *continuum* effects. The unitarity of $2 \to 2$ GBS amplitudes has been used as a tool to set limits on the scale of new physics or strong interactions, and on the mass of a heavy Higgs boson [209,214,215]. We pursue this idea in the context of CH models, as done in ref. [216].

Through the analysis of the GBS amplitudes and under the guidance of unitarity principles we set limits on the scale of resonance formation, in particular in the scalar channel which is only poorly described by lattice calculations. We will show that near the scale of leading-order (LO) unitarity violation the *continuum* of LET dominates the scattering amplitudes and prevents the formation of Breit-Wigner resonances. We will also argue that we can not only set constraints on the masses of resonances, but also on their couplings, if we assume basic criteria of saturation of unitarity and analyticity provided by the Inverse Amplitude Method (IAM) of unitarisation.

Following our assessment of resonance profiles via the study of unitarisation of GBS amplitudes, we estimate the potential to observe strong effects in realistic observables, whether resonances or strong *continuum* effects dominate the amplitudes. We analyze the production cross sections of heavy vector resonances through weak boson fusion (VBF) and Drell-Yan (DY) and non-resonant and scalar-resonant scenarios of strong VBS in $pp \to jjZZ \to jj4\ell$ channel.

In light of the results from the study of the amplitudes unitarity, we study the possibility of observing signals of strong VBS and heavy vector production at the LHC and a future 100 TeV collider.

In order to analyse unitarity, it is imperative to include higher order terms due to the strong relation between perturbativity and unitarity. Since the CCWZ Lagrangian in eq. 4.44 is an effective *non-renormalizable* theory, each order in the perturbation expansion has to be accompanied by a tower of higher dimension operators in order to carry out the renormalisation program. The $d = 4$ Lagrangian is given by

$$\begin{aligned} \mathcal{L}_4 &= L_0\langle x^\mu x^\nu x_\mu x_\nu\rangle + L_1\langle x^\mu x_\mu\rangle\langle x^\nu x_\nu\rangle \\ &+ L_2\langle x^\mu x^\nu\rangle\langle x_\mu x_\nu\rangle + L_3\langle x^\mu x_\mu x^\nu x_\nu\rangle\,, \end{aligned} \tag{4.69}$$

where the L_i are the so-called bare low energy constants, which represent the relative strengths encoded by the respective terms in the Lagrangian. The $\langle\rangle$ symbols stands for the trace, Tr, of the operators. These are unknown and we set them using the constraints from the unitarisation methods.

When talking about unitarity, we always refer to the unitarity of the S-matrix. It is well known in perturbation theory that the evolution of a state $|i\rangle$ to another one $|f\rangle$, at time $t \to \infty$, in general to be defined as *asymptotical* states, is described in term of the S-matrix,

$$\lim_{f\to\infty} |t\rangle = S|i\rangle\,. \tag{4.70}$$

The relevant matrix element is therefore proportional to

$$|\langle f|S|i\rangle|^2 \, . \tag{4.71}$$

Summing up the probability of finding all possible final states leads us to the condition of unitarity of the scattering matrix S

$$\sum_f |\langle f|S|i\rangle|^2 = \sum_f \langle i|S^\dagger|f\rangle\langle f|S|i\rangle = \langle i|S^\dagger S|i\rangle = 1 \, , \tag{4.72}$$

where we have used the completeness relation $\sum_f |f\rangle\langle f| = \mathrm{id}$. Splitting the S matrix as $S = \mathbb{1} + T$, where $\mathbb{1}$ encodes the non-interaction probability, we find the expression of the *optical* theorem,

$$(T - T^\dagger) = iT^\dagger T \, . \tag{4.73}$$

When we compute T using perturbation theory, we are fated to be incomplete due to the lack of higher order terms. In this approximation, it is possible that an apparent violation of unitarity is present. The typical example of this behaviour is exactly the scattering of gauge-bosons, in the absence (or partial absence) of the Higgs boson, or, at lower energies, meson-meson scattering. In this way one loses the predictability of resonances, which is one of the most typical feature of strongly interacting theories; nevertheless, different methods exist to enhance the applicability region to higher energies. These methods have been implemented and studied in the context of the full $2 \to 6$ matrix elements framework for strong VBS in Ref. [217].

A phenomenological approach to describe the physics beyond the perturbative regime in Goldstone scattering is given by unitarisation models. Forcing the amplitudes of GBS to satisfy the unitarity condition and maintain the low energy behaviour. Unitarisation models are intended to represent the approximate magnitude of these amplitudes beyond the perturbative regime and have been able, in some cases, to describe the first resonances of QCD. In view of the great similarities between low energy QCD and the Electroweak physics, the ideas of unitarisation models have been translated to a strong symmetry breaking sector in many studies [15, 218–223]. They are not complete quantum field theories and, in particular, they typically violate crossing symmetry, but despite those deficiencies, these models still carry out their phenomenological purpose of estimating the magnitude of strong VV scattering cross sections much above the perturbative regime. Several Unitarisation Methods have been proposed within the studies of scattering of pions, exactly our case of study, and inspire the current work. Examples are the Padé approximant [224], the N/D approach [225] or the explicit introduction of resonances [226], the K-matrix already developed in the '40s [227, 228].

Besides violating crossing symmetry, the K-matrix unitarisation procedure spoils the singularity structure of the fixed-order amplitudes. In the N/D protocol, unitarity is exactly restored with the extra quality of improved analytical properties, at the cost of introducing a new mass parameter [229]. A special case of the N/D method is the so-called Inverse Amplitude Method (IAM), which maintains the proper analytical structure of fixed order calculation with the correct branching cuts and without the need

for extra parameters. It also produces very interesting phenomenological consequences in the context of strong vector boson scattering. It has been widely and successfully used in the description of low energy pion-pion scattering and has given remarkable results describing meson dynamics beyond the perturbative regime, reproducing the first resonances in each isospin-spin channel up to 1.2 GeV [230]. For certain values of the chiral coefficients, the unitarized amplitudes, both by N/D and IAM protocols, present poles that can be interpreted as dynamically generated resonances.

In dealing with strongly interacting particles, it is usual to project the amplitudes with definite angular momentum J

$$\begin{aligned} \mathcal{A}(s,t) &= 32\pi \sum_{J=0}^{\infty} a_J(s)(2J+1)P_J(\cos\theta), \\ a_J(s) &= \frac{1}{32\pi\, s}\int_{-s}^{0} \mathrm{d}t \mathcal{A}(s,t,u)P_J(x)\,, \end{aligned} \tag{4.74}$$

where x is the cosine of the scattering angle and $P_J(x)$ are the Legendre polynomials, and $\mathcal{A}(s,t,u)$ is the amplitude for the scattering under consideration, expressed in terms of the Mandelstam variables. In this basis it is easy to derive directly from the unitarity of the S matrix expressed in eq. 4.72 the partial-wave unitarity condition, under the conditions $s > s_{th}$, so, above the threshold energy, s_{th}, for the process, and below inelastic thresholds,

$$\mathrm{Im}\, a_J(s) = |a_J(s)|^2\,. \tag{4.75}$$

In order to force elasticity (and thus make direct use of eq. 4.75) it is customary to expand the amplitudes in definite conserved quantum numbers before expanding them in partial waves.

We derive the Inverse Amplitude Method using dispersion theory, as shown in ref. [230], which we follow for the below derivation. Basically any partial wave obtained from a relativistic Quantum Field Theory present a complex structure in the s plane. This should exhibit a cut structure from the threshold value, s_{th}, to ∞. Applying Cauchy's theorem to the amplitude, it is possible to recover integral equations known as dispersion relations. Usually it is possible to write "subtracted" dispersion relations, in the case of a general complex function $f(z) \neq 0$ as $|z| \to \infty$, which is indeed our case. This is basically the relation for $f(s) - f(0)$, that simplifies as

$$f(s) = f(0) + \frac{s}{\pi}\int \frac{\mathrm{d}s'}{s'}\frac{\mathrm{Im}f(s')}{s'-s-i\epsilon}\,, \tag{4.76}$$

as $\mathrm{Im}f(0) = 0$.

Going back to partial-wave amplitudes, we could write a three-times subtracted dispersion relation as

$$a_{IJ}(s) = C_0 + C_1 s + C_2 s^2 + \frac{s^3}{\pi}\int_{M^2}^{\infty} \frac{\mathrm{Im}a_{IJ}(s')\mathrm{d}s'}{s'^3(s'-s-i\epsilon)} + \mathrm{LC}(a_{IJ})\,, \tag{4.77}$$

with C_i the subtraction coefficients and M the general threshold mass for the process. LC defines the left cut contribution. The number of subtraction depends on the order of

accuracy we are employing in our calculation. Our amplitudes at leading and next-to-leading order $a^{(0)}(s)$ and $a^{(1)}$ present both cuts and we can compute them perturbatively

$$a^{(0)}(s) = a_0 + a_1 s \,, \tag{4.78}$$

$$a^{(1)}(s) = b_0 + b_1 s + b_2 s^2 + \frac{s^3}{\pi}\int_{M^2}^{\infty} \frac{\mathrm{Im}a^{(1)}(s')\mathrm{d}s'}{s'^3(s'-s-i\epsilon)} + \mathrm{LC}(a^{(1)}) \,. \tag{4.79}$$

The IAM relies on the fact the function $1/a_{IJ}$ exhibits the same analytic structure as a_{IJ} itself, apart from some pole contribution. Thus, writing $G(s) = (a_{IJ}^{(0)})^2/a_{IJ}$, we can write the subtracted version

$$G(s) = G_0 + G_1 s + G_2 s^2 + \frac{s^3}{\pi}\int_{M^2}^{\infty} \frac{\mathrm{Im}G(s')\mathrm{d}s'}{s'^3(s'-s-i\epsilon)} + \mathrm{LC}(G(s) + \mathrm{PC} \,, \tag{4.80}$$

where PC denotes the pole contributions, and G_i the usual subtracted terms. Expanding eq. 4.80 and substituting with eqs. 4.78 and 4.79, we can compute

$$\frac{a_{IJ}^{(0)^2}}{a_{IJ}} \sim a_0 + a_1 s - b_0 - b_1 - b_2 s^2 - \frac{s^3}{\pi}\int_{M^2}^{\infty} \frac{\mathrm{Im}a_{IJ}^{(1)}(s')\mathrm{d}s'}{s'^3(s'-s-i\epsilon)} + \mathrm{LC}(a_{IJ}^{(1)}(s)) + \mathrm{PC} \sim a_{IJ}^{(0)} - a_{IJ}^{(1)} \,. \tag{4.81}$$

We approximated $\mathrm{Im}G \sim -\mathrm{Im}a_{IJ}^{(1)}$ on the cut and neglected pole contributions. So, finally, we can write the formula for the IAM procedure we employ to force unitarisation

$$a_{IJ} \sim \frac{a_{IJ}^{(0)\,2}}{a_{IJ}^{(0)} - a_{IJ}^{(1)}} \,. \tag{4.82}$$

4.3.1. Unitarity constraints in $SU(4)/Sp(4)$ VBS

In the chiral Lagrangian of pions the $\pi\pi$ scattering amplitudes can be expanded in the usual definite isospin I [213, 225]. The generalisation of such procedure is presented for the case of $SU(2N)/Sp(2n)$ theories in ref. [231], and we redirect there for details on the calculations of the amplitudes. For SU(4)/Sp(4), just like isospin, we expect that specially at high energies Sp(4) is approximately unbroken and we can therefore expand the $2 \to 2$ NGB scattering in definite multiplets of Sp(4), as

$$\mathbf{5} \otimes \mathbf{5} = \mathbf{1} \oplus \mathbf{10} \oplus \mathbf{14} \,, \tag{4.83}$$

and assume they correspond to pure elastic channels, with no mixing among them. We note that the Higgs boson is also part of the NGB scattering. The VBS topology can be seen as a special case of this scattering, with the longitudinal modes related to the eaten NGB π^i (i=1,2,3) through the equivalence theorem.

From the $d = 2$ Lagrangian in eq. 4.41 we get the LO amplitudes. We will consider only the leading spin, *i.e.* the scalar $J = 0$ for the singlet channel $\mathbf{1} \equiv A$, $a_{A0}(s)$, the vector $J = 1$ for the $\mathbf{10} \equiv B$ representation (since the $J = 0$ amplitude vanishes), $a_{B1}(s)$,

and the scalar for $\mathbf{14} \equiv C$, $a_{C0}(s)$. The corresponding partial wave amplitudes at LO are:

$$a^{(0)}_{A0}(s) = \frac{s}{16\pi f^2}\,, \tag{4.84}$$

$$a^{(0)}_{B1}(s) = \frac{s}{192\pi f^2}\,, \tag{4.85}$$

$$a^{(0)}_{C0}(s) = \frac{-s}{64\pi f^2}\,. \tag{4.86}$$

A real-valued amplitude can never satisfy the unitarity condition, eq. 4.75. The absorptive and imaginary part of the amplitude comes at first order at loop level, and fulfils the perturbative unitarity relation

$$\mathrm{Im}\, a^{(1)}(s) = |a^{(0)}(s)|^2\,, \tag{4.87}$$

where $a^{(1)}(s)$ is the correction from the effective energy expansion. As long as perturbativity is under control this relation is sufficient to avoid unitarity violation, which makes the relation between unitarity and perturbativity evident. This observation allows us to define another criterion of unitarity, which is

$$|a(s)| < 1\,. \tag{4.88}$$

Therefore, according to eq. 4.84 unitarity is fated to be violated at energies

$$\sqrt{s} \gtrsim 4\sqrt{\pi} f\,. \tag{4.89}$$

Since from EWPO we expect $\sin\theta \lesssim 0.2$, we need to reach partonic energies of the order of $\sqrt{\hat{s}} \gtrsim 8$ TeV to observe strong VBS effects. Such energies could, in principle, be at the extreme corner of the LHC, but it seems more feasible to reach those energies at a higher energy machine, such as a 100 TeV collider. Even for lower angles, *e.g.* $\theta = 0.1$, unitarity violation would take place around $\sqrt{s} \sim 16$ TeV, which is within the reach of a 100 TeV machine.

The next-to-leading order (NLO) correction to the partial wave amplitudes, which includes the tree level diagrams involving dimension-6 operators, eq. 4.69, and one-loop diagrams, is given by

$$a^{(1)}_{A0}(s) = \frac{s^2}{32\pi f^4}\left[\frac{1}{16\pi^2}\left(\frac{29}{12} + \frac{46}{18}\log\left(\frac{s}{\mu^2}\right) + 2\pi i\right) + \frac{2}{3}\widehat{L_A}(\mu)\right]\,, \tag{4.90}$$

$$a^{(1)}_{B1}(s) = \frac{s^2}{32\pi f^4}\left[\frac{1}{16\pi^2}\left(-\frac{35}{432} + \frac{1}{12}\log\left(\frac{s}{\mu^2}\right) + \frac{1}{72}\pi i\right) + \frac{2}{3}\widehat{L_B}(\mu)\right]\,, \tag{4.91}$$

$$a^{(1)}_{C0}(s) = \frac{s^2}{32\pi f^4}\left[\frac{1}{16\pi^2}\left(\frac{83}{144} - \frac{4}{9}\log\left(\frac{s}{\mu^2}\right) + \frac{1}{8}\pi i\right) + \frac{2}{3}\widehat{L_C}(\mu)\right]\,. \tag{4.92}$$

We defined the following combinations of Wilson coefficients:

$$\begin{aligned}
\widehat{L_A}(\mu) &= \widehat{L_0}(\mu) + 68\widehat{L_1}(\mu) + 36\widehat{L_2}(\mu) + 17\widehat{L_3}(\mu)\,,\\
\widehat{L_B}(\mu) &= 2\widehat{L_0}(\mu) - 4\widehat{L_1}(\mu) + 2\widehat{L_2}(\mu) - \widehat{L_3}(\mu)\,,\\
\widehat{L_C}(\mu) &= 8\widehat{L_1}(\mu) + 16\widehat{L_2}(\mu) + 2\widehat{L_3}(\mu)\,.
\end{aligned} \tag{4.93}$$

$\widehat{L_I}(\mu)$ are renormalised in the $\overline{MS}$ scheme and run according to the renormalisation group equations,

$$\widehat{L_I}(\mu) = \widehat{L_I}(\mu_0) + \frac{k_I}{16\pi^2}\log\left(\frac{\mu}{\mu_0}\right) , \tag{4.94}$$

with $k_I = -43/6,\ 1/4,\ -4/3$ for $I = A,\ B,\ C$, respectively. Of the 4 coefficients only 2 are independent for what concerns this process. In particular we have

$$\widehat{L_C}(\mu) = \frac{2}{7}\left(\widehat{L_A}(\mu) + 10\widehat{L_B}(\mu)\right) . \tag{4.95}$$

The correction is always in the direction of making unitarity bounds stronger. We show in fig. 4.1 the energy where unitarity is lost in the $A0$ channel, at NLO (Λ_{NLO}) as a function of $\widehat{L_A}(8\text{ TeV})$ and at LO (vertical black line, Λ_{LO}) for $\sin\theta = 0.2$. The result for different θ is very similar, indeed if we choose the renormalisation scale proportional to $\sqrt{s}$, $\mu \propto \sqrt{s}$ we find that the amplitudes depend only on the ratio s/f^2 apart from logarithmic corrections from the running of the effective coefficients. We also show in the shaded areas the regions where the K-factor $K \equiv |a^{NLO}(s)|/|a^{LO}(s)| - 1$ is $K > 50\%$ (blue area), $K < -50\%$ (green area) and $K > 100\%$ (brown area), where perturbativity is jeopardised. We define $a^{NLO}(s) = a^{(0)}(s) + a^{(1)}(s)$ and $a^{LO}(s) = a^{(0)}(s)$.

We notice that the NLO correction can never further postpone unitarity violation and therefore the LO limit, Λ_{LO}, is an important physical scale. This observation has interesting consequences. If the NLO corrections to $|a(s)|$ are positive, they will lead to a broad *continuum* enhancement at least as strong as the LO amplitude or to resonance formation *before* the scale of LO unitarity violation, *i.e.*, the mass of the resonance obeys $M \lesssim \Lambda_{LO}$. For the scalar $A0$ channel this implies $M_\sigma \lesssim 1.7\text{ TeV}/\sin\theta$, which is more stringent than lattice results on the scalar spectrum of $SU(2)$ gauge theory with 2 Dirac fermions, which provide $M_\sigma = 4.7(2.6)\text{ TeV}/\sin\theta$. If the NLO corrections are negative at $\sqrt{s} < \Lambda_{LO}$, they must grow rapidly to cross the LO amplitude before Λ_{LO} and should be very likely controlled by a more strongly bounded and narrower resonance. In either case, the LO amplitude enhancement can be regarded as the weakest and smoothest possible strong effect in GBS before unitarity violation.

We concentrate here on the IAM due to its good analytical properties and the dynamical generation of resonances, which we aim to compare with the effective description of sec. 4.2. The IAM defines the unitarised amplitude

$$a_{IJ}^{IAM}(s) = \frac{a_{IJ}^{(0)}(s)}{1 - \frac{a_{IJ}^{(1)}(s)}{a_{IJ}^{(0)}(s)}} . \tag{4.96}$$

For low energies this amplitude restores the chiral amplitudes while fully satisfying the unitarity condition. From the denominator of the IAM amplitudes a mass and a running

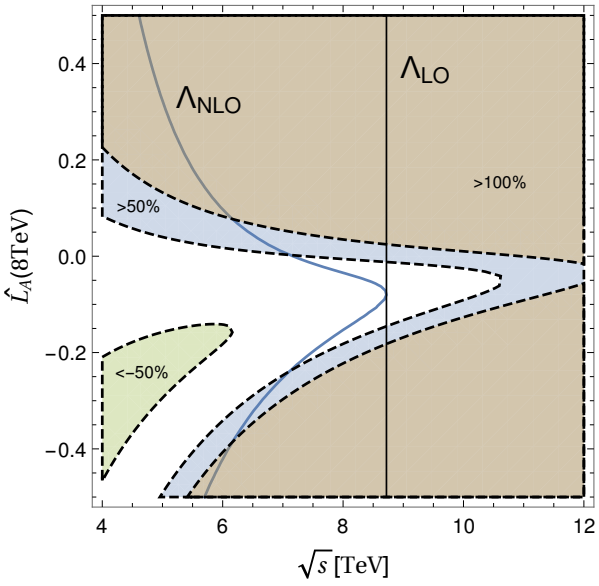

Figure 4.1.: Unitarity violation scale of $a_{A0}(s)$ as a function of $\widehat{L_A}(8\text{ TeV})$ for $\sin\theta = 0.2$ at NLO (blue solid) and LO (black solid). Also shown the regions of perturbativity loss $K \equiv |a^{NLO}(s)|/|a^{LO}(s)| - 1 > 50\%$ (blue shaded area), $K > 100\%$ (brown area) and $K < -50\%$ (green area).

width can be extracted

$$\begin{aligned} M_A^2 &= \frac{2f^2}{\frac{1}{16\pi^2}\left(\frac{29}{12}\right) + \frac{2}{3}\widehat{L_A}(M_A)}, \quad \Gamma_A = \frac{M_A^3}{16\pi f^2}, \\ M_B^2 &= \frac{(f^2/6)}{\frac{1}{16\pi^2}\left(-\frac{35}{432}\right) + \frac{2}{3}\widehat{L_B}(M_B)}, \quad \Gamma_B = \frac{M_B^3}{192\pi f^2}, \\ M_C^2 &= \frac{-(f^2/2)}{\frac{1}{16\pi^2}\left(\frac{83}{144}\right) + \frac{2}{3}\widehat{L_C}(M_C)}, \quad \Gamma_C = \frac{M_C^3}{64 f^2}\,. \end{aligned} \tag{4.97}$$

The amplitudes can then be written in a particularly simple form by choosing a dynamical renormalization scale $\mu = \sqrt{s}$,

$$a_{IJ}^{IAM}(s) = \frac{-\Gamma_I/M_I}{s - M_I^2 + i\frac{\Gamma_I}{M_I}s + 32\pi s \frac{\Gamma_I}{M_I}\frac{k_I}{16\pi^2}\log\left(\frac{\sqrt{s}}{M_I}\right)} \tag{4.98}$$

with k_I given in eq. 4.94.

As a specific example and benchmark scenario we now make use of lattice results $M_V \equiv M_B = 3.2(5)\text{ TeV}/\sin\theta$. The corresponding effective coefficient can be extracted from eq. 4.97, $L_B(M_V) = 2.225 \times 10^{-3}$, and it is independent of θ. The $J = 1$ partial wave amplitude for this scenario is shown for $\sin\theta = 0.2(0.15)$ in fig. 4.2. We use renormalisation scale $\mu = \sqrt{s}$.

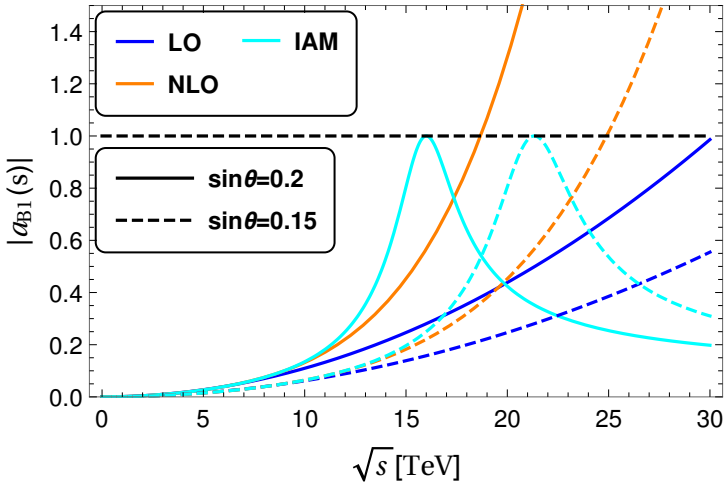

Figure 4.2.: Absolute value of partial wave amplitude $a_{B1}^{IAM}(s)$ shown together with $a_{B1}^{NLO}(s)$ and $a_{B1}^{LO}(s)$ for $\sin\theta = 0.2$ and 0.15.

For the scalar channel the lattice result $M_\sigma \equiv M_A = 4.7(2.6)$ TeV$/\sin\theta$ has very large uncertainty. The mass of an eventual resonance is also proportional to the scale f, thus we define the parameters

$$\upsilon_I \equiv \frac{M_I \sin\theta}{\text{TeV}}, \quad I = A, B, C\,. \tag{4.99}$$

The effective coefficient for channel A is $L_A(M_A) = -0.0229556 + 0.181548/\upsilon_A^2$. The corresponding unitarised amplitude is shown in fig. 4.3 for different values of υ_A. For large values of $\upsilon_A \gtrsim 1.5$ a broad enhancement takes the place of the typical Breit-Wigner peak of a resonance.

We now look at unitarisation of the C channel. As mentioned before, the effective coefficients are linearly dependent according to eq. 4.95; therefore, if we choose to fix lattice inspired $\upsilon_B = 3.2$, we find the relation among υ_C and υ_A, shown in fig. 4.4. We conclude that this eventual resonance must be at higher scales.

4.3.2. Vector Resonances

Both in this and the following sections, we use the chiral Lagrangians described in section 4.2 including vector and scalar states to estimate their parameters in the light of unitarity considerations just explored. Let us start with the vector case.

At tree-level the projections can all be computed from the single master amplitude $\mathcal{A}(s,t,u)$ of the process $\pi^+\pi^- \to \pi^0\pi^0$. The vector states contribute with trilinear couplings to the NGBs and also by modifying the quartic coupling of NGBs to recover

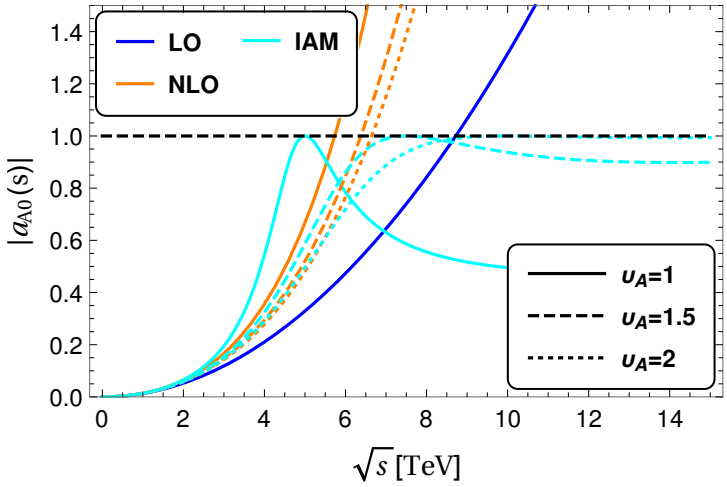

Figure 4.3.: Absolute value of partial wave amplitude $a_{A0}^{IAM}(s)$ shown together with $a_{A0}^{NLO}(s)$ and $a_{A0}^{LO}(s)$.

the correct LET behaviour, giving

$$\mathcal{A}(s,t,u) = -g_V^2 \left(\frac{s-u}{t-M_V^2} + \frac{s-t}{u-M_V^2} + \frac{3s}{M_V^2} \right) . \tag{4.100}$$

The projections are given by

$$\begin{aligned} \mathcal{A}_A(s,t,u) &= 5\mathcal{A}(s,t,u) + \mathcal{A}(t,s,u) + \mathcal{A}(u,t,s) , \\ \mathcal{A}_B(s,t,u) &= \mathcal{A}(t,s,u) - \mathcal{A}(u,s,t) , \\ \mathcal{A}_C(s,t,u) &= \mathcal{A}(t,s,u) + \mathcal{A}(u,s,t) . \end{aligned} \tag{4.101}$$

Further expanding in partial waves we get

$$a_{A0}^v(s) = -\frac{g_V^2}{8\pi} \left[(2 + 3\frac{s}{M_V^2}) - 2(\frac{M_V^2}{s} + 2) \log(1 + \frac{s}{M_V^2}) \right] , \tag{4.102}$$

$$\begin{aligned} a_{B1}^v(s) = \frac{g_V^2}{32\pi} \Bigg[& \frac{s}{3(s-M_V^2)} - \frac{s}{2M_V^2} \\ & -(\frac{M_V^2}{s} + 2) \left(2 - (2\frac{M_V^2}{s} + 1) \log(1 + \frac{s}{M_V^2}) \right) \Bigg] . \end{aligned} \tag{4.103}$$

The $J = 1$ amplitude is shown in fig. 4.5 for $\sin\theta = 0.2$ and lattice inspired value of mass $M_V = 3.2$ TeV$/\sin\theta$. We show 3 different values of the vector coupling $a_V = 0.8$, 1, 1.2. We can see that a_V must be close to 1 to better describe the dynamical inspired IAM amplitude. Moreover, the departure from $a_V = 1$ creates large deviations from

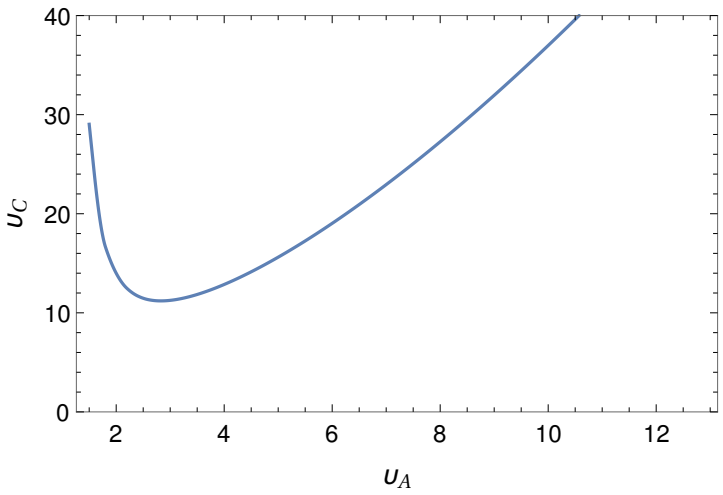

Figure 4.4.: Value of v_C as a function of v_A for fixed value of $v_B = 3.2$.

the LO amplitude at low energy. We therefore take $a_V = 1$ as a *natural* value. The total width of the decay into the NGBs is given by $\Gamma_V = \frac{g_V^2}{48\pi} M_V$. The choice $a_V = 1$ reproduces the total width provided by IAM method, eq. 4.97.

A remark about the EW and photon exchange follows. It is well known that low-mass boson exchange leads to large logarithmic enhancements due to the so-called "exceptional" phase-space regions, *e.g.*, the terms $\log(1 + \frac{s}{M_V^2})$ when $t \to 0$. These large logarithms usually need to be resummed for improved perturbative calculations. Nevertheless, this EW physics is not relevant for the present analysis, belonging to a different energy scale for the process under consideration [209, 212].

4.3.3. Scalar isosinglet σ

The σ contribution to the master amplitude is given by

$$\mathcal{A}(s,t,u) = -g_\sigma^2 \frac{s}{f^2} \frac{s}{s - M_\sigma^2}\,, \tag{4.104}$$

with $g_\sigma = \kappa'/2$.

The total width of σ into NGBs is given by $\Gamma_\sigma = 5\frac{g_\sigma^2 m_\sigma^3}{32\pi f^2}$. Requiring a width similar to IAM leads to $g_\sigma \sim 0.63$.

We show in the left-hand panel of fig. 4.6 the $a_{A0}(s)$ amplitudes, including the σ contribution for $g_\sigma = 0.63$ and $v_A = 1$. We also show the contribution from the v state with $a_V = 1$, which further postpone unitarity violation. In the right-hand panel, we show the equivalent $a_{B1}(s)$ amplitudes, including the σ contribution.

For larger values of $v_A \gtrsim 1$ the growing behaviour of the LO piece renders difficult for a resonance to unitarise the amplitude. This fact is illustrated in fig. 4.7 where we show

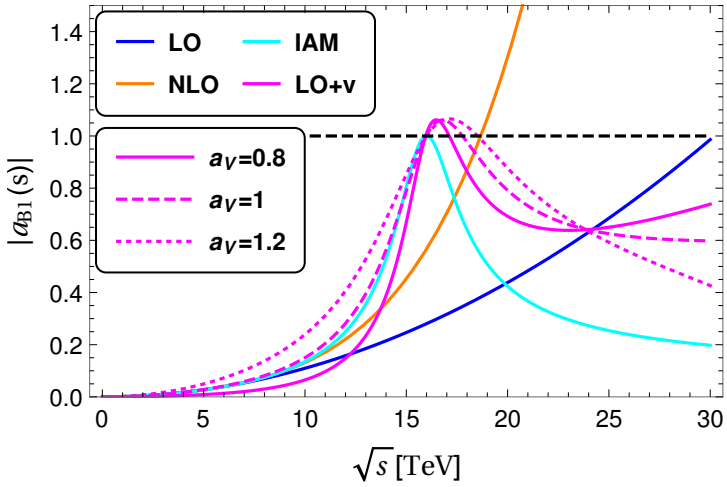

Figure 4.5.: Absolute value of partial wave amplitude $a^0_{B1}(s) + a^v_{B1}(s)$ together with LO, NLO and IAM equivalents, for three values of $a_V = 0.8,\ 1,\ 1.2$ and $\sin\theta = 0.2$.

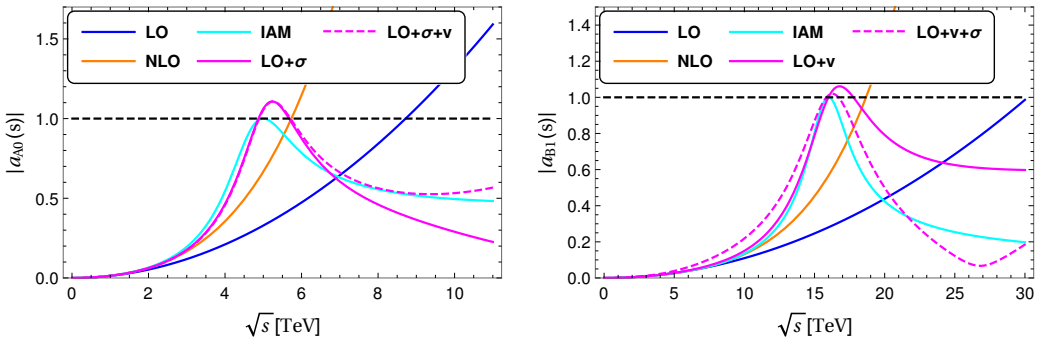

Figure 4.6.: *Left* panel: absolute value of partial wave amplitudes $a^0_{A0}(s)+a^\sigma_{A0}(s)+a^v_{A0}(s)$ together with LO, NLO and IAM equivalents. *Right* panel: equivalent amplitudes for $B1$ channel, $a^0_{B1}(s) + a^\sigma_{B1}(s) + a^v_{B1}(s)$. Parameters are $v_A = 1$, $\sin\theta = 0.2$, $g_\sigma = 0.63$.

the $a_{A0}(s)$ amplitudes for 3 values of $v_A = 0.5,\ 1,\ 1.5$, using the IAM unitarisation model (solid curve), the fixed width σ resonance (dashed) or a running width, $\Gamma_{fix} \to \frac{\Gamma_{run}}{M}s$, (dotted). The resummation of the self-energy diagrams lead to momenta dependent widths, or *running widths*, which are typically important for heavy and broad resonances. An *ad-hoc* incorporation of such running width, is however, not usually recommendable due to large extra mis-cancellations which worsen unitarity problems at higher energies,

and can be cured with a running width gauge invariant method as in ref. [232]. It can be seen that values of M_σ too close or larger than unitarity violation scale, $M_\sigma \sim \Lambda_{LO}$, prevent any meaningful use of resonant propagation and a broad *continuum* appears instead. Moreover, close to the peak the running width approach slightly ameliorates the lineshape description.

Similarly, large couplings can also jeopardise the resonant description and violate unitarity. Extra contributions to the width can dampen down and unitarise the amplitude, but nevertheless not helping in the description of the lineshape. In fig. 4.8 we show the $a_{A0}(s)$ amplitudes for 3 values of g_σ using the IAM unitarisation model (cyan), a fixed width (solid) and a running width (dashed).

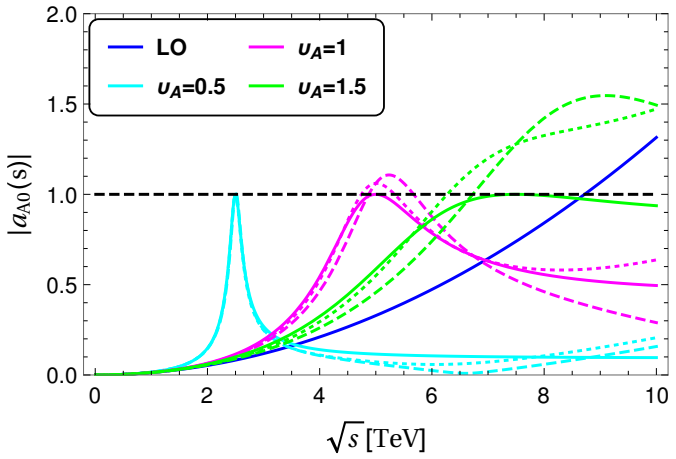

Figure 4.7.: Absolute value of partial wave amplitudes $a^0_{A0}(s) + a^\sigma_{A0}(s)$ for $\upsilon_A = 0.5$, 1, 1.5, using the IAM unitarisation model (solid curve), a fixed width σ resonance (dashed) and a running width (dotted).

4.4. Experimental signatures at Future Colliders

So far we have discussed the implications of the Composite Higgs model in the coset $SU(4)/Sp(4)$ with respect to the Standard Model realisation at amplitude level. In the SM prediction, the Higgs exchange would provide an almost exact cancellation of the contributions in the scattering of longitudinal gauge bosons. Introducing the Higgs as a pseudo-Nambu Goldstone boson coming from the symmetry breaking pattern $SU(4)/Sp(4)$ we have seen there is a miscancellation of the various diagrams parametrised by the vacuum misalignment angle, θ. This leads to a general enhancement of the amplitudes of the longitudinal boson scattering, and from this follows the need for a unitarisation procedure, as the process violates the unitarity requirement. Ideally, the enhancement translates to the typical observable of the process we are considering, but from the point of view of the experiment this is not as simple as the situation we

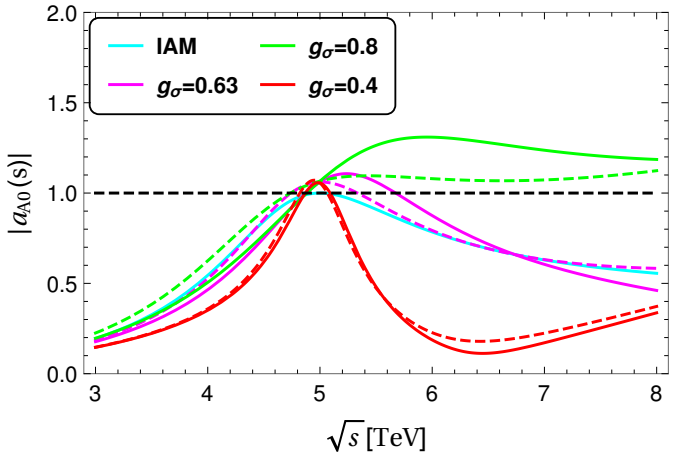

Figure 4.8.: Absolute value of partial wave amplitudes $a^0_{A0}(s) + a^\sigma_{A0}(s)$ for $g_\sigma = 0.4$, 0.63, 0.8, using a fixed width (solid curve) and a running width (dashed) compared to the IAM (cyan).

have depicted.

At the LHC proton-proton collisions happen, so the VBS process is embedded into a bigger class of scattering processes. The real emission of a gauge boson from the quarks contained in the proton leads to the generation of a particular signature, two energetic forward-backward jets. This, together with the final state coming from the core process - vector boson scattering - gives a particular signature. Other topologies of diagrams, which have no similarity to VBS also belong to the same process class, $VVjj$ at order $\mathcal{O}(\alpha_{\mathrm{EW}})^4$. We expect anyway that there will be an enhancement in the VBS topology, and this has to be traced in all the experimental observables. In particular, the invariant mass distribution of the VV system is sensitive to virtual particle exchange, in our LET case, to the Higgs particle, and then to the modification introduced by the new coupling. This observable is then also the suitable one when studying the exchange of new particles like the σ we have introduced in eq. 4.66 and the vectors of eq. 4.57.

Historically a more detailed phenomenological study of VBS signatures starts among the '80's and '90's, [14,15,215,233]. Of course, the focus there is on the Higgs exchange, and there are still discussion of Higgless scenarios. After the Higgs boson discovery the target is shifting to other models and issues, in particular the search for an explanation of the dynamical generation of the Higgs boson itself and of the Electroweak Symmetry Breaking in general. We refer the reader to [13] for an excellent summary of studies pre- and post-Higgs discovery. The use of unitarisation methods is largely standard practice, for VBS. With our work, we want to address a systematic treatment for the general search of Beyond Standard Model VBS unitarisation effects.

The characterisation of the VBS signal has been extensively discussed. Of the different channels it comprises, WW, WZ and ZZ, each with their decay channels, WW and

WZ suffer from non-negligible background contributions, $t\bar{t}$ process in particular, and in general by reconstruction issues. For all channels the estimation of the irreducible background is something to address carefully. Everyone agrees on the fact that the $ZZ \to 4\ell$ is the cleanest channel. It has few backgrounds to consider - the SM electroweak $ZZjj$ and the QCD ZZ plus jets production. From the point of view of the experimental reconstruction, it is as well an optimal candidate. However, it is penalised by a very tiny cross-section. The decay channel to $ZZ \to 2\ell 2\nu$ has a great impact on the sensitivity calculation, but has some issues on the MET requirements and reconstruction. In the following, we will discuss just the $ZZ \to 4\ell$ channel, for the reasons cited above. To account for the tiny rate of events, a luminosity range of the order of $\sim 1\text{ab}^{-1}$ are required, combined with multi-TeV centre of mass energies.

Striking signatures of the $VVjj$ signals include two energetic forward jets, peaked at $p_T \sim M_V/2$. In this case, usual high-p_T jet requirements will not work, suppressing most of the signal contribution. The absence of color flow (at leading order) in the partonic subprocess generates the large gap in pseudorapidities between the two jets stemming from the initial proton bunch, generating also a large invariant mass for the two tagged jets. This selection criterion particularly helps in suppressing the QCD background. As we want to investigate the high invariant mass tail of the ZZ system, further requirements on the hardness of this and related observables are implemented.

In previous sections we found that the dynamically inspired parameters are $a_V \sim 1$ and $M_V \sim 3.2\ \text{TeV}/\sin\theta$ in the vector sector and $g_\sigma = 0.63$ and $M_\sigma \lesssim 1.2\ \text{TeV}/\sin\theta$ in the scalar sector. Alternatively, LET behaviour gives a meaningful benchmark scenario for the non-resonant *continuum* (below unitarity violation). In all cases, the scenario is $\sin\theta < 0.2$. In the following we study these scenarios in realistic observables at hadron colliders.

Composite vector states can have a large mixing with the SM weak bosons, which generates minimal coupling to fermions. We assume there is no direct coupling to fermions, although this is a possibility. Complementary production modes, either via Drell Yan (DY) or via Vector Boson Fusion (VBF), as well as complementary decay modes into fermions or bosons are neglected. We will discuss the vector phenomenology in section 4.4.1. Similarly, the σ scalar resonance mixes with the Higgs boson and generates minimal couplings to SM fermions proportional to their masses, which would lead to its production through gluon fusion via a loop of top-quarks. However, this mixing should be small and the dominant channel has to be VBF production with decay to weak bosons. This signature falls in the same class of process of strong VBS, $VV \to VV$. Due to the intrinsic high compositeness scale of CH models for $\sin\theta \lesssim 0.2$, these typical strong effects will more likely be observable at a future 100 TeV machine than at the LHC.

In proton-proton collisions, VBS is embedded in more complicated processes where a quark in each proton emits a gauge boson, V. These scatter amongst themselves and produce two Vs along with the 2 extra remnant jets in the forward-backward region of the detector. The Vs subsequently decay into jets and/or leptons. This process has been scrutinised for a long time [14, 233–249] with an increasing degree of sophistication, in particular in the context of CH models [16, 17] and for Walking Technicolor with the

Higgs identified as the first scalar excitation [250], and more recently for a future 100 TeV collider [13, 22, 251].

The goal we pursue in sec. 4.4.2 is to assess the possibility of distinguishing the CH scenario from the SM predictions, looking at the high energy region of $M(VV)$. In the CH scenario an overall excess or a resonance is expected. We consider only the simplest and cleanest VBS channel where 2 Z decay into leptons, $pp \to jjZZ \to jj4\ell$. The only relevant backgrounds are SM electroweak $ZZjj$ and QCD ZZ+jets production. Other VBS channels, WW, WZ and other decay channels will definitely improve the discriminant power presented here [251].

4.4.1. Vector Phenomenology

To get cross sections and branching ratios (BR) for the composite vectors we make use of the full model presented in ref. [201]. It was implemented in the UFO format [252] via the FeynRules package [253] and is available in the HEPMDB[2]. We use the PDF set NNPDF 2.3 at LO [254][3]. We use MadGraph [256] to compute the cross sections for both DY and VBF productions. For the calculation of VBF cross sections we have selected the minimum set of gauge invariant diagrams in $pp \to VVjj$ which contain the VBF topology and applied a minimum transverse energy on the jets, $p_T(j) > 20$ GeV, to avoid singularities.

The heavy masses of these states $M_V \gtrsim 16$ TeV (since $\sin\theta \lesssim 0.2$) have to be probed at higher energies than those available at the LHC. A 100 TeV machine like the FCC is the natural candidate. The limits on production cross section times branching ratio ($\sigma \times BR$) of general vectorial resonance ρ at the FCC have been derived in Ref. [257]. This study is based on the exclusion sensitivities of two LHC analyses [258, 259] and on the scaling of cross sections due to the evolution of the parton luminosities. The limits are provided as a function of the resonance mass, M_ρ, for two different decay channels: $\rho \to \ell^+\ell^-$ and $\rho \to WZ$, and two integrated luminosities $L = 1\,, 10\,\text{ab}^{-1}$. In tab. 4.1 we show the exclusion limits at 95%CL on $\sigma \times$ BR for $\sin\theta = 0.2$, corresponding to $M_\rho \sim 16$ TeV (apart from mixing effects), and $\sin\theta = 0.15$ with $M_\rho \sim 21.3$ TeV.

From the vast spectrum of 15 vector states, the iso-triplet $V^{0,\pm}$ will be the most dominantly produced. The second triplet $S^{0,\pm}$ is only a bit heavier, nearly degenerate with $V^{0,\pm}$, but has lower cross section once decays into fermions and weak bosons are included. It could dominate in the Higgs decay channels, which were not considered in Ref. [257]. The $A^{0,\pm}$ states will also be produced in a proton-proton collision, but they are heavier and will be more difficult to observe. Other states do not mix with SM particles and are much harder to produce. Therefore, it is safe to assume the first observed peak will come from the $V^{0,\pm}$ states and we will neglect the other contributions.

Once $\sin\theta = 0.2,\ 0.15$, $M_V = 3.2\ \text{TeV}/\sin\theta$ and $M_{\mathcal{A}} = 3.5\ \text{TeV}/\sin\theta$ are fixed, we are left with 2 extra free parameters: $\widetilde{g}$ and r. For $r = 1$ the decay into fermions dominates.

[2] http://hepmdb.soton.ac.uk/hepmdb:0416.0200

[3] Only the first two families of quarks are included, even though the third family is known to be important for a centre of mass energy of 100 TeV [255].

$L[\text{ab}^{-1}]$	decay	$M_\rho = 16$ TeV	$M_\rho = 21.3$ TeV
1	$\ell^+\ell^-$	2.28×10^{-6} pb	3.7×10^{-6} pb
10	$\ell^+\ell^-$	4.01×10^{-7} pb	7.49×10^{-7} pb
1	WZ	4.0×10^{-4} pb	3.78×10^{-4} pb
10	WZ	3.73×10^{-5} pb	5.41×10^{-5} pb

Table 4.1.: Exclusion limits at 95%CL on the $\sigma\times$ BR production process $pp \to \rho$, in two different decay modes, $\rho \to \ell^+\ell^-$ and $\rho \to WZ$. Values for two different luminosities, 1 and $10\,\text{ab}^{-1}$ and two different masses, $M_\rho = 16$ TeV (21.3 TeV) are extracted from [257]. Centre-of-mass energy of $\sqrt{s} = 100$ TeV.

Once r departs from 1, the diboson decay channel becomes more important and rapidly overcomes the fermion channel.

In fig. 4.9 we can see the excluded region at 95% of confidence level in the plane $(\tilde{g}, r)$ for $\sin\theta = 0.2$ (*left* panel) and $\sin\theta = 0.15$ (*right* panel). The full parameter space for $\theta = 0.2$ can be excluded with a luminosity $L = 10\,\text{ab}^{-1}$ (dashed line). For $\theta = 0.15$ there is a region $\tilde{g} \gtrsim 8$ and $|r-1| \gtrsim 0.1$ which will not be excluded with 10ab^{-1}.

Lines of dynamically inspired $|a_V| = 1$ are also depicted in the plots.

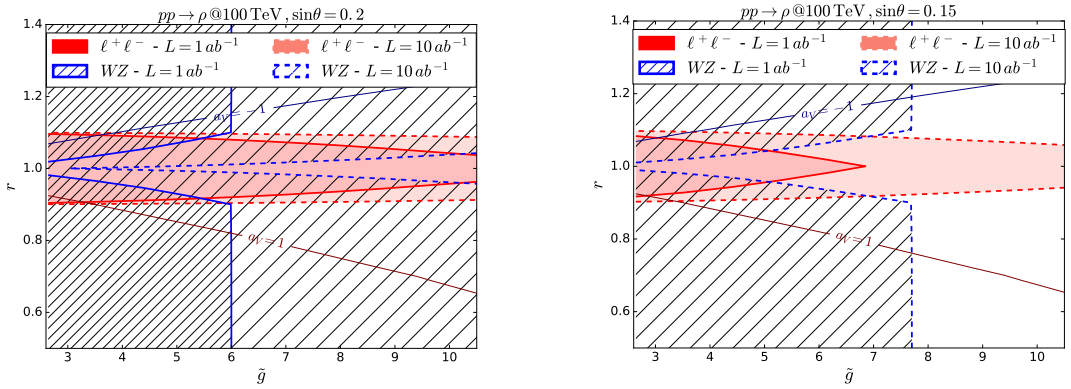

(a) (b)

Figure 4.9.: 95% CL exclusion regions in $(\tilde{g}, r)$-plane for $\sin\theta = 0.2$ (*left*) and $\sin\theta = 0.15$ (*right*) in the $\rho \to WZ$ (blue contour, hashed) and $\rho \to \ell^+\ell^-$ (red, shaded) channels. $L = 1\,\text{ab}^{-1}$ (solid contour) and $L = 10\,\text{ab}^{-1}$.

4.4.2. Strong VBS in $pp \to jjZZ \to jj4\ell$

To model the non-resonant excess and the σ resonance we have implemented the Lagrangian in eq. 4.66 in the UFO format via the FeynRules package. We consider the

following benchmark scenarios:

LET non-resonant enhancement: this is the Lagrangian in eq. 4.66 without σ. It is the simplest and most conservative effect of strong VBS in CH models and is a general feature not specific to the SU(4)/Sp(4) realisation. The observation of this excess gives an indirect probe of the Higgs coupling to weak bosons [13]. At the LHC, the measurement of hZZ coupling can reach 3% accuracy in the most optimistic case or 5% in a more realistic scenario (at 1 standard deviation) [260]. These deviations correspond to $\sin\theta \sim 0.24$ and ~ 0.31 respectively. We show that even with only the $ZZ \to 4\ell$ channel we may exclude $\sin\theta = 0.2$. We consider also $\sin\theta = 0.15, 0.1$. We note that the energies beyond LO unitarity violation have negligible contribution for our analysis.

Scalar σ resonance: we summarise the analysed benchmark scenarios we have considered in table 4.2 . The first 4 scenarios in the table will be analysed for a 100 TeV machine and the last one is an optimistic case to be analysed at LHC energies.

$\sin\theta$	v_A	M_σ[TeV]	Γ_σ[TeV]	g_σ	collider
0.2	1.2	6	2.81	0.63	FCC
0.15	0.9	6	1.58	0.63	FCC
0.1	0.6	6	0.7	0.63	FCC
0.1	0.8	8	2.69	0.8	FCC
0.2	0.8	4	1.34	0.8	LHC

Table 4.2.: Parameters of benchmark scenarios for the CH model with σ resonance.

Events for the process $pp \to jjZZ \to e^+e^-\mu^+\mu^-jj$ have been simulated at LO with the multi-purpose generator SHERPA [34]. We imported the UFO model through the BSM module [261] available for the COMIX matrix element generator [102]. All the samples were generated at LO accuracy, and are showered through the CSSHOWER module, the Catani-Seymour dipole based shower [62]. Description of the relevant process handled by such modules within SHERPA have been present in chapter 2. We have used dynamical factorisation and renormalisation scales $\mu_F^2 = \mu_R^2 = \left(p^\mu_{Z_1} + p^\mu_{Z_2}\right)^2$. The NNLO CT14 PDF set [262] in the 4 flavour scheme has been employed [4]. The SM parameters used are: $\alpha_{EW} = 1/127.9$, $M_Z = 91.18\,\text{GeV}$, $G_F = 1.16639 \times 10^{-5}\,\text{GeV}$ and $\alpha_S(M_Z) = 0.118$. Besides the CH scenario described above, we produced events for the relevant backgrounds: SM EW ZZjj, and the QCD ZZ+jets, merged up to the second jet at LO accuracy through the MEPS@LO [263] algorithm as implemented in SHERPA.

We would like to stress out the importance of gauge invariance in this study. The cancellations are so delicate that even fixed width effects can produce a large *fake* enhancement at high energies. One way out is to use the complex mass scheme to restore

[4] Here again the 3rd family PDF, including the top-quark, may play an important role at 100 TeV. This would lead to a process with 2 b-jets in the final state, allowing for a b-tagging on the forward jets, and could be treated as a different process.

gauge invariance. Our approach is instead to set all the widths of the gauge bosons to zero, since due to the implemented generation cuts we do not have kinematic regions where the internal boson propagators go on-shell. Z-bosons are decayed a posteriori with the SHERPA decay handler.

An analysis routine has been implemented in the RIVET framework [264]. Final state particles are identified within $|\eta| < 6$. One pair of isolated opposite charged muons and one of electrons with $p_{T,\text{min}} = 30\,\text{GeV}$ and $|\eta_\ell| < 4$ are identified to reconstruct the Z bosons. If more than one lepton of the same type is present we take the one with highest p_T. The reconstructed Z mass is required to be in the window $65\ \text{GeV} < m(Z) < 115\ \text{GeV}$, in order to suppress the non-ZZ backgrounds. Jets are reconstructed with the anti-k_T clustering algorithm, with $R = 0.4$ and $p_{T,\text{min}} = 30$ GeV. Moreover, typical kinematic selection cuts to enhance VBS topology have been implemented for LHC (FCC): the two jets are back-to-back in the forward-backward region of the detector forming a system with large invariant mass, while the Z-bosons are central and highly energetic. These cuts are summarised in tab. 4.3.

cut	100 TeV	14 TeV
2 jets	$p_{T,j} > 30$ GeV , $\|\eta\| > 3.5$, $\eta_{j_1} \cdot \eta_{j_2} < 0$	$p_{T,j} > 30$ GeV , $\|\eta_j\| > 3.$, $\eta_{j_1} \cdot \eta_{j_2} < 0$
ZZ invariant mass	$m_{ZZ} > 3$TeV	$m_{ZZ} > 3$TeV
di-jet invariant mass	$m_{jj} > 1$ TeV	$m_{jj} > 1$ TeV
Zs centrality	$\|\eta_{Z_i}\| < 2.$	$\|\eta_{Z_i}\| < 2.$
Zs momentum	$p_{T,Z_i} > 1$ TeV	$p_{T,Z_i} > 0.5$ TeV

Table 4.3.: Selection cuts implemented in the analyses at the FCC and LHC.

For the statistical assessment we performed a simple counting experiment analysis. We define $S = \sigma_S L$ and $B = \sigma_B L$, where L is the considered integrated luminosity and $\sigma_{S,B}$ are the effective cross sections after the application of all selection cuts for the CH scenario (S) and for the SM prediction (B), both comprising QCD ZZ+jets. We have multiplied the final cross section by a factor of 2 assuming the decay channels with 2 pairs of identical leptons can be reconstructed with similar efficiency to the channel $2e2\mu$. We model the probability to observe a number of events k with a smeared Poisson and mean value λ, given by either S or B,

$$\mathcal{P}(k;\lambda,\epsilon) = \frac{1}{2\epsilon}\int_{1-\epsilon}^{1+\epsilon} \mathrm{d}x\, e^{-x\lambda}\frac{(x\lambda)^k}{k!} \tag{4.105}$$

where ϵ models a flat systematic and theoretical uncertainty, related to scale dependence and experimental systematic error.

QCD corrections to boson-boson production via vector boson fusion [265–268] at the LHC turn out to be below 10%. At the FCC this is expected to be even lower. EW corrections, on the other hand, are known to increase with energy and can be very large and negative for VBS [269]. In $W^\pm W^\pm$ channel at the LHC the EW correction

is $k \sim -25\%$ for $M(\ell^\pm\ell^\pm) \gtrsim 500$ GeV for LHC energies. To partially account for such large corrections we consider a flat error up to $\epsilon = 40\%$.

A good estimator of the discriminatory power of the analysis is given by the probability to exclude the SM assuming one of the CH scenarios describes Nature. This probability is given by

$$1 - \beta = \sum_{k=m}^{\infty} \mathcal{P}(k; S) \tag{4.106}$$

where m is defined by

$$\sum_{k=0}^{m} \mathcal{P}(k; B) = 95\%^{5}. \tag{4.107}$$

Non-resonant excess at 100 TeV

The non-resonant enhancement cannot be observed at the LHC, due to its tiny rate, we therefore study this scenario at a 100 TeV collider. We investigate in more detail possible signatures at the LHC in 4.4.1, for the strongest channel, the vector production.

In fig. 4.10 (*left* panel) we show the distributions of the reconstructed ZZ system invariant mass, for the scenario with $\sin\theta = 0.2\,, 0.15\,, 0.1$. The corresponding $1-\beta$ is shown in the right panel as a function of luminosity, L. The central solid line assumes a systematic error $\epsilon = 20\%$. The upper and lower dashed lines refer to no-systematic and $\epsilon = 40\%$, respectively. The vertical dashed line highlights the benchmark value of luminosity used in the limits set on the vectorial resonances, $L = 10\,\text{ab}^{-1}$. The line $1-\beta = 0.5$ indicates the exclusion assuming the *mode* of the distribution is observed.

We can see that for the case $\sin\theta = 0.2$ we have a probability $1-\beta \gtrsim 50\%$ of excluding the SM already around $L \sim 3\,\text{ab}^{-1}$. For $\sin\theta = 0.15$ we need more statistics, with $L \gtrsim 25\text{ab}^{-1}$ we can reach a good probability to exclude the SM. For $\sin\theta = 0.1$ the situation is more complicated and considering the other VBS channels is unavoidable.

Heavy scalar at 100 TeV

The σ resonance has a more pronounced excess at lower energies and a better probability to be observed. In fig. 4.11 (a) we present the invariant mass of the reconstructed ZZ system for the resonant scenarios listed in tab. 4.2. We note that the σ resonance postpones the unitarity violation with respect to the plain LET scenario, and the high energy behaviour beyond the resonance peak approaches the SM prediction for a large energy range. For this reason we add a selection $M(ZZ) < 10$ TeV to avoid contamination from non-resonant areas. In fig. 4.11 (b) the corresponding $1-\beta$ are shown. We note a probability $1-\beta > 50\%$ even for $\sin\theta = 0.15$, which could be in particular stronger than vector resonance searches.

[5] To ensure exact 95% in the formula above we use fractional values in the sum.

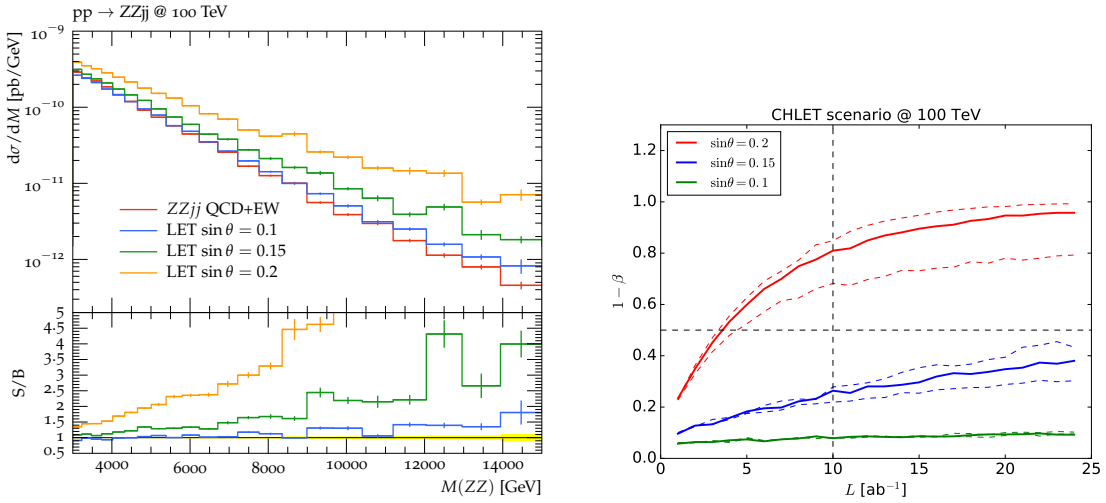

(a) (b)

Figure 4.10.: In (a) the ZZ system reconstructed invariant mass distribution for $\sin\theta = 0.1, 0.15, 0.2$ in the non-resonant excess scenario and the SM backgrounds (EW ZZjj and QCD ZZ+jets). In (b) the corresponding $1-\beta$.

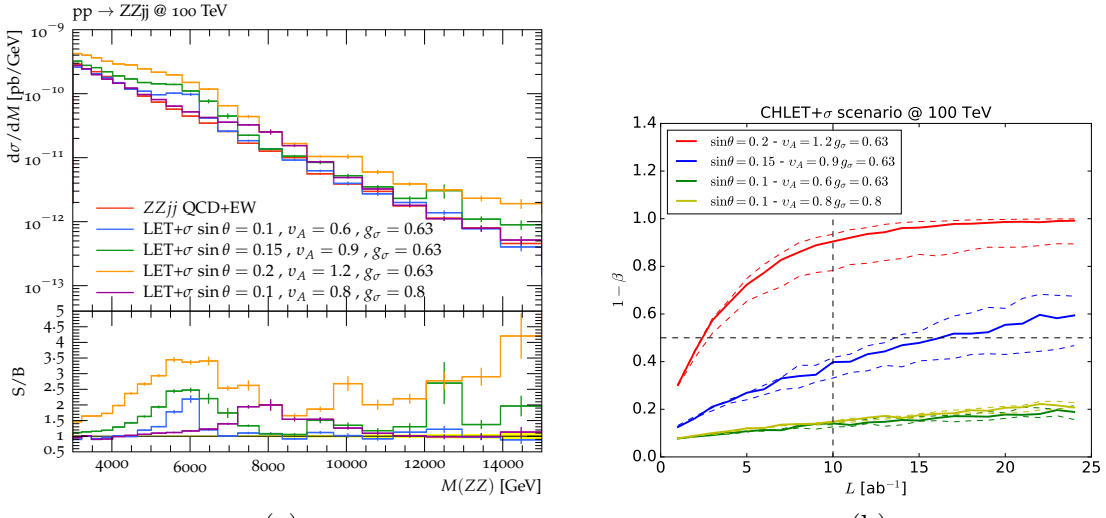

(a) (b)

Figure 4.11.: In (a) the ZZ system reconstructed invariant mass distribution in the σ resonant excess scenarios, tab. 4.2, and in (b) the corresponding $1-\beta$.

Heavy scalar at the LHC

The LHC is not the most obvious machine to observe signal of strong VBS in CH models due to the high intrinsic compositeness scales. However, nothing prevents some dynamical mechanism from producing a lighter state.

BSM searches through VBS have been analysed by the ATLAS and CMS collaborations [258, 270, 271]. In [272] in particular the production of scalar resonances in VBS in the $ZZ \to 4\ell$ channel at $\sqrt{s} = 14$ TeV, for $L = 300 - 3000\text{fb}^{-1}$ has been considered. For a resonance of mass $M_\sigma = 1$ TeV with $g_\sigma = 2.5$ they predict a sensitivity of 9.4 standard deviations at $3\,\text{ab}^{-1}$. Unfortunately, our motivated scenarios have larger masses and smaller couplings. We consider here $g_\sigma = 0.8$, $M_\sigma = 4$ TeV as an optimistic case.

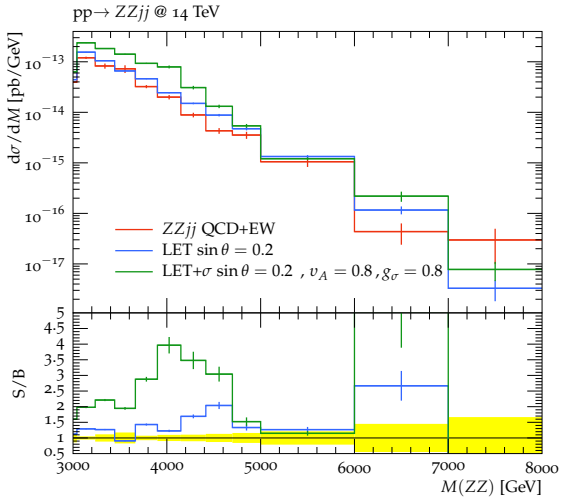

Figure 4.12.: ZZ invariant mass at the LHC for the composite scenario devised for LHC ($g_\sigma = 0.8$, $M_\sigma = 4$ TeV) and the SM backgrounds (EW ZZjj and QCD ZZ+jets).

In fig. 4.12, we show the invariant mass of the reconstructed ZZ system at $\sqrt{s} = 14$ TeV. The effective cross section found is only $\sigma = 2.9 \times 10^{-4}\,\text{ab}$. As already noted, the ZZ channel has the smallest cross-section amongst the VBS channels and including all the other channels is imperative for this search. Another source of improvement could come from the mixing of σ with the Higgs, which at this mass could give some small gluon fusion contribution. Further and more detailed study is required.

4.5. Conclusion

In this chapter we present new results for a possible analysis of Vector Boson Scattering events at a future 100 TeV hadron collider. We study this process within a particular realisation of the Composite Higgs model with coset $SU(4)/Sp(4)$.

The VBS process is one of the most challenging to measure at the LHC, due to its tiny rate, and the large backgrounds coming from top quarks production. Always with the aim of showing the potential of a 100 TeV future collider, we first present a novel prescription to impose the free parameters of the model, in order to generate meaningful events at a future collider. We use the unitarity of the amplitude, a first principle required in quantum field theory for describing real objects, as paradigm to constrain the couplings of the new particles present in the models. Through a direct comparison of the analytically unitarised amplitudes, and those partially unitarised by the presence of a resonance, we derived the optimal parameters for the model.

We present an analysis of the $pp \to ZZjj$ process, and extract sensitivity reaches at a future circular collider, getting a concrete indication of which luminosity would be required to rule out (or discovery) such new particles predicted in this scenario. We perform the same analysis at the LHC, in order to show that this is completely out its sensitivity reach. Further studies are needed, in order to complete the analysis adding the missing channels of the VBS process, which would account for a even greater sensitivity, given the higher cross sections, compared to the $ZZjj$ channel. An interesting outcome to be inspected would be also a possible sensitivity estimation of the indirect Higgs self-coupling, which would prove the FCC also a valuable precision machine.

CHAPTER 5

Conclusions

5.1. Conclusions

The LHC Run 1 and 2 have been the most exciting times in high-energy particle physics. The experimental confirmation of the existence of the Higgs boson has finally completed the already successful theory that is the Standard Model of particle physics. Nevertheless, it is already necessary to consider what could be next. The CERN is already scheduling a High Luminosity LHC run in ten years from now, in which more data will be collected, and perhaps an increase in centre-of-mass energy could even be implemented.

New frontiers for the forthcoming colliders are already being investigated at CERN. There are two main options: the precision and the energy frontiers. While the first would be interesting if new physics is discovered at the LHC, the second is the most likely if no new physics is discovered in the coming years. In this thesis we have revised some of the physics opportunities at a $\sqrt{s} = 100$ TeV hadron-hadron collider. This can be regarded as a bigger version of the LHC, where particles of masses of the order of tens of TeV could be observed.

Monte Carlo event generators, which have become a standard tool in the LHC era, allow us to study the possible physics outcomes of such a machine. More precision and attention to details is always needed in developing these powerful tools, in order to better simulate what happens during the collisions. The present thesis analyses two aspects of Monte Carlo programs to be employed at a 100 TeV collider.

We first present, in chapter 3, attempts for the automation of resummation of soft-gluons for global event shape variables within SHERPA, following the Caesar formalism. We have shown how resummed results could be used to analyse the colour flow in the event, allowing us to verify whether subleading contributions at the LHC can become relevant at an FCC-hh machine. This can be seen, in particular, in the comparison of large-N_C versus full colour treatment in section 3.1.2, where we verify that there is

no major change in going from a $\sqrt{s} = 14$ TeV collider to a 100 TeV one. An importance sampling Monte Carlo method has been implemented for the evaluation of the single-logarithmic function, $\mathcal{F}(v)$, sketching an algorithm for reaching convergence while calculating the function. This serves as starting point for a possible implementation of the $\mathcal{F}$ function through the parton shower within SHERPA.

New results regarding jet-rate predictions at a future circular collider at $\sqrt{s} = 100$ TeV have been presented. We performed an analysis comparing analytical results at next-to-double-logarithmic approximation (NDLA), computed through the generating functional mechanism, and parton showered events within SHERPA. These novel contributions shed new light on the relation between resummation and parton showers, and could actually help the community in designing further developments in all-order calculations, in sight of the future particle physics experiments.

The second main topic of the thesis has dealt with the analysis of one of the possible extensions of the Standard Model, the Composite Higgs scenario. We studied the possibility of detecting Vector Boson Scattering at a $\sqrt{s} = 100$ TeV. We have shown the implications of Goldstone Boson Scattering unitarity in the spectra of Composite Higgs scenarios, in particular for the coset we have chosen $SU(4)/Sp(4)$. We have made definite predictions for the possible range of the mass of an eventual σ-like composite scalar resonance, which can be described as a Breit-Wigner peak only if $M_\sigma \lesssim 1.2 \text{ TeV}/\sin\theta$. For masses heavier than this, the non-resonant growing behaviour overcomes and dilutes any possible peak, building up a continuum picture. Inspired by models of unitarisation which proved to be successful in predicting the first resonances in pion-pion and pion-kaon scattering data, we estimate the parameters of the Composite Higgs effective description, with which we simulate the Goldstone Boson Scattering at a $\sqrt{s} = 100$ TeV collider.

Limits on the production cross section of heavy composite vectors in the Fundamental Minimal Composite Higgs Model, $SU(4)/Sp(4)$, and a first assessment of strong Vector Boson Scattering in CH in the simplest channel $pp \to jjZZ \to jj4\ell$ have been provided. In the best case scenario, the non-resonant behaviour could, in principle, be detected, and indirect limits on the hVV coupling could be placed, with a precision of a few percent. Luminosity increase, up to $\mathcal{L} \sim 10\,\text{ab}^{-1}$, will be needed in order to have a meaningful set of events for the scenario with smallest vacuum misalignment angle θ.

To trace an outlook of this work, we expose two main branches. Regarding resummation, it would be a great achievement to build an algorithm that samples the $\mathcal{F}$ function through the parton shower algorithm already implemented in SHERPA. In this way a complete, automated software for generating resummed prediction in a Monte Carlo fashion will be available, allowing then to use resummed analytical results in the same way we do today with the parton showers. Furthermore, this tool could be used to better understand the logarithmic structure of parton showers. To enhance the results we found for the jet rates, it would be interesting to implement, within the generating functional formalism, the initial state radiation contributions, which up to now have not been considered, and a better way of including the dependence on the jet algorithm. The discrepancy between the resummation result and the parton shower outcome is particularly

enhanced in the gluon production, which is mostly affected by strong effects.

Concerning the study of Composite Higgs models at a future collider, a possible improvement of our analysis could come from the inclusion of other Vector Boson Scattering channels, like $WWjj$ and $WZjj$, which both have bigger cross sections, but necessitate a longer study of background sources. By including this, stronger limits could be placed on the production of resonances and non-resonant scenarios. A careful analysis and comparison of the precision with which the Higgs couplings could be indirectly measured would also be interesting and allow a better design and analysis of the possibilities at a future FCC-hh collider.

APPENDIX A

Conventions

A.0.1. γ matrices

$$\gamma^0 = \begin{pmatrix} 1 & 0 & 0 & 0 \\ 0 & 1 & 0 & 0 \\ 0 & 0 & -1 & 0 \\ 0 & 0 & 0 & -1 \end{pmatrix}, \qquad \gamma^1 = \begin{pmatrix} 0 & 0 & 0 & 1 \\ 0 & 0 & 1 & 0 \\ 0 & -1 & 0 & 0 \\ -1 & 0 & 0 & 0 \end{pmatrix},$$

$$\gamma^2 = \begin{pmatrix} 0 & 0 & 0 & -i \\ 0 & 0 & i & 0 \\ 0 & i & 0 & 0 \\ -i & 0 & 0 & 0 \end{pmatrix}, \qquad \gamma^3 = \begin{pmatrix} 0 & 0 & 1 & 0 \\ 0 & 0 & 0 & -1 \\ -1 & 0 & 0 & 0 \\ 0 & 1 & 0 & 0 \end{pmatrix}.$$

$$\gamma^5 = \begin{pmatrix} 0 & 0 & 0 & 1 \\ 0 & 0 & 0 & 1 \\ 1 & 0 & 0 & 0 \\ 0 & 1 & 0 & 0 \end{pmatrix}$$

A.0.2. $SU(3)$ generators

$$\lambda_1 = \begin{pmatrix} 0 & 1 & 0 \\ 1 & 0 & 0 \\ 0 & 0 & 0 \end{pmatrix} \quad \lambda_2 = \begin{pmatrix} 0 & -i & 0 \\ i & 0 & 0 \\ 0 & 0 & 0 \end{pmatrix} \quad \lambda_3 = \begin{pmatrix} 1 & 0 & 0 \\ 0 & -1 & 0 \\ 0 & 0 & 0 \end{pmatrix}$$
$$\lambda_4 = \begin{pmatrix} 0 & 0 & 1 \\ 0 & 0 & 0 \\ 1 & 0 & 0 \end{pmatrix} \quad \lambda_5 = \begin{pmatrix} 0 & 0 & -i \\ 0 & 0 & 0 \\ i & 0 & 0 \end{pmatrix}$$
$$\lambda_6 = \begin{pmatrix} 0 & 0 & 0 \\ 0 & 0 & 1 \\ 0 & 1 & 0 \end{pmatrix} \quad \lambda_7 = \begin{pmatrix} 0 & 0 & 0 \\ 0 & 0 & -i \\ 0 & i & 0 \end{pmatrix} \quad \lambda_8 = \frac{1}{\sqrt{3}} \begin{pmatrix} 1 & 0 & 0 \\ 0 & 1 & 0 \\ 0 & 0 & -2 \end{pmatrix}.$$

A.0.3. $SU(4)/Sp(4)$ generators

$$S^{1,2,3} = \frac{1}{2} \begin{pmatrix} \sigma^i & 0 \\ 0 & 0 \end{pmatrix}, \qquad S^{4,5,6} = \frac{1}{2} \begin{pmatrix} 0 & 0 \\ 0 & -\sigma^{T,i} \end{pmatrix},$$
$$S^{7,8,9} = \frac{1}{2\sqrt{2}} \begin{pmatrix} 0 & i\sigma^i \\ -i\sigma^i & 0 \end{pmatrix}, \qquad S^{10} = \frac{1}{2\sqrt{2}} \begin{pmatrix} 0 & 1 \\ 1 & 0 \end{pmatrix},$$
$$X^1 = \frac{1}{2\sqrt{2}} \begin{pmatrix} 0 & \sigma_3 \\ \sigma_3 & 0 \end{pmatrix}, \qquad X^2 = \frac{1}{2\sqrt{2}} \begin{pmatrix} 0 & i \\ -i & 0 \end{pmatrix},$$
$$X^3 = \frac{1}{2\sqrt{2}} \begin{pmatrix} 0 & \sigma_1 \\ \sigma_1 & 0 \end{pmatrix}, \qquad X^4 = \frac{1}{2\sqrt{2}} \begin{pmatrix} 0 & \sigma_2 \\ \sigma_2 & 0 \end{pmatrix},$$
$$X^5 = \frac{1}{2\sqrt{2}} \begin{pmatrix} 1 & 0 \\ 0 & -1 \end{pmatrix}.$$

APPENDIX B

Monte Carlo algorithms

In multidimensional integration, Monte Carlo algorithms are often preferred to standard numerical methods, as for example, numerical quadrature rules. This is because the scaling of the convergence error is always $1/\sqrt{N}$, independently of the dimension of the integral.

Given an integral

$$I = \int \mathrm{d}^d x f(x) \,, \tag{B.1}$$

where x is a vector with dimension d, the law of large number ensures that

$$\lim_{N\to\infty} \frac{1}{N} \sum_{n=1}^{N} f(x_n) = I \,. \tag{B.2}$$

The variance of the function can be expressed as

$$\sigma^2(f) = \int \mathrm{d}^d x \, (f(x) - I)^2 \,. \tag{B.3}$$

As direct consequence of eq. B.2, it follows that

$$\int \mathrm{d}x_1 \int \mathrm{d}x_N \left(\frac{1}{N} \sum_{n=1}^{N} f(x_n) - I \right)^2 = \frac{\sigma^2(f)}{N} \,. \tag{B.4}$$

defining in this way the average error for a Monte Carlo estimate as $\sigma(f)/\sqrt{N}$. As an exact value for $\sigma(f)$ is not always simple to compute, the following estimate is usually employed

$$S^2 = \frac{1}{N-1} \sum_{n=1}^{N} (f(x_n) - E)^2 \,. \tag{B.5}$$

Importance sampling belongs to the variance reduction techniques. The idea behind this is the fact that some regions of the parameter space have exactly more "importance" for the evaluation of the integral. Sampling more frequently these values allow to reduce the estimator variance. Distributions employed in the algorithm are then biased with the modified distribution allowing to sample more "important" values, but the output is correct by a weight, such that the final estimator is unbiased. The weight is given by the likelihood ratio of the true underlying distribution with the biased simulation distribution.

Importance sampling corresponds to a change of integration variables

$$\int \mathrm{d}x f(x) = \int \frac{f(x)}{p(x)} p(x) \mathrm{d}x = \int \frac{f(x)}{p(x)} \mathrm{d}P(x) \,, \tag{B.6}$$

where

$$p(x) \equiv= \frac{\partial^d}{\partial x_1, \ldots, \partial x_n} P(x) \,. \tag{B.7}$$

If we choose $p(x)$ to be positive-valued, $p(x) \geq 0$ and normalised to one, $\int \mathrm{d}x p(x) = 1$, we can treat $p(x)$ as a probability density function. Then, generating random $x_1, \ldots, x_N$ according to the probability $P(x)$, we have the following estimator for the integral I

$$E = \frac{1}{N} \sum_{n=1}^{N} \frac{f(x_n)}{p(x_n)} \,. \tag{B.8}$$

It directly follows that the variance estimator is

$$S^2 = \frac{1}{N} \sum_{n=1}^{N} \left(\frac{f(x_n)}{p(x_n)} \right)^2 - E^2 \,. \tag{B.9}$$

APPENDIX C

Generating functionals details

Following ref. [143], we write the splitting function for the gluon, through the Altarelli-Parisi splitting kernels $P_{gg}(z)$ and $P_{qg}(z)$,

$$\mathcal{P}_g(E,\xi) = \int_{\xi_R}^{\xi} \frac{d\xi'}{\xi'} \int_{E_R/E}^{1} dz \frac{\alpha_s(k_t^2)}{2\pi} \left[P_{gg}(z) + P_{qg}(z)\right] \ , \tag{C.1}$$

which gives to NDLA

$$\begin{aligned}\mathcal{P}_g(E,\xi) = \bar{\alpha}_s \ln\left(\frac{\xi}{\xi}_R\right) \left[C_A \ln\left(\frac{E}{E_R}\right) - b_0\right] + \\ \frac{1}{2} C_A b_0 \bar{\alpha}_s^2 \ln\left(\frac{\xi}{\xi}_R\right) \ln\left(\frac{E}{E_R}\right) \left[2\ln\left(\frac{E}{E_R}\right) + \ln\left(\frac{\xi}{\xi}_R\right)\right] \ ,\end{aligned} \tag{C.2}$$

and the gluon Sudakov factor is

$$\Delta_g(E,\xi) = \exp\left[-\mathcal{P}_g(E,\xi)\right] \ . \tag{C.3}$$

Note that all this is independent of the value of p, so that all the inclusive generalized k_t algorithms are equivalent at this level of precision.

Writing

$$\begin{aligned}\mathcal{N}_q(\kappa = ma, \lambda = nb) = f_{m,n} \\ \mathcal{N}_g(\kappa = ma, \lambda = nb) = g_{m,n} \ ,\end{aligned} \tag{C.4}$$

we have

$$\frac{\partial^2 \mathcal{N}_g}{\partial\kappa\,\partial\lambda} \approx \frac{1}{ab}\left[g_{m+1,n+1} - g_{m+1,n} - g_{m,n+1} + g_{m,n}\right] \tag{C.5}$$

and

$$\frac{c_g \mathcal{N}_g}{(2\kappa+\lambda+\mu)} \approx \frac{c_g}{4}\left[\frac{g_{m+1,n+1}}{2(m+1)a+(n+1)b+\mu}+\frac{g_{m+1,n}}{2(m+1)a+nb+\mu}\right. \tag{C.6}$$

$$\left.+\frac{g_{m,n+1}}{2ma+(n+1)b+\mu}+\frac{g_{m,n}}{2ma+nb+\mu}\right]. \tag{C.7}$$

Equating these expressions, one can solve iteratively for $g_{m+1,n+1}$ starting from the boundary values $g_{0,n} = g_{m,0} = 1$.

To include the finite parts of the splitting functions, we may write (3.70) and (3.73) with equivalent precision as

$$\frac{\partial^2 \mathcal{N}_{q,g}}{\partial\kappa\partial\lambda} = c_{q,g}\left(1 - d_{q,g}\frac{\partial}{\partial\kappa}\right)\frac{\mathcal{N}_g}{2\kappa+\lambda+\mu}\,, \tag{C.8}$$

where $c_{q,g} = C_{F,A}/b_0$ and

$$d_q = \frac{3}{4}\,, \quad d_g = \frac{11}{12} + \frac{n_f}{6N^3}\,. \tag{C.9}$$

The partial derivative equations (C.8) can be solved numerically by a simple extension of the method outlined above. For the discretized κ-derivative, we use

$$\frac{\partial \mathcal{N}_g}{\partial\kappa} \approx \frac{1}{2a}\left[g_{m+1,n+1} + g_{m+1,n} - g_{m,n+1} - g_{m,n}\right]\,. \tag{C.10}$$

We can then write the right-hand side of (C.8) as

$$\frac{c_g}{4}\left[\frac{(1-\delta_g)g_{m+1,n+1}}{2(m+1)a+(n+1)b+\mu}+\frac{(1-\delta_g)g_{m+1,n}}{2(m+1)a+nb+\mu}\right.$$

$$\left.+\frac{(1+\delta_g)g_{m,n+1}}{2ma+(n+1)b+\mu}+\frac{(1+\delta_g)g_{m,n}}{2ma+nb+\mu}\right], \tag{C.11}$$

where

$$\delta_g = \frac{2}{a}d_g = \frac{2}{a}\left(\frac{11}{12}+\frac{n_f}{6N^3}\right)\,, \tag{C.12}$$

and equate this to (C.5).

Similarly, to obtain the quark jet multiplicity we write

$$\frac{\partial^2 \mathcal{N}_q}{\partial\kappa\,\partial\lambda} \approx \frac{1}{ab}\left[f_{m+1,n+1} - f_{m+1,n} - f_{m,n+1} + f_{m,n}\right]\,, \tag{C.13}$$

equate this to (C.11) with c_g, δ_g replaced by

$$c_q = \frac{C_F}{b_0}\,, \quad \delta_q = \frac{3}{2a} \tag{C.14}$$

to obtain the discrete equivalent of (3.70), and solve iteratively for $f_{m+1,n+1}$ starting from the boundary values $f_{0,n} = f_{m,0} = 1$.

ACKNOWLEDGEMENTS

First of all I would like to thank my supervisor prof. Steffen Schumann for wanting me in his group, and for the great time we had in the last three years together. I am in debt with him for all the things I have learned so far. Special thanks go to prof. Arnulf Quadt, my second supervisor, who supported my research through these years. Second, I would like to thank especially my collaborator Dr. Diogo Buarque Franzosi, without him it would not be possible to write this thesis and finish the PhD. Thanks a lot, also for the wonderful time we had together. I take to occasion to thank all the other collaborators with which I shared a part of my PhD: Erik Gerwick, Simone Marzani and Stefan Höche. A very big thanks goes to Jennifer, who correct this thesis: without her this work would be much worse. I am not joking.

Thanks also to MCnet, the Marie Curie Network who partly funded my research, and also shaped me as a researcher now oriented to the private sector. It was so nice to meet all the people, students and professors, from other universities around Europe, sharing knowledge and experiences. Special thanks go to prof. Fabio Maltoni, who invited me in Louvain.

I would like to thank all the students of the department with which I shared my days as PhD: from my group, Enrico, Danilo, Stefan and Federica (for some time) and all the master students I met, to the students of the other groups of the department. I thank Matteo, who has been the first person I met in Göttingen, with whom I shared not only the physics, but also two houses and lot of beers. Greetings also to Antonio, who completed the italian group of the II. Physikalisches Institut. I thank Mrs. Bernadette Tyson and all the secretaries of the department. With Bernadette I used to share some lunchtime, together with Dr. Zinonas Zinonos: they have been very nice moments.

Let's move out from our department: I would like to thank prof. Salvatore Manmana, with whom I shared lot of interesting discussions. He has been always very kind with me, supporting my work and giving me lot of advises. Simone, thank you, for all the coffee we shared.

Outside the physics department I had a great time: I would like to thank all the people I met out there, in particular Emanuele (thank you for the keyboard I used, and the wine), Fabio, Gabriele, Giuseppe, Mattia, Marco and Raffaella, and all the other people met at the Italian Mission in the catholic church St. Micheal (Anna, Claudia, Chiara, Silvia, Serafina e Vito and many others). I would like to thank all the germans there that let me feel like at home, the priest who gave me access to the organ, Stefanie and Michael. All of this has been fundamental for my staying in Göttingen.

Thanks also to all the friends with which I shared my life in Germany, the majority of them physicists: Marco and Elisa, Paolo and Laura and family, Giuseppe and Titta and family, Linda, Nicola from Magdeburg, Matteo Pasi, Ralf and family, Giacomo. Of course I would like to thank my parents, my sister Bianca and my brother Paolo, my grannies Beppa and Maria who always supported my work here, and came to visit, also during Christmas. My uncle Massimo and my aunt Anna who made as well up to here, and stay with us for some days. I should quote all my other relatives here, but there is

not enough space. I should quote also all my friends from Italy: too many. Greetings go to the heroic guys who came in Göttingen: Nik, Zemelo, Jimmy and Dadde.

Last but not least, I thank my family: Annalisa and Caterina. During these three years lot of things happened. I thank you Annalisa for following me up to here, without you this would not have been possible. Things are always better than one expects. Caterina will have the indelible trace of our staying in Göttingen, since she was born here. Thanks God, our family is the greatest achievement of our staying here.

Bibliography

[1] S. L. Glashow, *Partial-symmetries of weak interactions*, *Nuclear Physics* **22** (1961) 579 – 588.

[2] S. Weinberg, *A model of leptons*, *Phys. Rev. Lett.* **19** (Nov, 1967) 1264–1266.

[3] A. Salam and J. C. Ward, *Electromagnetic and weak interactions*, *Phys. Lett.* **13** (1964) 168–171.

[4] ATLAS collaboration, G. Aad et al., *Observation of a new particle in the search for the Standard Model Higgs boson with the ATLAS detector at the LHC*, *Phys. Lett.* **B716** (2012) 1–29, [1207.7214].

[5] CMS collaboration, S. Chatrchyan et al., *Observation of a new boson at a mass of 125 GeV with the CMS experiment at the LHC*, *Phys. Lett.* **B716** (2012) 30–61, [1207.7235].

[6] E. L. Berger, J. Gao, C. P. Yuan and H. X. Zhu, *NNLO QCD Corrections to t-channel Single Top-Quark Production and Decay*, *Phys. Rev.* **D94** (2016) 071501, [1606.08463].

[7] M. Grazzini, S. Kallweit, S. Pozzorini, D. Rathlev and M. Wiesemann, W^+W^- *production at the LHC: fiducial cross sections and distributions in NNLO QCD*, *JHEP* **08** (2016) 140, [1605.02716].

[8] A. Gehrmann-De Ridder, T. Gehrmann, E. W. N. Glover, A. Huss and T. A. Morgan, *The NNLO QCD corrections to Z boson production at large transverse momentum*, *JHEP* **07** (2016) 133, [1605.04295].

[9] E. L. Berger, J. Gao and H. X. Zhu, *Differential Distributions for t-channel Single Top-Quark Production and Decay at Next-to-Next-to-Leading Order in QCD*, 1708.09405.

[10] ATLAS collaboration, G. Aad et al., *Measurement of multi-jet cross sections in proton-proton collisions at a 7 TeV center-of-mass energy*, *Eur. Phys. J.* **C71** (2011) 1763, [1107.2092].

[11] *Measurement of the inclusive differential jet cross section in pp collisions at s=2.76 tev*, *Physics Letters B* **722** (2013) 262 – 272.

[12] CMS Collaboration collaboration, S. Chatrchyan, V. Khachatryan, A. M. Sirunyan, A. Tumasyan, W. Adam, T. Bergauer et al., *Measurement of the inclusive jet cross section in pp collisions at* $\sqrt{s} = 7$ TeV, *Phys. Rev. Lett.* **107** (Sep, 2011) 132001.

[13] M. Szleper, *The Higgs boson and the physics of WW scattering before and after Higgs discovery*, 1412.8367.

[14] D. A. Dicus, J. F. Gunion and R. Vega, *Isolating the scattering of longitudinal W+'s at the SSC using like sign dileptons*, *Phys. Lett.* **B258** (1991) 475–481.

[15] J. Bagger, V. D. Barger, K.-m. Cheung, J. F. Gunion, T. Han, G. A. Ladinsky et al., *The Strongly interacting W W system: Gold plated modes*, *Phys. Rev.* **D49** (1994) 1246–1264, [hep-ph/9306256].

[16] A. Ballestrero, G. Bevilacqua, D. Buarque Franzosi and E. Maina, *How well can the LHC distinguish between the SM light Higgs scenario, a composite Higgs and the Higgsless case using VV scattering channels?*, *JHEP* **11** (2009) 126, [0909.3838].

[17] R. Contino, D. Marzocca, D. Pappadopulo and R. Rattazzi, *On the effect of resonances in composite Higgs phenomenology*, *JHEP* **10** (2011) 081, [1109.1570].

[18] CMS collaboration, A. M. Sirunyan et al., *Measurement of vector boson scattering and constraints on anomalous quartic couplings from events with four leptons and two jets in proton-proton collisions at sqrt(s) = 13 TeV*, 1708.02812.

[19] L. C. Collaboration, "International linear collider." http://www.linearcollider.org/ILC.

[20] CERN, "Fcc-ee study." http://tlep.web.cern.ch/.

[21] CERN, "Fcc-hh study." https://fcc.web.cern.ch.

[22] M. L. Mangano et al., *Physics at a 100 TeV pp collider: Standard Model processes*, 1607.01831.

[23] D. J. Gross and F. Wilczek, *Ultraviolet Behavior of Nonabelian Gauge Theories*, *Phys. Rev. Lett.* **30** (1973) 1343–1346.

[24] H. D. Politzer, *Reliable Perturbative Results for Strong Interactions?*, *Phys. Rev. Lett.* **30** (1973) 1346–1349.

[25] F. Wilczek, *Asymptotic freedom: From paradox to paradigm*, *Proc. Nat. Acad. Sci.* **102** (2005) 8403–8413, [hep-ph/0502113].

[26] M. Gell-Mann, *The Eightfold Way: A Theory of strong interaction symmetry*, *California Institut of Technology, Pasadena* **CTSL-20, TID-12608** (1961) .

[27] Particle Data Group collaboration, C. Patrignani et al., *Review of Particle Physics*, *Chin. Phys.* **C40** (2016) 100001.

[28] H. D. Politzer, *Gluon Corrections to Drell-Yan Processes*, *Nucl. Phys.* **B129** (1977) 301–318.

[29] H. D. Politzer, *QCD Off the Light Cone and the Demise of the Transverse Momentum Cutoff*, *Phys. Lett.* **70B** (1977) 430–432.

[30] T. Muta, *Foundations of Quantum Chromodynamics: An Introduction to Perturbative Methods in Gauge Theories, (3rd ed.)*, vol. 78 of *World scientific Lecture Notes in Physics*. World Scientific, Hackensack, N.J., 2010.

[31] R. P. Feynman, *The Behavior Of Hadron Collisions At Extreme Energies*, in *Noz, M.e. (ed.), Kim, Y.s. (ed.): Special Relativity And Quantum Theory* 289-304. (in *stony Brook 1969, Proceedings, Conference On High Energy Collisions* 237-258) And Preprint - Feynman, R.p. (69,rec.dec.) 23 P. (see Book Index), In *Brown, L.M. (ed.): Selected papers of Richard Feynman* 497-518*, 1989.

[32] J. Bellm et al., *Herwig 7.0/Herwig++ 3.0 release note*, *Eur. Phys. J.* **C76** (2016) 196, [1512.01178].

[33] T. Sjöstrand, S. Ask, J. R. Christiansen, R. Corke, N. Desai, P. Ilten et al., *An Introduction to PYTHIA 8.2*, *Comput. Phys. Commun.* **191** (2015) 159–177, [1410.3012].

[34] T. Gleisberg, S. Hoeche, F. Krauss, M. Schonherr, S. Schumann, F. Siegert et al., *Event generation with SHERPA 1.1*, *JHEP* **02** (2009) 007, [0811.4622].

[35] T. Kinoshita, *Mass singularities of Feynman amplitudes*, *J. Math. Phys.* **3** (1962) 650–677.

[36] T. D. Lee and M. Nauenberg, *Degenerate Systems and Mass Singularities*, *Phys. Rev.* **133** (1964) B1549–B1562.

[37] F. Bloch and A. Nordsieck, *Note on the Radiation Field of the electron*, *Phys. Rev.* **52** (1937) 54–59.

[38] G. Altarelli and G. Parisi, *Asymptotic Freedom in Parton Language*, *Nucl. Phys.* **B126** (1977) 298–318.

[39] Y. L. Dokshitzer, *Calculation of the Structure Functions for Deep Inelastic Scattering and e+ e- Annihilation by Perturbation Theory in Quantum Chromodynamics.*, *Sov. Phys. JETP* **46** (1977) 641–653.

[40] V. N. Gribov and L. N. Lipatov, *Deep inelastic e p scattering in perturbation theory*, *Sov. J. Nucl. Phys.* **15** (1972) 438–450.

[41] R. K. Ellis, W. J. Stirling and B. R. Webber, *QCD and collider physics*, *Camb. Monogr. Part. Phys. Nucl. Phys. Cosmol.* **8** (1996) 1–435.

[42] Y. L. Dokshitzer, V. A. Khoze, A. H. Mueller and S. I. Troian, *Basics of perturbative QCD*. 1991.

[43] M. D. Schwartz, *Quantum Field Theory and the Standard Model*. Cambridge University Press, 2014.

[44] G. Sterman and S. Weinberg, *Jets from quantum chromodynamics*, *Phys. Rev. Lett.* **39** (Dec, 1977) 1436–1439.

[45] G. P. Salam, *Towards Jetography*, *Eur. Phys. J.* **C67** (2010) 637–686, [0906.1833].

[46] J. E. Huth et al., *Toward a standardization of jet definitions*, in *1990 DPF Summer Study on High-energy Physics: Research Directions for the Decade (Snowmass 90) Snowmass, Colorado, June 25-July 13, 1990*, pp. 0134–136, 1990.

[47] JADE collaboration, W. Bartel et al., *Experimental Studies on Multi-Jet Production in e+ e- Annihilation at PETRA Energies*, *Z. Phys.* **C33** (1986) 23.

[48] JADE collaboration, S. Bethke et al., *Experimental Investigation of the Energy Dependence of the Strong Coupling Strength*, *Phys. Lett.* **B213** (1988) 235–241.

[49] Y. L. Dokshitzer, G. D. Leder, S. Moretti and B. R. Webber, *Better jet clustering algorithms*, *JHEP* **08** (1997) 001, [hep-ph/9707323].

[50] M. Wobisch and T. Wengler, *Hadronization corrections to jet cross-sections in deep inelastic scattering*, in *Monte Carlo generators for HERA physics. Proceedings, Workshop, Hamburg, Germany, 1998-1999*, pp. 270–279, 1998. hep-ph/9907280.

[51] S. Catani, Y. L. Dokshitzer, M. Olsson, G. Turnock and B. R. Webber, *New clustering algorithm for multi - jet cross-sections in e+ e- annihilation*, *Phys. Lett.* **B269** (1991) 432–438.

[52] M. Cacciari, G. P. Salam and G. Soyez, *The Anti-k(t) jet clustering algorithm*, *JHEP* **04** (2008) 063, [0802.1189].

[53] S. Catani and M. H. Seymour, *A General algorithm for calculating jet cross-sections in NLO QCD*, *Nucl. Phys.* **B485** (1997) 291–419, [hep-ph/9605323].

[54] S. Frixione, Z. Kunszt and A. Signer, *Three jet cross-sections to next-to-leading order*, *Nucl. Phys.* **B467** (1996) 399–442, [hep-ph/9512328].

[55] D. A. Kosower, *Antenna factorization of gauge theory amplitudes*, *Phys. Rev.* **D57** (1998) 5410–5416, [hep-ph/9710213].

[56] A. Gehrmann-De Ridder, T. Gehrmann and E. W. N. Glover, *Antenna subtraction at NNLO*, *JHEP* **09** (2005) 056, [hep-ph/0505111].

[57] S. Catani and L. Trentadue, *Resummation of the QCD Perturbative Series for Hard Processes*, *Nucl. Phys.* **B327** (1989) 323–352.

[58] A. H. Mueller, *On the Multiplicity of Hadrons in QCD Jets*, *Phys. Lett.* **B104** (1981) 161–164.

[59] A. Bassetto, M. Ciafaloni, G. Marchesini and A. H. Mueller, *Jet Multiplicity and Soft Gluon Factorization*, *Nucl. Phys.* **B207** (1982) 189–204.

[60] Y. L. Dokshitzer, V. S. Fadin and V. A. Khoze, *Double Logs of Perturbative QCD for Parton Jets and Soft Hadron Spectra*, *Z. Phys.* **C15** (1982) 325.

[61] V. V. Sudakov, *Vertex parts at very high-energies in quantum electrodynamics*, *Sov. Phys. JETP* **3** (1956) 65–71.

[62] S. Schumann and F. Krauss, *A Parton shower algorithm based on Catani-Seymour dipole factorisation*, *JHEP* **03** (2008) 038, [0709.1027].

[63] D. Amati, A. Bassetto, M. Ciafaloni, G. Marchesini and G. Veneziano, *A Treatment of Hard Processes Sensitive to the Infrared Structure of QCD*, *Nucl. Phys.* **B173** (1980) 429–455.

[64] OPAL collaboration, G. Abbiendi et al., *Measurement of event shape distributions and moments in $e^+e^- \to$ hadrons at 91 GeV - 209 GeV and a determination of α_s*, *Eur. Phys. J.* **C40** (2005) 287–316, [hep-ex/0503051].

[65] C. Adloff et al., *Investigation of power corrections to event shape variables measured in deep-inelastic scattering*, *The European Physical Journal C - Particles and Fields* **14** (2000) 255–269.

[66] Y. L. Dokshitzer, G. Marchesini and B. R. Webber, *Dispersive approach to power behaved contributions in QCD hard processes*, *Nucl. Phys.* **B469** (1996) 93–142, [hep-ph/9512336].

[67] M. Dasgupta and G. P. Salam, *Resummation of nonglobal QCD observables*, *Phys. Lett.* **B512** (2001) 323–330, [hep-ph/0104277].

[68] OPAL collaboration, P. D. Acton et al., *A Global determination of α_s (M(z0)) at LEP*, *Z. Phys.* **C55** (1992) 1–24.

[69] J. C. Collins, D. E. Soper and G. F. Sterman, *Transverse Momentum Distribution in Drell-Yan Pair and W and Z Boson Production*, *Nucl. Phys.* **B250** (1985) 199–224.

[70] G. Altarelli, R. D. Ball and S. Forte, *Singlet parton evolution at small x: A Theoretical update*, in *QCD: Perturbative or nonperturbative? Proceedings, 17th Autumn School, Lisbon, Portugal, September 29-October 4, 1999*, pp. 249–278, 2000. hep-ph/0001157.

[71] R. D. Ball and S. Forte, *Summation of leading logarithms at small x*, *Physics Letters B* **351** (1995) 313 – 324.

[72] S. Catani, L. Trentadue, G. Turnock and B. R. Webber, *Resummation of large logarithms in e+ e- event shape distributions*, *Nucl. Phys.* **B407** (1993) 3–42.

[73] C. W. Bauer, S. Fleming and M. E. Luke, *Summing Sudakov logarithms in B →X(s gamma) in effective field theory*, *Phys. Rev.* **D63** (2000) 014006, [hep-ph/0005275].

[74] M. Beneke, A. P. Chapovsky, M. Diehl and T. Feldmann, *Soft collinear effective theory and heavy to light currents beyond leading power*, *Nucl. Phys.* **B643** (2002) 431–476, [hep-ph/0206152].

[75] E. Farhi, *Quantum chromodynamics test for jets*, *Phys. Rev. Lett.* **39** (Dec, 1977) 1587–1588.

[76] S. Frixione and B. R. Webber, *Matching nlo qcd computations and parton shower simulations*, *Journal of High Energy Physics* **2002** (2002) 029.

[77] P. Nason, *A new method for combining nlo qcd with shower monte carlo algorithms*, *Journal of High Energy Physics* **2004** (2004) 040.

[78] S. Frixione, P. Nason and C. Oleari, *Matching nlo qcd computations with parton shower simulations: the powheg method*, *Journal of High Energy Physics* **2007** (2007) 070.

[79] S. Catani, F. Krauss, B. R. Webber and R. Kuhn, *Qcd matrix elements + parton showers*, *Journal of High Energy Physics* **2001** (2001) 063.

[80] F. Krauss, *Matrix elements and parton showers in hadronic interactions*, *Journal of High Energy Physics* **2002** (2002) 015.

[81] L. Lönnblad, *Correcting the colour-dipole cascade model with fixed order matrix elements*, *Journal of High Energy Physics* **2002** (2002) 046.

[82] M. L. Mangano, M. Moretti and R. Pittau, *Multijet matrix elements and shower evolution in hadronic collisions: $wb\bar{b}$+n-jets as a case study*, *Nuclear Physics B* **632** (2002) 343 – 362.

[83] L. Lönnblad and S. Prestel, *Matching tree-level matrix elements with interleaved showers*, *Journal of High Energy Physics* **2012** (2012) 19.

[84] S. Höche, F. Krauss, M. Schönherr and F. Siegert, *Qcd matrix elements + parton showers. the nlo case*, *Journal of High Energy Physics* **2013** (2013) 27.

[85] ATLAS collaboration, G. Aad et al., *Measurement of the transverse momentum and ϕ^*_η distributions of DrellâĂŞYan lepton pairs in protonâĂŞproton collisions at $\sqrt{s} = 8$ TeV with the ATLAS detector*, *Eur. Phys. J.* **C76** (2016) 291, [1512.02192].

[86] M. H. Seymour, *Matrix-element corrections to parton shower algorithms*, *Computer Physics Communications* **90** (1995) 95 – 101.

[87] T. Sjöstrand, S. Mrenna and P. Skands, *Pythia 6.4 physics and manual*, *Journal of High Energy Physics* **2006** (2006) 026.

[88] E. C. Poggio, H. R. Quinn and S. Weinberg, *Smearing method in the quark model*, *Phys. Rev. D* **13** (Apr, 1976) 1958–1968.

[89] K. G. Wilson, *Nonlagrangian models of current algebra*, *Phys. Rev.* **179** (1969) 1499–1512.

[90] K. G. Wilson and J. B. Kogut, *The Renormalization group and the epsilon expansion*, *Phys. Rept.* **12** (1974) 75–200.

[91] B. Andersson, G. Gustafson, G. Ingelman and T. Sjostrand, *Parton Fragmentation and String Dynamics*, *Phys. Rept.* **97** (1983) 31–145.

[92] X. Artru and G. Mennessier, *String model and multiproduction*, *Nucl. Phys.* **B70** (1974) 93–115.

[93] R. D. Field and S. Wolfram, *A QCD Model for e+ e- Annihilation*, *Nucl. Phys.* **B213** (1983) 65–84.

[94] T. Sjöstrand and M. van Zijl, *A multiple-interaction model for the event structure in hadron collisions*, *Phys. Rev. D* **36** (Oct, 1987) 2019–2041.

[95] T. Sjöstrand, *Colour Reconnections from LEP to Future Colliders*, in *Proceedings, Parton Radiation and Fragmentation from LHC to FCC-ee: CERN, Geneva, Switzerland, November 22-23, 2016*, pp. 144–148, 2017.

[96] R. Corke and T. Sjostrand, *Interleaved Parton Showers and Tuning Prospects*, *JHEP* **03** (2011) 032, [1011.1759].

[97] T. Sjostrand and P. Z. Skands, *Multiple interactions and the structure of beam remnants*, *JHEP* **03** (2004) 053, [hep-ph/0402078].

[98] A. Buckley et al., *General-purpose event generators for LHC physics*, *Phys. Rept.* **504** (2011) 145–233, [1101.2599].

[99] ATLAS collaboration, G. Aad et al., *Study of Jet Shapes in Inclusive Jet Production in pp Collisions at $\sqrt{s} = 7$ TeV using the ATLAS Detector*, *Phys. Rev.* **D83** (2011) 052003, [1101.0070].

[100] L. J. Dixon, *A brief introduction to modern amplitude methods*, in *Proceedings, 2012 European School of High-Energy Physics (ESHEP 2012): La Pommeraye, Anjou, France, June 06-19, 2012*, pp. 31–67, 2014. 1310.5353. DOI.

[101] F. Krauss, R. Kuhn and G. Soff, *AMEGIC++ 1.0: A Matrix element generator in C++*, *JHEP* **02** (2002) 044, [hep-ph/0109036].

[102] T. Gleisberg and S. Hoeche, *Comix, a new matrix element generator*, *JHEP* **12** (2008) 039, [0808.3674].

[103] F. A. Berends and W. T. Giele, *Recursive Calculations for Processes with n Gluons*, *Nucl. Phys.* **B306** (1988) 759–808.

[104] C. F. Berger, Z. Bern, L. J. Dixon, F. F. Cordero, D. Forde, H. Ita et al., *Automated implementation of on-shell methods for one-loop amplitudes*, *Phys. Rev. D* **78** (Aug, 2008) 036003.

[105] F. Cascioli, P. Maierhöfer and S. Pozzorini, *Scattering amplitudes with open loops*, *Phys. Rev. Lett.* **108** (Mar, 2012) 111601.

[106] S. Actis, A. Denner, L. Hofer, A. Scharf and S. Uccirati, *Recursive generation of one-loop amplitudes in the Standard Model*, *JHEP* **04** (2013) 037, [1211.6316].

[107] S. Actis, A. Denner, L. Hofer, J.-N. Lang, A. Scharf and S. Uccirati, *RECOLA: REcursive Computation of One-Loop Amplitudes*, *Comput. Phys. Commun.* **214** (2017) 140–173, [1605.01090].

[108] G. P. Lepage, *Vegas: An Adaptive Multidimensional Integration Program*, 1980.

[109] R. Kleiss, W. J. Stirling and S. D. Ellis, *A New Monte Carlo Treatment of Multiparticle Phase Space at High-energies*, *Comput. Phys. Commun.* **40** (1986) 359.

[110] P. D. Draggiotis, A. van Hameren and R. Kleiss, *SARGE: An Algorithm for generating QCD antennas*, *Phys. Lett.* **B483** (2000) 124–130, [hep-ph/0004047].

[111] A. van Hameren and C. G. Papadopoulos, *A Hierarchical phase space generator for QCD antenna structures*, *Eur. Phys. J.* **C25** (2002) 563–574, [hep-ph/0204055].

[112] S. Höche and S. Prestel, *The midpoint between dipole and parton showers*, *The European Physical Journal C* **75** (2015) 461.

[113] J.-C. Winter, F. Krauss and G. Soff, *A Modified cluster hadronization model*, *Eur. Phys. J.* **C36** (2004) 381–395, [hep-ph/0311085].

[114] T. Sjostrand and M. van Zijl, *A Multiple Interaction Model for the Event Structure in Hadron Collisions*, *Phys. Rev.* **D36** (1987) 2019.

[115] J. Rojo, *Parton Distributions at a 100 TeV Hadron Collider*, *PoS* **DIS2016** (2016) 275, [1605.08302].

[116] E. Bothmann, P. Ferrarese, F. Krauss, S. Kuttimalai, S. Schumann and J. Thompson, *Aspects of perturbative QCD at a 100 TeV future hadron collider*, *Phys. Rev.* **D94** (2016) 034007, [1605.00617].

[117] T. Golling et al., *Physics at a 100 TeV pp collider: beyond the Standard Model phenomena*, *CERN Yellow Report* (2017) 441–634, [1606.00947].

[118] R. Contino et al., *Physics at a 100 TeV pp collider: Higgs and EW symmetry breaking studies*, *CERN Yellow Report* (2017) 255–440, [1606.09408].

[119] J. M. Butterworth, A. R. Davison, M. Rubin and G. P. Salam, *Jet substructure as a new higgs-search channel at the large hadron collider*, *Phys. Rev. Lett.* **100** (Jun, 2008) 242001.

[120] S. D. Ellis, C. K. Vermilion and J. R. Walsh, *Techniques for improved heavy particle searches with jet substructure*, *Phys. Rev. D* **80** (Sep, 2009) 051501.

[121] D. Krohn, J. Thaler and L.-T. Wang, *Jet trimming*, *Journal of High Energy Physics* **2010** (2010) 84.

[122] D. Krohn, M. D. Schwartz, M. Low and L.-T. Wang, *Jet Cleansing: Pileup Removal at High Luminosity*, *Phys. Rev.* **D90** (2014) 065020, [1309.4777].

[123] M. Cacciari and G. P. Salam, *Pileup subtraction using jet areas*, *Physics Letters B* **659** (2008) 119 – 126.

[124] D. Schulte, *FCC-hh conceptual machine desing - CDR plan and status*, *FCC Week 2017* .

[125] D. Schulte, *FCC-hh Design Highlights*, *ICFA Beam Dyn. Newslett.* **72** (2017) 99–109.

[126] S. Kluth, P. A. Movilla Fernandez, S. Bethke, C. Pahl and P. Pfeifenschneider, *A Measurement of the QCD color factors using event shape distributions at s**(1/2) = 14-GeV to 189-GeV*, *Eur. Phys. J.* **C21** (2001) 199–210, [hep-ex/0012044].

[127] T. Sjostrand, P. Eden, C. Friberg, L. Lonnblad, G. Miu, S. Mrenna et al., *High-energy physics event generation with PYTHIA 6.1*, *Comput. Phys. Commun.* **135** (2001) 238–259, [hep-ph/0010017].

[128] G. Corcella, I. G. Knowles, G. Marchesini, S. Moretti, K. Odagiri, P. Richardson et al., *HERWIG 6: An Event generator for hadron emission reactions with interfering gluons (including supersymmetric processes)*, *JHEP* **01** (2001) 010, [hep-ph/0011363].

[129] CMS collaboration, V. Khachatryan et al., *Study of hadronic event-shape variables in multijet final states in pp collisions at sqrt(s) = 7 TeV*, *JHEP* **10** (2014) 87, [1407.2856].

[130] ATLAS collaboration, G. Aad et al., *Measurement of charged-particle event shape variables in $\sqrt{s} = 7$ TeV proton-proton interactions with the ATLAS detector*, *Phys. Rev.* **D88** (2013) 032004, [1207.6915].

[131] T. Becher, B. D. Pecjak and D. Y. Shao, *Factorization for the light-jet mass and hemisphere soft function*, *JHEP* **12** (2016) 018, [1610.01608].

[132] A. Banfi, G. P. Salam and G. Zanderighi, *Principles of general final-state resummation and automated implementation*, *JHEP* **03** (2005) 073, [hep-ph/0407286].

[133] E. Gerwick, S. Hoeche, S. Marzani and S. Schumann, *Soft evolution of multi-jet final states*, *JHEP* **02** (2015) 106, [1411.7325].

[134] G. 't Hooft, *A Planar Diagram Theory for Strong Interactions*, *Nucl. Phys.* **B72** (1974) 461.

[135] N. Kidonakis, G. Oderda and G. F. Sterman, *Evolution of color exchange in QCD hard scattering*, *Nucl. Phys.* **B531** (1998) 365–402, [hep-ph/9803241].

[136] Yu. L. Dokshitzer and G. Marchesini, *Soft gluons at large angles in hadron collisions*, *JHEP* **01** (2006) 007, [hep-ph/0509078].

[137] F. Maltoni, K. Paul, T. Stelzer and S. Willenbrock, *Color flow decomposition of QCD amplitudes*, *Phys. Rev.* **D67** (2003) 014026, [hep-ph/0209271].

[138] M. Sjodahl and J. Thorén, *Decomposing color structure into multiplet bases*, *JHEP* **09** (2015) 055, [1507.03814].

[139] A. Schofield and M. H. Seymour, *Jet vetoing and Herwig++*, *JHEP* **01** (2012) 078, [1103.4811].

[140] M. Mangano, S. Parke and Z. Xu, *Duality and multi-gluon scattering*, *Nuclear Physics B* **298** (1988) 653 – 672.

[141] M. Dasgupta and G. P. Salam, *Resummed event shape variables in DIS*, *JHEP* **08** (2002) 032, [hep-ph/0208073].

[142] A. Banfi, G. P. Salam and G. Zanderighi, *Phenomenology of event shapes at hadron colliders*, *JHEP* **06** (2010) 038, [1001.4082].

[143] E. Gerwick, S. Schumann, B. Gripaios and B. Webber, *QCD Jet Rates with the Inclusive Generalized kt Algorithms*, *JHEP* **04** (2013) 089, [1212.5235].

[144] A. Altheimer et al., *Boosted objects and jet substructure at the LHC. Report of BOOST2012, held at IFIC Valencia, 23rd-27th of July 2012*, *Eur. Phys. J.* **C74** (2014) 2792, [1311.2708].

[145] D. Krohn, J. Thaler and L.-T. Wang, *Jet Trimming*, *JHEP* **02** (2010) 084, [0912.1342].

[146] CMS collaboration, A. M. Sirunyan et al., *Search for anomalous couplings in boosted* WW/WZ $\to \ell\nu\mathrm{q}\bar{\mathrm{q}}$ *production in proton-proton collisions at* $\sqrt{s} = 8$ *TeV*, *Phys. Lett.* **B772** (2017) 21âĂŞ42, [1703.06095].

[147] CMS collaboration, V. Khachatryan et al., *Identification techniques for highly boosted W bosons that decay into hadrons*, *JHEP* **12** (2014) 017, [1410.4227].

[148] T. Plehn, G. P. Salam and M. Spannowsky, *Fat Jets for a Light Higgs*, *Phys. Rev. Lett.* **104** (2010) 111801, [0910.5472].

[149] G. Kasieczka, T. Plehn, T. Schell, T. Strebler and G. P. Salam, *Resonance Searches with an Updated Top Tagger*, *JHEP* **06** (2015) 203, [1503.05921].

[150] ATLAS collaboration, G. Aad et al., *Identification of boosted, hadronically decaying W bosons and comparisons with ATLAS data taken at* $\sqrt{s} = 8$ *TeV*, *Eur. Phys. J.* **C76** (2016) 154, [1510.05821].

[151] S. Schätzel and M. Spannowsky, *Tagging highly boosted top quarks*, *Phys. Rev.* **D89** (2014) 014007, [1308.0540].

[152] A. J. Larkoski and J. Thaler, *Aspects of jets at 100 TeV*, *Phys. Rev.* **D90** (2014) 034010, [1406.7011].

[153] T. Cohen, R. T. D'Agnolo, M. Hance, H. K. Lou and J. G. Wacker, *Boosting Stop Searches with a 100 TeV Proton Collider*, *JHEP* **11** (2014) 021, [1406.4512].

[154] A. J. Larkoski, F. Maltoni and M. Selvaggi, *Tracking down hyper-boosted top quarks*, *JHEP* **06** (2015) 032, [1503.03347].

[155] K. Konishi, A. Ukawa and G. Veneziano, *Jet Calculus: A Simple Algorithm for Resolving QCD Jets*, *Nucl. Phys.* **B157** (1979) 45–107.

[156] S. Catani, Y. L. Dokshitzer, F. Fiorani and B. R. Webber, *Average number of jets in e+ e- annihilation*, *Nucl. Phys.* **B377** (1992) 445–460.

[157] A. Abdesselam et al., *Boosted objects: a probe of beyond the standard model physics*, *EPHJA,C71,1661.2011* **C71** (2011) 1661, [1012.5412].

[158] T. Plehn and M. Spannowsky, *Top Tagging*, *J. Phys.* **G39** (2012) 083001, [1112.4441].

[159] A. Altheimer et al., *Jet Substructure at the Tevatron and LHC: New results, new tools, new benchmarks*, 1201.0008.

[160] M. Dasgupta, A. Fregoso, S. Marzani and G. P. Salam, *Towards an understanding of jet substructure*, *JHEP* **09** (2013) 029, [1307.0007].

[161] M. Dasgupta, A. Fregoso, S. Marzani and A. Powling, *Jet substructure with analytical methods*, *Eur. Phys. J.* **C73** (2013) 2623, [1307.0013].

[162] A. J. Larkoski, S. Marzani, G. Soyez and J. Thaler, *Soft Drop*, *JHEP* **05** (2014) 146, [1402.2657].

[163] M. Dasgupta, L. Schunk and G. Soyez, *Jet shapes for boosted jet two-prong decays from first-principles*, 1512.00516.

[164] A. J. Larkoski, I. Moult and D. Neill, *Analytic Boosted Boson Discrimination*, 1507.03018.

[165] C. Frye, A. J. Larkoski, M. D. Schwartz and K. Yan, *Factorization for groomed jet substructure beyond the next-to-leading logarithm*, 1603.09338.

[166] J. Gallicchio and M. D. Schwartz, *Quark and Gluon Tagging at the LHC*, *Phys. Rev. Lett.* **107** (2011) 172001, [1106.3076].

[167] B. Bhattacherjee, S. Mukhopadhyay, M. M. Nojiri, Y. Sakaki and B. R. Webber, *Associated jet and subjet rates in light-quark and gluon jet discrimination*, *JHEP* **04** (2015) 131, [1501.04794].

[168] M. Cacciari, G. P. Salam and G. Soyez, *FastJet user manual*, *Eur.Phys.J.* **C72** (2012) 1896, [1111.6097].

[169] S. Höche and S. Prestel, *The midpoint between dipole and parton showers*, *Eur. Phys. J.* **C75** (2015) 461, [1506.05057].

[170] M. Dasgupta, F. Dreyer, G. P. Salam and G. Soyez, *Small-radius jets to all orders in QCD*, *JHEP* **04** (2015) 039, [1411.5182].

[171] M. Dasgupta, F. A. Dreyer, G. P. Salam and G. Soyez, *Inclusive jet spectrum for small-radius jets*, 1602.01110.

[172] Y. Delenda, R. Appleby, M. Dasgupta and A. Banfi, *On QCD resummation with k(t) clustering*, *JHEP* **12** (2006) 044, [hep-ph/0610242].

[173] D. Adams et al., *Towards an Understanding of the Correlations in Jet Substructure*, *Eur. Phys. J.* **C75** (2015) 409, [1504.00679].

[174] S. Höche, F. Krauss and S. Prestel, *Implementing NLO DGLAP evolution in Parton Showers*, 1705.00982.

[175] S. Höche and S. Prestel, *Triple collinear emissions in parton showers*, 1705.00742.

[176] G. Panico and A. Wulzer, *The Composite Nambu-Goldstone Higgs*, *Lect. Notes Phys.* **913** (2016) pp.1–316, [1506.01961].

[177] P. Ferrarese, "Searching for top partners at the large hadron collider." Dipartimento di Fisica ed Astronomia G. Galilei.

[178] F. Englert and R. Brout, *Broken Symmetry and the Mass of Gauge Vector Mesons*, *Phys. Rev. Lett.* **13** (1964) 321–323.

[179] P. W. Higgs, *Broken symmetries, massless particles and gauge fields*, *Phys. Lett.* **12** (1964) 132–133.

[180] CMS collaboration, S. Chatrchyan et al., *Observation of a new boson with mass near 125 GeV in pp collisions at* $\sqrt{s}$ *= 7 and 8 TeV*, *JHEP* **06** (2013) 081, [1303.4571].

[181] S. Weinberg, *Baryon and Lepton Nonconserving Processes*, *Phys. Rev. Lett.* **43** (1979) 1566–1570.

[182] Super-Kamiokande Collaboration collaboration, K. Abe, Y. Haga, Y. Hayato, M. Ikeda, K. Iyogi, J. Kameda et al., *Search for proton decay via* $p \to e^+\pi^0$ *and* $p \to \mu^+\pi^0$ *in* 0.31 *megaton· years exposure of the super-kamiokande water cherenkov detector*, *Phys. Rev. D* **95** (Jan, 2017) 012004.

[183] S. Weinberg, *Baryon- and lepton-nonconserving processes*, *Phys. Rev. Lett.* **43** (Nov, 1979) 1566–1570.

[184] V. N. Aseev, A. I. Belesev, A. I. Berlev, E. V. Geraskin, A. A. Golubev, N. A. Likhovid et al., *Upper limit on the electron antineutrino mass from the troitsk experiment*, *Phys. Rev. D* **84** (Dec, 2011) 112003.

[185] Planck collaboration, P. A. R. Ade et al., *Planck 2015 results. XIII. Cosmological parameters*, *Astron. Astrophys.* **594** (2016) A13, [1502.01589].

[186] D. B. Kaplan and H. Georgi, *SU(2) x U(1) Breaking by Vacuum Misalignment*, *Phys. Lett.* **B136** (1984) 183–186.

[187] D. B. Kaplan, H. Georgi and S. Dimopoulos, *Composite Higgs Scalars*, *Phys. Lett.* **B136** (1984) 187–190.

[188] H. Georgi and D. B. Kaplan, *Composite Higgs and Custodial SU(2)*, *Phys. Lett.* **B145** (1984) 216.

[189] G. Panico and A. Wulzer, *The Composite Nambu-Goldstone Higgs*, *Lect. Notes Phys.* **913** (2016) pp.1–316, [1506.01961].

[190] B. Bellazzini, C. Csáki and J. Serra, *Composite Higgses*, *Eur. Phys. J.* **C74** (2014) 2766, [1401.2457].

[191] G. von Gersdorff, E. Pontón and R. Rosenfeld, *The Dynamical Composite Higgs*, *JHEP* **06** (2015) 119, [1502.07340].

[192] T. A. Ryttov and F. Sannino, *Ultra Minimal Technicolor and its Dark Matter TIMP*, *Phys. Rev.* **D78** (2008) 115010, [0809.0713].

[193] J. Galloway, J. A. Evans, M. A. Luty and R. A. Tacchi, *Minimal Conformal Technicolor and Precision Electroweak Tests*, *JHEP* **10** (2010) 086, [1001.1361].

[194] G. Cacciapaglia and F. Sannino, *Fundamental Composite (Goldstone) Higgs Dynamics*, *JHEP* **04** (2014) 111, [1402.0233].

[195] S. R. Coleman, J. Wess and B. Zumino, *Structure of phenomenological Lagrangians. 1.*, *Phys. Rev.* **177** (1969) 2239–2247.

[196] C. G. Callan, Jr., S. R. Coleman, J. Wess and B. Zumino, *Structure of phenomenological Lagrangians. 2.*, *Phys. Rev.* **177** (1969) 2247–2250.

[197] S. R. Coleman and E. J. Weinberg, *Radiative Corrections as the Origin of Spontaneous Symmetry Breaking*, *Phys. Rev.* **D7** (1973) 1888–1910.

[198] E. Katz, A. E. Nelson and D. G. E. Walker, *The Intermediate Higgs*, *JHEP* **08** (2005) 074, [hep-ph/0504252].

[199] B. Gripaios, A. Pomarol, F. Riva and J. Serra, *Beyond the Minimal Composite Higgs Model*, *JHEP* **04** (2009) 070, [0902.1483].

[200] A. Arbey, G. Cacciapaglia, H. Cai, A. Deandrea, S. Le Corre and F. Sannino, *Fundamental Composite Electroweak Dynamics: Status at the LHC*, 1502.04718.

[201] D. Buarque Franzosi, G. Cacciapaglia, H. Cai, A. Deandrea and M. Frandsen, *Vector and Axial-vector resonances in composite models of the Higgs boson*, *JHEP* **11** (2016) 076, [1605.01363].

[202] M. Bando, T. Kugo and K. Yamawaki, *Nonlinear Realization and Hidden Local Symmetries*, *Phys. Rept.* **164** (1988) 217–314.

[203] R. Arthur, V. Drach, M. Hansen, A. Hietanen, C. Pica and F. Sannino, *SU(2) gauge theory with two fundamental flavors: A minimal template for model building*, *Phys. Rev.* **D94** (2016) 094507, [1602.06559].

[204] G. Cacciapaglia, H. Cai, A. Deandrea, T. Flacke, S. J. Lee and A. Parolini, *Composite scalars at the LHC: the Higgs, the Sextet and the Octet*, *JHEP* **11** (2015) 201, [1507.02283].

[205] G. Ferretti, *Gauge theories of Partial Compositeness: Scenarios for Run-II of the LHC*, 1604.06467.

[206] M. J. G. Veltman, *Second Threshold in Weak Interactions*, *Acta Phys. Polon.* **B8** (1977) 475.

[207] M. J. G. Veltman, *Large Higgs Mass and mu - e Universality*, *Phys. Lett.* **B70** (1977) 253–254.

[208] B. W. Lee, C. Quigg and H. B. Thacker, *The Strength of Weak Interactions at Very High-Energies and the Higgs Boson Mass*, *Phys. Rev. Lett.* **38** (1977) 883–885.

[209] B. W. Lee, C. Quigg and H. B. Thacker, *Weak Interactions at Very High-Energies: The Role of the Higgs Boson Mass*, *Phys. Rev.* **D16** (1977) 1519.

[210] G. Passarino, *Large Masses, Unitarity and One Loop Corrections*, *Phys. Lett.* **B156** (1985) 231–235.

[211] G. Passarino, *W W scattering and perturbative unitarity*, *Nucl. Phys.* **B343** (1990) 31–59.

[212] J. M. Cornwall, D. N. Levin and G. Tiktopoulos, *Derivation of Gauge Invariance from High-Energy Unitarity Bounds on the s Matrix*, *Phys. Rev.* **D10** (1974) 1145.

[213] S. Weinberg, *Pion scattering lengths*, *Phys. Rev. Lett.* **17** (1966) 616–621.

[214] G. Passarino, *Ww scattering and perturbative unitarity*, *Nuclear Physics B* **343** (1990) 31 – 59.

[215] M. S. Chanowitz and M. K. Gaillard, *The TeV Physics of Strongly Interacting W's and Z's*, *Nucl. Phys.* **B261** (1985) 379–431.

[216] D. Buarque Franzosi and P. Ferrarese, *Implications of Vector Boson Scattering Unitarity in Composite Higgs Models*, 1705.02787.

[217] A. Ballestrero, D. Buarque Franzosi, L. Oggero and E. Maina, *Vector Boson scattering at the LHC: counting experiments for unitarized models in a full six fermion approach*, *JHEP* **03** (2012) 031, [1112.1171].

[218] A. Alboteanu, W. Kilian and J. Reuter, *Resonances and Unitarity in Weak Boson Scattering at the LHC*, *JHEP* **11** (2008) 010, [0806.4145].

[219] J. M. Butterworth, B. E. Cox and J. R. Forshaw, *WW scattering at the CERN LHC*, *Phys. Rev.* **D65** (2002) 096014, [hep-ph/0201098].

[220] M. S. Chanowitz, *Strong W W scattering in unitary gauge*, *Phys. Lett.* **B373** (1996) 141–146, [hep-ph/9512358].

[221] M. S. Chanowitz, *Gauge invariant formulation of strong W W scattering*, *Phys. Lett.* **B388** (1996) 161–166, [hep-ph/9608324].

[222] K.-i. Hikasa and K. Igi, *Strongly interacting WW sector with a scalar resonance*, *Phys. Lett.* **B261** (1991) 285–288.

[223] A. Dobado, M. J. Herrero, J. R. Pelaez and E. Ruiz Morales, *CERN LHC sensitivity to the resonance spectrum of a minimal strongly interacting electroweak symmetry breaking sector*, *Phys. Rev.* **D62** (2000) 055011, [hep-ph/9912224].

[224] A. Dobado, M. J. Herrero and T. N. Truong, *Unitarized Chiral Perturbation Theory for Elastic Pion-Pion Scattering*, *Phys. Lett.* **B235** (1990) 134–140.

[225] G. F. Chew and S. Mandelstam, *Theory of low-energy pion pion interactions*, *Phys. Rev.* **119** (1960) 467–477.

[226] G. Ecker, J. Gasser, A. Pich and E. de Rafael, *The Role of Resonances in Chiral Perturbation Theory*, *Nucl. Phys.* **B321** (1989) 311–342.

[227] S. Gupta, *Quantum Electrodynamics*, vol. New York. 1981.

[228] J. S. Schwinger, *Quantum electrodynamics. I A covariant formulation*, *Phys. Rev.* **74** (1948) 1439.

[229] J. A. Oller, *The Case of a WW dynamical scalar resonance within a chiral effective description of the strongly interacting Higgs sector*, *Phys. Lett.* **B477** (2000) 187–194, [hep-ph/9908493].

[230] A. Dobado and J. R. Pelaez, *A Global fit of pi pi and pi K elastic scattering in ChPT with dispersion relations*, *Phys. Rev.* **D47** (1993) 4883–4888, [hep-ph/9301276].

[231] J. Bijnens and J. Lu, *Meson-meson Scattering in QCD-like Theories*, *JHEP* **03** (2011) 028, [1102.0172].

[232] D. Buarque Franzosi, F. Maltoni and C. Zhang, *Effective field theory approach to the Higgs lineshape*, *Phys. Rev.* **D87** (2013) 053015, [1211.4835].

[233] J. Bagger, V. D. Barger, K.-m. Cheung, J. F. Gunion, T. Han, G. A. Ladinsky et al., *CERN LHC analysis of the strongly interacting W W system: Gold plated modes*, *Phys. Rev.* **D52** (1995) 3878–3889, [hep-ph/9504426].

[234] M. J. Duncan, G. L. Kane and W. W. Repko, *W W Physics at Future Colliders*, *Nucl. Phys.* **B272** (1986) 517–559.

[235] D. A. Dicus and R. Vega, *WW Production From PP Collisions*, *Phys. Rev. Lett.* **57** (1986) 1110–1112.

[236] R. N. Cahn, S. D. Ellis, R. Kleiss and W. J. Stirling, *Transverse Momentum Signatures for Heavy Higgs Bosons*, *Phys. Rev.* **D35** (1987) 1626.

[237] V. D. Barger, T. Han and R. J. N. Phillips, *Improved Transverse Mass Variable for Detecting Higgs Boson Decays Into Z Pairs*, *Phys. Rev.* **D36** (1987) 295.

[238] R. Kleiss and W. J. Stirling, *Tagging the Higgs*, *Phys. Lett.* **B200** (1988) 193–199.

[239] V. D. Barger, T. Han and R. J. N. Phillips, *Improving the Heavy Higgs Boson Two Charged Lepton - Two Neutrino Signal*, *Phys. Rev.* **D37** (1988) 2005–2008.

[240] V. D. Barger, K.-m. Cheung, T. Han and R. J. N. Phillips, *Strong W^+W^+ scattering signals at pp supercolliders*, *Phys. Rev.* **D42** (1990) 3052–3077.

[241] U. Baur and E. W. N. Glover, *Tagging the Higgs boson in p p —¿ W+ W- j j*, *Phys. Lett.* **B252** (1990) 683–689.

[242] V. D. Barger, K.-m. Cheung, T. Han and D. Zeppenfeld, *Single forward jet tagging and central jet vetoing to identify the leptonic WW decay mode of a heavy Higgs boson*, *Phys. Rev.* **D44** (1991) 2701.

[243] D. A. Dicus, J. F. Gunion, L. H. Orr and R. Vega, *Isolating purely leptonic signals for strong W scattering using antitagging jet tagging, and lepton isolation*, *Nucl. Phys.* **B377** (1992) 31–54.

[244] V. D. Barger, R. J. N. Phillips and D. Zeppenfeld, *Mini - jet veto: A Tool for the heavy Higgs search at the LHC*, *Phys. Lett.* **B346** (1995) 106–114, [hep-ph/9412276].

[245] D. L. Rainwater and D. Zeppenfeld, *Observing $H \to W^*W^* \to e^\pm\mu\mp \not{p}_T$ in weak boson fusion with dual forward jet tagging at the CERN LHC*, *Phys. Rev.* **D60** (1999) 113004, [hep-ph/9906218].

[246] E. Accomando, A. Ballestrero, S. Bolognesi, E. Maina and C. Mariotti, *Boson-boson scattering and Higgs production at the LHC from a six fermion point of view: Four jets + l nu processes at O(alpha(em)**6)*, *JHEP* **03** (2006) 093, [hep-ph/0512219].

[247] A. Ballestrero, G. Bevilacqua and E. Maina, *A Complete parton level analysis of boson-boson scattering and ElectroWeak Symmetry Breaking in lv + four jets production at the LHC*, *JHEP* **05** (2009) 015, [0812.5084].

[248] A. Ballestrero, D. Buarque Franzosi and E. Maina, *Vector-Vector scattering at the LHC with two charged leptons and two neutrinos in the final state*, *JHEP* **06** (2011) 013, [1011.1514].

[249] A. Ballestrero, D. Buarque Franzosi and E. Maina, *Exploring alternative symmetry breaking mechanisms at the LHC with 7, 8 and 10 TeV total energy*, *JHEP* **05** (2012) 083, [1203.2771].

[250] D. Buarque Franzosi and R. Foadi, *Probing Near-Conformal Technicolor through Weak Boson Scattering*, *Phys. Rev.* **D88** (2013) 015013, [1209.5913].

[251] B. Jager, L. Salfelder, M. Worek and D. Zeppenfeld, *Physics Opportunities for Vector-Boson Scattering at a Future 100 TeV Hadron Collider*, 1704.04911.

[252] C. Degrande, C. Duhr, B. Fuks, D. Grellscheid, O. Mattelaer et al., *UFO - The Universal FeynRules Output*, *Comput.Phys.Commun.* **183** (2012) 1201–1214, [1108.2040].

[253] A. Alloul, N. D. Christensen, C. Degrande, C. Duhr and B. Fuks, *FeynRules 2.0 - A complete toolbox for tree-level phenomenology*, *Comput. Phys. Commun.* **185** (2014) 2250–2300, [1310.1921].

[254] R. D. Ball et al., *Parton distributions with LHC data*, *Nucl. Phys.* **B867** (2013) 244–289, [1207.1303].

[255] T. Han, J. Sayre and S. Westhoff, *Top-Quark Initiated Processes at High-Energy Hadron Colliders*, *JHEP* **04** (2015) 145, [1411.2588].

[256] J. Alwall, R. Frederix, S. Frixione, V. Hirschi, F. Maltoni, O. Mattelaer et al., *The automated computation of tree-level and next-to-leading order differential cross sections, and their matching to parton shower simulations*, *JHEP* **07** (2014) 079, [1405.0301].

[257] A. Thamm, R. Torre and A. Wulzer, *Future tests of Higgs compositeness: direct vs indirect*, *JHEP* **07** (2015) 100, [1502.01701].

[258] CMS collaboration, V. Khachatryan et al., *Study of vector boson scattering and search for new physics in events with two same-sign leptons and two jets*, *Phys. Rev. Lett.* **114** (2015) 051801, [1410.6315].

[259] CMS collaboration, V. Khachatryan et al., *Search for new resonances decaying via WZ to leptons in proton-proton collisions at* $\sqrt{s} = 8$ *TeV*, *Phys. Lett.* **B740** (2015) 83–104, [1407.3476].

[260] C. Mariotti and G. Passarino, *Higgs boson couplings: measurements and theoretical interpretation*, 1612.00269.

[261] S. Hoeche, S. Kuttimalai, S. Schumann and F. Siegert, *Beyond Standard Model calculations with Sherpa*, *Eur. Phys. J.* **C75** (2015) 135, [1412.6478].

[262] S. Dulat, T.-J. Hou, J. Gao, M. Guzzi, J. Huston, P. Nadolsky et al., *New parton distribution functions from a global analysis of quantum chromodynamics*, *Phys. Rev.* **D93** (2016) 033006, [1506.07443].

[263] S. Hoeche, F. Krauss, S. Schumann and F. Siegert, *QCD matrix elements and truncated showers*, *JHEP* **05** (2009) 053, [0903.1219].

[264] A. Buckley, J. Butterworth, L. Lonnblad, D. Grellscheid, H. Hoeth, J. Monk et al., *Rivet user manual*, *Comput. Phys. Commun.* **184** (2013) 2803–2819, [1003.0694].

[265] B. Jager, C. Oleari and D. Zeppenfeld, *Next-to-leading order QCD corrections to W+W- production via vector-boson fusion*, *JHEP* **07** (2006) 015, [hep-ph/0603177].

[266] B. Jager, C. Oleari and D. Zeppenfeld, *Next-to-leading order QCD corrections to Z boson pair production via vector-boson fusion*, *Phys. Rev.* **D73** (2006) 113006, [hep-ph/0604200].

[267] G. Bozzi, B. Jager, C. Oleari and D. Zeppenfeld, *Next-to-leading order QCD corrections to W+ Z and W- Z production via vector-boson fusion*, *Phys. Rev.* **D75** (2007) 073004, [hep-ph/0701105].

[268] B. Jager, C. Oleari and D. Zeppenfeld, *Next-to-leading order QCD corrections to W+ W+ jj and W- W- jj production via weak-boson fusion*, *Phys. Rev.* **D80** (2009) 034022, [0907.0580].

[269] B. Biedermann, A. Denner and M. Pellen, *Large electroweak corrections to vector-boson scattering at the Large Hadron Collider*, 1611.02951.

[270] *Studies of Vector Boson Scattering And Triboson Production with an Upgraded ATLAS Detector at a High-Luminosity LHC*, Tech. Rep. ATL-PHYS-PUB-2013-006, CERN, Geneva, Jun, 2013.

[271] ATLAS collaboration, *Measurements of the Higgs boson production cross section via Vector Boson Fusion and associated WH production in the $WW^* \to \ell\nu\ell\nu$ decay mode with the ATLAS detector at $\sqrt{s}$ = 13 TeV*, Tech. Rep. ATLAS-CONF-2016-112, CERN, Geneva, Nov, 2016.

[272] T. ATLAS-Collaboration, *Studies of Vector Boson Scattering with an Upgraded ATLAS Detector at a High-Luminosity LHC*, Tech. Rep. ATL-PHYS-PUB-2012-005, CERN, Geneva, Nov, 2012.